

# **Novel Pseudocyclopeptides Containing 1,4- Disubstituted 1,2,3-Triazole Subunits for Anion Recognition**

vom Fachbereich Chemie der Technischen Universität  
zur Verleihung des akademischen Grades 'Doktor der Naturwissenschaften'  
genehmigte Dissertation

**D 386**



Datum der wissenschaftlichen Aussprache: 21.07.2017

Vorgelegt von  
**Disha Mungalpara**  
**Betreuer: Prof. Dr. Stefan Kubik**  
Kaiserslautern 2017

Die vorliegende Arbeit wurde unter der Leitung von Prof. Dr. Stefan Kubik im Zeitraum von Juni 2013 bis Juni 2017 im Fachbereich Chemie der Technischen Universität Kaiserslautern angefertigt.

Betreuer: Prof. Dr. S. Kubik

Prüfungskommission

Vorsitzender: Prof. Dr. Hans-Jörg Krüger

1. Gutachter: Prof. Dr. Stefan Kubik

2. Gutachter: Jr. Prof. Dr. Frederic Patureau

Hiermit versichere ich, dass ich die vorliegende Arbeit selbstständig verfasst und keine anderen als die angegebenen Quellen und Hilfsmittel verwendet habe sowie Literaturzitate kenntlich gemacht wurden. Ich erkläre außerdem, dass diese Dissertation weder in gleicher, noch in anderer Form bereits in einem anderen Prüfungsverfahren vorlag.

Kaiserslautern, den .....

Disha Mungalpara

Teile dieser Arbeit wurden bereits veröffentlicht:

1. D. Mungalpara, H. Kelm, A. Valkonen, K. Rissanen, S. Keller, S. Kubik "Oxoanion binding to a cyclic pseudopeptide containing 1,4-disubstituted 1,2,3-triazole moieties" *Org. Biomol. Chem.* 2017, **15**, 102-113.
2. D. Mungalpara, A. Valkonen, K. Rissanen, S. Kubik "Efficient stabilisation of a dihydrogenphosphate tetramer and a dihydrogenpyrophosphate dimer by a cyclic pseudopeptide containing 1,4-disubstituted 1,2,3-triazole moieties" *Chem. Sci.* 2017, **8**, 6005-6013.
3. D. Mungalpara, S. Stegmüller, S. Kubik "A neutral halogen bonding macrocyclic anion receptor based on a pseudocyclopeptide with three 5-iodo-1,2,3-triazole subunits" *Chem. Commun.* 2017, **53**, 5095-5098.

## **Acknowledgment**

It is my pleasure to take this opportunity to acknowledge the people that have contributed directly or indirectly to the successful outcome of this work. First and foremost, I owe deepest gratitude to my supervisor, Prof. Dr. Stefan Kubik, who gave me the opportunity to work in his group and for providing invaluable support and guidance, at the same time granting me freedom in the planning and conduction of the work. I am truly thankful not only for the knowledge acquired from Prof. Dr. Stefan Kubik but also for the advice and friendly discussions, which meant a great deal to me.

I would like to thank Jr. Prof. Dr. Frederic Patureau and Prof. Dr. Hans-Jörg Krüger for helping with the revision of my thesis.

I wish to express my gratitude Prof. Dr. Kari Rissanen and Dr. Arto Valkonen for their extensive help in solving challenging crystal structures. I want to also thank Dr. Herald Kelm and Dr. Richard Goddard for their great support in X-ray Crystallography.

My special thanks to Prof. Dr. Sandro Keller who have assisted in the interpretation of complicated ITC results.

I express thanks to Prof. Krüger and his coworkers who generously shared their chemicals, dry solvents and other lab facilities with us. I am grateful to Mrs. Christiana Müller, who taught me special NMR techniques and helped in the solving difficulties associated with the NMR measurements. Also, I wish to acknowledge Simone Stegmüller for assisting during HPLC-MS measurements.

I am also thankful to our chemical store team (Ludvik, Frank, Jürgen). It was interesting to discuss non-chemistry topics (meditation, moral education and other life lessons) with Ludvik whenever I went for chemical order.

My special thanks to neighbour cum co-worker Ligia for the great friendship. My appreciation also extends to all my current (Beatrice, Daniel, Fabian, Julia, Lena) and the former (Michaela, Astrid, Serap, Björn, Steffen, Christian, Alex, Michael) lab members for making the work atmosphere very friendly.

I am overwhelmingly grateful to my husband (Chirag) for his endless support and encouragement. I am fully indebted to friends (Shailja, Ridhhi and Dimple di) and my family members (Avani, Jay, and my parents) for their love, support, and understanding.

# Table of Content

Table of Content .....	IV
List of Figures .....	VI
List of Tables.....	VIII
Abbreviations.....	IX
Nomenclature.....	X
<b>1 Chapter 1- Intoduction .....</b>	<b>2</b>
1.1 Anion Recognition .....	3
1.1.1 Significance of Anion Recognition .....	4
1.1.2 Strategy to Design Receptors for Anion Recognition .....	5
1.2 State of Art .....	9
1.2.1 Triazole C-H as anion binding motif.....	9
1.2.2 Triazole C-I as anion binding motif .....	13
1.3 Scope of the doctoral work .....	19
<b>2 Chapter 2 - Anion binding to a cyclic pseudopeptide containing 1,4-disubstituted 1,2,3-triazole moieties .....</b>	<b>22</b>
2.1 Scope of the work.....	23
2.2 Results .....	25
2.2.1 Synthesis.....	25
2.2.2 Structural Assignment and Anion Binding Properties .....	29
2.3 Discussion .....	35
2.4 Summary .....	36
2.5 Publication.....	38
<b>3 Chapter 3 - Efficient stabilization of phosphate aggregates by a cyclic pseudopeptide containing 1,4-disubstituted 1,2,3-triazole moieties .....</b>	<b>52</b>
3.1 Scope of the Work.....	53
3.2 Results .....	55
3.2.1 Synthesis.....	55
3.2.2 Structural Assignment and Anion Binding Properties .....	59
3.3 Discussion .....	63
3.4 Summary .....	65
3.5 Manuscript.....	66
<b>4 Chapter 4 - A neutral halogen bonding macrocyclic anion receptor based on a pseudocyclopeptide with three 5-iodo-1,2,3-triazole subunits .....</b>	<b>76</b>
4.1 Scope of the Work.....	77
4.2 Results .....	78
4.2.1 Synthesis.....	78
4.2.2 Structural Assignment and Anion Binding Properties .....	81
4.3 Discussion .....	85
4.4 Summary .....	86
4.5 Publication.....	87

<b>5</b>	<b>Conclusion and Outlook .....</b>	<b>91</b>
<b>6</b>	<b>References .....</b>	<b>94</b>
<b>7</b>	<b>Appendix I.....</b>	<b>97</b>
<b>8</b>	<b>Appendix II.....</b>	<b>126</b>
<b>9</b>	<b>Appendix III .....</b>	<b>161</b>

## List of Figures

Figure 1	Schematic representation of anion recognition.....	3
Figure 2	Schematic representation of anion binding that includes solvent reorganization..	3
Figure 3	Possible application of anion receptors. ....	5
Figure 4	Examples of typical anion binding motifs. ....	6
Figure 5	Examples of novel anion binding motifs. ....	7
Figure 6	Cu(I)-Catalyzed 1,3-dipolar cycloaddition reaction affording a 1,4-disubstituted 1,2,3-triazole unit. The red arrow indicates the dipole moment $\mu$ of the 1,2,3-triazole unit in Debye (D). ....	9
Figure 7	Similarities of trans-amides and cis-amides with 1, 4-disubstituted (a) and 1,5-disubstituted (b) 1,2,3-triazoles. ....	12
Figure 8	One pot synthesis of 1,4-disubstituted 5-iodo-1,2,3-triazoles by using Cu(I)-catalyzed 1,3-dipolar cycloaddition in the presence of triiodide. The red arrow indicates the dipole moment ( $\mu$ ) of the 5-iodo-1,2,3-triazole unit.....	14
Figure 9	Schematic representation of the electrostatic interaction between the $\sigma$ hole of the iodine atom in a 1,4-disubstituted 5-iodo-1,2,3-triazole ring and an anion.....	14
Figure 10	Comparison of crystal structures of cyclopeptide <b>19</b> (a) and cyclic pseudohexapeptide <b>20</b> (b) with the calculated structure of cyclic pseudohexapeptide <b>16</b> (c). In the cases of <b>19</b> and <b>20</b> , solvent molecules are omitted for the clarity. The structure of <b>16</b> was calculated by using Spartan 04 for Macintosh (Wavefunction, Inc.) with the MMFF force field and without considering solvent molecules.....	25
Figure 11	Synthesis of the linear trimer <b>25a</b> . ....	26
Figure 12	Synthesis of the cyclic pseudopeptide <b>16</b> . ....	27
Figure 13	HPLC chromatogram of the cyclization reaction <b>CR3</b> after 24 h (a), 48 h (b), and 72 h (c). ....	28
Figure 14	HPLC chromatogram of cyclization reaction <b>CR4</b> after 24 h (a) 48 h (b) 96 h (c) 120 h (d) 144 h (e) and 168 h (f). After 96 h the reaction was heated to 35 °C. .	29
Figure 15	<sup>1</sup> H-NMR spectra of solutions containing 0.1 mM (a), 0.25 mM (b), 0.50 mM (c), 0.75 mM (d), and 1.00 mM (e) of <b>16</b> in 5 vol% DMSO- <i>d</i> <sub>6</sub> /acetone- <i>d</i> <sub>6</sub> . The signals assigned are indicated in the structure on the right hand side by using the same color code.....	30
Figure 16	<sup>1</sup> H-NMR spectrum of <b>16</b> (1 mM) in 5 vol% DMSO- <i>d</i> <sub>6</sub> /acetone- <i>d</i> <sub>6</sub> in the absence (a) and the presence of 5 equiv. of TBA iodide (b), nitrate (c) hydrogen sulfate (d) bromide (e), chloride (f), dihydrogenphosphate (g), and sulfate (h).....	31
Figure 17	<sup>1</sup> H-NMR spectra of <b>16</b> and TBA chloride in 5 vol% DMSO- <i>d</i> <sub>6</sub> /acetone- <i>d</i> <sub>6</sub> at mol fractions X of the partner ranging between 0.0 and 0.9 mol% of TBA chloride and a total concentration of 1 mM. ....	32
Figure 18	Job plots for the chloride complex of <b>16</b> in 5 vol% DMSO- <i>d</i> <sub>6</sub> /acetone- <i>d</i> <sub>6</sub> . The three curves were constructed by following the courses of the N-H (stars), TriC-H (circles), and C*-H (squares) signals in the NMR spectra depicted in Figure 17. ....	32

Figure 19	$^1\text{H-NMR}$ spectra of <b>16</b> (0.5 mM) in 5 vol% $\text{DMSO-}d_6/\text{acetone-}d_6$ containing increasing equivalents of TBA chloride, specified to the left of each spectrum. 33
Figure 20	Binding isotherms obtained in the NMR titration of <b>16</b> with TBA chloride by following the shifts of the TriC-H (a), N-H (b), and C*-H (c) signals. Fitting of isotherms was performed by using HypNMR2008. .... 34
Figure 21	Calculated structure of cyclic pseudopeptide <b>17</b> : side view (a) top view (b). The calculations were performed by using the MMFF force-field implemented in Spartan 10. A Monte-Carlo conformational search was performed without restricting the number of considered conformations. After initiating the calculation, 39366 conformations were expected to be calculated. The search aborted after 122 conformations, however, after which no further improvement could be achieved. .... 54
Figure 22	Synthesis of linear tetramer <b>28a</b> . .... 55
Figure 23	Synthesis of the cyclic pseudooctapeptide <b>17</b> . .... 56
Figure 24	HPLC chromatograms of the cyclization reaction in tert-butanol/water, 1:1 (v/v) after 24 h (a), 48 h (b), and 72 h (c). Extra 5 mol% of $\text{Cu}(\text{MeCN})_4\text{PF}_6$ and TBTA were added after every 24 h. .... 57
Figure 25	$^1\text{H-NMR}$ spectra recorded in $\text{DMSO-}d_6$ of the product mixture (a), and of the major (b) and the minor (c) component of the isolated mixture. The signals assigned are indicated in the structure on the right hand side by using the same color code. The signals denoted with the blue and the black dots represent the ones of the minor and the major product, respectively. .... 58
Figure 26	Crystal structures of $(\mathbf{17}\cdot\text{DHP})_2$ (a) $(\mathbf{17}\cdot\text{DHPP})_2$ (b) $((S)\mathbf{17}\cdot\text{DHPP})_2$ (c) $((R)\mathbf{17}\cdot\text{DHPP})_2$ (d) complexes. .... 60
Figure 27	$^1\text{H-NMR}$ spectra of <b>17</b> (0.5 mM) in 2.5 vol% $\text{D}_2\text{O}/\text{DMSO-}d_6$ in the absence (a) and the presence of TBA sulfate (0.5 equiv) (b), DHP (2 equiv) (c), HPP (0.5 equiv) (d), DHPP (0.5 equiv) (e). The signals denoted with the green and the red dots represent the ones of <b>17</b> in the free and complexed states, respectively. .... 61
Figure 28	Calculated structures of pseudopeptide <b>18</b> (a), crystal structure of <b>16</b> (b) and calculated structure of the chloride complex of <b>18</b> (c). DFT calculations were performed by using the B3LYP functional implemented in Spartan 10 (Wavefunction, Inc.) with the 6-311G* basis set. .... 77
Figure 29	Synthesis of linear pseudoheptapeptide <b>30</b> . .... 78
Figure 30	Synthesis of the pseudocycloheptapeptide <b>18</b> . .... 79
Figure 31	Conversion of the model monomer <b>31</b> into the azide <b>31a</b> . .... 80
Figure 32	HPLC chromatograms of the cyclization reaction under condition <b>CR1</b> obtained after 24 h (a) 72 h (b), and 120 h (c). .... 81
Figure 33	$^1\text{H-NMR}$ spectrum of <b>18</b> (1 mM) in 2.5 vol% $\text{H}_2\text{O}/\text{DMSO-}d_6$ in the absence (a) and the presence of 5 equiv. of TBA nitrate (b), DHP (c), fluoride (d), sulfate (e), iodide (f), bromide (g) chloride (h). The signals assigned are indicated in the structure on the right hand side by using the same color code. .... 83

## List of Tables

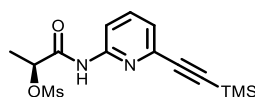
Table 1	Amount of reagents used for the cyclization of <b>25a</b> in tert-butanol/water, 1:1 (v/v) at 25 °C. ....	28
Table 2	Stability constants of the chloride, bromide, hydrogen sulfate (HS), and nitrate complexes of <b>16</b> in 5 vol% DMSO- <i>d</i> <sub>6</sub> /acetone- <i>d</i> <sub>6</sub> determined by NMR titrations. ....	35
Table 3	Main signals ( <i>m/z</i> ) present in the ESI mass spectra of solutions of <b>17</b> (0.5 mM) in DCM containing different anions as their respective TBA salts. ....	59
Table 4	Stability constants and thermodynamic parameters of the TBA sulfate complexes of <b>16</b> and <b>17</b> in 2.5 vol% water/DMSO. ....	62
Table 5	Stability constants and thermodynamic parameters of the TBA DHP and DHPP complexes of <b>17</b> in 2.5 vol% water/DMSO. ....	62
Table 6	Attempted cyclization reactions involving <b>30c</b> by using different copper sources and solvents. All reactions were performed at 25 °C. ....	80
Table 7	Main signals ( <i>m/z</i> ) present in the ESI mass spectra of solution of <b>18</b> (1 mM) in 50 vol% DMSO/ACN containing 1 equiv of different anions as their TBA salts....	82
Table 8	Stability constants and thermodynamic parameters of the TBA halide complexes of <b>18</b> in 2.5 vol% H <sub>2</sub> O/DMSO- <i>d</i> <sub>6</sub> or 2.5 vol% H <sub>2</sub> O/DMSO. ....	84

## Abbreviations

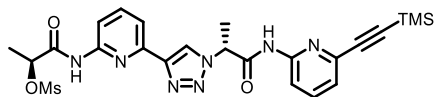
ACN	Acetonitrile
CuAAC	Copper-catalyzed alkyne-azide cycloaddition
CuIAAC	Copper-catalyzed iodoalkyne-azide cycloaddition
DCM	Dichloromethane
DHP	Dihydrogen phosphate
DHPP	Dihydrogen pyrophosphate
DMSO	Dimethyl sulfoxide
ESI	Electrospray Ionization
HB	Hydrogen Bonding
HPLC	High-Performance Liquid Chromatography
HPP	Hydrogen pyrophosphate
HS	Hydrogen sulfate
ITC	Isothermal Titration Calorimetry
MALDI-TOF	Matrix Assisted Laser Desorption Ionization-Time of Flight
MS	Mass Spectrometry
NMR	Nuclear Magnetic Resonance
NOESY	Nuclear Overhauser Effect Spectroscopy
ROESY	Rotational Frame Nuclear Overhauser Effect Spectroscopy
TBA	Tetrabutylammonium
TBTA	Tris(benzyltriazolylmethyl)amine
TEA	Triethylamine
THF	Tetrahydrofuran
TMA	Tetramethylammonium
TMS	Trimethylsilane
XB	Halogen Bonding

# Nomenclature

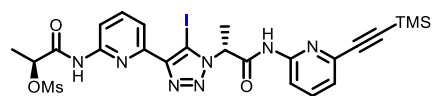
Linear monomer **21**



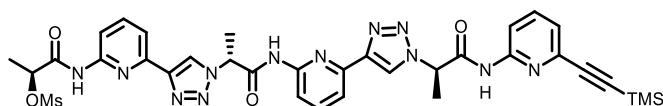
Linear dimer **24**



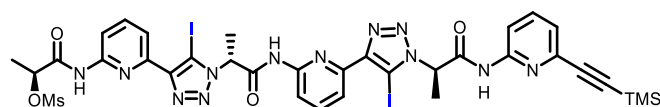
Linear dimer **29**



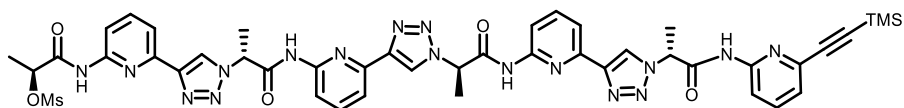
Linear trimer **25**



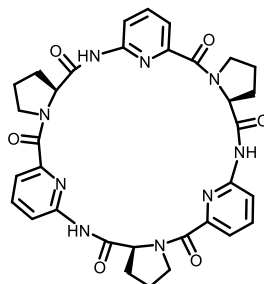
Linear trimer **30**



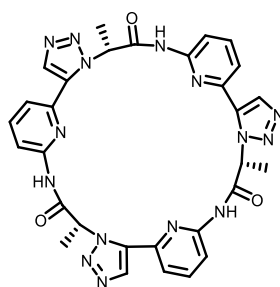
Linear tetramer **28**



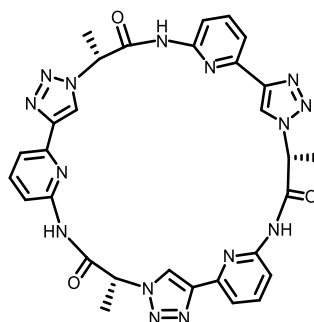
Cyclic hexapeptide **19**



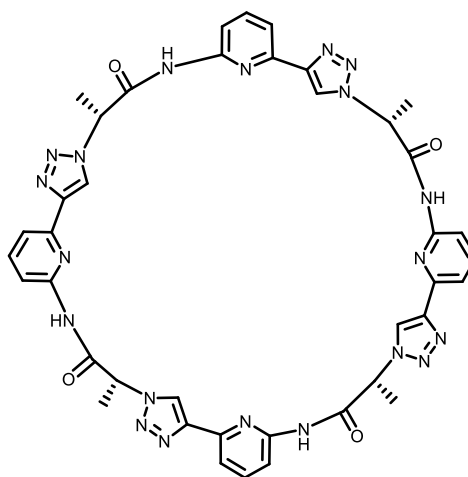
Cyclic  
pseudo-hexapeptide **20**



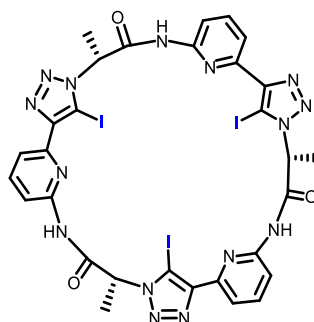
Cyclic  
pseudo-hexapeptide **16**



Cyclic  
pseudooctapeptide **17**



Cyclic  
pseudohexapeptide **18**



# Chapter 1

---

## Introduction

**1 Chapter 1- Intoduction**

## 1.1 Anion Recognition

Anion recognition is a phenomenon in which a molecule selectively binds to a negatively charged substrate using reversible, typically non-covalent or coordinative interactions (Figure 1).<sup>1,2</sup>

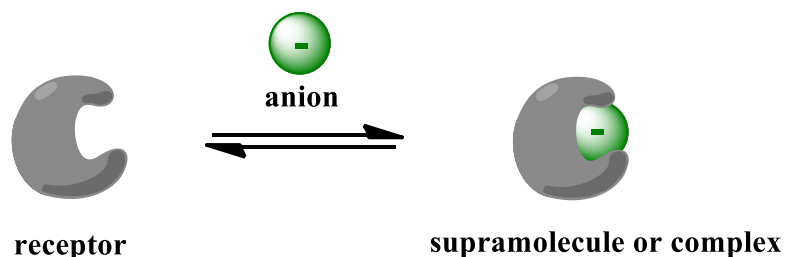


**Figure 1** Schematic representation of anion recognition.

In the aforementioned process, the molecule used to bind the anion is referred to as the receptor or host. The receptor molecule has strategically arranged convergent binding sites that can interact with the anion to form a product, which is also called a complex or a supramolecule. Selective anion binding can be achieved if the electronic character and geometry of the binding pocket of the receptor complements those of the anion. Moreover, the binding sites in a receptor should be spatially organized in such a way that they attract the anion without generating unfavorable repulsive interactions.

The anion binding event often begins with a conformational reorganization of the receptor to arrange the binding sites in the optimal way to bind the anion and simultaneously to minimize steric hindrance. When a receptor does not need to undergo a large change in its conformation for binding to occur, the receptor is *preorganized*.<sup>2</sup> It is important to mention that a conformational reorganization of the receptor is associated with an entropic and possibly enthalpic penalty that reduce complex stability. Preorganized receptors thus typically form more stable complexes than non-preorganized ones.

Also, solvation, i.e. the interaction of solvent molecules with the receptor and the anion, plays a substantial role in anion recognition.<sup>3</sup>

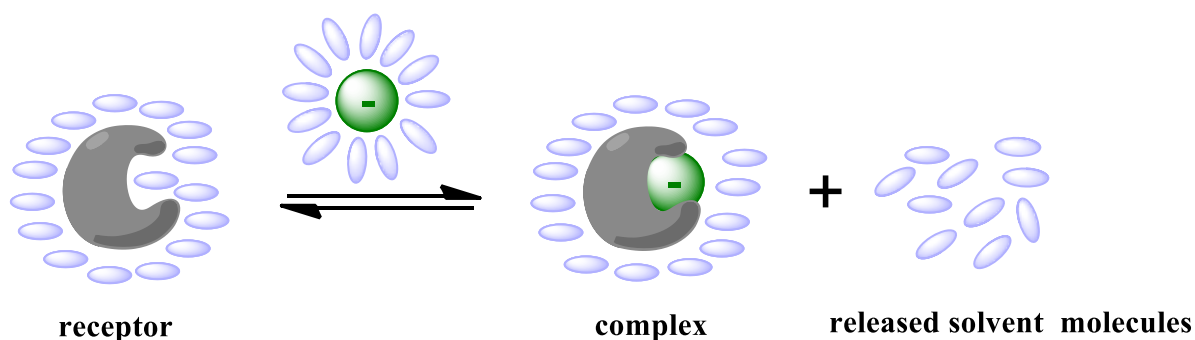


**Figure 2** Schematic representation of anion binding that includes solvent reorganization.

As shown in Figure 2, the receptor and the substrate are surrounded by solvent molecules in solution. During complexation, some of these interactions with the solvent molecules are broken to allow the receptor to interact with the anion. The Gibbs free energy gained by complex formation should overcompensate the energy required for desolvation. Moreover, the release of solvent molecules from a receptor and an anion during complex formation into the bulk increases the entropy, while the conformational restriction of the binding partners causes a loss of entropy. Thus, the final balance of all the enthalpic and entropic contributions determine the affinity of a receptor to an anion in a particular solvent.<sup>3</sup>

### 1.1.1 Significance of Anion Recognition

In the past few decades, anion coordination chemistry has experienced an exponential growth that is partly related to the significance of anion recognition in various fields as shown schematically in Figure 3.<sup>4, 5, 6, 7</sup>

For instance, the presence or concentration of toxic or environmentally deleterious anions can be monitored through anion sensing. Anion sensing by means of molecular receptors can be achieved if the recognition of an anion by a receptor produces a response, be it optical (change of color or fluorescence), electrochemical, or associated with a sol-gel transition. Anion receptors can also be employed to remove toxic anions ( $\text{TcO}_4^-$ ,  $\text{CN}^-$ ,  $\text{AsO}_4^{3-}$ ) from the environment via selective extraction. In metallurgy, metallate anions or ion pairs can be extracted by anion recognition.<sup>8</sup>

In biology, anions are transported across membranes by specific proteins in order to maintain the optimum concentration within the cell and the cellular compartments. Defects in these proteins affect their transporting ability, thus causing a number of diseases such as cystic fibrosis,<sup>9</sup> certain types of Bartter syndrome,<sup>10 11</sup> Pendred syndrome,<sup>12</sup> congenital chloride diarrhea,<sup>13</sup> and other genetic diseases. These disorders could be treated by replacing the malfunctioning proteins with synthetic anion receptors that can transport anions across phospholipid membranes.

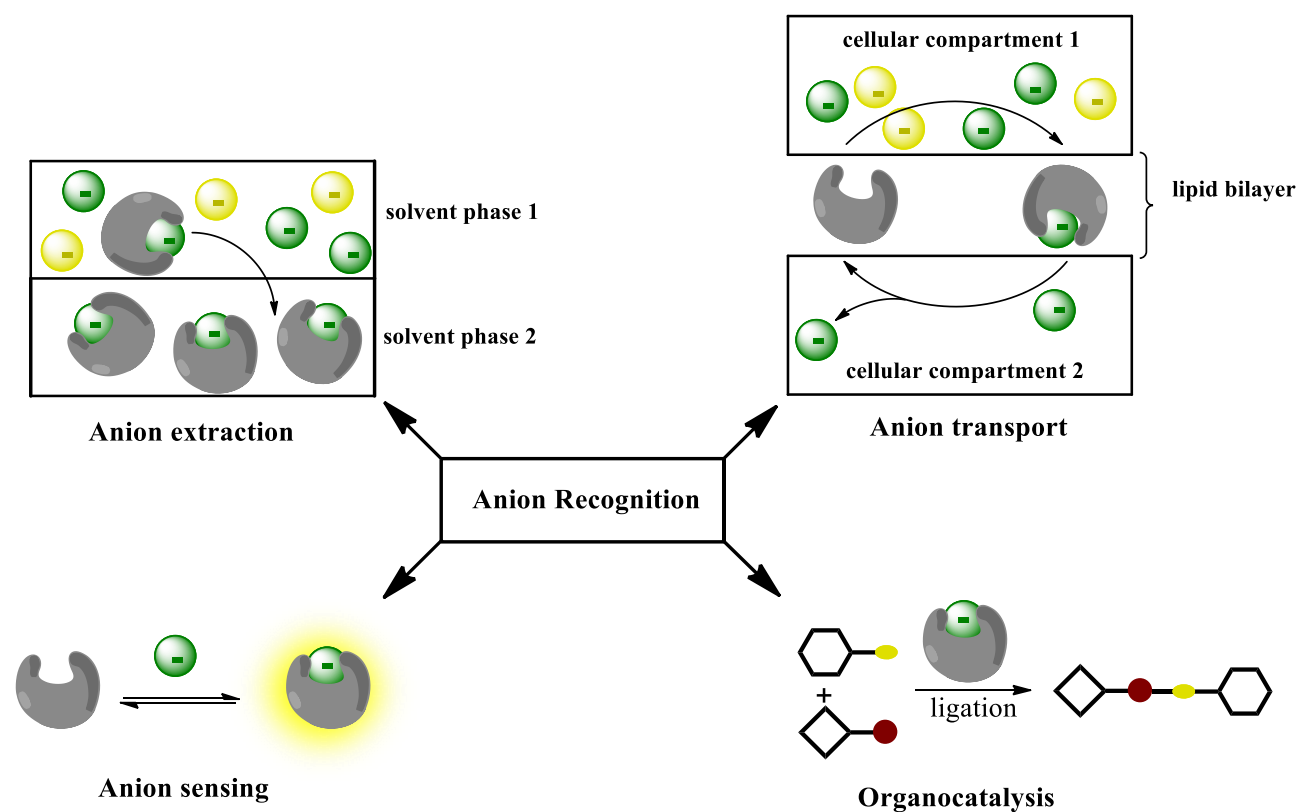


**Figure 3** Possible application of anion receptors.

Molecular recognition is also of central importance in bio- and organocatalysis. That anion receptors can also contribute as catalysts to the field of organocatalysis has nevertheless been recognized only recently.<sup>5, 14, 15</sup>

### 1.1.2 Strategy to Design Receptors for Anion Recognition

The key factors that should be considered during the design of a selective host are the properties of the anion that should be bound. Specifically, the binding pocket of the receptor should ideally be complementary to the structure of the target anion. In addition, it should contain appropriate acidic groups that can engage in non-covalent attractive interactions with the anion. A strategy to realize such a pocket involves arranging appropriate anion binding sites in a convergent arrangement around a cavity. The examples of typical anion binding motifs are depicted in Figure 4.<sup>16, 7, 17</sup>

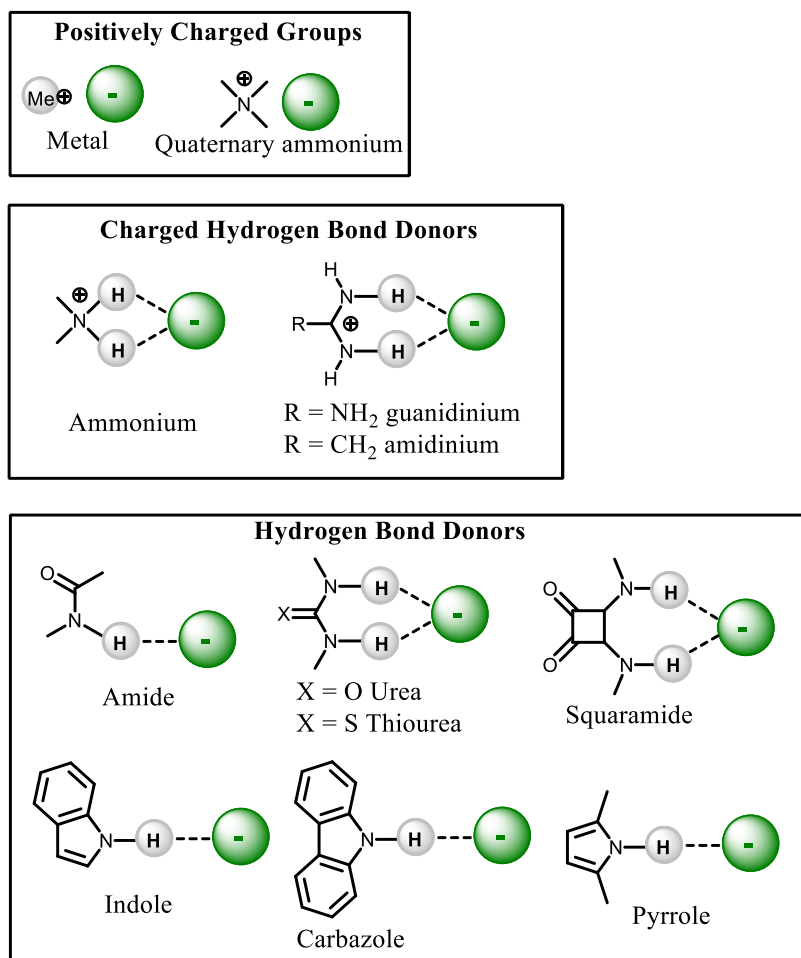


**Figure 4** Examples of typical anion binding motifs.

One strategy to recognize anions makes use of their Lewis bases nature, which enables selective and strong coordination to suitable Lewis acidic metal ions.<sup>18, 19, 20</sup> The coordination bonds thus formed have a high degree of directionality and often a high thermodynamic stability. Quaternary ammonium ions can be used in receptors to mediate anion affinity by electrostatic interaction.<sup>21, 22, 23</sup>

Hydrogen bond donors are functional groups in which one or more hydrogen atoms are connected to an electronegative atom (oxygen, sulfur, or nitrogen). The electronegative atom reduces the electron density on the hydrogen atom directly attached to it. The resultant electron deficient hydrogen atom interacts with the anion by an attractive force called hydrogen bond.<sup>24</sup> It is noteworthy that the strength of the resulting hydrogen bond reflects the sum of different interactions, namely, dipole-dipole interaction, London dispersion, and charge-transfer interactions. The strength of hydrogen bonds, which ranges in a wide range (2-180 kJ/mol),<sup>25</sup> and their good directionality render this type of interaction very useful for anion recognition.

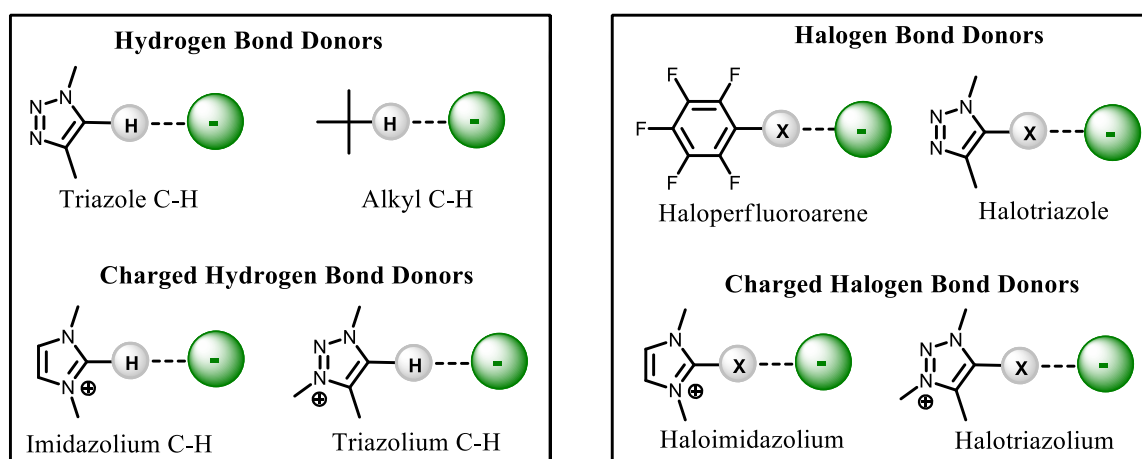


**Figure 5** Examples of novel anion binding motifs.

Recent investigations have shown that polarized C-H groups can also engage in hydrogen bonding interactions with anions (Figure 5). The C<sup>5</sup>-H bond of 1,4-disubstituted 1,2,3-triazole rings, in particular, represents a versatile anion binding motif.<sup>26, 27, 28, 29</sup> This bond was found to be a stronger hydrogen bond donor than aliphatic C-H bonds due to its large dipole moment, which is almost collinear with the C-H bond, and has the positive end oriented in the direction of the hydrogen atom. The triazole C-H is, however, a weaker donor than conventional hydrogen bond donors. Another advantage of 1,2,3-triazoles is their easy accessibility by means of copper(I)-catalyzed azide-alkyne cycloaddition.<sup>30</sup>

A strategy to recognize anions that has only been recently found wider application is by means of halogen bonding (XB) interactions.<sup>31</sup> A halogen bond is an attractive non-covalent interaction between an electrophilic region in a covalently bonded halogen atom and a Lewis base (anion).<sup>32, 33, 34, 35</sup> The halogen bond ability of halogens increases as they become larger ( $F^- \ll Cl^- < Br^- < I^-$ ). These interactions have long been exploited as a tool in crystal engineering for their powerful ability to direct supramolecular self-assembly<sup>36</sup> whereas molecular recognition in solution using halogen bonding has been overlooked for some time.

Halogen bonding interactions  $R-X \cdots A^-$  have some characteristic features. The interatomic  $X \cdots A^-$  distance is, for example, shorter than the sum of the van-der-Waals radii of the two interacting atoms and the optimal angle of the interactions is close to  $180^\circ$ .<sup>37, 38</sup> The interaction strength of halogen bonding lies in the range 10-200 kJ/mol,<sup>39</sup> which is similar to that of hydrogen bonding interactions. However, XB interactions have an increased preference for linearity and are more hydrophobic in nature than HB interactions. Figure 5 shows commonly employed halogen bond donors for the development of anion receptors.

Incorporation of a positive charge into HB or XB donor motifs (termed charged hydrogen/halogen bond donors) increases the degree of polarization of hydrogen/halogen bonds,

thus strengthening the corresponding interactions. The charged nature of the resulting receptors also cause electrostatic interaction to contribute to binding. Charged receptors are also typically better soluble in polar solvents so that anion binding studies become possible under more competitive conditions. Examples of charged hydrogen bond and halogen bond donors are also included in Figure 4 and Figure 5.

## 1.2 State of Art

### 1.2.1 Triazole C-H as anion binding motif

The 1,2,3-triazole unit has many properties that make it well suited as a building block in anion receptors. Firstly, the heterocycle is readily prepared using Cu(I)-catalyzed 1,3-dipolar cycloadditions (Figure 6).<sup>30, 40, 41</sup>

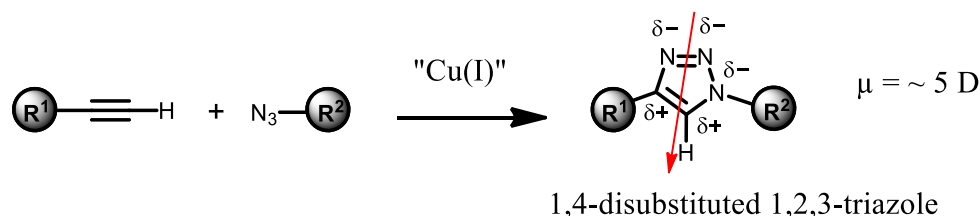


**Figure 6** Cu(I)-Catalyzed 1,3-dipolar cycloaddition reaction affording a 1,4-disubstituted 1,2,3-triazole unit. The red arrow indicates the dipole moment  $\mu$  of the 1,2,3-triazole unit in Debye (D).

Secondly, the electronic structure of the triazole ring is highly relevant for anion binding.<sup>29, 27</sup> The three electronegative and  $sp^2$  hybridized nitrogen atoms resided together on one side of the ring while the C-H bond resides on the opposite side. This arrangement creates a large dipole moment with its axis almost collinear with the C-H bond and the positive end located at the C-H group. The electronegativity of C<sup>5</sup>-carbon atom is further augmented by its  $sp^2$  hybridization and the presence of the clustered nitrogen atoms. As a consequence, the proton on C<sup>5</sup> is capable of engaging in hydrogen bonding interactions with anions. In this context, the geometry of the 1,2,3-triazole offers favorable features for constructing macrocyclic receptors. It is planar and has only minor steric bulk. The two substituents in 1- and 4- position of five-membered ring are arranged at a slightly larger angle than two meta-oriented substituents in a six-membered aromatic ring thus decreasing the steric hindrance with nearby groups.

The first example of a triazole C-H containing receptor is macrocycle **1** (Chart 1), which was prepared from the respective 1,3-diethynyl benzene and 1,3-diazido benzene precursors by means of copper-catalyzed azide-alkyne cycloaddition.<sup>42</sup> Compound **1** coordinates to chloride in dichloromethane with high affinity ( $K_a = 1.3 \times 10^5 \text{ M}^{-1}$ ). Size selectivity was observed because **1** forms less stable complexes with smaller fluoride and larger bromide and iodide anions. This receptor was developed in the Flood group in which various structural analogs of **1** were also prepared and investigated with respect to their anion coordination properties.<sup>27</sup>

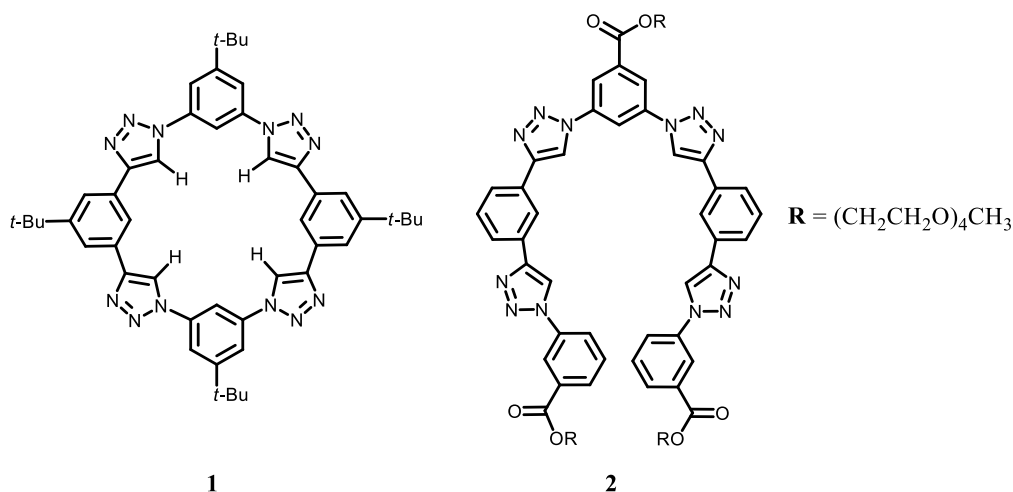


### Chart 1

Almost simultaneously, the anion binding properties of oligomer **2** (Chart 1), the acyclic analog of **1**, comprising alternating triazolyl and 1,3-disubstituted phenylene subunits were reported. Like macrocycle **1**, **2** binds to inorganic anions via C-H $\cdots$ anion interactions.<sup>43</sup> Anion binding studies demonstrated that **2** adopts a helical conformation in the presence of suitable anions with all the triazole C-H bonds directed towards the guest anion within the central cavity. Oligomer **2** binds to both chloride and bromide in acetone-*d*<sub>6</sub> at 25 °C with respective binding constants of  $K_a = 1.7 \times 10^4 \text{ M}^{-1}$  and  $K_a = 1.2 \times 10^4 \text{ M}^{-1}$ . However, the binding affinity of **2** is significantly lower for iodide due to the larger radius and an improper fit of this anion within the helix cavity. The increase of the length of oligomer **2** and introduction of chiral side-chains on every second phenylene subunits afforded **3** (Chart 2).<sup>44</sup> This compound adopts a two-turn helical conformation in water/acetonitrile further stabilized by  $\pi$ -stacking of the overlapping strands and solvophobic effects. The presence of chloride and bromide causes inversion of helicity, with the latter anion having the largest effect. This helix inversion in response to an achiral stimulus is unique. The authors claim that it is induced by halide binding to the chiral side chains of **3**, which alters the transfer of helicity of the substituents to the aromatic backbone, thus producing an inversion from left- to right-handed helicity.<sup>44</sup>



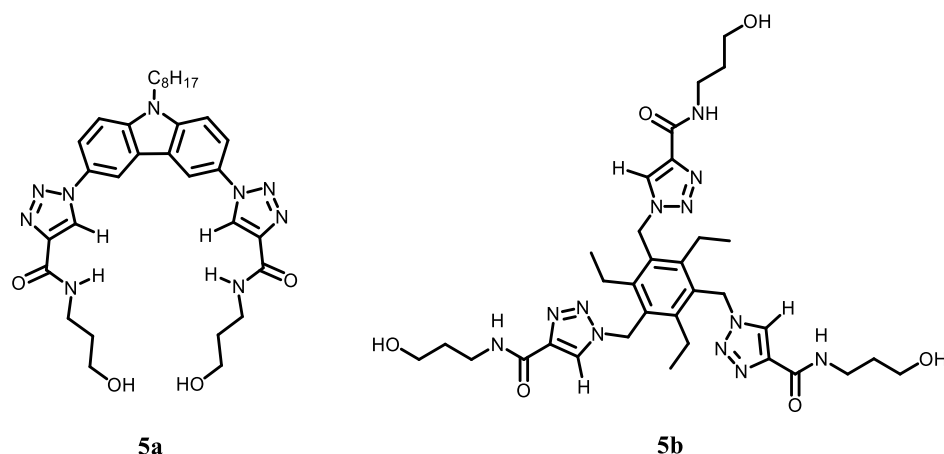


#### Chart 4

In terms of structure, triazole subunits have other key features that extends beyond anion coordination chemistry into the field of peptidomimetics.<sup>51, 52</sup> 1,2,3-Triazole rings share both electronic and topological characteristics with amide groups (Figure 7), in that both groups are of similar size and possess similar H-bonding donor and acceptor capabilities.<sup>53, 54, 55</sup> In addition, the incorporation of a 1,2,3-triazole ring into a molecule provides access to both “*trans*” and “*cis*” peptide mimics according to the substitution pattern on the triazole. Specifically, 1,4-disubstituted 1,2,3-triazoles mimic the *trans* whereas 1,5-substituted 1,2,3-triazoles the *cis* conformation of the amide bond.<sup>56, 57</sup>

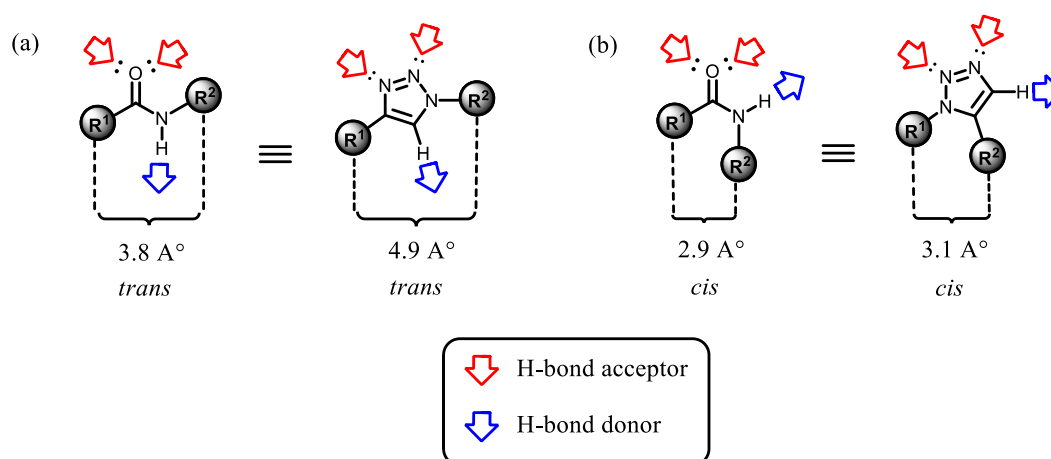


**Figure 7** Similarities of *trans*-amides and *cis*-amides with 1, 4-disubstituted (a) and 1,5-disubstituted (b) 1,2,3-triazoles.

Advantage of 1,2,3-triazoles is their proteolytic and metabolic stability with respect to amide bonds.<sup>56, 58</sup> Thus, the use of 1,2,3-triazole as bioisosteres for amide bonds has been recognized for some time. Davis et al. reported the triazolo peptide **6b**, an analog of the anticancer compound (**6a**) (Chart 5).<sup>59</sup> In their work, the authors studied the utility of different moieties as amide bond surrogates. Evaluation of the compounds in vitro revealed that only the 1,4-

disubstituted 1,2,3-triazole moiety could be incorporated in the cyclopeptide without reduction of its cytotoxicity.

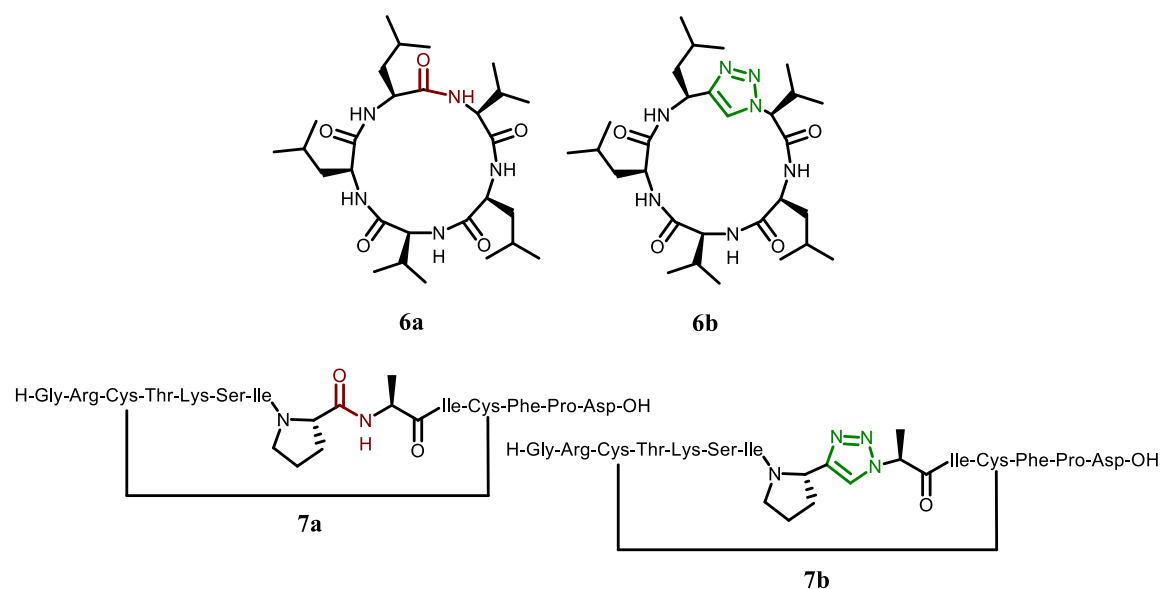


### Chart 5

The *trans*-amide bond of compound **7a** (compound **7a** is a Sunflower trypsin inhibitor 1 (SFTI-1) and act as protease inhibitor) was replaced by a 1,2,3-triazole unit between the prolyl and the alanyl residue.<sup>60</sup> In this work, the authors reported the use of both 1,4- and 1,5- disubstituted 1,2,3-triazole as amide bond surrogates. Only compound **7b**, which mimics the *trans* conformation of parent macrocycle **7a**, exhibits biological activity.<sup>60</sup>

### 1.2.2 Triazole C-I as anion binding motif

1,4-Disubstituted 5-iodo-1,2,3-triazole (iodotriazole) moieties have recently gained increasing attention as XB donors in anion receptors.<sup>61</sup> Similar to the prototriazole analog, iodotriazole rings are readily prepared by using a copper(I)-catalyzed cycloaddition between an azide and a terminal alkyne in the presence of an iodinating agent (triiodide) in one pot (Figure 8).<sup>62,63</sup> In analogy to the C-H bond polarization within 1,2,3-triazoles, a significant C-X bond polarization can be expected in 5-iodo-1,2,3-triazoles due to the presence of three nitrogen ring atoms.<sup>64</sup> Other structural properties such as planarity and ring size of prototriazole are essentially preserved in iodotriazoles.

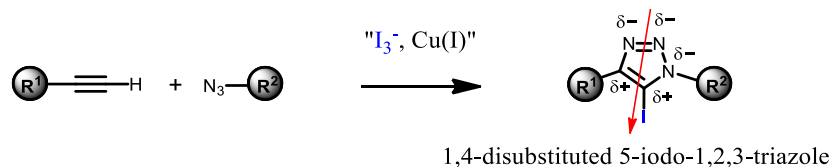


**Figure 8** One pot synthesis of 1,4-disubstituted 5-iodo-1,2,3-triazoles by using Cu(I)-catalyzed 1,3-dipolar cycloaddition in the presence of triiodide. The red arrow indicates the dipole moment ( $\mu$ ) of the 5-iodo-1,2,3-triazole unit.

A number of computational and experimental studies indicated that an anisotropic distribution of electron density around the iodine atom in the 1,4-disubstituted 5-iodo-1,2,3-triazole subunit generates a localized region of depleted electron density along the C-I axis, termed as  $\sigma$  hole.<sup>65</sup> Electrostatic interactions between the  $\sigma$  hole and electron donating species such as anions are termed halogen bonding (XB) (Figure 9).<sup>35</sup> XB interactions are considered to be of comparable strength to HB interactions but have a stricter linear geometry and different steric requirements. These properties render the 1,4-disubstituted 5-iodo-1,2,3-triazole subunit an attractive anion binding motif for incorporation into the binding pockets of anion receptors.

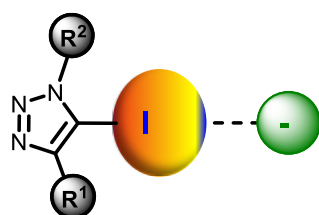


**Figure 9** Schematic representation of the electrostatic interaction between the  $\sigma$  hole of the iodine atom in a 1,4-disubstituted 5-iodo-1,2,3-triazole ring and an anion.

Several anion receptors containing iodotriazole subunits have been reported in the past few years. Schubert *et al.* prepared bidentate receptors **8a-b** in which a carbazole scaffold is symmetrically functionalized with two iodotriazole units (Chart 6).<sup>66</sup> X-ray crystallographic and NMR spectroscopic experiments indicated that intramolecular OH $\cdots$ N hydrogen bond interactions in **8b** preorganize the two triazole into a *syn-syn* arrangement, which is optimal for anion recognition. Isothermal titration calorimetry in THF indicated that bromide and chloride form 2:1 complexes in which one anion binds to two receptor molecules with the accumulated binding constants  $K_a$  equal to  $2.1 \times 10^8 \text{ M}^{-2}$  and  $2.2 \times 10^8 \text{ M}^{-2}$ , respectively. The complexation is enthalpically and entropically favored. Receptor **8a**, lacking the OH groups, forms less stable complexes with the same anions due to the greater entropic penalty that has to be paid during

complex formation with respect to **8b**. This outcome confirms that the preorganization of **8b** has a favorable effect on anion affinity.

In the bimetallic bis-triazole pyrimidine derived receptors **9a-b** (Chart 6), the chelation of the two Re(I) centers preorganizes the triazole groups as well as increases the degree of polarization of the C-I and C-H bonds.<sup>67</sup> The binding affinity and selectivity of the iodine containing receptor **9b** for a range of halides and oxoanions are quite different from the ones of the structural analog **9a**, containing two prototriazole moieties. Halides, hydrogen carbonate, and acetate have higher affinities for **9b** in 50 vol% CDCl<sub>3</sub>/CD<sub>3</sub>OD, whereas **9a** is a slightly superior ligand for H<sub>2</sub>PO<sub>4</sub><sup>-</sup>, ClO<sub>4</sub><sup>-</sup>, SO<sub>4</sub><sup>2-</sup>, and NO<sub>3</sub><sup>-</sup>. Moreover, **9a** shows little discrimination among the monovalent anions ( $92 \leq K_a \leq 548 \text{ M}^{-1}$ ), whereas a clear selectivity for I<sup>-</sup> ( $K_a > 10^4 \text{ M}^{-1}$ ) was observed in the case of XB receptor **9b**.

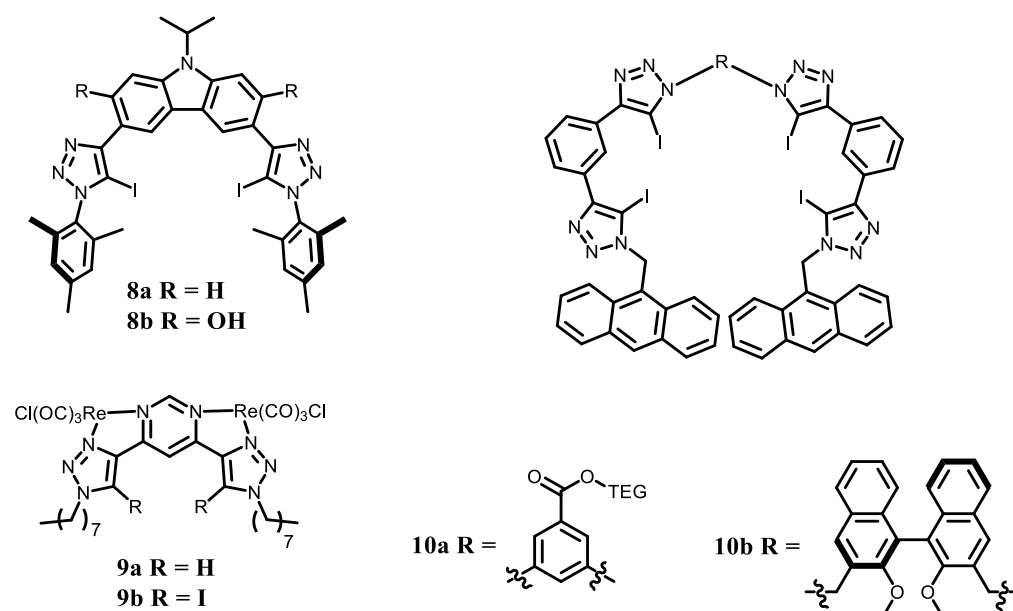


### Chart 6

Subsequently, Beer's group introduced the acyclic receptors **10a-b**, comprising four iodotriazole subunits (Chart 6).<sup>68</sup> The neutral tetradentate XB foldamer **10a** exhibits higher affinity for iodide ( $K_a = 2.7 \times 10^3 \text{ M}^{-1}$ ) over the smaller halides, carboxylate, and dihydrogen phosphate (DHP) anions in 50 vol% CDCl<sub>3</sub>/acetone-*d*<sub>6</sub>. The foldamer **10b** with a chiral (*S*)-binaphthol subunit is able to distinguish between the enantiomers of chiral amino acids. The highest enantioselectivity was observed for tryptophan ( $K_D/K_L = 1.69$ ), followed by leucine ( $K_D/K_L = 1.52$ ) and alanine ( $K_D/K_L = 0.79$ ), which correlates with the steric bulk of the amino acid side chain.

The same group recently introduced a neutral all-XB [2]rotaxane **11**, which is equipped with three convergent iodotriazole donors (Chart 7).<sup>69</sup> This host displays a significantly improved selectivity for halide anions over AcO<sup>-</sup> in CHCl<sub>3</sub> compared to an acyclic model system,

comprising the isolated bis-iodotriazole Re(I) complex. The halide selectivity trend ( $\text{Cl}^- > \text{Br}^- > \text{I}^-$ ) suggests a size complementarity between the [2]rotaxane's binding cavity and the  $\text{Cl}^-$  anion. Importantly, no interactions between the metal-free analog of rotaxane **11** and halide anions were observed, which highlights the pivotal role of the Re(I) center in preorganizing and polarizing the ring bis-iodotriazole XB donor groups.

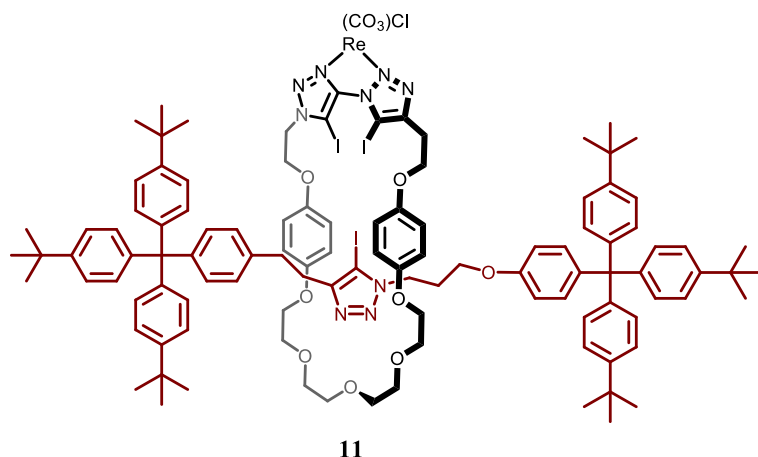


#### Chart 7

Beer *et al.* prepared the tetrapodal receptor **12b** (Chart 8) by installing four iodotriazole containing arms onto a picket-fence-style Zn(II) metalloporphyrin scaffold.<sup>70</sup> Anions are bound by **12b** via XB interactions to the four C-I groups and by coordinative interactions with the Lewis acidic Zn(II) center. The anion recognition properties of **12b** and of its structurally analogous HB receptor **12a** (Chart 8) were investigated by means of UV-visible titration experiments in  $\text{CHCl}_3$ , acetone, and acetonitrile. Both receptors prefer the complexation of oxoanions over halide anions, with the trend in halide binding affinities correlating with the charge density of the anion ( $\text{Cl}^- > \text{Br}^- > \text{I}^-$ ). The XB receptor **12b** has a higher affinity for halides than the HB receptor in all three solvents, whereas the same trend was not observed for the oxoanions. Moreover, the anion affinities of both receptors were shown to strongly depend on the solvent (acetone > acetonitrile > chloroform).

The 3,5-bis-(iodotriazole)-pyridinium subunit was incorporated into [2]catenane **13b** (Chart 8) by using a chloride-templated ring-closing metathesis ‘clipping’ reaction.<sup>71</sup> This receptor binds to halides with a markedly higher affinity than the all-HB catenane **13a** (Chart 8). Compound **13b** has a strong preference for  $\text{I}^-$  and  $\text{Br}^-$  over the smaller  $\text{Cl}^-$  anion in 45:45:10  $\text{CDCl}_3/\text{CD}_3\text{OD}/\text{D}_2\text{O}$ . Interestingly, **13b** binds to oxoanions,  $\text{AcO}^-$ , and  $\text{H}_2\text{PO}_4^-$  too weakly for binding affinity to be quantified. Single crystal X-ray structural analysis confirms the incorporation of the halides into the cavity of **13b**.

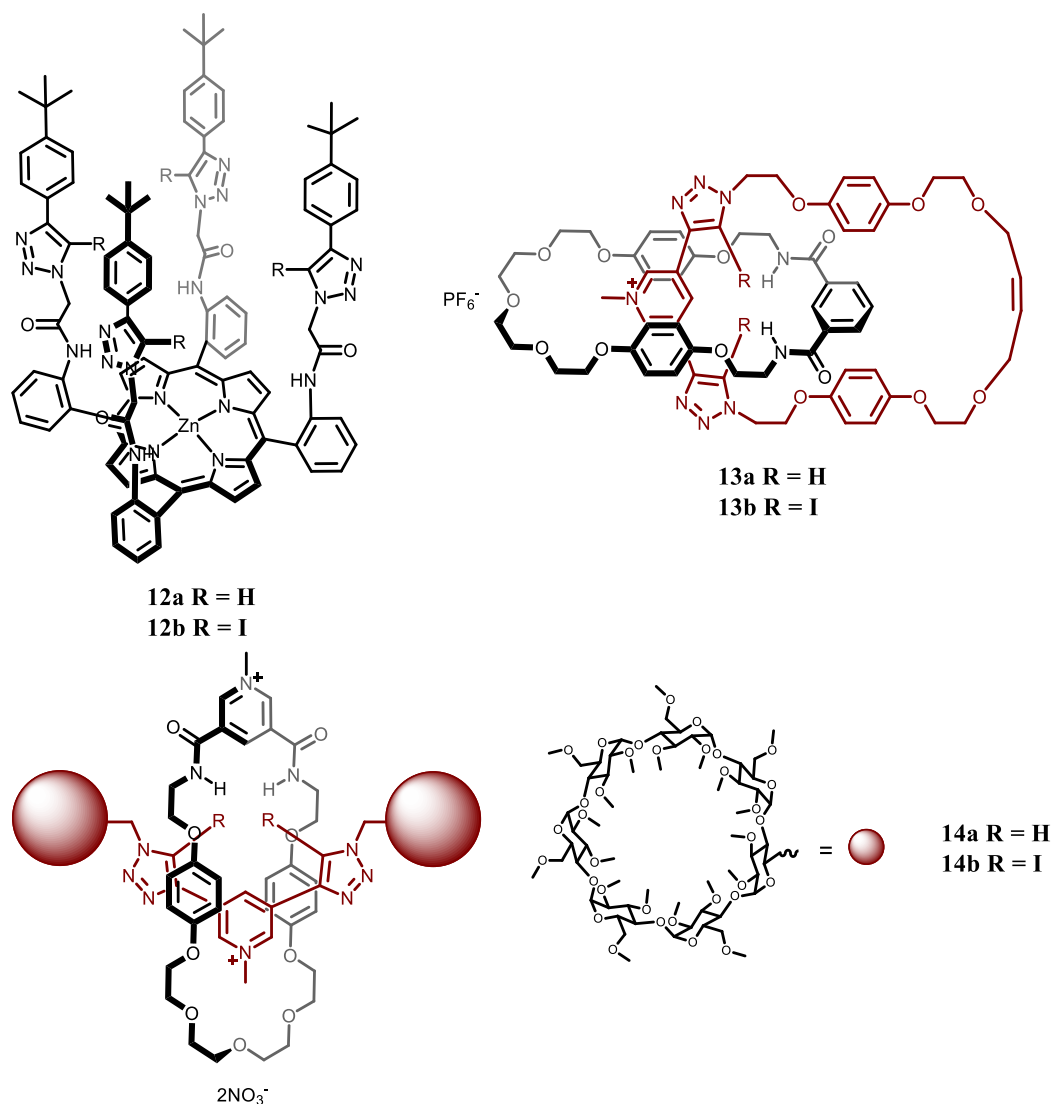


### Chart 8

Clipping of a ring around a bis-iodotriazole pyridinium subunit with two appended permethylated  $\beta$ -cyclodextrin stoppers afforded the water soluble dicationic [2]rotaxane **14b** (Chart 8).<sup>72</sup>  $^1\text{H-NMR}$  titration experiments revealed that halide and sulfate affinities of the prototriazole analog **14a** (Chart 8) in  $\text{D}_2\text{O}$  are modest whereas the [2]rotaxane **14b** containing the XB donors binds strongly to these anions. Iodide affinity of the XB rotaxane **14b** ( $K_a = 2.2 \times 10^3 \text{ M}^{-1}$ ) is particularly improved over that of **14a** ( $K_a = 20 \text{ M}^{-1}$ ). The complexation of iodide by **14a** is enthalpically disfavored and entropically driven as a consequence of the release of  $\text{D}_2\text{O}$  molecules from the host and guest upon anion binding. Conversely, the binding of  $\text{I}^-$  by the bis-iodotriazole rotaxane **14b** is entropically unfavorable and driven by a favorable enthalpic contribution which suggests the formation of strong  $\text{C-I}\cdots\text{I}^-$  bonds.

Most anion receptors containing 1,4-disubstituted 5-iodo-1,2,3-triazole (iodotriazole) building blocks reported so far are non-cyclic, containing typically up to four iodotriazole subunits as

binding sites or feature interlocked molecular components such as the receptors developed in the Beer group.<sup>61</sup> Macrocyclic receptors with a converging arrangement of several halogen-bond donors are, however, rare. The only example is a family of cyclophanes developed by Beer *et al.* featuring two bromoimidazolium units in the ring that bind halides in 90 vol% CH<sub>3</sub>OH/H<sub>2</sub>O by combining electrostatic interactions with XB. In addition, there is a single example of a cyclic receptor, namely **15a** (Chart 9) comprising a crown ether embedded 5-iodo-1,2,3-triazole ring. This ion-pair receptor simultaneously binds to both the anion and the cation of sodium iodide (Chart 9).<sup>64</sup> Affinity in 75 vol% CD<sub>2</sub>Cl<sub>2</sub>/CD<sub>3</sub>CN is low due to the poor solubility of sodium iodide in organic solvent and the non-ideal fit of the sodium with the cation cavity. However, **15a** exhibits overall higher affinity for NaI ( $K_a = 541 \text{ M}^{-1}$ ) than the prototriazole containing macrocycle **15b** ( $K_a = 174 \text{ M}^{-1}$ ).

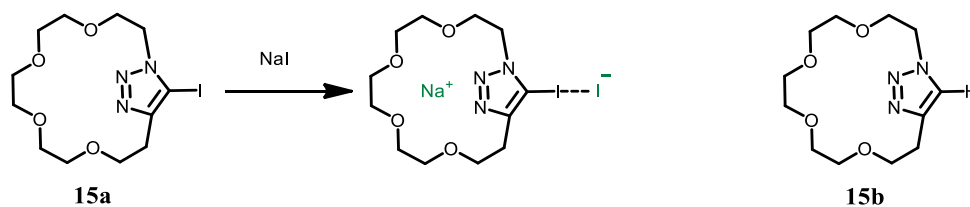


Chart 9

### 1.3 Scope of the doctoral work

The main objectives of this thesis were to develop novel cyclic pseudopeptides containing multiple binding sites for anion recognition and investigate their anion affinity.

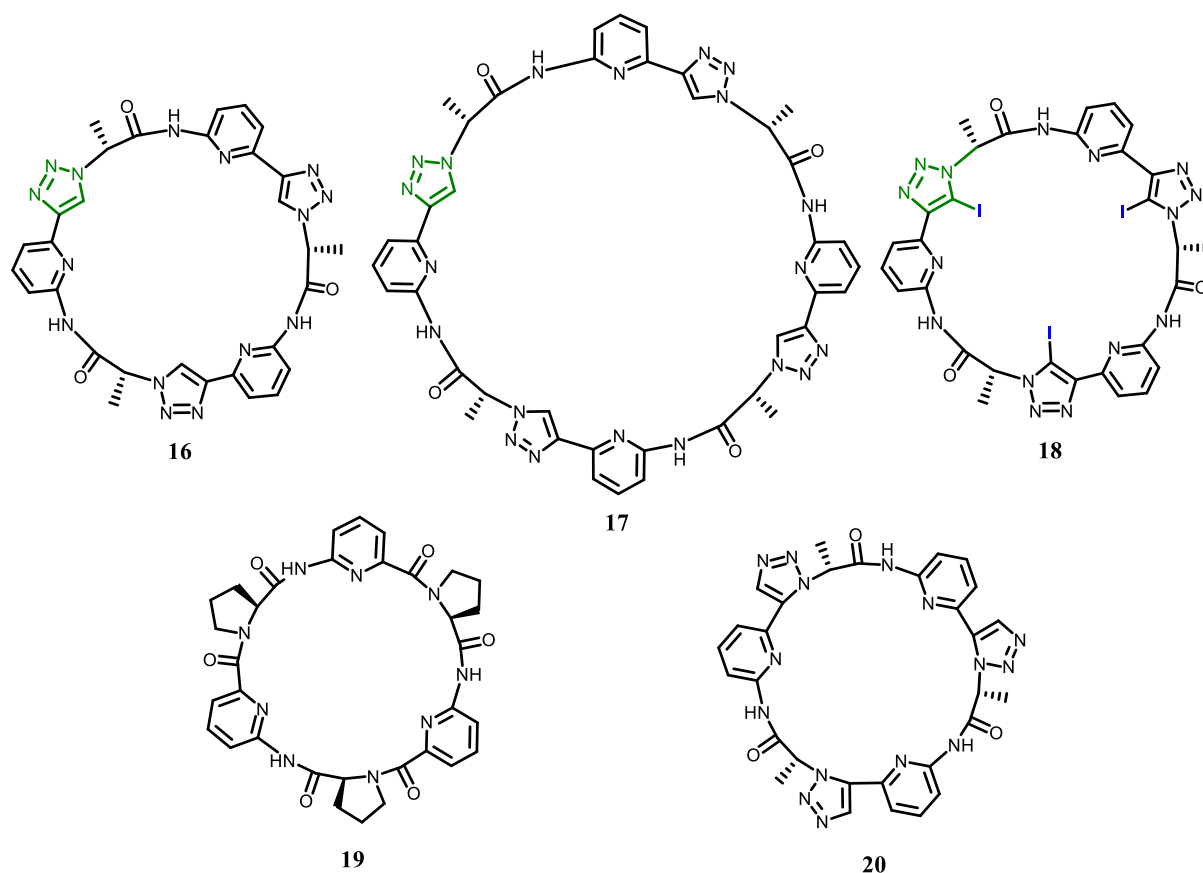


Chart 10

Cyclic pseudoheptapeptide **16** (Chart 10) is structurally based on an anion-binding cyclopeptide **19** and an anion-binding cyclic pseudopeptide **20** previously reported in the Kubik group.<sup>73, 74</sup> The main structural difference is the presence of the 1,4-disubstituted 1,2,3 triazole subunits that also induce a larger cavity diameter with respect to the previous receptors. Cyclic pseudopeptide **16** was expected to feature a converging arrangement of amide N-H groups and triazole C-H groups, which should thus both be able to contribute to anion binding. My work involved the synthesis of **16** and the assessment of the influence of the triazole units on anion affinity.

The results obtained for **16** indicated that the larger analog, cyclic pseudoheptapeptide **17** (Chart 10), could also possess interesting binding properties because of its higher flexibility with respect to **16**, its larger cavity, and higher number of triazole C-H and amide N-H groups. Pseudopeptide **17** was therefore included into the work.

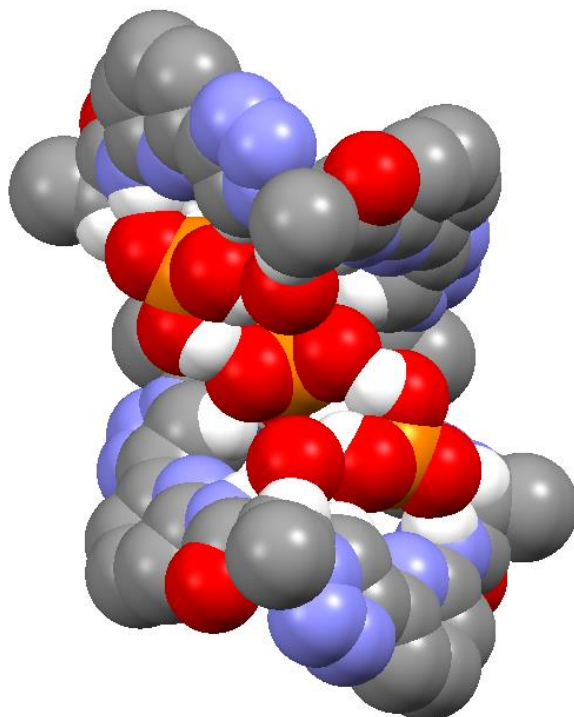
The third pseudopeptide developed during this thesis is the cyclic pseudoheptapeptide **18** (Chart 10) that is structurally related to **16** but contains iodine atoms in the 5-position of the triazole

subunits. This compound should therefore have a smaller cavity diameter than **16** and should be able to exhibit a converging arrangement of amide N-H and triazole C-I groups which should thus both be able to engage in interactions with anions. My work involved the synthesis of **18** and the assessment of the influence of the iodine atoms on anion affinity.

# Chapter 2

---

## Anion binding to a cyclic pseudopeptide containing 1,4-disubstituted 1,2,3-triazole moieties



[D. Mungalpara, H. Kelm, A. Valkonen, K. Rissanen, S. Keller, S. Kubik "Oxoanion binding to a cyclic pseudopeptide containing 1,4-disubstituted 1,2,3-triazole moieties" *Org. Biomol. Chem.* 2017, **15**, 102-113]. Copyright by the Royal Society of Chemistry (RSC). Reproduced with permission.

My work that led to this publication comprised the synthetic work including the characterization of the prepared compounds and their crystallization. In addition, I performed all binding studies by using ITC and NMR spectroscopy. Dr. Herald Kelm helped in solving the crystal structure of the free cyclic pseudopeptide. Prof. Dr. Kari Rissanen and Dr. Arto Valkonen solved the crystal structure of the receptor-DHP complex. Prof. Dr. Sandro Keller helped in the interpretation of the ITC results. Prof. Dr. Stefan Kubik acted as scientific supervisor.

**2 Chapter 2 - Anion binding to a cyclic pseudopeptide containing 1,4-disubstituted 1,2,3-triazole moieties**

## 2.1 Scope of the work

Cyclic hexapeptide **19** (Chart 11), comprising alternating 6-aminopicolinic acid and L-proline subunits has been shown to efficiently bind to inorganic anions even in competitive aqueous solvent mixture such as 80 vol% water/methanol.<sup>73</sup> The X-ray crystal structure analysis of the trihydrate of **19** shows that the peptide adopts a  $C_3$  symmetric conformation in the crystal. All the protons of the N-H groups are arranged in a convergent fashion. This can be explained by the presence of the pyridine units that destabilize arrangements of the neighboring carbonyl oxygen atoms pointing into the direction of the free electron pairs on the ring nitrogen atoms (Chart 11). Another characteristic structural feature of **19** is that the tertiary amides adopt the *cis* conformation causing the planes of the aromatic units to lie approximately parallel to the  $C_3$  axis of the macrocycle.

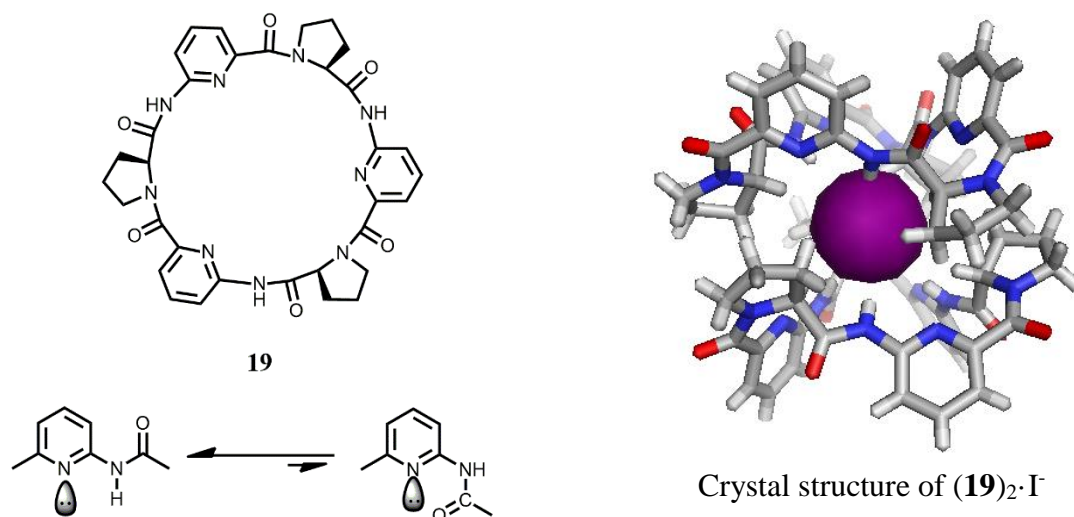


### Chart 11

In 80 vol% water/methanol, **19** has highest affinity for iodide and sulfate. Complexation of these anions involves sandwiching them between two cyclopeptide rings, producing  $(\mathbf{19})_2 \cdot (\text{anion})_1$  complexes (Chart 11). The stability of these complexes in aqueous media is attributed to the shielding of the bound anion from the surrounding solvent and hydrophobic interactions between the cyclopeptide rings. <sup>1</sup>H-NMR spectroscopy and isothermal titration calorimetry showed that the overall stability constants of the iodide and sulfate complexes of **19** amount to *ca.*  $10^5 \text{ M}^{-2}$  in 80 vol% water/methanol.<sup>73</sup> Interestingly, protonated oxoanions such as hydrogen phosphate or dihydrogen phosphate anions bind significantly less strongly to **19** because of repulsive interactions between the protons on these anions and the hydrogen bond donors inside the cavity between two cyclopeptide rings.

In subsequent work, the unusual binding properties of **19** were transferred to a structural analog, namely the cyclic pseudopeptide **20** (Chart 12) that features similar conformations.<sup>74</sup> In **20**, the pyridine units also induce converging arrangement of the N-H groups. The tertiary amide groups in **19** are replaced by 1,5-disubstituted 1,2,3-triazole rings that are known to act as surrogates for *cis*-peptide bonds.<sup>75</sup> Pseudopeptide **20** was shown to also interact with anions in highly competitive media although its propensity to form sandwich type complexes is lower than that of **19**.<sup>74</sup>

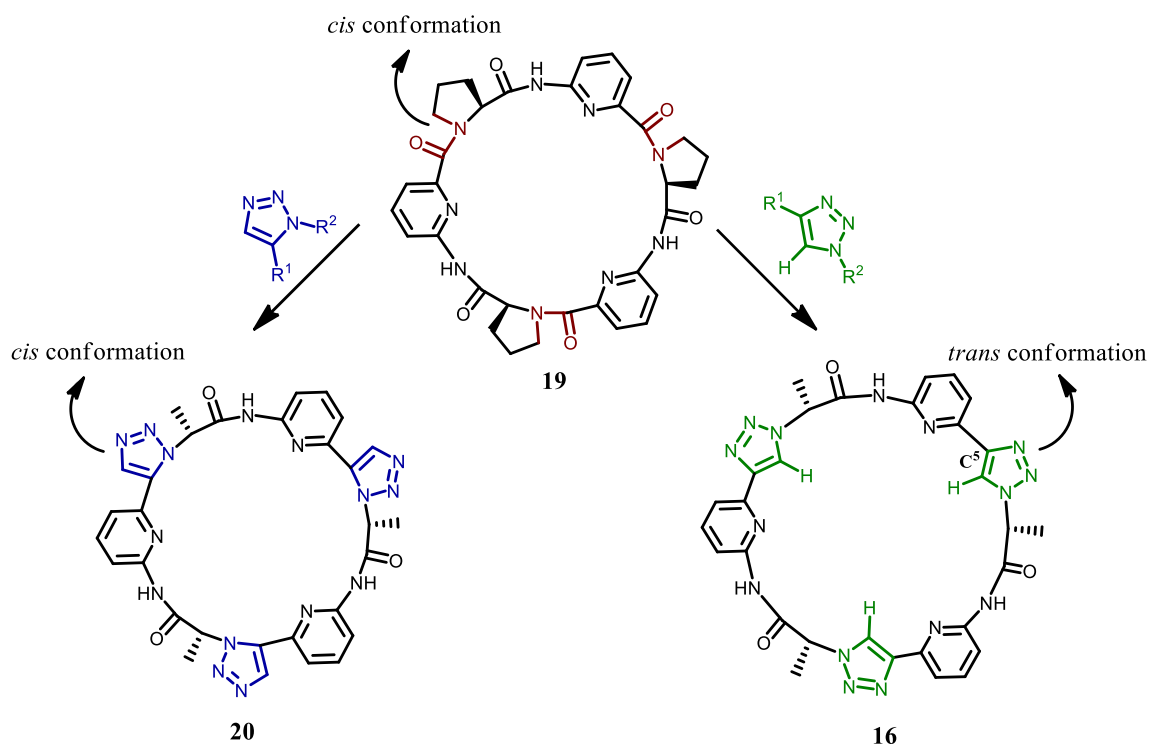


**Chart 12**

In this work, the family of anion-binding cyclopeptides and pseudopeptides should be extended to compound **16**, containing 1,4-disubstituted triazole rings (Chart 12). This pseudopeptide should again feature converging N-H groups due to the orienting effects of the pyridine nitrogen atoms. However, the conformation of **16** should significantly differ from the ones of **19** or **20** because of the structural relationship of 1,4-disubstituted triazoles to *trans*-amides.<sup>51</sup> The advantage of **16** in terms of anion affinity should be a higher number of hydrogen bond donors with respect to **19** and **20** because the triazole C<sup>5</sup>-H groups should be able to participate in anion binding. To demonstrate the effect of the triazole units in **16** on the conformation, the solid-state structures of compounds **19**, **20**, and the calculated structure of **16** are compared in Figure 10.

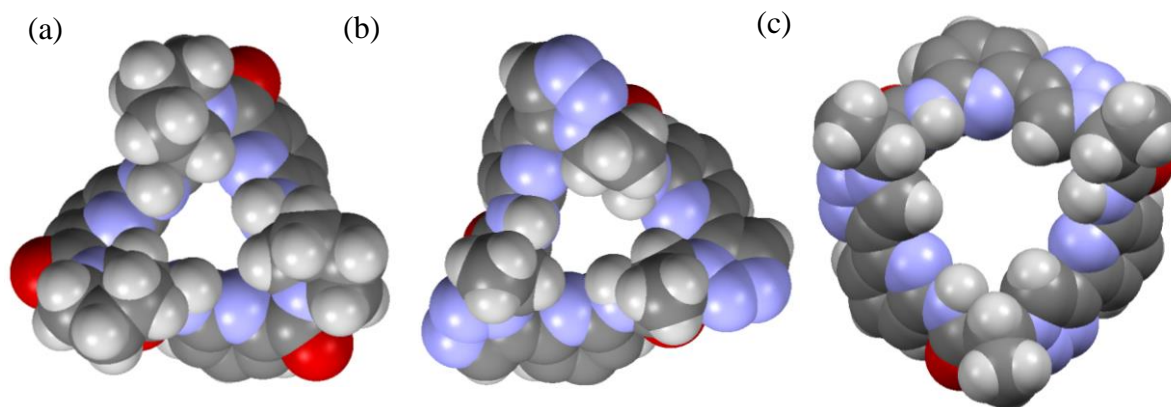


**Figure 10** Comparison of crystal structures of cyclopeptide **19** (a) and cyclic pseudohexapeptide **20** (b) with the calculated structure of cyclic pseudohexapeptide **16** (c). In the cases of **19** and **20**, solvent molecules are omitted for the clarity. The structure of **16** was calculated by using Spartan 04 for Macintosh (Wavefunction, Inc.) with the MMFF force field and without considering solvent molecules.

All three structures are approximately  $C_3$ -symmetric and share the converging arrangement of the N-H groups. The pseudopeptides **20** and **16** differ in the orientation of the triazole C-H groups. Whereas the triazole C-H groups point away from the anion binding site in **20** they are arranged close to the converging N-H groups in **16**, thus potentially allowing them to contribute to anion binding. In addition, the three macrocycles differ in the diameter of the ring, which is larger for **16** due to the 1,4-disubstituted triazole units than for **19** or **20**. Moreover, the aromatic rings in **16** are slightly more tilted than in **19** and **20**. In order to experimentally elucidate the effect of the 1,4-disubstituted 1,2,3-triazole units in **16** on anion binding, the objective of this thesis was to prepare this pseudopeptide, assign its conformation in solution and evaluate its binding properties.

## 2.2 Results

### 2.2.1 Synthesis

According to a retrosynthetic analysis, **16** can be assembled either from the monomer **21a** by using standard peptide synthesis, or from **21b** by using repeated Cu(I)-catalyzed click chemistry (Chart 13). Since carboxylic acids with a stereogenic center in  $\alpha$ -position that carries an additional triazole unit are extremely prone to racemization,<sup>76, 77</sup> the second approach was used to synthesize **16**.

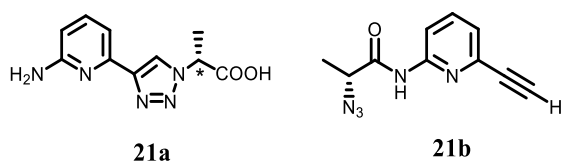


**Chart 13**

Firstly, the known linear monomer **21**<sup>77</sup> was converted into the azide **22** and the unprotected alkyne **23**, both of which were then coupled under the conditions of CuAAC to afford the linear dimer **24** (Figure 11). This dimer was further elongated to the linear trimer **25** by deprotecting the alkyne moiety in **24** and performing another azide-alkyne cycloaddition using **22** as the azide component.

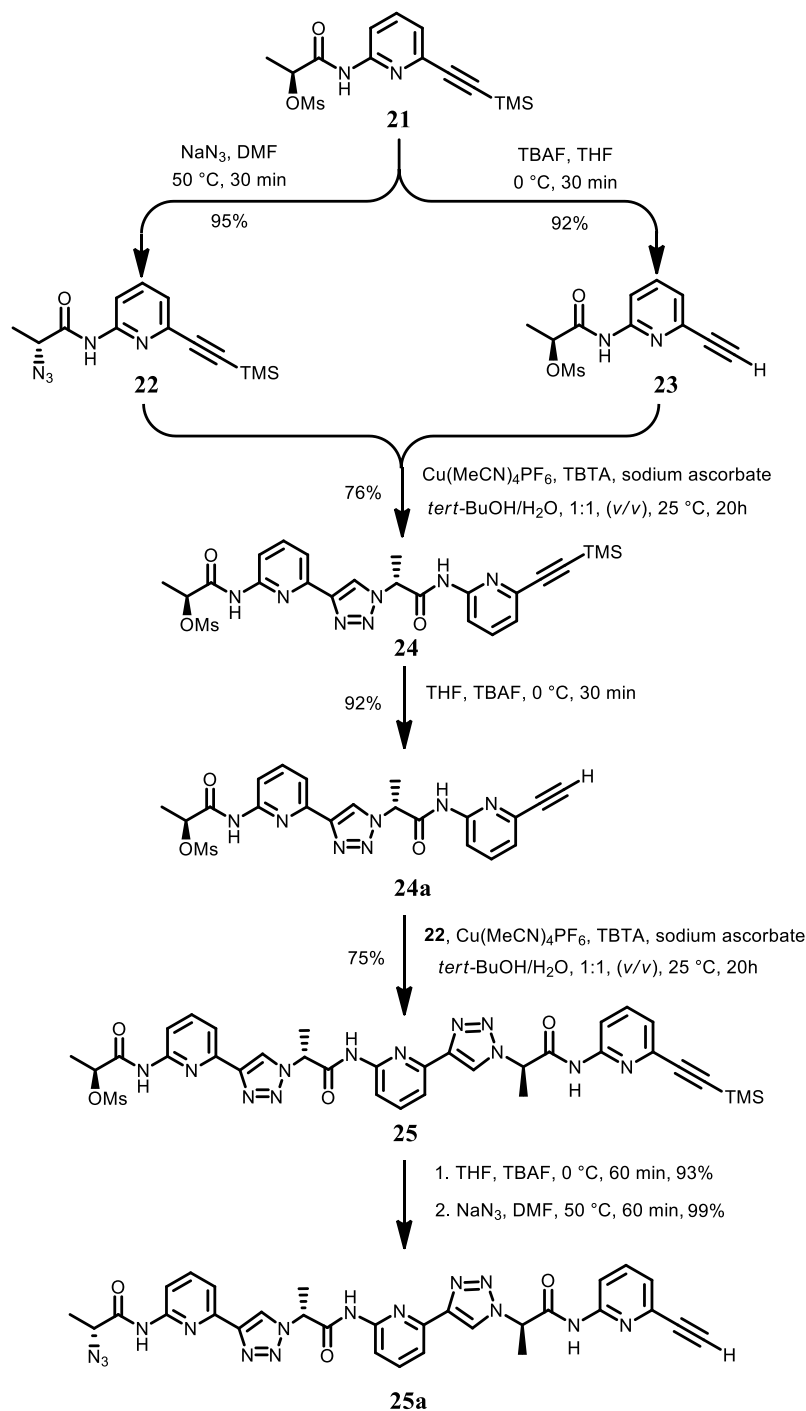


**Figure 11** Synthesis of the linear trimer **25a**.

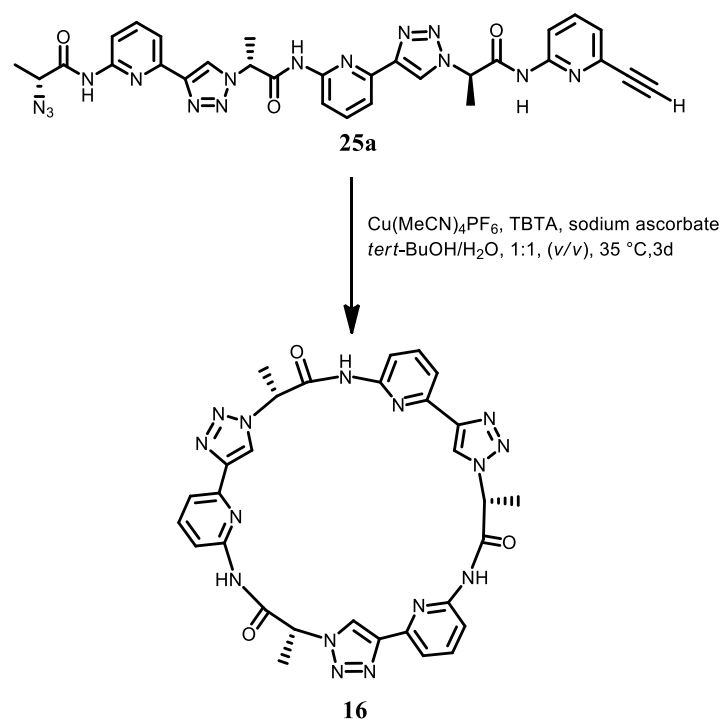


**Figure 12** Synthesis of the cyclic pseudopeptide **16**.

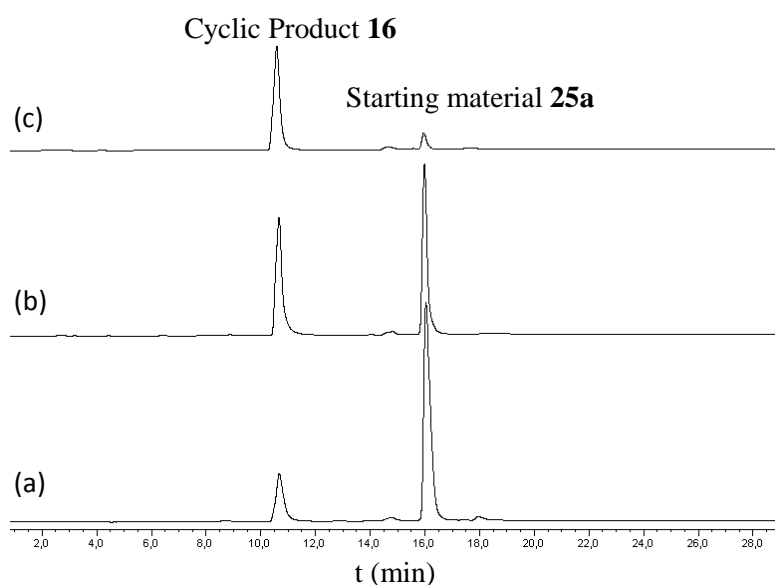
The linear timer **25** was made ready for cyclization by, first, cleaving the TMS group and then substituting the mesylate group with an azide group to afford **25a**. Initially, small-scale cyclizations were performed under different reaction conditions to find suitable conditions that afford **16**. The courses of these test reactions were followed by HPLC. The conditions employed are summarized in Table 1. All small-scale cyclization reactions were performed under dilute condition by dissolving **25a** in *tert*-butanol/water, 1:1 (v/v) at a concentration of 852  $\mu\text{M}$ . In reactions **CR1** and **CR2**, 50 mol% and 100 mol% of  $\text{Cu}(\text{MeCN})_4\text{PF}_6$ , TBTA, and sodium ascorbate were used, respectively. In reaction **CR3**, the reaction mixture was initially treated with 10 mol% of these reagents and additional 5 mol% of reagents ( $\text{Cu}(\text{MeCN})_4\text{PF}_6$  and TBTA) were added every 24 h till the complete disappearance of the peak associated with the starting material in the HPLC chromatogram.

**Table 1** Amount of reagents used for the cyclization of **25a** in *tert*-butanol/water, 1:1 (v/v) at 25 °C.

Entry	<b>25a</b> mg (μmol)	Solvent mixture (mL)	Cu(MeCN) <sub>4</sub> PF <sub>6</sub> (mol%)	TBTA (mol%)	Sodium ascorbate (mol%)
<b>CR1</b>	11.0 (17)	20	50	50	50
<b>CR2</b>	11.0 (17)	20	100	100	100
<b>CR3</b>	11.0 (17)	20	10+(2x5) <sup>a</sup>	10+(2x5) <sup>a</sup>	5
<b>CR4<sup>b</sup></b>	120.0 (186)	200	10+(5x5) <sup>a</sup>	10+(5x5) <sup>a</sup>	5

<sup>a</sup>5 mol% of Cu(MeCN)<sub>4</sub>PF<sub>6</sub>, TBTA, and sodium ascorbate were added to the reaction mixture **CR3** for 3 days after an initial reaction time of 24 h; <sup>b</sup>**CR4** reaction mixture was heated at 35 °C after 96 h.

The rates of cyclization in reactions **CR1** and **CR2** were very slow and large amounts of starting material were present even after 96 h. The conditions employed in **CR3** proved to be more beneficial for the cyclization. Figure 13 shows the chromatograms obtained after 24 h, 48 h, and 72 h under these conditions.

**Figure 13** HPLC chromatogram of the cyclization reaction **CR3** after 24 h (a), 48 h (b), and 72 h (c).

The peaks at 11 min and 16 min correspond to the product **16** and the starting material **25a**, respectively. The repeated addition of the reagents resulted in the gradual increase in the intensity of the product peak with the concomitant decrease of the educt peak. After 72 h, almost all of the starting material was consumed.

The cyclization was subsequently performed in four different solvents, namely, dichloromethane, 1,4-dioxane, 1,4-dioxane/water, 1:1 (v/v), and *tert*-butanol/water, 1:1 (v/v) using condition **CR3**. Among the tested solvents, the cyclization proceeded best in *tert*-butanol/water, 1:1 (v/v).

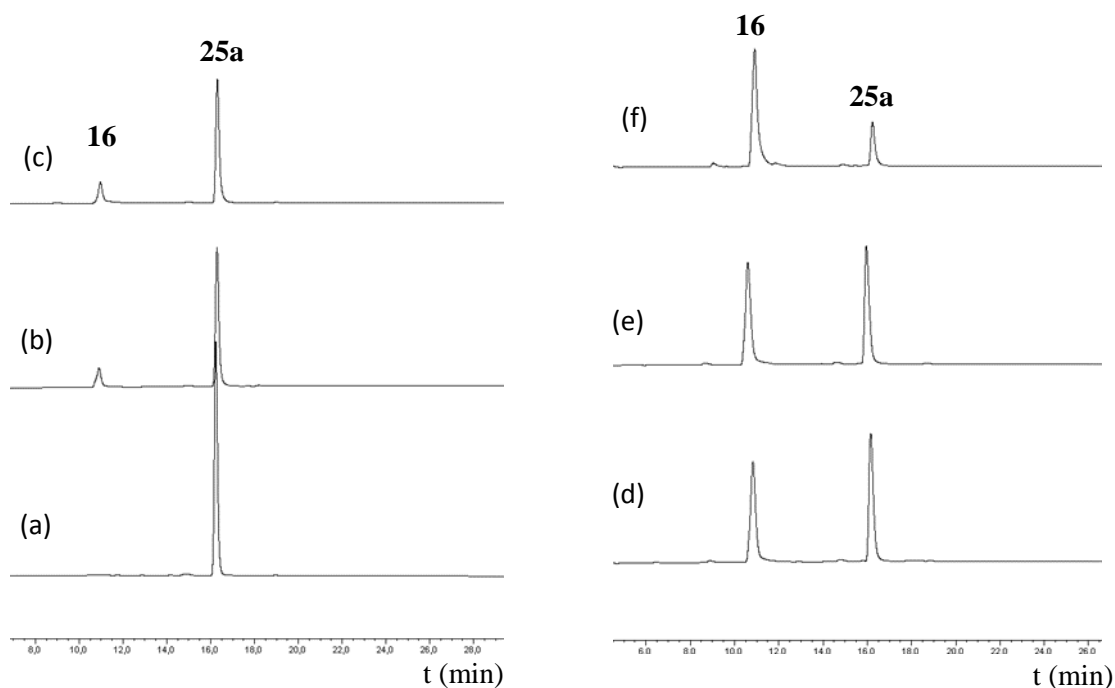


**Figure 14** HPLC chromatogram of cyclization reaction **CR4** after 24 h (a) 48 h (b) 96 h (c) 120 h (d) 144 h (e) and 168 h (f). After 96 h the reaction was heated to 35 °C.

A large-scale cyclization (**CR4**) was performed under the optimized conditions by using 120 mg of **25a**. According to the HPLC analysis, conversion was very slow and a large amount of starting material was present even after 96 h. Therefore, this reaction mixture was heated to 35 °C and addition of 5 mol% of the reagents ( $\text{Cu}(\text{MeCN})_4\text{PF}_6$  and TBTA) was continued. Under these conditions, almost all of the starting material was consumed after additional 72 h (Figure 14).

Thus, all the later cyclizations were performed using the optimized conditions at 35 °C. Purification of **16** was achieved by performing washing, extraction, and crystallization steps without requiring chromatography. The analytically pure product was isolated with a yield of *ca.* 30%. Further information about the synthesis of **16** and the purification is available in the respective publication (Chapter 2.5).<sup>78</sup>

### 2.2.2 Structural Assignment and Anion Binding Properties

X-ray crystallography showed that **16** adopts a conformation in the solid state with the N-H groups and the triazoles C-H groups converging towards the cavity center. NOESY NMR spectroscopy indicated that this conformation is also preferred in solution ( $\text{DMSO}-d_6$ ). Binding studies were performed in  $\text{D}_2\text{O}/\text{DMSO}-d_6$  or water/DMSO mixtures containing between 0.03 vol% and 5 vol% of water using  $^1\text{H}$ -NMR spectroscopy and microcalorimetry, respectively. The

results of these investigations are described in detail in the corresponding publication (Chapter 2.5).<sup>78</sup>

Anion binding investigations were also performed in 5 vol% DMSO-*d*<sub>6</sub>/acetone-*d*<sub>6</sub>. Initially, <sup>1</sup>H-NMR spectra were recorded of solutions containing **16** in concentration varying between 0.1 mM to 1.0 mM to see whether the pseudopeptide aggregates in this solvent within this concentration range. Figure 15 shows that the signals of **16** do not shift or exhibit broadening when increasing the concentration, suggesting that aggregation does not occur. Therefore, <sup>1</sup>H-NMR spectroscopic experiments were performed to evaluate qualitatively and quantitatively the anion binding properties of **16** in this solvent.

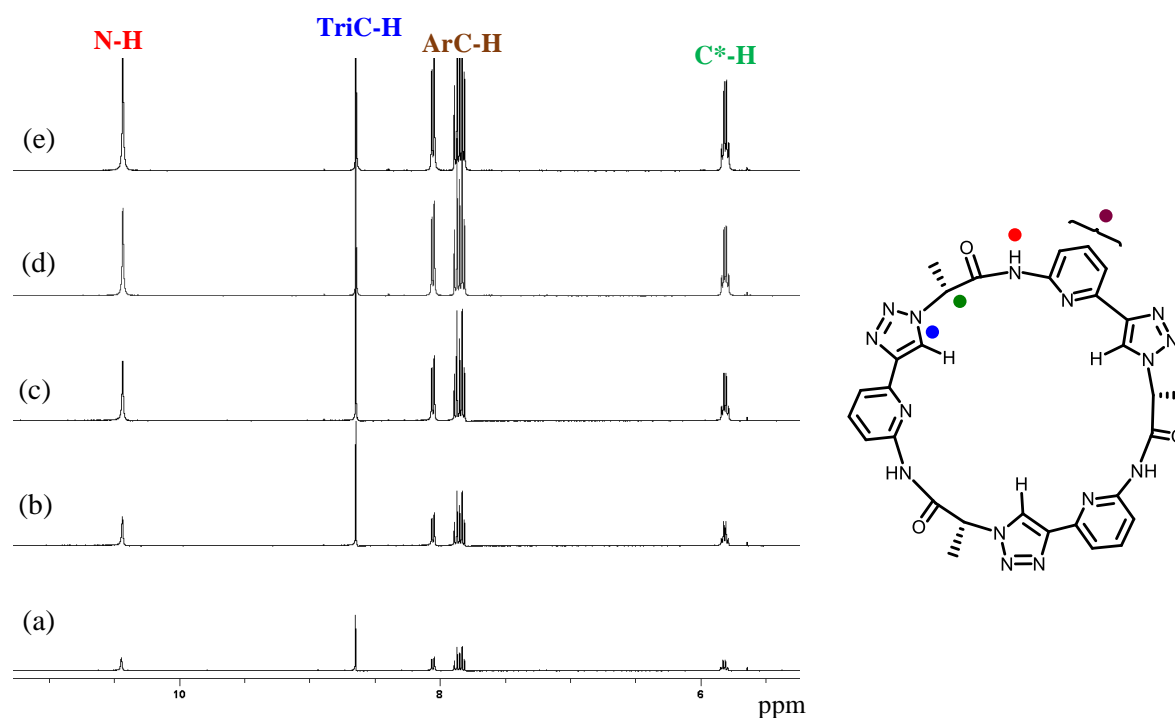


**Figure 15** <sup>1</sup>H-NMR spectra of solutions containing 0.1 mM (a), 0.25 mM (b), 0.50 mM (c), 0.75 mM (d), and 1.00 mM (e) of **16** in 5 vol% DMSO-*d*<sub>6</sub>/acetone-*d*<sub>6</sub>. The signals assigned are indicated in the structure on the right hand side by using the same color code.

To this end, the <sup>1</sup>H-NMR spectra of solutions of cyclic pseudopeptide **16** (1 mM) in 5 vol% DMSO-*d*<sub>6</sub>/acetone-*d*<sub>6</sub> that additionally contained 5 equiv of the tetrabutylammonium salts of various anions were recorded at 25 °C and compared with the spectrum of the free pseudopeptide in the same solvent. The corresponding NMR spectra are depicted in Figure 16. These spectra show that the anions mainly cause downfield shifts of three signals, namely, those of the N-H, TriC-H protons as well as the signals of the protons on the stereogenic centers of **16**, C\*-H. The signal belonging to the peripheral methyl groups (C\*-CH<sub>3</sub>) of **16** is also affected but to a significantly smaller extent. These qualitative binding experiments indicated that all the

investigated anions interact with **16** in 5 vol% DMSO- $d_6$ /acetone- $d_6$ . Assuming that binding strength is proportional to the extent of the induced signal shifts,  $\text{H}_2\text{PO}_4^-$  (DHP) is most strongly bound. In the case of the DHP and sulfate anions, the NH signal is not visible in the spectrum presumably because these anions promote H/D exchange. In addition, the signals of **16** broaden in the presence of sulfate anions.

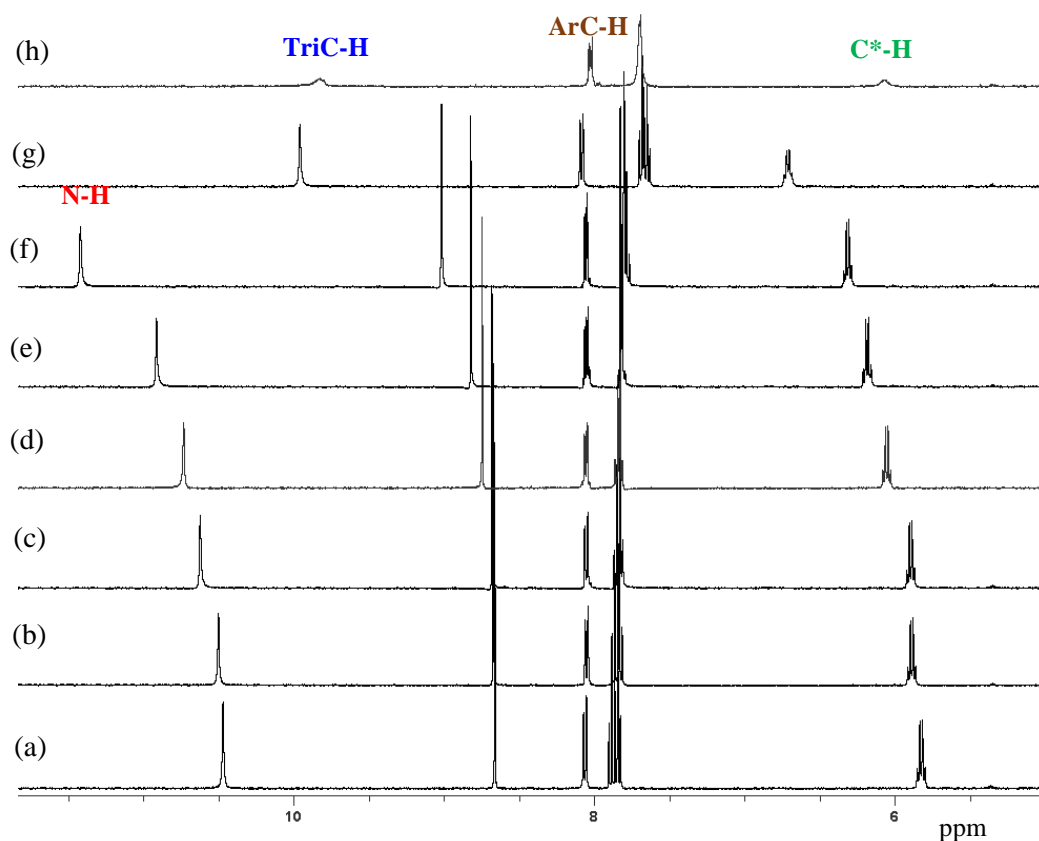


**Figure 16**  $^1\text{H}$ -NMR spectrum of **16** (1 mM) in 5 vol% DMSO- $d_6$ /acetone- $d_6$  in the absence (a) and the presence of 5 equiv. of TBA iodide (b), nitrate (c) hydrogen sulfate (d) bromide (e), chloride (f), dihydrogenphosphate (g), and sulfate (h).

Subsequently, Job's method of continuous variation was used to determine the stoichiometry of the chloride complex of **16**. The respective  $^1\text{H-NMR}$  spectra are depicted in Figure 17.

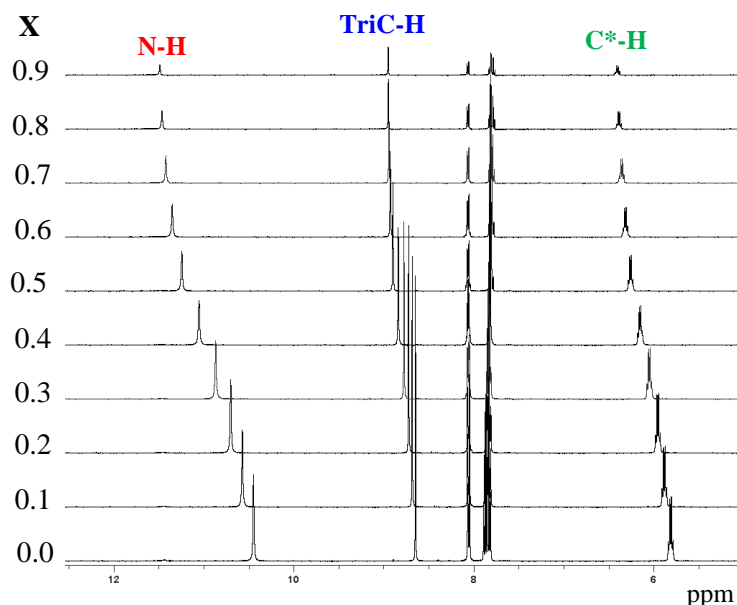


**Figure 17**  $^1\text{H-NMR}$  spectra of **16** and TBA chloride in 5 vol%  $\text{DMSO-}d_6/\text{acetone-}d_6$  at mol fractions  $X$  of the partner ranging between 0.0 and 0.9 mol% of TBA chloride and a total concentration of 1 mM.

The Job plots constructed by following the chemical shifts of the N-H, TriC-H, and C\*-H signals are displayed in Figure 18. These Job plots indicate that **16** preferentially forms a 1:1 complex with the chloride anion.

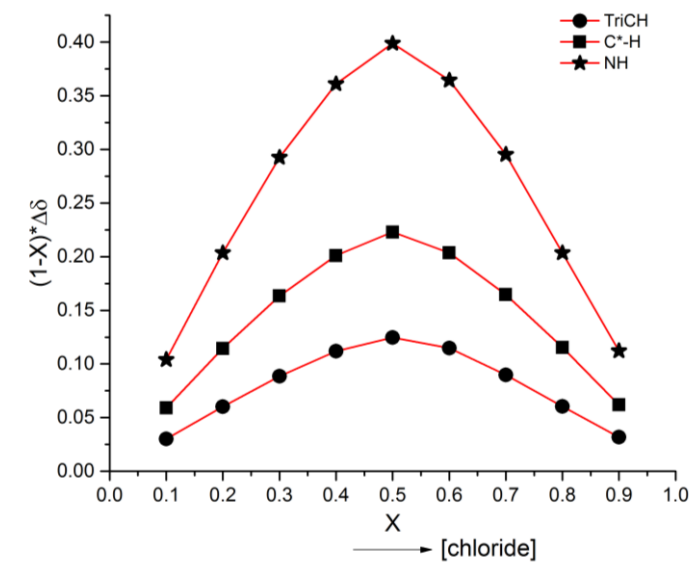


**Figure 18** Job plots for the chloride complex of **16** in 5 vol%  $\text{DMSO-}d_6/\text{acetone-}d_6$ . The three curves were constructed by following the courses of the N-H (stars), TriC-H (circles), and C\*-H (squares) signals in the NMR spectra depicted in Figure 17.

Subsequently, NMR titrations were performed by following the effects of the gradual addition of the TBA salts of chloride, bromide, hydrogen sulfate (HS) and DHP to a solution of **16** in 5 vol% DMSO- $d_6$ /acetone- $d_6$ . Under these conditions, the signals of the free receptor and its DHP complex are simultaneously visible in the spectra of a solutions containing less than one equivalent of the salt, showing that complex formation is slow on the NMR time-scale. Thus, the association constant of the DHP complex of **16** could not be determined. The broadening of the receptor signals in the presence of TBA sulfate also precluded quantification of the stability of the sulfate complex. Binding of the other anions is fast on the NMR time-scale, allowing binding isotherms to be constructed from the gradual shifts of the receptor signals observed when increasing the amount of the salt. As an example, the  $^1\text{H}$ -NMR spectra obtained in the titration with TBA chloride are depicted in Figure 19.

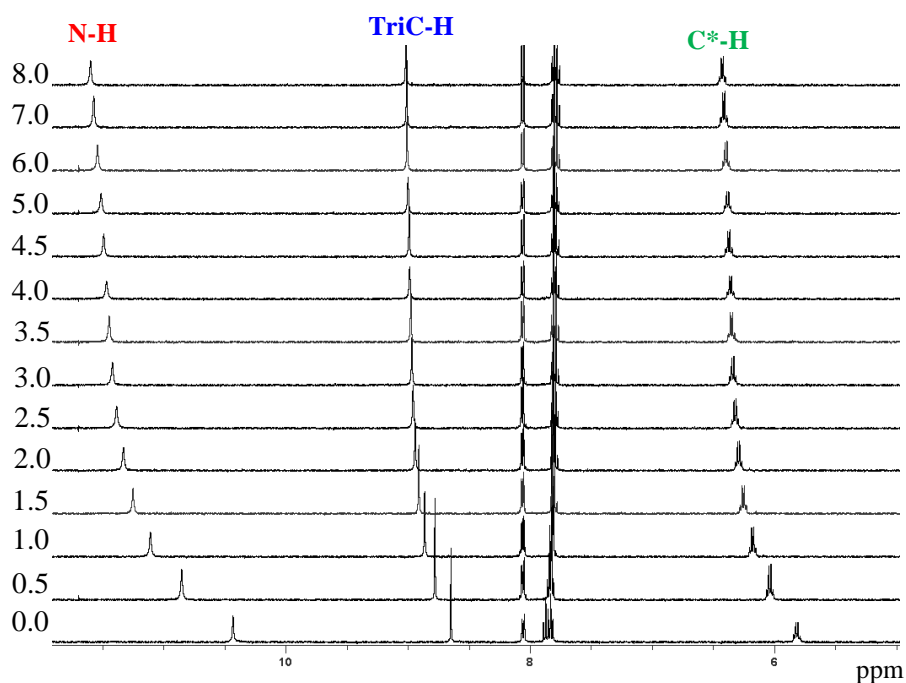


**Figure 19**  $^1\text{H}$ -NMR spectra of **16** (0.5 mM) in 5 vol% DMSO- $d_6$ /acetone- $d_6$  containing increasing equivalents of TBA chloride, specified to the left of each spectrum.

The isotherms obtained from the shifts of the N-H, TriC-H and C\*-H were globally fitted to different binding models by using HypNMR2008. The fitted isotherms are shown in graphs in Figure 20.

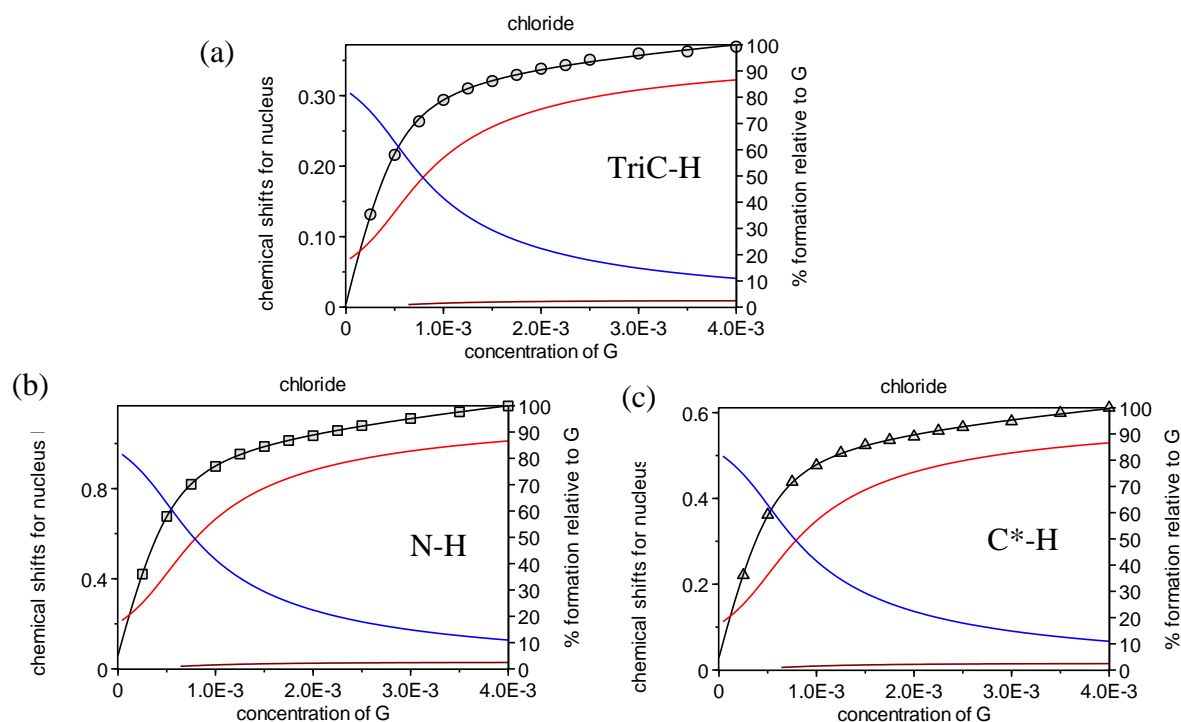


**Figure 20** Binding isotherms obtained in the NMR titration of **16** with TBA chloride by following the shifts of the TriC-H (a), N-H (b), and C\*-H (c) signals. Fitting of isotherms was performed by using HypNMR2008.

Fitting only gave satisfactory results if formation of higher complexes was considered in which two anions bind to the receptor. Only in the case of the nitrate complex were the results consistent with a 1:1 complex. Table 2 summarizes the obtained binding constants. In all cases, the first binding step is significantly stronger than the second one, with chloride anions forming the most stable 1:1 complex. Affinity decreases in the order of chloride > bromide > hydrogen sulfate > nitrate. The effect of the addition of TBA iodide to a solution of **16** in 5 vol% DMSO- $d_6$ /acetone- $d_6$  proved to be too weak to allow quantification of binding strength.

**Table 2** Stability constants of the chloride, bromide, hydrogen sulfate (HS), and nitrate complexes of **16** in 5 vol% DMSO-*d*<sub>6</sub>/acetone-*d*<sub>6</sub> determined by NMR titrations.

anion	log $K_{11}$ <sup>a</sup>	log $K_{12}$ <sup>b</sup>
chloride	4.0	1.5
bromide	3.4	2.4
HS	3.0	1.4
nitrate	2.4	-

<sup>a</sup>Equilibrium constant describing the formation of the 1:1 complex; <sup>b</sup>Equilibrium constant describing the formation of the **16**·(anion)<sub>2</sub> complex from the **16**·anion complex; errors are estimated to amount to *ca.* ±10%.

### 2.3 Discussion

X-ray crystallography and NOESY NMR spectroscopy confirm the  $C_3$  symmetric conformation of **16** as well as the expected convergent arrangement of three amide N-H and triazole C-H protons. Thus, the conformation observed in the solid state and solution is in good agreement with the conformation of the calculated one. The amide N-H and triazole C-H protons point towards the narrow opening of the receptor and create an electropositive binding site where an anion can coordinate to all six hydrogen donors.

In the less competitive solvent (5 vol% DMSO-*d*<sub>6</sub>/acetone-*d*<sub>6</sub>), pseudohexapeptide **16** interacts with a variety of anions as indicated by pronounced shifts of receptor signals upon addition of different TBA salts. The signals most affected are the ones of the N-H, triazole C-H, and the C\*-H protons, which all move downfield upon anion binding. As all of these protons are arranged at the narrow opening of the receptor one can assume that anion binding take place there. The extents of the signal shifts differ significantly among the different anions. In the case of halides, chloride induces the strongest shift and iodide the weakest. For the oxoanions, the anion effect is weakest for nitrate and strongest for sulfate and dihydrogenphosphate (DHP). Quantitative binding studies showed that complexation of DHP is slow on NMR time-scale and sulfate causes broadening of receptor signals. While this precluded quantification of binding strengths it shows qualitatively that very stable complexes are formed, consistent with the qualitative binding study. All other anions form complexes whose complexation/decomplexation rates are fast on the NMR time-scale. Among the anions investigated chloride forms the most stable 1:1 complex, which is consistent with the fact that chloride is a strongly coordinating anion. However, formation of higher complexes is observed, indicating that once the first anion is bound, binding sites remain empty on the receptor that allow complexation of a second anion.

Such  $\mathbf{16} \cdot (\text{anion})_2$  complexes are unusual as binding of the second anion has to overcome charge repulsion suggesting efficient stabilization. Similar types of complexes have been recently reported for the cyclic peptide unguisin A that can coordinate to two anions (chloride, bromide and bicarbonate).<sup>79</sup> The fact that the binding constants of the second binding steps are smaller than the ones of the first steps shows that the second anion is less efficiently stabilized than the first, also explaining why the second binding step is not visible in the job plot of chloride complex (Table 2). That two anions can be bound by **16** is probably a consequence of the size of the cavity.

In the competitive solvent (2.5 vol%  $\text{D}_2\text{O}/\text{DMSO-}d_6$ ), only binding of the more strongly coordinating oxoanions sulfate, DHP, and HPP is retained. These anions form complexes differing in stoichiometry. Sulfate and HPP complexation involves a stepwise process comprising formation of a  $\mathbf{16} \cdot \text{anion}$  complex followed by a  $(\mathbf{16})_2 \cdot (\text{anion})$  complex. Formation of the higher complexes indicates that **16** cannot saturate all acceptor sites of the anion so that the anions can recruit a second receptor molecule. In contrast, **16** binds to two DHP anions in solution. This stoichiometry is different from the one detected in the solid state where a trimer of DHP is stabilized by two pseudopeptide rings. While close spatial arrangement of two or more anions in the solid-state may look unusual, the tendency of DHP anions to form such aggregates is well known.<sup>80</sup> Charge repulsion upon DHP association can obviously be overcompensated by sufficiently strong hydrogen bonding interactions between two DHP anions.<sup>80, 81</sup> While isolated DHP aggregates are only weakly stable in a polar medium such as DMSO, suitable receptors such as pseudopeptide **16** can cause their efficient stabilization. The formation of a  $\mathbf{16}_2 \cdot (\text{DHP})_3$  complex as found in the solid state seems to be entropically unfavourable in solution so that only a  $\mathbf{16} \cdot (\text{DHP})_2$  complex was observed under these conditions.

## 2.4 Summary

The cyclic pseudohexapeptide **16** was successfully synthesized. X-ray crystallography showed that it adopts a conformation in the solid state with the N-H groups and the triazole C-H groups converging towards the cavity center. NOESY NMR spectroscopy indicated that this conformation is also preferred in solution ( $\text{DMSO-}d_6$ ).

Pseudopeptide **16** is only soluble in organic solvents such as 5 vol%  $\text{DMSO-}d_6/\text{acetone-}d_6$  and DMSO containing up to 5 vol% of water. In 5 vol%  $\text{DMSO-}d_6/\text{acetone-}d_6$ , **16** binds to chloride, bromide, nitrate, hydrogen sulfate, sulfate, and dihydrogen phosphate anions. Quantitative binding studies demonstrated that chloride, bromide, and hydrogen sulfate are bound in the forms of  $(\mathbf{16}) \cdot (\text{anion})_2$  complexes in this solvent mixture. The exact structure of these complexes

could not be determined. The binding of sulfate and DHP in 5 vol% DMSO-*d*<sub>6</sub>/acetone-*d*<sub>6</sub> is slow on the NMR time-scale.

In 2.5 vol% D<sub>2</sub>O/DMSO-*d*<sub>6</sub>, **16** only binds to strongly coordinating oxoanions. The respective complexes differ in their stoichiometries. In the case of DHP, two anions are bound by **16** in solution whereas sulfate and HPP complexation involves a stepwise process, comprising formation of a 1:1 complex followed by binding of second pseudopeptide ring. The stability constant associated with the second binding step is smaller in comparison to the first one in the case of sulfate complexation, while the two binding constants are of similar magnitude in the case of HPP binding.

## 2.5 Publication

## Organic &amp; Biomolecular Chemistry



PAPER

View Article Online  
View Journal | View IssueCite this: *Org. Biomol. Chem.*, 2017, **15**, 102

## Oxoanion binding to a cyclic pseudopeptide containing 1,4-disubstituted 1,2,3-triazole moieties†

Disha Mungalpara,<sup>a</sup> Harald Kelm,<sup>b</sup> Arto Valkonen,<sup>c</sup> Kari Rissanen,<sup>c</sup> Sandro Keller<sup>d</sup> and Stefan Kubik\*<sup>a</sup>

A macrocyclic pseudopeptide **3** is described featuring three amide groups and three 1,4-disubstituted 1,2,3-triazole units along the ring. This pseudopeptide was designed such that the amide NH groups and the triazole CH groups converge toward the cavity, thus creating an environment well suited for anion recognition. Conformational studies in solution combined with X-ray crystallography confirmed this pre-organisation. Solubility of **3** restricted binding studies to organic media such as 5 vol% DMSO/acetone or DMSO/water mixtures with a water content up to 5 vol%. These binding studies demonstrated that **3** binds to a variety of inorganic anions in DMSO/acetone including chloride, nitrate, sulfate, and dihydrogenphosphate anions. In the more competitive DMSO/water mixtures, only affinity to the more strongly coordinating oxoanions is retained. Quantitative binding studies showed that dihydrogen phosphate complexation in DMSO/water involves the dimer of the  $\text{H}_2\text{PO}_4^-$  anion. By contrast, sulfate and hydrogenpyrophosphate complexation involves a stepwise process comprising formation of a 1 : 1 complex followed by a  $2_{\text{R}} : 1_{\text{A}}$  complex in which two molecules of **3** (R) bind to a single anion (A). While the second binding equilibrium is associated with a much smaller stability constant in comparison with the first one in the case of sulfate complexation, the two binding constants are of similar magnitude in the case of the hydrogenpyrophosphate anion. Formation of the  $2_{\text{R}} : 1_{\text{A}}$  complex was attributed to the fact that the cavity size and rigidity of **3** prevents saturation of all hydrogen acceptor sites on the anionic guests.

Received 5th October 2016,  
Accepted 27th October 2016  
DOI: 10.1039/c6ob02172g

www.rsc.org/obc

## Introduction

There is hardly a field in organic chemistry today in which 1,2,3-triazole-based building blocks have not made an impact. Formation of 1,2,3-triazoles from azides and alkynes *via* 1,4-dipolar Huisgen cycloaddition<sup>1</sup> has, for example, become a potent ligation strategy with applications in organic synthesis,<sup>2</sup> chemical biology,<sup>3</sup> supramolecular chemistry,<sup>4</sup> and more. The major factor that triggered this development was the discovery

of the copper(i)-catalysed variant of the azide-alkyne cycloaddition by Meldal and Sharpless with which drawbacks of the thermal reaction such as low rate and low regioselectivity could be overcome.<sup>5</sup> Today, this cycloaddition is considered the prototype of a click-reaction,<sup>6</sup> whose importance is progressively increasing also because synthetic approaches to access triazoles are continuously being developed. Examples are the ruthenium(ii)-catalysed version that affords 1,5-disubstituted rather than 1,4-disubstituted 1,2,3-triazoles,<sup>7</sup> metal-free strain-promoted cycloadditions,<sup>8</sup> and more recently organocatalysed triazole syntheses.<sup>9</sup>

In the area of chemical biology, the azide-alkyne cycloaddition benefits from the bioorthogonality of azide and alkyne groups, which allows using this reaction even *in vivo*.<sup>3,8</sup> In addition, 1,2,3-triazoles are mimics of peptide bonds, not only in terms of geometry but also in their electronic properties, so that 1,4-disubstituted and 1,5-disubstituted 1,2,3-triazoles can serve as surrogates for, respectively, *trans*-peptide and *cis*-peptide bonds in peptide mimics.<sup>10</sup>

In supramolecular chemistry, the use of 1,2,3-triazoles often extends beyond simply linking two building blocks because triazoles also feature characteristic recognition elements, namely, the nitrogen atoms for coordination to transition metal ions and a hydrogen bond donor in the form of

<sup>a</sup>Technische Universität Kaiserslautern, Fachbereich Chemie – Organische Chemie, Erwin-Schrödinger-Straße, 67663 Kaiserslautern, Germany.  
E-mail: kubik@chemie.uni-kl.de

<sup>b</sup>Technische Universität Kaiserslautern, Fachbereich Chemie – Anorganische Chemie, Erwin-Schrödinger-Straße, 67663 Kaiserslautern, Germany

<sup>c</sup>University of Jyväskylä, Department of Chemistry, Nanoscience Center, P.O. Box 35, Jyväskylä FI-40014, Finland

<sup>d</sup>University of Kaiserslautern, Molecular Biophysics, Erwin-Schrödinger-Str. 13, 67663 Kaiserslautern, Germany

† Electronic supplementary information (ESI) available: <sup>1</sup>H NMR, <sup>13</sup>C NMR, and mass spectra of compounds **5**, **7**, **8**, **3**; NOESY NMR spectrum of **3**; <sup>1</sup>H NMR spectra of qualitative binding studies; Job plots and results of NMR titrations and of selected ITC titrations; details of crystal structures. CCDC 1504361 and 1505706. For ESI and crystallographic data in CIF or other electronic format see DOI: 10.1039/c6ob02172g

the CH group.<sup>4</sup> The hydrogen bonding ability of 1,2,3-triazoles combined with the ease of their synthesis renders them particularly potent and versatile building blocks for the construction of anion receptors.<sup>11</sup> Significant contributions in this area came from the groups of Flood,<sup>12</sup> Craig,<sup>13</sup> Hecht,<sup>14</sup> Beer,<sup>15</sup> and Schubert.<sup>16</sup> Notably, anion-binding properties of receptors with triazole subunits can be further modulated by converting triazole into triazolium derivatives or by replacing the proton on the CH group with a halogen and making use of halogen-bonding for anion coordination.<sup>17</sup> In addition, triazole residues and other anion binding elements, such as carboxamide groups, have also been combined to develop anion receptors.<sup>18</sup>

In earlier work, we used the 1,2,3-triazole units in cyclic pseudopeptide **1** mainly for structural purposes, namely, to induce conformations similar to those found for cyclopeptide **2** (Fig. 1a).<sup>19</sup> This cyclopeptide was shown to possess high affinity for sulfate and iodide anions even in competitive aqueous solvent mixtures.<sup>20</sup> Anion affinity turned out to be partly due to the rigid and well preorganised structure of **2** featuring *cis*-amides at the tertiary amide bonds and a converging arrangement of the NH and proline C<sup>α</sup>H protons, which serve as hydrogen bond donors. The orientation of the NH groups can be explained by the presence of the pyridine nitrogen atoms that destabilise arrangements with ring nitrogen and carbonyl oxygen atoms located in close proximity (Fig. 1b).

Based on these results, pseudopeptide **1** was devised by retaining the pyridine units of **2** and replacing the *cis*-amides with 1,5-disubstituted 1,2,3-triazole units.<sup>19</sup> Because of the structural relationship of *cis*-amides and 1,5-disubstituted 1,2,3-triazole rings, **1** and **2** were expected to adopt similar overall conformations, which turned out to be the case. As a consequence, **1** also interacts with sulfate and halide anions in competitive aqueous media, although characteristic differences in the binding properties of the two receptors were noted.<sup>19</sup>

To access new macrocyclic motifs for anion recognition, the approach of incorporating 1,2,3-triazole units along the backbone of such pseudopeptides has now been extended to compound **3** containing 1,4-disubstituted triazole rings. This pseudopeptide should again feature conformations with converging NH groups due to the orienting effects of the pyridine nitrogen

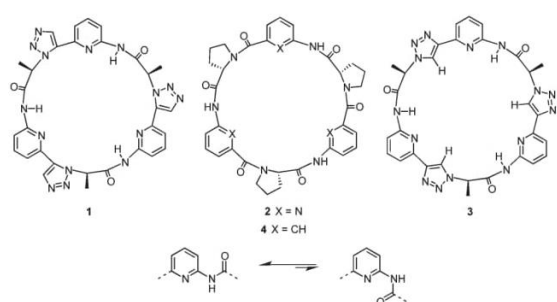


Fig. 1 Structures of macrocyclic receptors **1**–**4** (top) and effect of the ring nitrogen atom on the orientation of the adjacent amide group (bottom).

atoms. These conformations should, however, substantially differ from the ones of **1** or **2** because of the structural relationship of 1,4-disubstituted triazoles to *trans*-amides. Thus, **3** conformationally likely resembles cyclopeptides such as **4**, which also interact with anions, albeit in organic media.<sup>21</sup> The advantages of **3** should be a better preorganisation for anion binding in comparison with **4** and a higher number of hydrogen bond donors with respect to receptors **1**, **2**, and **4** because the triazole CH groups in **3** could participate in the interactions with the substrate.

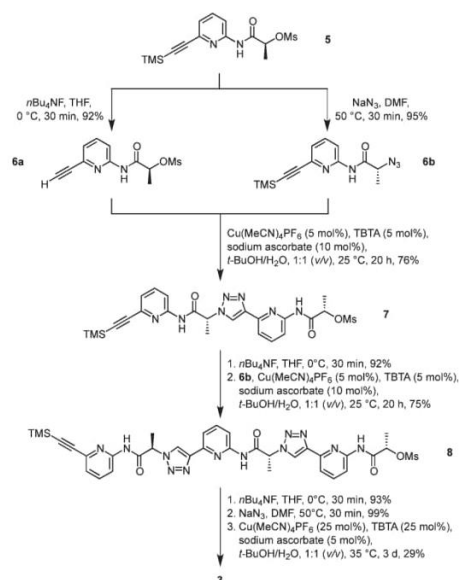
Here, we show how the 1,4-disubstituted triazole units affect the conformation of **3** and how the combination of NH and triazole CH hydrogen donor groups along the ring affects the anion binding properties of this pseudopeptide.

## Results and discussion

### Synthesis

Pseudopeptide **3** was prepared along a similar route as the analogue **1**.<sup>19</sup> The known monomer **5**, featuring a trimethylsilyl-protected alkyne group on one end and a mesylate group on the other, acted as the central building block (Scheme 1). Chain elongation involved initial conversion of **5** into the derivatives **6a** and **6b** by cleaving the TMS group with tetrabutylammonium fluoride (TBAF) and replacing the mesylate with an azide group under inversion of the configuration at the stereogenic centre, respectively. Compounds **6a** and **6b** now contained the necessary functional groups to couple them by using a copper(i)-catalysed azide–alkyne cycloaddition.

The resulting dimer **7** was chain-elongated along a similar route to the trimer **8**, which was subsequently deprotected on



Scheme 1 Synthesis of cyclic pseudopeptide **3**.

the alkyne group and then transformed into the azide. Finally, cyclisation in the presence of copper(I) afforded the desired product **3**. Isolation of **3** involved a couple of washing, extraction, and crystallisation steps but did not require chromatography. The isolated yield of product typically amounted to *ca.* 30%, which is acceptable for such types of macrocyclisation reactions. The alternative approach of using standard peptide chemistry for the synthesis of **3** is not feasible because the required building blocks would contain a stereogenic centre flanked by a carboxylate and a triazole ring, which is typically rather prone to racemisation once the carboxylate group is activated.<sup>22</sup>

### Structural analysis

X-ray crystallography of crystals grown from DMSO confirmed the expected constitution of **3**. The solid-state structure shows that this pseudopeptide crystallises with 5 molecules of DMSO, one of which resides inside the bowl-shaped cavity defined by the aromatic subunits (Fig. 2).

Three DMSO molecules are located on the opposite side of the cavity, interacting with the pseudopeptide *via* hydrogen bonds between the DMSO oxygen atoms and the pseudopeptide NH groups. The fifth DMSO molecule is disordered with a 0.65:0.35 occupancy ratio. The orientation with the lower abundance shares the space with an additional water molecule. As expected, all three NH protons of **3** point into the direction of the narrow cavity opening as a consequence of the conformational control exerted by the pyridine nitrogen atoms. Importantly, the three 1,2,3-triazole protons point into the same direction as the NH groups, indicating that all six hydrogen donors of **3** could participate in anion binding.

To illustrate the effect of the triazole units in **3** on pseudopeptide conformation, the solid-state structures of compounds **1** and **3** are compared in Fig. 3. Both structures are approximately  $C_3$ -symmetric and share the converging arrangement of the NH group. They differ in the orientations of the triazole

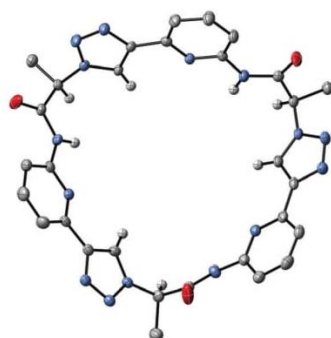


Fig. 2 Molecular structure of **3**·5DMSO·0.35H<sub>2</sub>O in the solid state with the thermal ellipsoids shown at the 50% probability level. Solvent molecules and hydrogen atoms except those on the NH and triazole CH groups as well as those on the stereogenic centres C\*H are omitted for clarity.

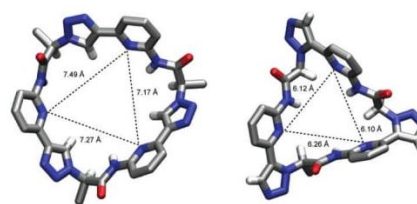


Fig. 3 Comparison of the solid-state molecular structures of **3**·5DMSO·0.35H<sub>2</sub>O (left) and **1**·C<sub>3</sub>H<sub>6</sub>O·H<sub>2</sub>O (right). Solvent molecules and hydrogen atoms except those on the NH and triazole CH groups as well as those on the stereogenic centres C\*H are omitted for clarity.

CH groups and in the diameters of the rings, with the one of **3** being larger due to the 1,4-connections on the triazole units. Taking the distance of the ring nitrogen atoms in **1** and **3** as a measure for ring size shows that this distance increases from an averaged 6.16 Å to an averaged 7.31 Å when going from **1** to **3**. As the aromatic rings in **3** are also slightly more tilted than in **1**, pseudopeptide **3** has a shallower cavity somewhat reminiscent of that found in the *N*-methylquinuclidinium iodide complex of **4**.<sup>21</sup> Overall, the solid-state structure provides evidence that **3** should likely be able to interact with anions, but differences with respect to the anion properties of **1** are to be expected.

Characterisation of the solution structure was strongly affected by the poor solubility of **3**, which was significantly lower than that of **1**. While **1** is soluble in a wide range of solvent mixtures ranging from water/methanol mixtures over acetone and DMSO to chloroform, **3** is not soluble in aqueous methanol mixtures. Concentrations sufficiently high for NMR analyses could be obtained only in DMSO or in organic solvents containing at least 5 vol% of DMSO.

Comparison of the <sup>1</sup>H NMR spectra of **3** in 5 vol% DMSO-*d*<sub>6</sub>/CDCl<sub>3</sub>, 5 vol% DMSO-*d*<sub>6</sub>/acetone-*d*<sub>6</sub>, DMSO-*d*<sub>6</sub>, and 2.5 vol% DMSO-*d*<sub>6</sub>/D<sub>2</sub>O showed that the pseudopeptide adopts an averaged  $C_3$ -symmetric conformation in all of these solvents (Fig. 4a). The signals are sharp, with the exception of those in the spectrum recorded in the chloroform mixture, in which some signal broadening was observed. Increasing the DMSO content of the mixtures caused a pronounced downfield shift of the NH signal, demonstrating the tendency of DMSO molecules to interact with the NH groups of **3**, as also observed in the crystal structure. Also the signal of the triazole CH shifts, but the ones of other protons are not affected to a large extent.

The NOESY NMR of **3** in DMSO-*d*<sub>6</sub> exhibits crosspeaks between the signal of the protons on the stereogenic centres of **3** and those belonging to the NH and the triazole CH groups (Fig. 4b). These crosspeaks account for a spatial proximity of the corresponding protons. As no crosspeak between the signal of the NH protons and that of the H<sup>3</sup> protons on the aromatic residues was observed, the pseudopeptide seems to adopt an average conformation in solution similar to that found in the solid state.

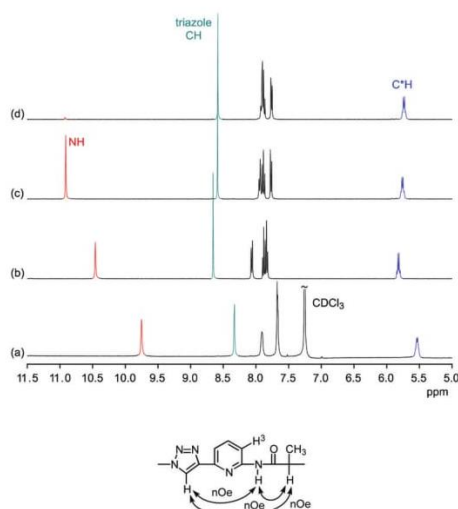


**Fig. 4** Comparison of the  $^1\text{H}$  NMR spectra of **3** in 5 vol% DMSO- $d_6$ /CDCl $_3$  (a), 5 vol% DMSO- $d_6$ /acetone- $d_6$  (b), DMSO- $d_6$  (c), and 2.5 vol% D $_2$ O/DMSO- $d_6$  (d) (top) and schematic representation of the crosspeaks found in the NOESY NMR spectrum of **3** in DMSO- $d_6$  (bottom).

### Qualitative binding studies

Information about the ability of **3** to interact with anions was obtained by evaluating the effects of various anions on the  $^1\text{H}$  NMR spectrum of **3**. Initially, we used 5 vol% DMSO- $d_6$ /acetone- $d_6$  as solvent and recorded  $^1\text{H}$  NMR spectra of 1 mM solutions of **3** after addition of 5 equiv. of different tetrabutylammonium (TBA) salts (Fig. 5). These investigations showed that the anions mainly cause downfield shifts of three signals, namely, those of the NH, triazole CH, and the C\*H on the stereogenic centre. The signal belonging to the peripheral methyl groups of **3** is also affected, but to a significantly smaller extent (not shown).

The extents of the signal shifts differ significantly among the different anions. In the halide series, chloride causes the strongest effect and iodide the weakest. For the oxoanions, the anion effect is weakest for nitrate and strongest for sulfate and dihydrogenphosphate (DHP). In the case of the latter two anions, the NH signal is not visible in the spectrum presumably because these anions promote exchange. In addition, the signals of **3** broaden in the presence of sulfate anions.

In the more competitive solvent mixture 2.5 vol% D $_2$ O/DMSO- $d_6$ , no interactions of halides or nitrate with **3** could be detected, and the only investigated anions that cause changes in the  $^1\text{H}$  NMR spectrum of **3** are DHP and sulfate anions (see ESI $^\dagger$ ). Again, mainly the triazole CH and C\*H signals shift (the NH signal is not visible in this solvent mixture because of H/D exchange), indicating that the mode of anion binding is not affected by the change of the solvent.

These results indicate that anion binding most likely occurs at the smaller cavity opening of **3**, where the NH, triazole CH, and C\*H protons converge. Thus, the expected direct participation of the triazole moieties of **3** in anion

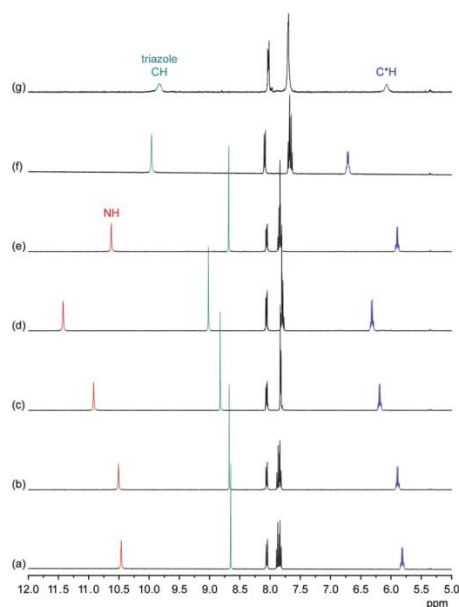


**Fig. 5**  $^1\text{H}$  NMR spectrum of **3** (1 mM) in 5 vol% DMSO- $d_6$ /acetone- $d_6$  in the absence (a) and the presence of 5 equiv. of TBA iodide (b), bromide (c), chloride (d), nitrate (e), dihydrogenphosphate (f), and sulfate (g). The signals of the NH, triazole and C\*H protons are marked in red, green, and blue, respectively.

binding is indeed evident. Assuming that the extents of the signal shifts correlate with binding strength, anion affinity of **3** in 5 vol% DMSO- $d_6$ /acetone- $d_6$  reflects the normal coordinating ability of anions, being stronger for more strongly coordinating anions such as the oxoanions sulfate and DHP and the small chloride anion. In the more competitive D $_2$ O/DMSO- $d_6$  mixture, anion binding is weakened to such an extent that only complex formation with the oxoanions is retained. Thus, the ability of **1** to bind anions even in highly competitive protic solvents $^{19}$  is lost upon moving one substituent on each triazole unit from the 5 into the 4 position despite the good preorganisation of **3** for anion binding and the presence of the three additional hydrogen-bond donors along the ring that contribute to anion recognition. This shows how important the unique conformation of **1** (and of **2**) is for anion binding in protic media.

Nevertheless, pseudopeptide **3** possesses characteristic properties not observed for **1** or **2** such as an affinity for DHP anions and we therefore concentrated on quantitatively evaluating the interactions of **3** with oxoanions in DMSO.

### Quantitative binding studies

**Sulfate binding.** Initial information about the stoichiometry of the sulfate complex of **3** was derived from a Job plot, which was obtained by following characteristic signal shifts in the  $^1\text{H}$  NMR spectra of solutions containing different mole fractions but a constant total concentration of **3** and TBA sulfate. This Job plot indicated that sulfate binding follows a simple

1 : 1 equilibrium in 2.5 vol% D<sub>2</sub>O/DMSO-*d*<sub>6</sub> (see ESI†). The shapes of the binding isotherms subsequently obtained from isothermal titration calorimetry (ITC) and NMR titrations showed that the equilibrium is more complex, however. Although binding is indeed mainly governed by a 1 : 1 complex, a 2<sub>R</sub> : 1<sub>A</sub> complex in which two molecules of **3** (R) bind to a single anion (A) has to be considered when the receptor is present in excess.

The results of the ITC titrations are summarized in Table 1. These titrations were performed in different solvent mixtures to elucidate effects of solvent composition on complex stability. Each titration was typically performed in triplicate with freshly prepared solutions of **3** and TBA sulfate, and the thermodynamic parameters were derived by fitting the obtained isotherms to a model that considers binding of up to two receptors (R) to one anion (A), thereby allowing for the formation of both 1 : 1 and 2<sub>R</sub> : 1<sub>A</sub> complexes. Although weak binding of a second receptor was evident from the isotherms, only the stability constants of the 1 : 1 complex could be accurately determined. For the second binding event only an upper limit of  $K_{21}$  could be reasonably estimated.<sup>23</sup>

An NMR titration performed in 2.5 vol% D<sub>2</sub>O/DMSO-*d*<sub>6</sub>, whose results are also included in Table 1, yielded similar results. The binding constant  $K_{11}$  resulting from this titration is in excellent agreement with the one obtained by ITC in the same solvent mixture. Moreover, the sigmoidal shape of the binding isotherms resulting from this titration (see ESI†) provided clear evidence for the formation of higher complexes, consistent with the ITC titrations. Unfortunately, also in this case the second, weaker binding constant turned out to be difficult to quantify. Based on the regression analysis one can only safely state that  $K_{21}$  is at least two orders of magnitude smaller than  $K_{11}$ . This ratio of the stepwise binding constants shows that substantial amounts of the 2<sub>R</sub> : 1<sub>A</sub> complex are formed only when **3** is present in excess, which explains why this complex is not visible in the Job plot.<sup>24</sup>

According to the results of the binding studies, the stability of the 1 : 1 complex between **3** and a sulfate anion is relatively unaffected by solvent composition. Interestingly, complex stability is slightly higher in 2.5 vol% H<sub>2</sub>O/DMSO than in the solvent mixtures containing less and more water. Although the difference is small, it mirrors the effect of water on the anion-induced shift of the triazole signal in the NMR spectra. Fig. 6 shows that addition of D<sub>2</sub>O to a DMSO-*d*<sub>6</sub> solution of the

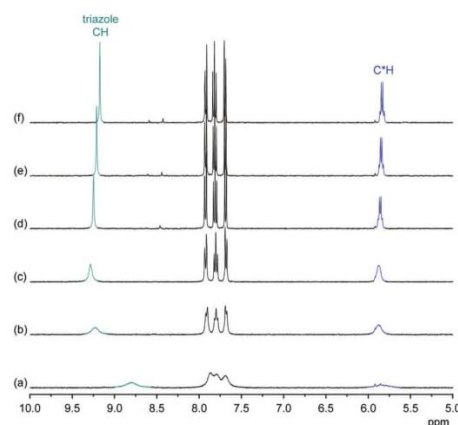


Fig. 6 <sup>1</sup>H NMR spectrum of **3** (1 mM) in the presence of 5 equiv. of TBA sulfate in D<sub>2</sub>O/DMSO-*d*<sub>6</sub> mixtures with the D<sub>2</sub>O content amounting to 0.03 vol% (a), 1 vol% (b), 2 vol% (c), 3 vol% (d), 4 vol% (e), and 5 vol% (f). The signals of the triazole and C\*H protons are marked in green and blue, respectively.

sulfate complex of **3** causes the triazole CH and C\*H signals to shift *downfield* in the <sup>1</sup>H NMR spectrum until a D<sub>2</sub>O content of 2 vol% is reached, with a concomitant sharpening of the signals. Only when further increasing the D<sub>2</sub>O content of the solution is the expected upfield shift of these signals that indicates weakening of anion-binding being observed. In the absence of TBA sulfate, the <sup>1</sup>H NMR spectrum of **3** is practically unaffected when varying the D<sub>2</sub>O content of the D<sub>2</sub>O/DMSO-*d*<sub>6</sub> mixture between 0.03% and 5% (see ESI†).

The effect of water on the <sup>1</sup>H NMR spectrum of the sulfate complex of **3** and the quantitative results of the binding studies indicate that small amounts of water seem to reinforce sulfate complexation. A possible explanation could be that sulfate anions associated with one or more water molecules better fit the available space in the cavity of **3** similarly as in the DHP complex of **3** (*vide infra*) in which one water molecule was found to bridge hydrogen bond donors along the receptor cavity and oxygen atoms of the anion. Note that under the conditions used for recording the NMR spectra in Fig. 6 (*i.e.*, excess of sulfate), the presence of a higher complex containing more than one pseudopeptide ring can be neglected.

Table 1 Thermodynamic parameters of the interaction of TBA sulfate with **3** in H<sub>2</sub>O/DMSO mixtures containing different amounts of H<sub>2</sub>O. Uncertainties (in parentheses) indicate 68.3% confidence intervals as calculated by error-surface projection<sup>25</sup>

Vol% H <sub>2</sub> O in H <sub>2</sub> O/DMSO	log $K_{11}$ <sup>a</sup>	log $K_{21}$ <sup>b</sup>	$\Delta H_{11}^{\circ}$ <sup>c</sup>	$T\Delta S_{11}^{\circ}$ <sup>c</sup>
0.03 <sup>d</sup>	4.08 (4.00 to 4.15)	<3.2	39.7 (37.5 to 42.2)	62.9
2.5	4.39 (4.36 to 4.42)	<2.4	-14.1 (-14.4 to -13.8)	11.0
	4.22 <sup>e</sup>	<2.1 <sup>e</sup>		
5	4.05 (4.00 to 4.09)	<2.3	-21.6 (-22.7 to -20.6)	1.5

<sup>a</sup> Equilibrium constant describing the formation of the 1 : 1 complex. <sup>b</sup> Equilibrium constant describing the formation of the 2<sub>R</sub> : 1<sub>A</sub> complex from the 1 : 1 complex. <sup>c</sup> Enthalpies and entropies associated with the formation of the 1 : 1 complex in kJ mol<sup>-1</sup>. <sup>d</sup> Maximum water content of the DMSO (99.6%) used. <sup>e</sup> Determined by NMR titration with an estimated error of 10%.

**Table 2** Thermodynamic parameters of the interaction of TBA DHP with **3** in H<sub>2</sub>O/DMSO mixtures containing different amounts of H<sub>2</sub>O. Uncertainties (in parentheses) indicate 68.3% confidence intervals as calculated by error-surface projection<sup>25</sup>

Vol% H <sub>2</sub> O in H <sub>2</sub> O/DMSO	log $K_{11}$ <sup>a</sup>	log $K_{12}$ <sup>b</sup>	$\Delta H_{11}^{\circ}$ <sup>c</sup>	$T\Delta S_{11}^{\circ}$ <sup>c</sup>	$\Delta H_{12}^{\circ}$ <sup>c</sup>	$T\Delta S_{12}^{\circ}$ <sup>c</sup>
0.03 <sup>d</sup>	3.85 (3.50 to 4.20)	3.53 (3.03 to 4.03)	-9.8 (-11.5 to -8.7)	12.2	-16.7 (-20.1 to -11.5)	3.4
2.5	3.46 (3.17 to 3.76)	3.22 (2.82 to 3.62)	-7.2 (-10.2 to -5.6)	12.5	-24.1 (-27.7 to -17.4)	-5.7
	3.21 <sup>e</sup>	3.10 <sup>e</sup>				
5	3.57 (3.37 to 3.79)	2.82 (2.57 to 3.06)	-2.8 (-3.4 to -2.3)	17.6	-26.1 (-27.3 to -24.6)	-10.0

<sup>a</sup> Equilibrium constant describing the formation of the 1:1 complex. <sup>b</sup> Equilibrium constant describing the formation of the 1<sub>R</sub>:2<sub>A</sub> complex from the 1:1 complex. <sup>c</sup> Enthalpies and entropies associated with the formation of the 1:1 and 1:2 complexes in kJ mol<sup>-1</sup>. <sup>d</sup> Maximum water content of the DMSO (99.6%) used. <sup>e</sup> Determined by NMR titration with an estimated error of 10%.

Formation of the 1:1 complex is endothermic in DMSO and becomes increasingly exothermic when the solvent mixture contains more water. Conversely, the large favourable contribution of entropy to complex formation in DMSO decreases. Note that the enthalpies and entropies associated with the formation of the 2<sub>R</sub>:1<sub>A</sub> complexes are not considered in Table 1 because the much lower stability of this complex renders their estimation unreliable.

In spite of the clearly visible trends of  $\Delta H_{11}^{\circ}$  and  $T\Delta S_{11}^{\circ}$  with solvent composition, correlating them with direct receptor-anion interactions or solvation effects is not straightforward because the effects of water molecules involved in complex formation are difficult to estimate.

These binding studies thus demonstrated that sulfate complexation of receptors **1**, **2**, and **3** follows related models: all three compounds have a tendency to form complexes with sulfate anions in which two receptor units bind to a single anion. The reasons of forming these higher complexes differ, however. In the case of **2** and to a lesser extent **1**, 2<sub>R</sub>:1<sub>A</sub> complexes are found in polar protic solvents, and a major driving force of their formation comes from hydrophobic effects between the two receptor rings. Increasing the water content of the solvent thus leads to a strengthening of the second binding step with respect to the first one.<sup>19,26</sup> By contrast, sulfate binding of **3** takes place in organic media and is likely caused by the tendency of the anion to saturate its hydrogen-bond acceptor sites. If this cannot be achieved in the 1:1 complex, a second receptor molecule is recruited. Formation of this higher complex is, however, weak in the case of sulfate complexation and becomes even weaker when the water content of the solution increases. Hydrophobic effects between the receptor units in the corresponding 2<sub>R</sub>:1<sub>A</sub> complex of **3** are absent in DMSO and probably not even possible because of the significantly different conformations of **1** and **3**.

**Dihydrogenphosphate binding.** Similar investigations were performed to study DHP binding to **3**. These investigations demonstrated that the binding model underlying the corresponding interactions differs from the one observed for sulfate complexation. First evidence was obtained from a Job plot, which showed that complexes dominate in solution containing two DHP anions bound to one molecule of **3**. The corresponding 1<sub>R</sub>:2<sub>A</sub> stoichiometry was then confirmed by ITC and NMR titrations as well as X-ray crystallography. Binding constants and thermodynamic parameters derived

from titrations in different solvent mixtures are compiled in Table 2.

This table shows that the results of ITC and NMR titrations are in very good agreement, this time providing reliable information about the stability constants associated with both binding steps.

In contrast to sulfate binding, the stability constants associated with the 1:1 complex continuously decrease with increasing water content. Moreover, complex formation is exothermic in DMSO and becomes enthalpically less favourable the more water is present. Conversely, the favourable contribution of entropy increases in the same direction.

Once the 1:1 complex is formed, binding of a second DHP anion is favourable as indicated by the fact that the second binding step is strongly exothermic and associated with a stability constant almost equal in size as the one associated with the corresponding 1:1 complex.

The tendency of forming the 1<sub>R</sub>:2<sub>A</sub> complexes decreases when increasing the water content of the solvent, a trend that is mainly caused by entropy as the binding enthalpy of forming the 1<sub>R</sub>:2<sub>A</sub> complex becomes even more favourable in solvent mixtures containing more water. Because of the continuous decrease of  $K_{12}$ , the overall stability of the DHP complex of **3** decreases with increasing water content of the solvent, consistent with the effect of water on the <sup>1</sup>H NMR spectrum of this complex (see ESI†). Moreover, binding of the second DHP anion is weakly cooperative in DMSO and 2.5 vol% H<sub>2</sub>O/DMSO, but not in 5 vol% H<sub>2</sub>O/DMSO.‡

Structural information about the DHP complex of **3** was obtained from a crystal structure. Crystals were grown by slow evaporation of a solution of **3** (1.2 mM) in DMSO/acetone, 1:1 (v/v) containing 2 equiv. of TBADHP. The arrangement of anions and **3** in these crystals is depicted in Fig. 7. Accordingly, two molecules of **3** bind to three DHP anions in the solid state; the 3/TBADHP ratio therefore deviates from the

‡ For completely independent binding steps one would expect a 4 times smaller association constant  $K_{12}$  for the second binding step with respect to  $K_{11}$  of the 1:1 complex. The reason is that the rate constant of forming the 1:1 complex is statistically two times higher than that of forming the 1:2 complex, while the dissociation rate constant of the 1:2 complex is twice that of the 1:1 complex. Since the ratio of the rate constant of formation and the rate constant of dissociation gives the equilibrium constant, it follows that  $K_{12} = K_{11}/4$  in the absence of cooperativity.<sup>33</sup>

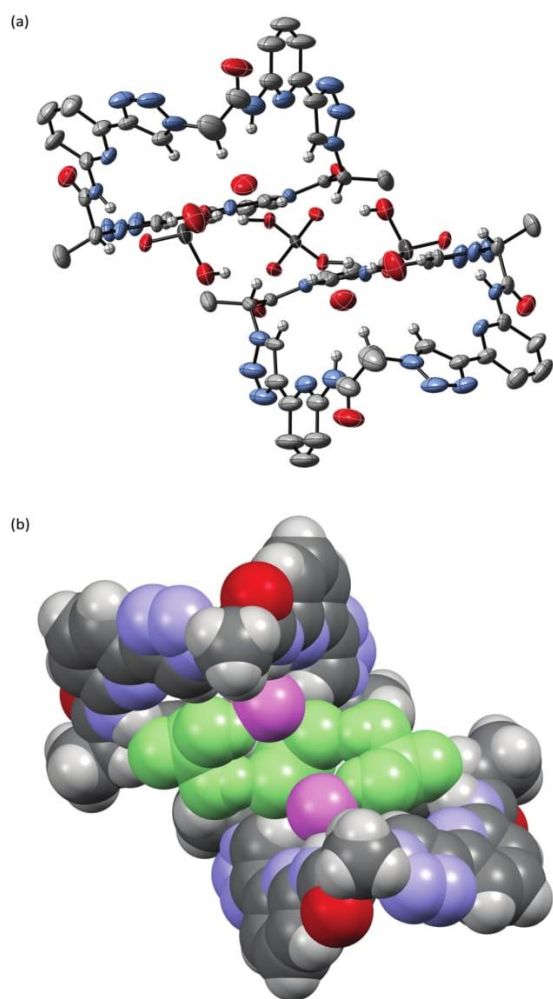


Fig. 7 Molecular structure of  $3 \cdot 1.5\text{TBADHP} \cdot 2.5\text{DMSO} \cdot 1.7\text{H}_2\text{O}$  (a) showing the 2 : 3 association of **3**, the DHP anions, and the water molecules in the solid state with the thermal ellipsoids shown at the 50% probability level. The DMSO molecules, the TBA cations, the minor component of the water disorder, and the hydrogen atoms except those on the NH and triazole CH groups as well as those on the stereogenic centres C\*H are omitted for clarity. (b) Shows the same structure as a space-filling model with the DHP trimer in green and the water molecules in pink to better illustrate the arrangement of the binding partners.

one found in solution and amounts to 2 : 3. The conformation of **3** in the complex  $3 \cdot 1.5\text{TBADHP} \cdot 2.5\text{DMSO} \cdot 1.7\text{H}_2\text{O}$  is similar as that observed in  $3 \cdot 5\text{DMSO} \cdot 0.35\text{H}_2\text{O}$  shown in Fig. 2 (for an overlay, see ESI<sup>†</sup>). Thus, complex formation does not require a substantial conformational reorganisation of the pseudopeptide. In  $3 \cdot 1.5\text{TBADHP} \cdot 2.5\text{DMSO} \cdot 1.7\text{H}_2\text{O}$  one of the DMSO molecules resides in the concave cavity of **3**, while the others are located outside where also the TBA counterions, one of which is disordered on a symmetry element, can be found. The DHP anions form a tight hydrogen-bonded trimer with short, 2.46 and 2.51 Å, P–O⋯O=P distances between O2⋯O5

and O3⋯O6, respectively (Fig. S2<sup>†</sup>). Each pseudopeptide ring hydrogen bonds to the terminal anions of the DHP trimer while the central anion is hydrogen bonded to both of the macrocycles. Ten of the twelve oxygen atoms of the DHP trimer interact with hydrogen bond donors along the pseudopeptide rings, two NH groups and three triazole CH groups per ring. With O⋯N distances of 2.76 and 2.92 Å the lengths of the hydrogen bonds to the NH groups are shorter than the ones to the triazole C–H groups, whose O⋯C distances amount to 3.19, 3.24, and 3.53 Å. Two water molecules are also present in the complex, one per pseudopeptide, which bridge the bound anions and the third NH group of each ring. There is no evidence that the pyridine or triazole nitrogen atoms of **3** participate in complex formation as they do not act as hydrogen bond acceptors with the OH groups of the DHP anions.

While close spatial arrangement of the three anions in this structure may look unusual, the tendency of DHP anions to form such aggregates and even higher ones is well known.<sup>27–29</sup> Charge repulsion upon DHP association can obviously be overcompensated by sufficiently strong hydrogen bonding interactions. While isolated DHP aggregates are only weakly stable in a polar medium such as DMSO,<sup>29f</sup> suitable receptors can cause their stabilisation.<sup>29</sup> Fig. 7 provides evidence that **3** belongs to this category due to its ring size and proper arrangement of hydrogen bond acceptors. The cavity of **3** seems to be slightly too large to accommodate two DHP anions, necessitating incorporation of an additional water molecule to fill the available space. Formation of  $2_{\text{R}} : 3_{\text{A}}$  complexes is likely entropically unfavourable, which explains why the binding mode is simpler in solution. The solid-state structure does, however, provide a plausible structural rationale for the observed complex stoichiometry in solution because it demonstrates that each pseudopeptide ring is able to interact with altogether two DHP anions.

The detected cooperativity in DHP complex formation indicates that the 1 : 1 complex between **3** and a DHP anion features a superior binding environment for the incoming anion than the empty pseudopeptide ring. Similar behaviour was reported for other systems.<sup>29a,d,e</sup> In the case of **3**, the water molecule found in the complex could play an additional role. Our results furthermore demonstrate that the presence of water in the medium mainly weakens the second binding event, leading to an overall reduction of complex stability as the water content of the solvent mixture rises. Moreover, the structure of the complex shown in Fig. 7 provides information why complexes containing more than one pseudopeptide ring are not observed in the presence of DHP: in contrast to the sulfate complex of **3**, no hydrogen-bond acceptors of the complexed DHP anions remain vacant that would allow interactions with a second pseudopeptide ring.

**Hydrogenpyrophosphate binding.** Having seen that **3** has a large enough cavity to incorporate a DHP dimer, we wondered whether complexation of the hydrogenpyrophosphate (HPP) anion would also be possible. The respective binding studies revealed that the effects of HPP again differ from those of the previous two anions. Specifically, addition of HPP to a solution

of **3** in 2.5 vol% D<sub>2</sub>O/DMSO-*d*<sub>6</sub> led to separate signals for free and complexed receptor species in the <sup>1</sup>H NMR spectrum when less than 1 equiv. of HPP was present, demonstrating that complex formation is slow on the NMR timescale. As a consequence, no Job plot could be recorded. Increasing the HPP concentration caused a progressive increase in the intensity of the signal assigned to the triazole proton of complexed **3**. At the same time, the corresponding signal of free **3** became smaller but also shifted downfield (Fig. 8), which could indicate that HPP binding is more complex than a simple 1:1 binding equilibrium.

The shapes of the binding isotherms of the ITC titration support this assumption. These isotherms exhibit clear steps showing that HPP complexation is associated with several equilibria (see ESI†). The first two steps signify the initial (exothermic) formation of a 2<sub>R</sub>:1<sub>A</sub> complex containing two units of **3** and the subsequent transformation of this complex into a 1:1 complex. In the presence of a large excess of anions, a further process takes place possibly involving formation of higher complexes or other aggregation phenomena.

In the absence of detailed knowledge about these higher-order complexes, data fitting was restricted to the concentration regime comprising up to slightly more than one equivalent of HPP, in which the 2<sub>R</sub>:1<sub>A</sub> and 1:1 complexes dominate. From this part of the binding isotherm, high binding constants of log *K*<sub>11</sub> = 6.62 and log *K*<sub>21</sub> = 5.64 were calculated for the HPP complex of **3** in 2.5 vol% H<sub>2</sub>O/DMSO. It should be noted that these constants represent lower estimates because contributions to the binding isotherms from additional equilibria (as suggested by the transitions observed at much higher anion concentrations) were neglected.

Both stability constants are significantly higher than those of the complexes of the other two anions in the same solvent mixture, possibly explaining why the complexation equilibrium of HPP is slow on the NMR timescale. The high stability of the HPP complex can partly be attributed to the threefold charge of the HPP anion and potentially also its better fit into

the cavity of **3**. As in the case of the sulfate complex, the HPP anion in the 1:1 complex seems to be able to engage in further interactions with a second pseudopeptide molecule, but this interaction is significantly stronger than that of sulfate, leading to a much higher overall stability of the HPP complex (log *K*<sub>T</sub> = 12.26).

Replacing DHP with HPP therefore has larger consequences than just replacing the two anions of the 1<sub>R</sub>:2<sub>A</sub> DHP complex of **3** by a larger and presumably better-fitting one. Since HPP has a lower degree of protonation than DHP, it has a high propensity to involve more than one pseudopeptide ring in complex formation. Moreover, the threefold negative charge on the HPP anion causes the second binding step to be much stronger than in the case of sulfate.

It should be noted that we also considered TBA trimetaphosphate as potential substrate for **3** because the size and the matching symmetric should render this anion an even better guest than HPP. Although the <sup>1</sup>H NMR spectrum of **3** exhibited the typical changes associated with anion binding in the presence of this anion, the binding isotherms obtained in the respective ITC titrations were even more complex than the ones of HPP complexation (see ESI†). While it is likely that stable 1:1 and 2<sub>R</sub>:1<sub>A</sub> complexes are again being formed, as also indicated by the corresponding Job plot (see ESI†), additional equilibria contribute so strongly to the binding isotherms that quantification of stability became unreliable.

## Conclusions

Complementing the family of anion receptors shown in Fig. 1 by compound **3** improved our understanding of the effects that govern preferred conformations and binding properties of these compounds. While **1** and **2** are structurally closely related because the 1,5-disubstituted triazole units in **1** well mimic the *cis*-amides found in **2**, altering the substitution pattern on the triazole units greatly affects conformational behaviour, solubility, and anion binding properties.

In terms of structure, **3** features the predicted converging arrangement of the NH and the triazole CH groups rendering this pseudopeptide well preorganised for anion binding. Moreover, the 1,4-disubstitution pattern of the triazole units causes the cavity diameter of **3** to be slightly larger than that of **1** and the binding site to be relatively exposed to the solvent. The combination and arrangement of two different types of hydrogen-bond donors thus creates an environment particularly suited to host larger oxoanions.

Solubility of **3** restricted binding studies to DMSO/acetone mixtures or to DMSO containing up to 5 vol% of water. In these solvents, anion affinity of **3** is substantial and binding indeed involves both the NH and the triazole CH groups. Moreover, the relatively open cavity of **3** allows the incorporation of protonated anions whose hydrogen-bond donor sites can be arranged away from the receptor as in the case of the DHP complex. By contrast, anion binding of **1** and **2** takes place in a cavity made up by two receptor molecules coming

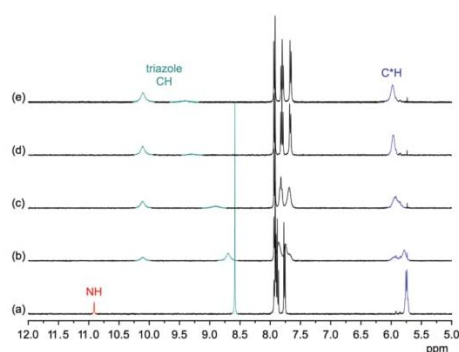


Fig. 8 <sup>1</sup>H NMR spectrum of **3** (1 mM) in 2.5 vol% D<sub>2</sub>O/DMSO-*d*<sub>6</sub> in the absence (a) and the presence of 0.25 (b), 0.50 (c), 0.75 (d), and 1.0 equiv. (e) of TBA HPP. The signals of the NH, triazole, and C\*H protons are marked in red, green, and blue, respectively.

together, which features only hydrogen-bond donors. Receptors **1** and **2** therefore do not interact with phosphate-derived anions. Changing the substitution pattern of the triazole units from the 1,5-disubstitution in **1** to the 1,4-disubstitution in **3** obviously completely alters this selectivity.

In spite of the presence of six anion binding sites along the ring, **3** seems to be unable to fully saturate the acceptor sites on sulfate or HPP anions, presumably because of cavity size and conformational rigidity. As a consequence, **3** tends to form complexes with certain anions in which more than one receptor molecule is involved in complex formation. The ring size of **3** furthermore causes water molecules to be required to mediate anion binding, as evident in the crystal structure of the DHP complex and possibly also the dependence of the stability of the sulfate complex on the water content on the solvent.

Future studies will therefore address improving solubility and simplifying the binding model underlying complex formation of **3**. The latter could be achieved, for example, by arranging additional binding sites around the cavity or by designing larger analogues of **3** that completely fold around the anionic guest. These structural modifications could also have a beneficial effect on receptor solubility. Pseudopeptide **3** therefore represents a highly promising scaffold for designing new anion receptors. Work in this context is currently underway.

## Experimental

### General details

TBA sulfate, TBA DHP, and TBA HPP are commercially available and were used after confirming purity by an elemental analysis. TBA trimetaphosphate was prepared by following a reported procedure.<sup>30</sup>

Analyses were carried out as follows: melting points, Müller SPM-X 300; NMR, Bruker AVANCE III 400 (peak assignments were confirmed by using H,H-COSY and HMQC spectra), spectra were referenced to the residual solvent signals (DMSO-*d*<sub>6</sub>:  $\delta^H = 2.50$  ppm,  $\delta^C = 39.5$  ppm); MALDI-TOF-MS, Bruker Ultraflex TOF/TOF; elemental analysis, Elementar vario Micro cube; optical rotation, Perkin Elmer 241 MC digital polarimeter (*d* = 10 cm); ITC, Microcal VP-ITC.

The following abbreviations are used: TBA, tetrabutylammonium; Epa, 6-ethynylpyridin-2-amine; Lac, CH<sub>3</sub>CHCO; Tri, 1,2,3-triazole; PyCloP, chlorotripyrrolidinophosphonium hexafluorophosphate; TBTA, tris[(1-benzyl-1*H*-1,2,3-triazol-4-yl)methyl]amine; HPP, hydrogenpyrophosphat; DHP, dihydrogenphosphate; TBAF, tetrabutylammonium fluoride.

### Syntheses

**TMS-Epa-(S)-Lac-OMs (5).** 6-[(Trimethylsilyl)ethynyl]pyridine-2-amine (13.0 g, 68.4 mmol), (*S*)-2-(methylsulfonyloxy)propionic acid (13.0 g, 77.3 mmol) and PyCloP (31.6 g, 75.0 mmol) were dissolved in dry dichloromethane (500 mL). The mixture was stirred for 2 d at 25 °C. Afterwards, the solvent was evaporated and the residue purified by column

chromatography with hexane/ethyl acetate, 2 : 1 (v/v) as eluent. The product was recrystallised from hexane/ethyl acetate, 2 : 1 (v/v) affording white needles. Yield: 13.0 g (38.1 mmol, 56%); m.p. 115–117 °C;  $[\alpha]_D^{25} = -45.4$  (*c* = 1, CHCl<sub>3</sub>); <sup>1</sup>H NMR (400 MHz, DMSO-*d*<sub>6</sub>)  $\delta$ : 11.01 (s, 1H, NH), 8.07 (d, 1H, <sup>3</sup>*J*(H, H) = 8.3 Hz, EpaH(5)), 7.84 (t, 1H, <sup>3</sup>*J*(H, H) = 8.0 Hz, EpaH(4)), 7.31 (dd, 1H, <sup>3</sup>*J*(H, H) = 7.5 Hz, <sup>4</sup>*J*(H, H) = 0.7 Hz, EpaH(3)), 5.23 (q, 1H, <sup>3</sup>*J*(H, H) = 6.7 Hz, LacCH), 3.25 (s, 3H, MsCH<sub>3</sub>), 1.52 (d, 3H, <sup>3</sup>*J*(H, H) = 6.7 Hz, LacCH<sub>3</sub>), 0.24 (s, 9H, TMSCH<sub>3</sub>); <sup>13</sup>C NMR (101 MHz, DMSO-*d*<sub>6</sub>)  $\delta$ : 168.2 (CO), 151.4 (EpaC(2)), 140.0 (EpaC(6)), 139.2 (EpaC(4)), 123.1 (EpaC(5)), 114.1 (EpaC(3)), 103.5 (Si-C≡C), 94.1 (Si-C≡C), 75.2 (LacCH), 38.0 (MsCH<sub>3</sub>), 18.6 (LacCH<sub>3</sub>), -0.40 (TMSCH<sub>3</sub>); MS (MALDI-TOF) *m/z* (%): [M - CH<sub>3</sub>SO<sub>3</sub>H + H]<sup>+</sup> 244.9 (97), [M - CH<sub>3</sub>SO<sub>3</sub>H + Na]<sup>+</sup> 267.0 (35), [M + H]<sup>+</sup> 341.1 (100), [M + Na]<sup>+</sup> 363.1 (68), [M + K]<sup>+</sup> 379.1 (33), [M + C<sub>3</sub>H<sub>6</sub>O + H]<sup>+</sup> 399.2 (51); elemental analysis calcd (%) for C<sub>14</sub>H<sub>20</sub>N<sub>2</sub>O<sub>4</sub>SSi: C 49.39, H 5.92, N 8.23, S 9.27; found C 49.17, H 5.91, N 8.16, S 9.42.

**H-Epa-(S)-Lac-OMs (6a).** TMS-Epa-(S)-Lac-OMs (2.0 g, 5.9 mmol) was dissolved in THF (20 mL) at 0 °C. To this solution, a solution of TBAF (2.8 g, 10.7 mmol) in THF (8 mL) was added dropwise. The reaction mixture was stirred for 30 min at 0 °C. Ethyl acetate (50 mL) and water (50 mL) were added, and the organic layer was separated. The aqueous phase was extracted three times with ethyl acetate (100 mL), and the combined organic layers were dried using MgSO<sub>4</sub>. The solvent was evaporated, and the residue purified on a silica gel column with hexane/ethyl acetate, 1 : 1 (v/v) as eluent. The product was obtained as a white powder. Yield: 1.4 g (5.4 mmol, 92%), MS (MALDI-TOF) *m/z* (%): [M + H]<sup>+</sup> 268.9 (100), [M + Na]<sup>+</sup> 291.0 (10), [M + K]<sup>+</sup> 279.1 (17).

**TMS-Epa-(R)-Lac-N<sub>3</sub> (6b).** TMS-Epa-(S)-Lac-OMs (1.9 g, 5.6 mmol) and sodium azide (600 mg, 9.2 mmol) were dissolved in DMF (20 mL) and the resulting mixture was heated at 50 °C for 30 min. Ethyl acetate (30 mL) and water (30 mL) were added, the organic layer was separated, and the aqueous phase was extracted with ethyl acetate three times (60 mL). The combined organic layers were dried using MgSO<sub>4</sub>. The solvent was evaporated, and the residue purified on a silica gel column with hexane/ethyl acetate, 3 : 1 (v/v) as eluent. Yield: 1.50 g (5.3 mmol, 95%), MS (MALDI-TOF) *m/z* (%): [M - N<sub>2</sub> + H]<sup>+</sup> 260.0 (31), [M - N<sub>2</sub> + Na]<sup>+</sup> 282.0 (55), [M + H]<sup>+</sup> 288.0 (33), [M + Na]<sup>+</sup> 310.0 (100), [M + K]<sup>+</sup> 326.0 (74).

**TMS-Epa-(R)-Lac-1,4-Tri-Epa-(S)-Lac-OMs (7).** H-Epa-(S)-Lac-OMs (1.4 g, 5.4 mmol) and TMS-Epa-(R)-Lac-N<sub>3</sub> (1.5 g, 5.3 mmol) were dissolved in *t*-BuOH/H<sub>2</sub>O, 1 : 1 (v/v) (150 mL), followed by the addition of a solution of TBTA (143 mg, 270 μmol, 5 mol%), Cu(MeCN)<sub>4</sub>PF<sub>6</sub> (101 mg, 270 μmol, 5 mol%), and sodium ascorbate (107 mg, 540 μmol, 10 mol%) in *t*-BuOH/H<sub>2</sub>O, 1 : 1 (v/v) (20 mL). The reaction mixture was stirred at 25 °C for 20 h and extracted with ethyl acetate three times (60 mL). The combined organic layers were washed with water twice and dried over MgSO<sub>4</sub>. The solvent was evaporated under vacuum, and the crude product was purified by column chromatography using ethyl acetate/hexane, 1 : 2 (v/v) as eluent. The product was obtained as a white solid. Yield: 2.2 g

(4.0 mmol, 76%); m.p. 109–111 °C;  $[\alpha]_D^{25} = -162.1$  ( $c = 0.1$ ,  $\text{CHCl}_3$ );  $^1\text{H NMR}$  (400 MHz,  $\text{DMSO-}d_6$ )  $\delta$ : 11.41 (s, 1H, NH), 10.77 (s, 1H, NH), 8.63 (s, 1H, TriH), 7.99–8.05 (m, 2H, EpaH(3)), 7.93 (t, 1H,  $^3J(\text{H}, \text{H}) = 7.9$  Hz, EpaH(4)), 7.83 (t, 1H,  $^3J(\text{H}, \text{H}) = 8.0$  Hz, EpaH(4)), 7.78 (dd, 1H,  $^3J(\text{H}, \text{H}) = 7.4$  Hz,  $^4J(\text{H}, \text{H}) = 0.8$  Hz, EpaH(5)), 7.31 (d, 1H,  $^3J(\text{H}, \text{H}) = 7.5$  Hz, EpaH(5)), 5.75 (q, 1H,  $^3J(\text{H}, \text{H}) = 7.1$  Hz, LacCH), 5.34 (q, 1H,  $^3J(\text{H}, \text{H}) = 6.5$  Hz, LacCH), 3.26 (s, 3H,  $\text{MsCH}_3$ ), 1.85 (d, 3H,  $^3J(\text{H}, \text{H}) = 7.1$  Hz, LacCH $_3$ ), 1.55 (d, 3H,  $^3J(\text{H}, \text{H}) = 6.7$  Hz, LacCH $_3$ ), 0.25 (s, 9H,  $\text{TMSCH}_3$ );  $^{13}\text{C NMR}$  (101 MHz,  $\text{DMSO-}d_6$ )  $\delta$ : 168.2 (CO), 168.1 (CO), 151.5 (EpaC(2)), 151.1 (EpaC(2)), 148.5 (EpaC(6)), 146.4 (TriC(4)), 140.0 (EpaC(6)), 139.5 (EpaC(4)), 139.4 (EpaC(4)), 123.2 (EpaC(5)), 122.8 (TriC(5)), 116.0 (EpaC(5)), 115.9 (EpaC(5)), 114.0 (EpaC(3)), 113.0 (EpaC(3)), 112.9 (EpaC(3)), 103.5 (Si–C $\equiv$ C), 94.2 (Si–C $\equiv$ C), 75.3 (LacC), 58.8 (LacC), 38.1 (MsCH $_3$ ), 18.7 (LacCH $_3$ ), 17.9 (LacCH $_3$ ), –0.4 (TMSCH $_3$ ); MS (MALDI-TOF)  $m/z$  (%):  $[\text{M} - \text{N}_2 - \text{CH}_3\text{SO}_3\text{H} + \text{H}]^+$  432.2 (16),  $[\text{M} - \text{CH}_3\text{SO}_3\text{H} + \text{H}]^+$  460.3 (100),  $[\text{M} - \text{N}_2 + \text{H}]^+$  528.3 (17),  $[\text{M} + \text{H}]^+$  556.3 (13),  $[\text{M} + \text{Na}]^+$  578.3 (30),  $[\text{M} + \text{K}]^+$  594.3 (14); elemental analysis calcd (%) for  $\text{C}_{24}\text{H}_{29}\text{N}_7\text{O}_5\text{SSi}$ : C 51.87, N 17.64, H 5.26, S 5.77 found C 51.60, N 17.34, H 5.40, S 5.60.

**H-Epa-(R)-Lac-1,4-Tri-Epa-(S)-Lac-OMs.** Dimer **7** (3.3 g, 5.9 mmol) was dissolved in THF (40 mL) at 0 °C. To this solution, a solution of TBAF (3.4 g, 12.9 mmol) in THF (20 mL) was added dropwise. This mixture was stirred for 30 min at 0 °C. Ethyl acetate (50 mL) and water (50 mL) were added, and after separation of the organic layer the aqueous phase was extracted three times using ethyl acetate (150 mL). The combined organic layers were dried using  $\text{MgSO}_4$ . The solvent was evaporated and the residue purified on a silica gel column with hexane/ethyl acetate, 1 : 1 (v/v) as eluent. The product was obtained as a white powder. Yield: 2.6 g (5.4 mmol, 92%), MS (MALDI-TOF)  $m/z$  (%):  $[\text{M} - \text{CH}_3\text{SO}_3\text{H} + \text{H}]^+$  388.2 (100),  $[\text{M} + \text{H}]^+$  484.3 (35),  $[\text{M} + \text{Na}]^+$  506.3 (48),  $[\text{M} + \text{K}]^+$  522.3 (8).

**TMS-Epa-[(R)-Lac-1,4-Tri-Epa] $_2$ -(S)-Lac-OMs (8).** Compounds **7** (2.6 g, 5.4 mmol) and **6b** (1.8 g, 6.3 mmol) were dissolved in  $t\text{-BuOH}/\text{H}_2\text{O}$ , 1 : 1 (v/v) (200 mL), followed by the addition of a solution of TBTA (143 mg, 270  $\mu\text{mol}$ , 5 mol%), Cu( $\text{MeCN}$ ) $_4\text{PF}_6$  (101 mg, 270  $\mu\text{mol}$ , 5 mol%), and sodium ascorbate (107 mg, 540  $\mu\text{mol}$ , 10 mol%) in  $t\text{-BuOH}/\text{H}_2\text{O}$ , 1 : 1 (v/v) (20 mL). The reaction mixture was stirred at 25 °C for 20 h and extracted with ethyl acetate three times (60 mL). The combined organic layers were washed with water twice and dried over  $\text{MgSO}_4$ . Ethyl acetate was evaporated under vacuum, and the crude product was purified by column chromatography using ethyl acetate/hexane, 2 : 1 (v/v) as eluent. Pure product was obtained as a white solid. Yield: 3.2 g (4.1 mmol, 75%); m.p. 195–200 °C (dec.);  $[\alpha]_D^{25} = -215.1$  ( $c = 0.1$ ,  $\text{CHCl}_3$ );  $^1\text{H NMR}$  (400 MHz,  $\text{DMSO-}d_6$ )  $\delta$ : 11.39 (s, 1H, NH), 11.24 (s, 1H, NH), 10.78 (s, 1H, NH), 8.65 (s, 1H, TriH), 8.64 (s, 1H, TriH), 7.91–8.05 (m, 5H, EpaH(4) + EpaH(3)), 7.83 (t, 1H,  $^3J(\text{H}, \text{H}) = 8.0$  Hz, EpaH(4)), 7.76–7.80 (m, 2H, EpaH(5)), 7.30 (d, 1H,  $^3J(\text{H}, \text{H}) = 7.5$  Hz, EpaH(5)), 5.85 (q, 1H,  $^3J(\text{H}, \text{H}) = 6.4$  Hz, LacCH), 5.75 (q, 1H,  $^3J(\text{H}, \text{H}) = 7.1$  Hz, LacCH), 5.31 (q, 1H,  $^3J(\text{H}, \text{H}) = 6.7$  Hz, LacCH), 3.25 (s, 3H,  $\text{MsCH}_3$ ), 1.87 (d, 3H,  $^3J(\text{H}, \text{H}) = 7.2$  Hz, LacCH $_3$ ), 1.85 (d, 3H,  $^3J(\text{H}, \text{H}) = 7.2$  Hz,

LacCH $_3$ ), 1.54 (d, 3H,  $^3J(\text{H}, \text{H}) = 6.7$  Hz, LacCH $_3$ ), 0.24 (s, 9H,  $^3J(\text{H}, \text{H}) = 7.1$  Hz,  $\text{TMSCH}_3$ );  $^{13}\text{C NMR}$  (101 MHz,  $\text{DMSO-}d_6$ )  $\delta$ : 168.2 (CO), 168.1 (CO), 151.5 (EpaC(2)), 151.2 (EpaC(2)), 151.1 (EpaC(2)), 148.6 (EpaC(6)), 148.5 (EpaC(6)), 146.5 (TriC(4)), 146.4 (TriC(4)), 140.1 (EpaC(6)), 139.6 (EpaC(4)), 139.5 (EpaC(4)), 139.4 (EpaC(4)), 123.2 (EpaC(5)), 122.8 (TriC(5)), 116.0 (EpaC(5)), 115.9 (EpaC(5)), 114.0 (EpaC(3)), 113.0 (EpaC(3)), 112.9 (EpaC(3)), 103.5 (Si–C $\equiv$ C), 94.2 (Si–C $\equiv$ C), 75.3 (LacC), 58.9 (LacC), 58.8 (LacC), 38.1 (MsCH $_3$ ), 18.7 (LacCH $_3$ ), 18.0 (LacCH $_3$ ), 17.9 (LacCH $_3$ ), –0.4 (TMSCH $_3$ ); MS (MALDI-TOF)  $m/z$  (%):  $[\text{M} - \text{CH}_3\text{SO}_3\text{H} + \text{H}]^+$  675.6 (100),  $[\text{M} - \text{CH}_3\text{SO}_3\text{H} + \text{H}_2 + \text{H}]^+$  677.7 (94),  $[\text{M} - \text{CH}_3\text{SO}_3\text{H} + \text{H}_2 + \text{Na}]^+$  699.7 (46),  $[\text{M} + \text{H}]^+$  771.7 (27),  $[\text{M} + \text{Na}]^+$  593.7 (17),  $[\text{M} + \text{C}_3\text{H}_6\text{O} + \text{H}]^+$  829.8 (37); elemental analysis calcd (%) for  $\text{C}_{34}\text{H}_{38}\text{N}_{12}\text{O}_6\text{SSi}$ : C 52.97, N 21.80, H 5.97, S 4.16 found C 52.59, N 21.51, H 5.00, S 3.90.

**H-Epa-[(R)-Lac-1,4-Tri-Epa] $_2$ -(S)-Lac-OMs.** Compound **8** (2.9 g, 3.8 mmol) was dissolved in THF (40 mL) at 0 °C. To this solution, a solution of TBAF (3.0 g, 11.4 mmol) in THF (20 mL) was added dropwise. The reaction mixture was stirred for 1 h at 0 °C. Ethyl acetate (50 mL) and water (50 mL) were added, and the organic layer was separated. The aqueous layer was extracted four times with ethyl acetate (100 mL), and the combined organic layers were dried using  $\text{MgSO}_4$ . The solvent was evaporated, and the residue purified on a silica gel column with ethyl acetate as eluent. The product was obtained as a white powder. Yield: 2.5 g (3.6 mmol, 93%), MS (MALDI-TOF)  $m/z$  (%):  $[\text{M} - \text{CH}_3\text{SO}_3\text{H} + \text{H}]^+$  603.5 (100),  $[\text{M} + \text{Na}]^+$  721.5 (27).

**H-Epa-[(R)-Lac-1,4-Tri-Epa] $_2$ -(R)-Lac-N $_3$ .** This reaction was performed with 0.36 mmol of starting material to avoid having to store larger amounts of the product, which is potentially prone to oligomerisation *via* thermal 1,3-dipolar cycloaddition, and because the subsequent cyclisation step turned out to be more efficient when performed on a smaller scale. The product from the previous step (252 mg, 0.36 mmol) and sodium azide (25 mg, 0.36 mmol) were dissolved in DMF (20 mL), and the reaction mixture was heated at 50 °C for 1 h. Ethyl acetate (30 mL) and water (30 mL) were added, and the organic layer was separated. The aqueous layer was extracted three times with ethyl acetate (50 mL), and the combined organic layers were dried over  $\text{MgSO}_4$ . The solvent was evaporated and the residue purified on a silica gel column with ethyl acetate as eluent to afford pure product as a white powder. Yield: 230 mg (0.36 mmol, 99%), MS (MALDI-TOF)  $m/z$  (%):  $[\text{M} - \text{N}_2 + \text{Na}]^+$  640.7 (77),  $[\text{M} - \text{N}_2 + \text{K}]^+$  656.7 (26),  $[\text{M} + \text{Na}]^+$  668.8 (100),  $[\text{M} + \text{K}]^+$  684.8 (36).

**cyclo[(R)-Lac-1,4-Tri-Epa] $_3$  (3).** The product from the previous step (230 mg, 356  $\mu\text{mol}$ ) was dissolved in a mixture of DMSO (2 mL) and  $t\text{-BuOH}/\text{H}_2\text{O}$ , 1 : 1 (v/v) (50 mL). The resulting solution was added dropwise to a suspension of TBTA (19 mg, 36  $\mu\text{mol}$ , 10 mol%), sodium ascorbate (3.5 mg, 18  $\mu\text{mol}$ , 5 mol%), and Cu( $\text{MeCN}$ ) $_4\text{PF}_6$  (13 mg, 35  $\mu\text{mol}$ , 10 mol%) in  $t\text{-BuOH}/\text{H}_2\text{O}$ , 1 : 1 (v/v) (250 mL) over a period of 30 min at 25 °C. The reaction mixture was stirred at 35 °C, and progress was followed by HPLC. Additional solid TBTA (9 mg, 18  $\mu\text{mol}$ , 5 mol%) and Cu( $\text{MeCN}$ ) $_4\text{PF}_6$  (7 mg, 18  $\mu\text{mol}$ , 5 mol%) were

added every 24 h until HPLC indicated full conversion, typically after 3 d. Ethyl acetate was added and the aqueous layer removed. The organic solvent was evaporated, and the residue was washed several times with acetone to remove the catalyst and TBTA and dried. The product was obtained analytically pure after recrystallisation from DMSO. Yield: 65 mg (101  $\mu\text{mol}$ , 29%); m.p. > 200 °C (dec);  $[\alpha]_{\text{D}}^{25} = +6.94$  ( $c = 0.1$ , DMSO);  $^1\text{H}$  NMR (400 MHz, DMSO- $d_6$ )  $\delta$ : 10.91 (s, 3H, NH), 8.59 (s, 3H, TriH), 7.94 (d, 2H,  $^3J(\text{H}, \text{H}) = 8.0$  Hz, EpaH(4)), 7.89 (t, 3H,  $^3J(\text{H}, \text{H}) = 7.8$  Hz, EpaH(5)), 7.77 (d, 3H,  $^3J(\text{H}, \text{H}) = 7.6$  Hz, EpaH(3)), 5.76 (q, 3H,  $^3J(\text{H}, \text{H}) = 6.7$  Hz, LacCH), 1.85 (d, 9H,  $^3J(\text{H}, \text{H}) = 6.9$  Hz, LacCH<sub>3</sub>);  $^{13}\text{C}$  NMR (101 MHz, DMSO- $d_6$ )  $\delta$ : 166.6 (CO), 151.2 (EpaC(2)), 148.4 (EpaC(6)), 146.3 (TriC(4)), 139.6 (EpaC(4)), 123.4 (TriC(5)), 116.0 (EpaC(5)), 113.1 (EpaC(3)), 59.1 (LacC), 16.1 (LacCH<sub>3</sub>); MS (MALDI-TOF)  $m/z$  (%):  $[\text{M} + \text{H}]^+$  646.5 (34),  $[\text{M} + \text{Na}]^+$  668.5 (100),  $[\text{M} + \text{K}]^+$  684.6 (19); elemental analysis calcd (%) for C<sub>30</sub>H<sub>27</sub>N<sub>15</sub>O<sub>3</sub>·DMSO·2H<sub>2</sub>O: C 50.58, N 27.65, H 4.91, S 4.22 found C 50.27, N 27.43, H 4.62, S 4.02.

**NMR titrations.** Stock solutions of **3** (1 mM), TBA DHP (10 mM), and TBA sulfate (3 mM) were prepared separately in 2.5 vol% D<sub>2</sub>O/DMSO- $d_6$ . Increasing amounts (0 to 300  $\mu\text{L}$ ) of the salt stock solution were added to 16 NMR tubes, each containing 300  $\mu\text{L}$  of the receptor stock solution. The total volume in each tube was made up to 600  $\mu\text{L}$  with 2.5 vol% D<sub>2</sub>O/DMSO- $d_6$ . All tubes were thoroughly shaken, and the  $^1\text{H}$  NMR spectra were recorded (256 scans, 400 MHz). Stability constants of the anion–receptor complexes were calculated by using HypNMR2008.<sup>31</sup>

**ITC titrations.** The ITC experiments were carried out in DMSO and water–DMSO mixtures containing 2.5 vol% or 5 vol% of water. The anionic substrates were used as their TBA salts. The salts and receptor **3** were weighed using an analytical precision balance, dissolved in known volumes of the respective solvent mixture, and loaded into the system for immediate analysis.

The measurements were carried out at 25 °C using a reference power of 25  $\mu\text{J s}^{-1}$ , a filter period of 2 s, a stirrer speed of 307 rpm. Other experimental parameters of the individual titrations are specified in the ESI.† Automated baseline assignment and peak integration of raw thermograms were accomplished by singular value decomposition and peak-shape analysis using NITPIC.<sup>32a</sup> Estimation of best-fit parameter values by weighted nonlinear least-squares fitting and calculation of 68.3% confidence intervals were performed with the public-domain software SEDPHAT,<sup>32b</sup> as explained in detail elsewhere.<sup>32c,d</sup>

## Acknowledgements

We thank Dr M. Meyer, Institut de Chimie Moléculaire de l'Université de Bourgogne (ICMUB), Dijon for help with the HypNMR software and Dr R. Goddard, Max-Planck-Institut für Kohlenforschung, Mülheim/Ruhr for performing preliminary crystallographic studies. K.R. thanks the Academy of Finland for financial support (Project Nos. 263256 and 292746).

## Notes and references

- 1 R. Huisgen, G. Szeimies and L. Möbius, *Chem. Ber.*, 1967, **100**, 2494–2507.
- 2 M. Meldal and C. W. Tornøe, *Chem. Rev.*, 2008, **108**, 2952–3015.
- 3 C. P. R. Hackenberger and D. Schwarzer, *Angew. Chem., Int. Ed.*, 2008, **47**, 10030–10074.
- 4 B. Schulze and U. S. Schubert, *Chem. Soc. Rev.*, 2014, **43**, 2522–2571.
- 5 (a) V. V. Rostovtsev, L. G. Green, V. V. Fokin and K. B. Sharpless, *Angew. Chem., Int. Ed.*, 2002, **41**, 2596–2599; (b) C. W. Tornøe, C. Christensen and M. Meldal, *J. Org. Chem.*, 2002, **67**, 3057–3064.
- 6 H. C. Kolb, M. G. Finn and K. B. Sharpless, *Angew. Chem., Int. Ed.*, 2001, **40**, 2004–2021.
- 7 B. C. Boren, S. Narayan, L. K. Rasmussen, L. Zhang, H. Zhao, Z. Lin, G. Jia and V. V. Fokin, *J. Am. Chem. Soc.*, 2008, **130**, 8923–8930.
- 8 J. C. Jewett and C. R. Bertozzi, *Chem. Soc. Rev.*, 2010, **39**, 1272–1279.
- 9 (a) C. G. S. Lima, A. Ali, S. S. van Berkel, B. Westermann and M. W. Paixão, *Chem. Commun.*, 2015, **51**, 10784–10796; (b) J. John, J. Thomas and W. Dehaen, *Chem. Commun.*, 2015, **51**, 10797–10806.
- 10 (a) D. S. Pedersen and A. Abell, *Eur. J. Org. Chem.*, 2011, 2399–2411; (b) I. E. Valverde and T. L. Mindt, *Chimia*, 2013, **67**, 262–266.
- 11 Y. Hua and A. H. Flood, *Chem. Soc. Rev.*, 2010, **39**, 1262–1271.
- 12 Y. Li and A. H. Flood, *Angew. Chem., Int. Ed.*, 2008, **47**, 2649–2652.
- 13 H. Juwarker, J. M. Lenhardt, D. M. Pham and S. L. Craig, *Angew. Chem., Int. Ed.*, 2008, **47**, 3740–3743.
- 14 R. M. Meudtner and S. Hecht, *Angew. Chem., Int. Ed.*, 2008, **47**, 4926–4930.
- 15 N. L. Kilah, M. D. Wise, C. J. Serpell, A. L. Thompson, N. G. White, K. E. Christensen and P. D. Beer, *J. Am. Chem. Soc.*, 2010, **132**, 11893–11895.
- 16 B. Schulze, C. Friebe, M. D. Hager, W. Günther, U. Köhn, B. O. Jahn, H. Görls and U. S. Schubert, *Org. Lett.*, 2010, **12**, 2710–2713.
- 17 (a) M. Erdélyi, *Chem. Soc. Rev.*, 2012, **41**, 3547–3557; (b) T. M. Beale, M. G. Chudzinski, M. G. Sarwar and M. S. Taylor, *Chem. Soc. Rev.*, 2013, **42**, 1667–1680; (c) L. C. Gilday, S. W. Robinson, T. A. Barendt, M. J. Langton, B. R. Mullaney and P. D. Beer, *Chem. Rev.*, 2015, **115**, 7118–7195; (d) G. Cavallo, P. Metrangolo, R. Milani, T. Pilati, A. Priimagi, G. Resnati and G. Terraneo, *Chem. Rev.*, 2016, **116**, 2478–2601; (e) D. Bulfield and S. M. Huber, *Chem. – Eur. J.*, 2016, **22**, 14434–14450.
- 18 (a) Y.-J. Li, L. Xu, W.-L. Yang, H.-B. Liu, S.-W. Lai, C.-M. Che and Y.-L. Li, *Chem. – Eur. J.*, 2012, **18**, 4782–4790; (b) L. Xu, Y. Li, Y. Yu, T. Liu, S. Cheng, H. Liu and Y. Li, *Org. Biomol. Chem.*, 2012, **10**, 4375–4380; (c) L. Cao, R. Jiang, Y. Zhu, X. Wang, Y. Li and Y. Li, *Eur. J. Org. Chem.*, 2014, 2687–2693.

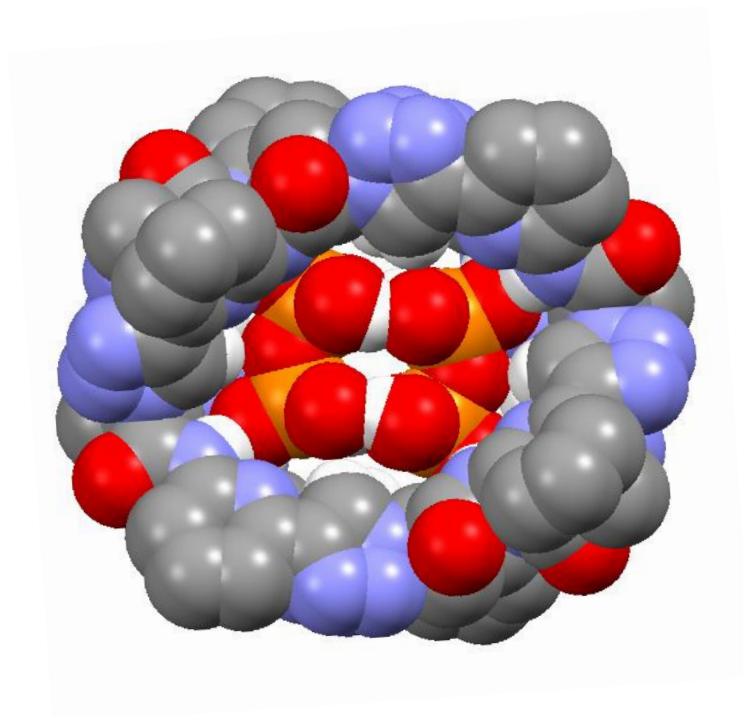
- 19 M. R. Krause, R. Goddard and S. Kubik, *J. Org. Chem.*, 2011, **76**, 7084–7095.
- 20 (a) S. Kubik, R. Goddard, R. Kirchner, D. Nolting and J. Seidel, *Angew. Chem., Int. Ed.*, 2001, **40**, 2648–2651; (b) S. Kubik and R. Goddard, *Proc. Natl. Acad. Sci. U. S. A.*, 2002, **99**, 5127–5132.
- 21 S. Kubik and R. Goddard, *J. Org. Chem.*, 1999, **64**, 9475–9486.
- 22 J. Zabrocki, J. B. Dunbar Jr., K. W. Marshall, M. V. Toth and G. R. Marshall, *J. Org. Chem.*, 1992, **57**, 202–209.
- 23 J. Broecker, C. Vargas and S. Keller, *Anal. Biochem.*, 2011, **418**, 307–309.
- 24 F. Ulatowski, K. Dąbrowa, T. Bałakier and J. Jurczak, *J. Org. Chem.*, 2016, **81**, 1746–1756.
- 25 G. Kemmer and S. Keller, *Nat. Protoc.*, 2010, **5**, 267–281.
- 26 Z. Rodriguez-Docampo, S. I. Pascu, S. Kubik and S. Otto, *J. Am. Chem. Soc.*, 2006, **128**, 11206–11210.
- 27 (a) N. Ohama, M. Machida, T. Nakamura and Y. Kunifuji, *Acta Crystallogr., Sect. C: Cryst. Struct. Commun.*, 1987, **43**, 962–964; (b) J. M. Karle and I. L. Karle, *Acta Crystallogr., Sect. C: Cryst. Struct. Commun.*, 1988, **44**, 1605–1608; (c) M. A. Hossain, M. Işiklan, A. Pramanik, M. A. Saeed and F. R. Fronczek, *Cryst. Growth Des.*, 2012, **12**, 567–571; (d) A. Rajbanshi, S. Wan and R. Custelcean, *Cryst. Growth Des.*, 2013, **13**, 2233–2237.
- 28 (a) F. Rull, A. Del Valle, F. Sobron and S. Veintemillas, *J. Raman Spectrosc.*, 1989, **20**, 625–631; (b) R. H. Wood and R. F. Platford, *J. Solution Chem.*, 1975, **4**, 977–982.
- 29 (a) V. Amendola, M. Boiocchi, D. Esteban-Gómez, L. Fabbrizzi and E. Monzani, *Org. Biomol. Chem.*, 2005, **3**, 2632–2639; (b) P. S. Lakshminarayanan, I. Ravikumar, E. Suresh and P. Ghosh, *Chem. Commun.*, 2007, 5214–5216; (c) P. Dydio, T. Zieliński and J. Jurczak, *Org. Lett.*, 2010, **12**, 1076–1078; (d) V. Blažek, N. Bregović, K. Mlinarić-Majerski and N. Basarić, *Tetrahedron*, 2011, **67**, 3846–3857; (e) V. Blažek, K. Molčanov, K. Mlinarić-Majerski, B. Kojić-Prodić and N. Basarić, *Tetrahedron*, 2013, **69**, 517–526; (f) N. Bregović, N. Cindro, L. Frkanec, K. Užarević and V. Tomišić, *Chem. – Eur. J.*, 2014, **20**, 15863–15871.
- 30 S. Mohamady and S. D. Taylor, *Org. Lett.*, 2013, **15**, 2612–2615.
- 31 C. Frassinetti, S. Ghelli, P. Gans, A. Sabatini, M. S. Moruzzi and A. Vacca, *Anal. Biochem.*, 1995, **231**, 374–382.
- 32 (a) S. Keller, C. Vargas, H. Zhao, G. Piszczek, C. A. Brautigam and P. Schuck, *Anal. Chem.*, 2012, **84**, 5066–5073; (b) J. C. D. Houtman, P. H. Brown, B. Bowden, H. Yamaguchi, E. Appella, L. E. Samelson and P. Schuck, *Protein Sci.*, 2007, **16**, 30–42; (c) G. Krainer, J. Broecker, C. Vargas, J. Fanghänel and S. Keller, *Anal. Chem.*, 2012, **84**, 10715–10722; (d) G. Krainer and S. Keller, *Methods*, 2015, **76**, 116–123.
- 33 G. Ercolani, *J. Am. Chem. Soc.*, 2003, **125**, 16097–16103.



# Chapter 3

---

## Efficient stabilization of phosphate aggregates by a cyclic pseudopeptide containing 1,4-disubstituted 1,2,3-triazole moieties



[D. Mungalpara, A. Valkonen, K. Rissanen, S. Kubik "Efficient stabilisation of a dihydrogenphosphate tetramer and a dihydrogenpyrophosphate dimer by a cyclic pseudopeptide containing 1,4-disubstituted 1,2,3-triazole moieties" *Chem. Sci.* **2017**, 8, 6003-6013]. Copyright by the Royal Society of Chemistry (RSC). Reproduced with permission.

My tasks of the work described in this publication involved the design, synthesis, purification, and characterization of the cyclic pseudooctapeptide. I also crystallized this compound in its free form and its phosphate complexes, and performed the binding studies by using ESI-MS, ITC, and NMR spectroscopy. Prof. Dr. Kari Rissanen and Dr. Arto Valkonen solved the crystal structures. Prof. Dr. Stefan Kubik acted as scientific supervisor.

**3 Chapter 3 - Efficient stabilization of phosphate aggregates by a cyclic pseudopeptide containing 1,4-disubstituted 1,2,3-triazole moieties**

### 3.1 Scope of the Work

The structural characterization of cyclic pseudopeptide **16** showed that it features the expected converging arrangement of the amide N-H and triazole C-H groups. High anion affinity was therefore observed in organic solvents in which **16** is soluble. The binding studies also revealed, however, that the interactions of **16** with the studied anions are often complex. The complexation typically involved the formation of higher complexes in which either more than one pseudopeptide binds to one anion or more than one anion binds to one pseudopeptide. This result was attributed to the fact that high conformational rigidity and the large cavity size of **16** do not allow the saturation of all hydrogen bond acceptor sites of oxoanions by a single pseudopeptide ring. A strategy to simplify complex formation would involve using a more flexible derivative of **16** that is able to fold around an anion, thus forming a 1:1 complex.

Molecular modeling indicated that a larger analog of **16**, cyclic pseudo-octa-peptide **17**, could be able to adopt folded conformations to wrap around an anion (Chart 14). Another advantage of **17** is the higher number of anion binding sites with respect to **16** that could also improve the anion affinity.

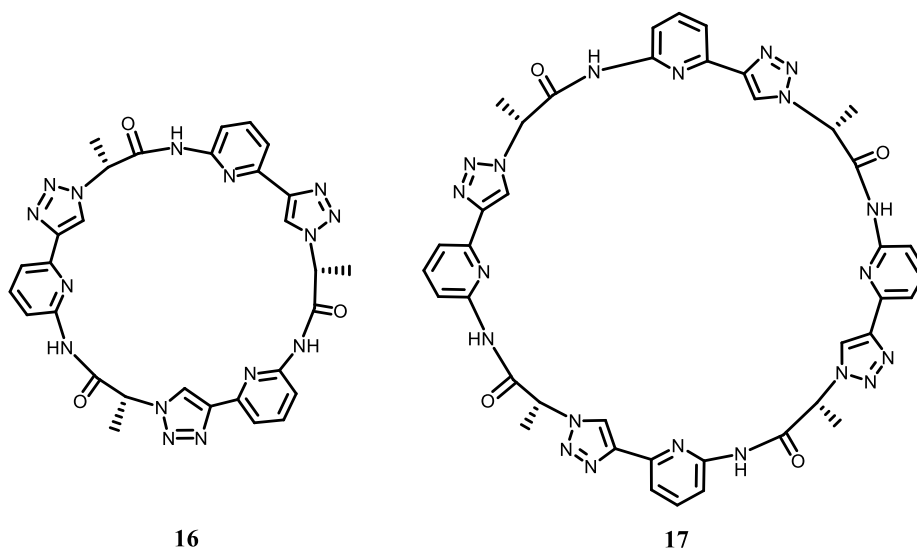
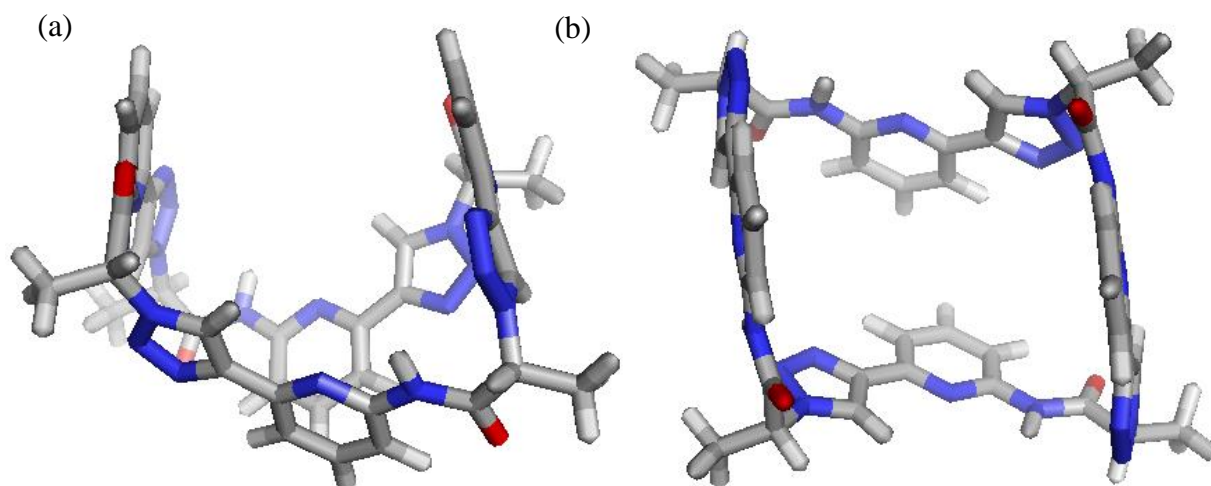


Chart 14

Figure 21 shows that **17** is able to adopt a conformation with all eight hydrogen bond donors of the amide N-H and triazole C-H groups arranged around the ring. Should an anion included into this cavity be able to interact with these binding sites, stabilization could be specifically high and should not involve formation of complexes with a higher stoichiometry. Based on this assumption, pseudopeptide **17** should be synthesized and its binding properties investigated.



**Figure 21** Calculated structure of cyclic pseudopeptide **17**: side view (a) top view (b). The calculations were performed by using the MMFF force-field implemented in Spartan 10. A Monte-Carlo conformational search was performed without restricting the number of considered conformations. After initiating the calculation, 39366 conformations were expected to be calculated. The search aborted after 122 conformations, however, after which no further improvement could be achieved.

## 3.2 Results

### 3.2.1 Synthesis

Synthesis of **17** was based on the strategy developed for **16**. The synthetic route is depicted in Figure 22 and Figure 23. The synthesis started with dimer **24**, which was also an intermediate in the synthesis of **16**. Compound **24** was converted into the azide **26** and the alkyne **27**, both of which were then coupled under CuAAC conditions to afford the linear tetramer **28** (Figure 22). The linear tetramer **28** was made ready for cyclization by, first, cleaving the TMS group and then substituting the mesylate group with an azide group to afford **28a** by using the established reaction conditions (Figure 22).

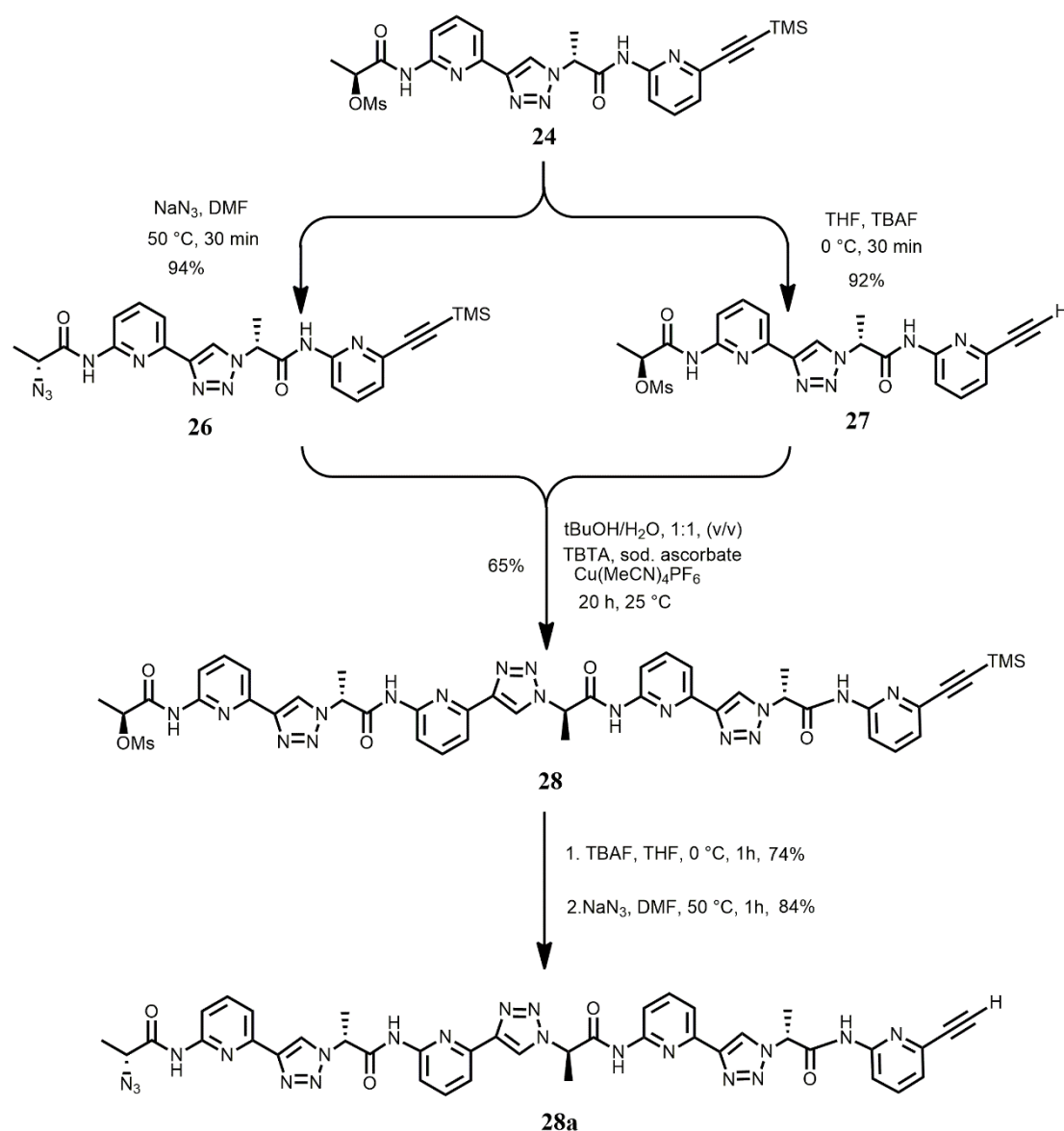
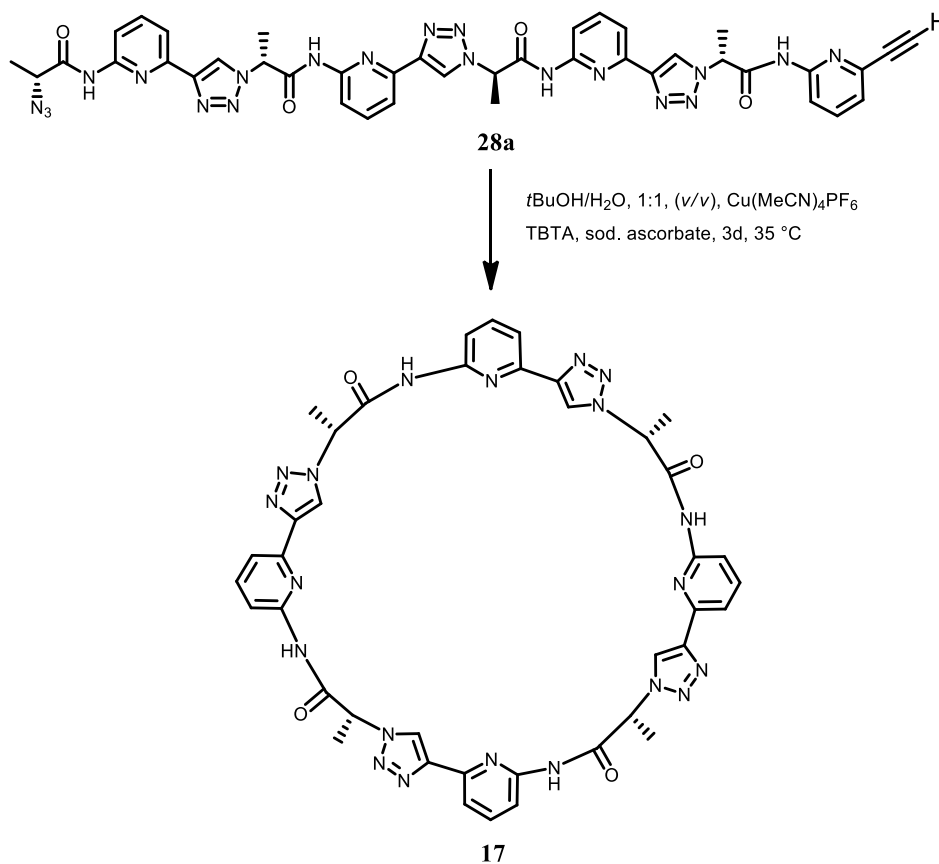


Figure 22 Synthesis of linear tetramer **28a**.

Compound **28a** was cyclized by using conditions also employed for the synthesis of **16** (Figure 23).



**Figure 23** Synthesis of the cyclic pseudooctaopeptide **17**.

For the cyclization, the linear tetramer **28a** was initially treated with 10 mol% of Cu(MeCN)<sub>4</sub>PF<sub>6</sub>, TBTA, and sodium ascorbate in *tert*-butanol/water, 1:1 (v/v) and the progression of the cyclization was followed by HPLC.

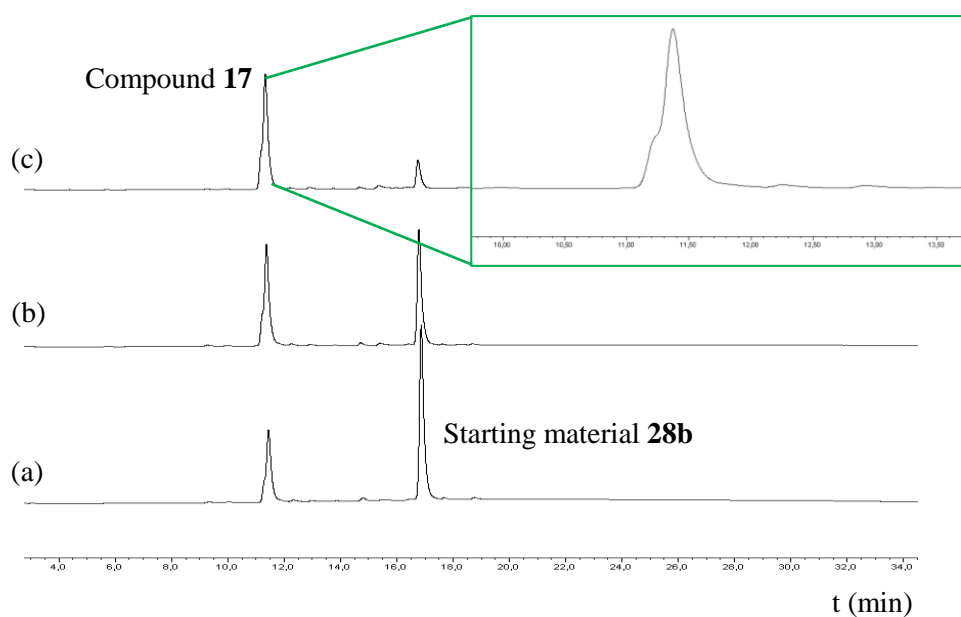


**Figure 24** HPLC chromatograms of the cyclization reaction in *tert*-butanol/water, 1:1 (v/v) after 24 h (a), 48 h (b), and 72 h (c). Extra 5 mol% of  $\text{Cu}(\text{MeCN})_4\text{PF}_6$  and TBTA were added after every 24 h.

By assuming that the product **17** and the starting material **28b** have same extinction coefficients, Figure 24 shows that conversion only amounted to *ca.* 30 % after 24 h with a large amount of the starting material still being present. Therefore, additional 5 mol% of  $\text{Cu}(\text{MeCN})_4\text{PF}_6$  and TBTA were added every day which caused the starting material to be nearly consumed after 72 h. The shape of the product peak at the end of the reaction indicated the presence of an impurity with almost the same retention time. Both products could be separated by column chromatography on silica gel using DCM/acetone 2:1 (v/v) as the eluent during work-up. MALDI-TOF mass spectrometric analysis showed that the two products have the same mass, indicating that they are isomers.

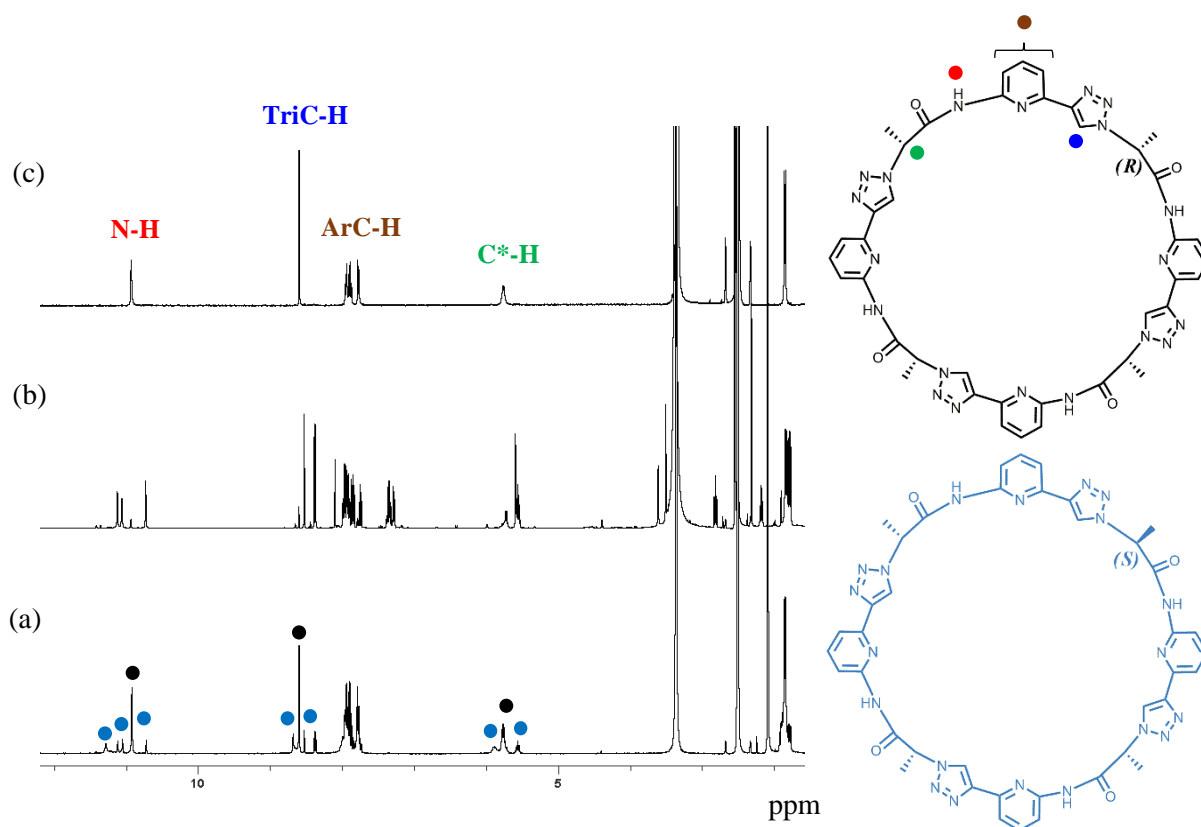


**Figure 25**  $^1\text{H-NMR}$  spectra recorded in  $\text{DMSO-}d_6$  of the product mixture (a), and of the major (b) and the minor (c) component of the isolated mixture. The signals assigned are indicated in the structure on the right hand side by using the same color code. The signals denoted with the blue and the black dots represent the ones of the minor and the major product, respectively.

The major fraction of the purified product has a simple  $^1\text{H-NMR}$  spectrum (Figure 25c), indicating that it is the desired  $C_4$  symmetric product. The minor fraction has a complex  $^1\text{H-NMR}$  spectrum (Figure 25b) which shows that this compound has a reduced symmetry. Preliminary X-ray crystallographic results indicated that this minor product contains one *S*-configured stereogenic center while all the others have the correct *R*-configuration (Figure 25). Formation of this product thus results from epimerization of a stereogenic center during one synthetic step. Since no evidence for the formation of diastereomers could be found in the  $^1\text{H-NMR}$  spectra of the linear precursors of **17**, epimerization likely only occurs during or after cyclization, which was performed at an elevated temperature.<sup>76</sup> Further information about the synthesis and purification of **17** is available in the manuscript (Chapter 3.5).

### 3.2.2 Structural Assignment and Anion Binding Properties

The results of the structural assignment of pseudopeptide **17** and of the anion binding studies are described in the manuscript (Chapter 3.5). Only the most important results will therefore be summarized here.

<sup>1</sup>H-NMR spectroscopy indicates that **17** adopts an averaged C<sub>4</sub> symmetrical conformation in DMSO-*d*<sub>6</sub>. The NOESY NMR spectrum in the same solvent shows that the amide N-H, triazole C-H, and the C\*-H are oriented in one direction.

Binding studies were restricted to three anions, namely, sulfate, DHP, and DHPP as guests in 2.5 vol% water/DMSO to allow comparison with the properties of the smaller analog **16**, whose interactions with anions were studied under analogous conditions. Binding studies were performed by using ESI mass spectrometry, <sup>1</sup>H-NMR spectroscopy, and microcalorimetry.

The ESI mass spectra of solutions of **17** (0.5 mM) in DCM containing the TBA salts of sulfate (1 equiv), DHPP (1 equiv), or DHP (2 equiv) show signals at *m/z* ratios that could be assigned to the respective anion complexes of the pseudopeptide. In the case of sulfate, a signal for the 1:1 complex was observed, whereas the signals visible in the spectra recorded in the presence of DHP and DHPP were consistent with (**17**·DHP)<sub>2</sub> and (**17**·DHPP)<sub>2</sub>, respectively (Table 3). These spectra thus indicate that only sulfate seems to form the expected 1:1 complex with **17** while the phosphate-derived anions prefer the formation of higher complexes.

**Table 3** Main signals (*m/z*) present in the ESI mass spectra of solutions of **17** (0.5 mM) in DCM containing different anions as their respective TBA salts.

anion	Equiv	<i>m/z</i>	Complex
sulfate	1.0	859.49	[ <b>17</b> -H] <sup>-</sup>
		1198.54	[( <b>17</b> ·SO <sub>4</sub> <sup>2-</sup> )·TBA] <sup>-</sup>
DHP	2.0	783.89	[( <b>17</b> DHP) <sub>2</sub> ·TBA] <sup>3-</sup>
		957.38	[ <b>17</b> ·DHP] <sup>-</sup>
		1297.00	[( <b>17</b> ·DHP) <sub>2</sub> ·TBA <sub>2</sub> ] <sup>2-</sup>
DHPP	1.0	771.89	[( <b>17</b> ·DHPP) <sub>2</sub> ·TBA] <sup>3-</sup>
		1279.02	[( <b>17</b> ·DHPP) <sub>2</sub> ·TBA <sub>2</sub> ] <sup>2-</sup>

X-ray crystallographic analysis of crystals of the DHP and DHPP complexes of **17** confirmed these stoichiometries, showing that the DHPP complex comprises a dimer of this anion sandwiched between two pseudopeptide rings while two pseudopeptides bind to a tetramer of the anion in the case of the DHP complex (Figure 26). When crystals of **17** were grown from acetone in the presence of TBA HPP, the sandwich-type complex between **17** and the DHPP

dimer was also found, indicating that complex formation is associated with anion protonation (Figure 26). Moreover, the thus obtained crystals are centrosymmetric and contain both enantiomers of **17**. The receptor therefore seems to racemize in the presence of (basic) HPP anions.

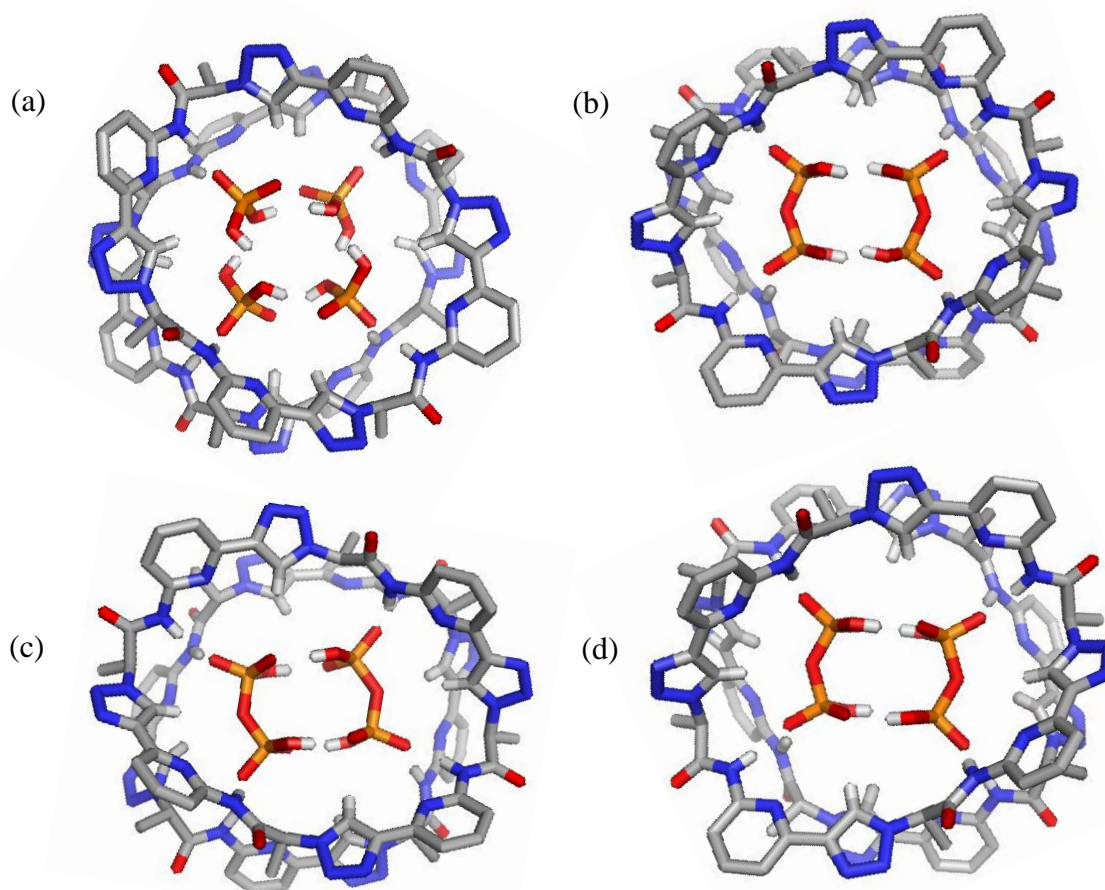


**Figure 26** Crystal structures of  $(\mathbf{17}\cdot\text{DHP})_2$  (a)  $(\mathbf{17}\cdot\text{DHPP})_2$  (b)  $((S)\mathbf{17}\cdot\text{DHPP})_2$  (c)  $((R)\mathbf{17}\cdot\text{DHPP})_2$  (d) complexes.

$^1\text{H-NMR}$  spectroscopy showed that complex formation also takes place in solution. Figure 27 shows the  $^1\text{H-NMR}$  spectra of solutions of **17** in 2.5 vol%  $\text{D}_2\text{O}/\text{DMSO-}d_6$  containing the TBA salts of DHP (2 equiv), HPP (0.5 equiv), DHPP (0.5 equiv), and sulfate (0.5 equiv) in comparison to the  $^1\text{H-NMR}$  spectrum of the free pseudopeptide.

In the presence of sulfate, signal shifts are observed of the triazole C-H and C\*-H signals of **17** that are qualitatively similar albeit smaller than the shifts observed in the  $^1\text{H-NMR}$  spectrum when TBA sulfate was added to pseudopeptide **16** in the same solvent. Since only a single set of signals is visible in the presence of substoichiometric amount of sulfate, complex formation is fast on the NMR time-scale. In contrast, two sets of signals appear in the spectra once a

phosphate derived anion is present, accounting for binding equilibria that are slow on the NMR time-scale. Moreover, the signal set belonging to the complex contains twice the number of signals in comparison to the spectrum of free receptor, which shows that the averaged  $C_4$  symmetry of **17** is reduced to  $C_2$  upon phosphate binding.

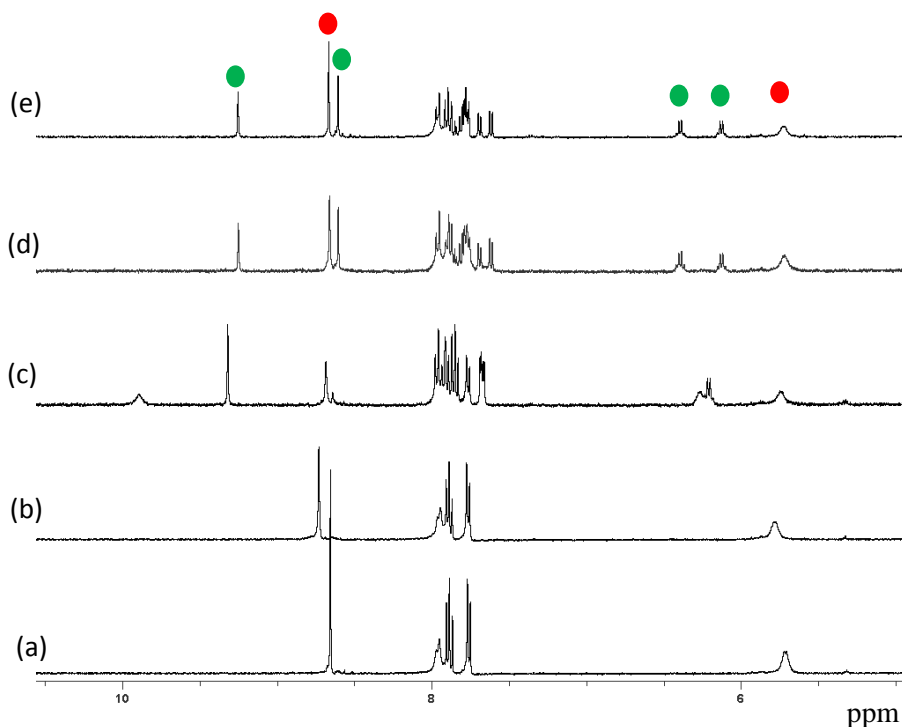


**Figure 27**  $^1\text{H-NMR}$  spectra of **17** (0.5 mM) in 2.5 vol%  $\text{D}_2\text{O}/\text{DMSO-}d_6$  in the absence (a) and the presence of TBA sulfate (0.5 equiv) (b), DHP (2 equiv) (c), HPP (0.5 equiv) (d), DHPP (0.5 equiv) (e). The signals denoted with the green and the red dots represent the ones of **17** in the free and complexed states, respectively.

ITC confirmed that TBA sulfate forms 1:1 complex with **17** in 2.5 vol% water/DMSO. The stability constant of the corresponding complex is one order of magnitude lower than that of the 1:1 sulfate complex of **16** (Table 4). Moreover, ring enlargement causes sulfate binding to go from exothermic for **16** to endothermic for **17**.

**Table 4** Stability constants and thermodynamic parameters of the TBA sulfate complexes of **16** and **17** in 2.5 vol% water/DMSO.

Receptor	$\log K_{11}^a$	$\log K_{21}^b$	$\Delta H_{11}^{\circ c}$ kJ/mol	$T\Delta S_{11}^{\circ c}$ kJ/mol
<b>16</b>	4.2	< 3.2	-9.8	12.2
<b>17</b>	3.2	-	6.1	23.6

<sup>a</sup>Equilibrium constant describing the formation of the 1:1 complex. <sup>b</sup>Equilibrium constant describing the formation of the **16**<sub>2</sub>·SO<sub>4</sub><sup>2-</sup> complex from the 1:1 complex. <sup>c</sup>Enthalpies and entropies associated with the formation of the 1:1 complexes.

The complexation of DHP and DHPP by **17** is strongly exothermic. Deriving binding constants for the individual binding steps associated with the formation of **17**<sub>2</sub>·(DHP)<sub>4</sub> and **17**<sub>2</sub>·(DHPP)<sub>2</sub> complexes from the binding isotherms proved to be not possible because too many species are involved in the equilibria. The sharp transition of the binding isotherm indicated, however, that complex formation proceeds in a cooperative fashion in the case of DHPP. On the other hand, the isotherm of the DHP complexation has a complex shape, thus, a part of isotherm was considered during the quantification of the stability constant. The binding isotherms were therefore fitted by using a simplified binding model that neglects the oligomerization equilibrium of the DHP and DHPP anions and assuming that the DHPP dimer or the DHP tetramer bind as a single entity to two molecules of **17** in a stepwise fashion. The thus obtained binding constants are summarized in Table 5.

**Table 5** Stability constants and thermodynamic parameters of the TBA DHP and DHPP complexes of **17** in 2.5 vol% water/DMSO.

Anion	$\log K_{11}^a$	$\log K_{21}^b$	$\log \beta$	$\Delta H^{\circ c}$ kJ/mol	$T\Delta S^{\circ c}$ kJ/mol
DHPP	6.3	6.4	12.7	-53.3	19.1
DHP <sup>d</sup>	5.6	4.0	9.6	-42.8	12.0

<sup>a</sup>Equilibrium constants describing the formation of the **17**·(DHP)<sub>4</sub>/**17**·(DHPP)<sub>2</sub> complexes. <sup>b</sup>Equilibrium constants describing the formation of the **17**<sub>2</sub>·(DHP)<sub>4</sub>/**17**<sub>2</sub>·(DHPP)<sub>2</sub> complexes from the respective **17**·(DHP)<sub>4</sub>/**17**·(DHPP)<sub>2</sub> complexes. <sup>c</sup>Cumulative enthalpies and entropies associated with the formation of the **17**<sub>2</sub>·(DHP)<sub>4</sub>/**17**<sub>2</sub>·(DHPP)<sub>2</sub> complexes.

### 3.3 Discussion

The design of **17** was based on the assumption that this pseudopeptide can fold around an anion so that formation of higher complexes that were observed for **16** could be avoided. According to  $^1\text{H-NMR}$  and NOESY NMR spectroscopy, **17** adopts an averaged  $C_4$  symmetric conformation in solution with all H-bond donors oriented into the same direction. The converging arrangement of neighboring N-H, TriC-H and C\*-H protons is also visible in the calculated structure of **17** (Figure 21). This calculated structure is, however,  $C_2$  symmetric and therefore less symmetric than the averaged conformation detected in solution because of the folding of the macrocycle. It is therefore reasonable to assume that **17** is flexible in solution, which causes averaging over several conformations, possibly including the ones that are most stable according to the calculations, so that a simple  $^1\text{H-NMR}$  spectrum results. The low solubility of **17** in organic solvents precluded measuring  $^1\text{H-NMR}$  spectra at lower than room temperature to confirm this assumption.

The presence of sulfate anions in 2.5 vol%  $\text{D}_2\text{O}/\text{DMSO-}d_6$  causes typical downfield shifts of H-bond donor protons of **17** in the  $^1\text{H-NMR}$  spectrum, indicating that the anion is hydrogen bonded to these protons. Microcalorimetry indicated formation of a 1:1 complex of moderate stability. Complexation is associated with a small favourable entropic and an unfavourable enthalpic contribution. The unfavorable enthalpy is attributed to the weak hydrogen bonding interactions between sulfate and the receptor due to the improper fit of the anion into the large cavity whereas the favourable entropy could be due to the release of solvent molecules from the receptor and the anion upon binding.

The complexation of phosphate derived anions by **17** is more interesting. Pseudopeptide **17** is able to stabilize a tetramer of DHP and a dimer of DHPP by sandwiching these anionic aggregates between two pseudopeptide rings. Pseudopeptide **17** therefore shares with the smaller analog **16** the ability to stabilize the aggregates of phosphate-derived anions. The respective complexes of **17** are, however, structurally better defined as the same stoichiometries were found in the solid state, in solution, and even in the gas phase. The cyclic arrangement of four DHP anions in the DHP complex of **17** has so far not been observed in other system. A DHPP dimer, has been observed in the respective complex of a pyrrole-derived receptor.<sup>82</sup>

While the conformation of the individual pseudopeptide rings are almost  $C_4$  symmetric in these complexes, the overall symmetry of the complexes is  $C_2$  because the two pseudopetides adopts an offset arrangement. This arrangement seems to be retained in

solution and the dynamic exchange is slow on the NMR time-scale as demonstrated by the splitting of the signals of **17** in the  $^1\text{H}$ -NMR spectrum into two signal sets upon complex formation.

No quantitative information about complex stability could be derived by NMR spectroscopy and the stability of the DHPP and DHP complexes was therefore evaluated in 2.5 vol% water/DMSO by using microcalorimetry.

These investigations indicate that the binding of these anions to **17** seems to proceed in a highly cooperative fashion, involving a single step in the binding isotherms. These isotherms were therefore fitted to a simplified binding model, which neglected the oligomerization equilibria of the anions. With a  $\log K_{11}$  of 6.3 and a  $\log K_{21}$  of 6.4, the stepwise binding constants of the DHPP complex are nearly equal in size, leading to a  $\log \beta$  of 12.7 for the overall stability of the complex. This  $\log \beta$  only qualitatively reflects the actual stability of the DHPP complex of **17** as the oligomerization equilibrium of the anion is neglected. The fact that the second stability constant is larger than  $\log (K_{11}/4)$  is consistent with cooperative binding.<sup>83</sup> The thermodynamic parameters associated with the overall binding constants indicate that DHPP and DHP binding is enthalpically (negative  $\Delta H$ ) as well as entropically favourable (positive  $T\Delta S$ ). Stability of the  $(\mathbf{17}\cdot\text{DHP})_2$  and  $(\mathbf{17}\cdot\text{DHPP})_2$  complexes is in fact so high that these complexes can even be transferred into the gas phase without decomposition as demonstrated by ESI mass spectrometry. The high stability of these complexes could be attributed to various attractive interactions between the complex components, namely, hydrogen-bonding between the anions, multiple hydrogen bonding interactions between the anion oligomers and the hydrogen bond donors of **17**, and dispersive interactions between the closely arranged pseudopeptide rings. In combination, these stabilizing effects allow to overcome charge repulsion of the individual anions.

The propensity of **17** to bind to the DHPP dimer is also reflected by the fact that the  $(\mathbf{17}\cdot\text{DHPP})_2$  complex even forms when TBA HPP was used instead of TBA DHPP as substrate. Complex formation thus causes a shift of the HPP/DHPP protonation equilibrium to the diprotonated form of the anion, which can then be bound. The protons required for this process likely derive from the water present in the solvent, which should cause the solution to become basic. The concomitant basicity of the solution would explain why the pseudopeptide seems to racemize in the presence of HPP.

In conclusion, by enlarging the ring of **16** to afford **17**, the anion binding equilibrium could be simplified but only for sulfate, with the corresponding complexes being not very

stable. A more interesting feature of pseudopeptide **17** is its ability to stabilize aggregates of phosphate-derived anions. The high stability of the corresponding complexes could allow the development of phosphate selective receptors whose selectivity derives from the unique ability of such anions to form higher aggregates.

### **3.4 Summary**

The cyclic pseudooctapeptide **17** containing 1,4-disubstituted 1,2,3-triazole moieties was synthesized. This pseudooctapeptide binds to the sulfate anion in 2.5 vol% water/DMSO in the form of a 1:1 complex with moderate affinity ( $\log K_a = 3.2$ ). Dihydrogen phosphate (DHP) and dihydrogen pyrophosphate (DHPP) anions are, however, strongly bound. Complexation of these anions involves sandwiching of a DHPP dimer or a DHP tetramer between two pseudopeptide rings. The structure of these complexes was determined by X-ray crystallography.  $^1\text{H-NMR}$  spectroscopy, mass spectrometry, and isothermal titration calorimetry showed that they are highly stable in solution (2.5 vol% water/DMSO) and in the gas phase. This stability was attributed to multiple hydrogen bonding between the individual anions and between the anion oligomers and the hydrogen bond donors of **17**. In addition, dispersive interactions between the closely arranged pseudopeptide rings in the sandwich complexes likely also contribute to complex stability.

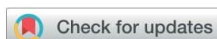
## 3.5 Manuscript

Chemical  
Science



EDGE ARTICLE

View Article Online  
View Journal | View Issue



Cite this: *Chem. Sci.*, 2017, 8, 6005

### Efficient stabilisation of a dihydrogenphosphate tetramer and a dihydrogenpyrophosphate dimer by a cyclic pseudopeptide containing 1,4-disubstituted 1,2,3-triazole moieties†‡

Disha Mungalpara,<sup>a</sup> Arto Valkonen,<sup>b</sup> Kari Rissanen<sup>b</sup> and Stefan Kubik<sup>\*a</sup>

A cyclic pseudooctapeptide **2** is described containing 1,4-disubstituted 1,2,3-triazole moieties. This compound features eight converging hydrogen bond donors along the ring, namely four amide NH and four triazole CH groups, which enable **2** to engage in interactions with anions. While fully deprotonated sulfate anions exhibit only moderate affinity for **2**, protonated anions such as dihydrogenpyrophosphate and dihydrogenphosphate anions are strongly bound. Complexation of the phosphate-derived anions involves sandwiching of a dihydrogenpyrophosphate dimer or a dihydrogenphosphate tetramer between two pseudopeptide rings. X-ray crystallography provided structural information, while <sup>1</sup>H NMR spectroscopy, mass spectrometry, and isothermal titration calorimetry demonstrated that these complexes are stable in solution (2.5 vol% water/DMSO) and can even be transferred without decomposition into the gas phase. The observed high thermodynamic stabilities are attributed to the mutual reinforcement of the interactions between the individual complex components, namely, hydrogen-bonding between the anions, multiple hydrogen bonding interactions between the anion aggregates and the triazole CH and NH hydrogen bond donors of **2**, and potential dispersive interactions between the closely arranged pseudopeptide rings. Pseudopeptide **2** thus represents a promising lead for the construction of phosphate receptors, whose binding selectivity makes use of the unique ability of certain anions to assemble into higher aggregates.

Received 16th June 2017  
Accepted 12th July 2017

DOI: 10.1039/c7sc02700a  
rsc.li/chemical-science

## Introduction

Coulomb's law states that particles with a like electrical charge repel each other.<sup>1</sup> As a consequence, two isolated cations or anions are expected to maximise their distance thus minimising the electrostatic repulsion. Repulsion can be avoided if the charges of the ions are screened by an appropriate ligand as in complexes of larger crown ethers folding around two cations,<sup>2</sup> or complexes of certain anion receptors binding to two halides.<sup>3</sup> A special situation arises in anion coordination chemistry<sup>4</sup> if the anion is protonated. In this case, Coulomb repulsion of the anions can be compensated by hydrogen-bonding interactions, allowing protonated anions to form dimers or larger aggregates in which every

individual component is negatively charged. While there recently has been controversy in the literature about the exact nature of the underlying interactions,<sup>5</sup> such aggregates are generally believed to be stabilised by attractive electrostatic interactions in the hydrogen bond that balance electrostatic repulsion.<sup>6</sup>

Aggregates of anions have been experimentally detected in the solid state,<sup>7–10</sup> and in solution.<sup>11</sup> They can be stabilised by organic ligands as the examples of complexes demonstrate containing hydrogensulfate anions,<sup>7a–f</sup> sulfate anions,<sup>7g</sup> sulfate anions bridged by water molecules,<sup>7h</sup> or dihydrogenphosphate anions.<sup>8–10</sup> Phosphates, in particular, have been shown to assemble into a wide variety of different structures, ranging from dimers<sup>8</sup> to larger linear<sup>9</sup> or cyclic oligomers.<sup>10</sup> There is ample evidence for the supramolecular stabilisation of anion aggregates in the solid state, but reports that demonstrate the survival of these complexes in solution are scarce.<sup>11</sup> A notable exception came from the Flood group who showed that their cyanostar receptor stabilises the hydrogensulfate dimer.<sup>12</sup> NMR spectroscopy clearly revealed the existence of the respective complex in chloroform. The authors were even able to detect the signal of the bridging protons in the anion dimer by NMR spectroscopy and they demonstrated the stability of the complex in the gas phase by mass spectrometry. In addition, a bis-calix[4]pyrrole receptor has recently been described by the

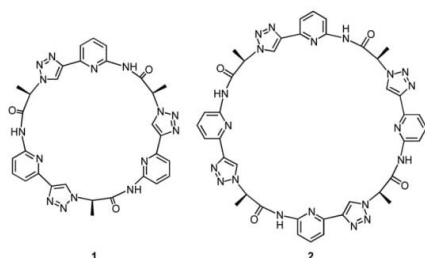
<sup>a</sup>Technische Universität Kaiserslautern, Fachbereich Chemie – Organische Chemie, Erwin-Schrödinger-Straße, 67663 Kaiserslautern, Germany. E-mail: kubik@chemie.uni-kl.de

<sup>b</sup>University of Jyväskylä, Department of Chemistry, Nanoscience Center, P.O. Box 35, Jyväskylä FI-40014, Finland

† In memoriam Fritz Vögtle (1939–2017).

‡ Electronic supplementary information (ESI) available: Synthetic details, NMR spectroscopic and MS spectrometric characterisation of **2**, NMR spectroscopic and mass spectrometric binding studies, ITC titrations, and crystal structures. CCDC 1555955–1555958. For ESI and crystallographic data in CIF or other electronic format see DOI: 10.1039/c7sc02700a

Sessler group, which was shown to bind two dihydrogenphosphate anions, two sulfate anions bridged by water molecules, and two pyrophosphate anions.<sup>13</sup>



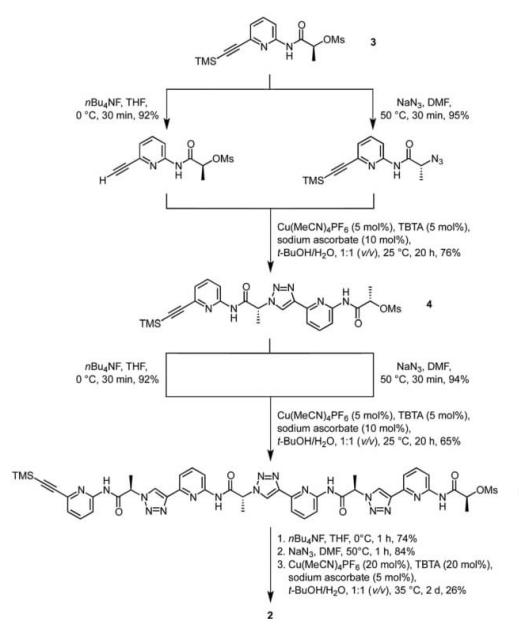
Our group recently introduced the cyclic pseudopeptide **1** containing 1,4-disubstituted 1,2,3-triazole moieties.<sup>14</sup> This compound prefers conformations in solution with the protons on the NH groups and those on the triazole moiety converging to the centre of the macrocycle, well preorganised for anion binding. Binding of oxoanions such as sulfate and dihydrogenphosphate (DHP) was detected in 2.5 vol% water/DMSO, but the binding equilibria were rather complex, likely because of the inability of **1** to saturate all hydrogen bond acceptors of the investigated anions. In the case of sulfate, we detected the formation of complexes with two receptor molecules binding to one anion. DHP recognition, on the other hand, involved binding of two DHP anions to one receptor in solution, a complex stoichiometry consistent with the dimer of the DHP anion acting as guest. The crystal structure of the corresponding complex revealed that two molecules of **1** bind to a linear DHP trimer in the solid state, confirming the ability of **1** to stabilise DHP aggregates.

Here, we show that the higher cyclic oligomer of **1**, cyclic pseudooctapeptide **2**, has an even more pronounced propensity to stabilise such anion aggregates. Compound **2** was originally synthesised in the hope that it would fold around oxoanions as some of the large macrocyclic receptors introduced by Katayev and Sessler,<sup>15</sup> thus yielding simple 1 : 1 complexes. We found, however, that **2** prefers to bind a DHP tetramer and a dimer of dihydrogenpyrophosphate (DHPP) anions by sandwiching these aggregates between two macrocyclic rings. The complexes persist in solution (2.5 vol% water/DMSO) and can also be detected in the gas phase. Considering that the DHP complex comprises six individual components this stability is remarkable, clearly illustrating the substantial stabilising effect of receptor **2**. Pseudopeptide **2** thus represents a promising lead compound for the construction of phosphate receptors, whose binding selectivity is not governed by size or shape complementarity between the host and individual anions but makes use of the unique ability of certain protonated anions to assemble into higher aggregates.

## Results and discussion

### Synthesis and structural characterisation

Synthesis of **2** was based on the strategy developed for **1** (Scheme 1). It started with building block **3** of which one



Scheme 1 Synthesis of cyclic pseudopeptide **2**.

portion was TMS deprotected and an equivalent portion converted into the azide by substitution of the mesylate group. The products thus obtained were then coupled under copper(I)-catalysis to afford dimer **4**. This dimer, which was also used for the synthesis of **1**,<sup>14</sup> was now chain elongated to the corresponding linear tetramer **5** by using a related three step sequence. The terminal groups of **5** were prepared for cyclisation and the subsequent cyclisation was then performed under dilution conditions to suppress oligomerisation. After chromatographic purification, **2** was obtained in analytically pure form.

It should be noted that a side product was isolated during purification that did not exhibit the simple <sup>1</sup>H NMR spectrum of the C<sub>4</sub> symmetric **2** but a more complex one. This side product also represents a cyclic tetramer according to MS whose reduced symmetry is presumably caused by partial epimerisation. Epimerisation likely only occurs during or after cyclisation since no evidence for the presence of stereoisomers could be found in the <sup>1</sup>H NMR spectra of the linear precursors.

<sup>1</sup>H NMR spectroscopy indicates that **2** adopts an averaged C<sub>4</sub> symmetric conformation in DMSO-*d*<sub>6</sub>. The NOESY NMR spectrum in the same solvent features crosspeaks between the NH, triazole CH, and the C<sup>\*</sup>H signals, the latter of which correspond to the protons on the stereogenic centres. These crosspeaks account for the spatial proximity of the respective sets of protons (see ESI<sup>†</sup>). Since no crosspeak is visible between the NH signal and the signal of the aromatic C<sup>3</sup>H, the preferred conformation of **1**, characterised by a converging arrangement of the NH, triazole CH, and C<sup>\*</sup>H protons, seems to be retained upon ring enlargement.

### Anion binding studies

Binding studies were restricted to 2.5 vol% water/DMSO as solvent and to the oxoanions sulfate, dihydrogenphosphate (DHP), and (di)hydrogenpyrophosphate [(D)HPP] as guests to allow comparison with the previous work on receptor **1**, whose interactions with the same anions was studied under analogous conditions.<sup>14</sup> Anions such as halides and nitrate were excluded because they did not exhibit detectable affinity to **1** in DMSO.

**Sulfate binding.** Addition of 2 equiv. of TBA sulfate to a solution of **2** in 2.5 vol% D<sub>2</sub>O/DMSO-*d*<sub>6</sub> produced downfield shifts of the triazole CH signal by 0.35 ppm and of the C\*H signal by 0.30 ppm. The extent of the shift of the triazole CH signal is significantly smaller than the one observed for the smaller pseudopeptide **1** under the same conditions (see ESI<sup>†</sup>), while that of the C\*H signal is larger.<sup>14</sup> The binding mode of the two receptors therefore seems to differ with the relatively moderate shift of the triazole CH signal indicating that interactions of **2** with the sulfate anion might be weaker than those of **1**.

The ESI mass spectrum of a solution of **2** in dichloromethane containing 1 equiv. of TBA sulfate, recorded in the negative mode, exhibits two major signals (see ESI<sup>†</sup>). Besides the signal of the deprotonated receptor also a strong signal is visible whose *m/z* ratio can be assigned to the 1 : 1 complex 2·SO<sub>4</sub><sup>2-</sup> with one TBA cation partially balancing the two negative charges. No evidence for the presence of higher complexes could be detected. The preferential formation of a 1 : 1 complex is also consistent with the shape of the ITC isotherm obtained by titrating **2** with TBA sulfate in 2.5 vol% H<sub>2</sub>O/DMSO. The resulting stability constant log *K*<sub>a</sub> amounts to 3.1 ( $\Delta H = +6.1$  kJ mol<sup>-1</sup>,  $T\Delta S = +23.6$  kJ mol<sup>-1</sup>), rendering the sulfate complex of **2** more than one order of magnitude less stable than the corresponding 1 : 1 complex of **1**.<sup>14</sup> Moreover, ring enlargement causes sulfate binding to go from exothermic for **1** to endothermic for **2** in 2.5 vol% water/DMSO.

The stoichiometry of the sulfate complex suggests that **2** can indeed fold around an anion as predicted, but binding seems to be not very efficient. While the exact mode of complex formation unfortunately could not be elucidated, it is very likely that it differs profoundly from the one observed for protonated phosphate-derived anions (*vide infra*).

**Dihydrogenpyrophosphate binding.** Crystals of the complex between **2** and DHPP with modest quality for X-ray crystallography were obtained from a solution of **2** in DMSO containing 1 equiv. of TBA DHPP. Fig. 1 shows that anion binding in the solid-state involves sandwiching of a hydrogen-bonded DHPP dimer between two pseudopeptide rings resulting in an overall C<sub>2</sub> symmetric complex. The hydrogen bonding pattern of the DHPP dimer commences through pairs of oxygen atoms on each phosphorus atom with O···O distances between 2.53 Å and 2.55 Å. The four remaining oxygen atoms point into the corners of the rectangular complex, interacting with the pseudopeptide rings. It should be noted that a similar hydrogen-bonded DHPP dimer has recently been found in the complexes of non-cyclic pyrrole-derived receptors developed in the Sessler group.<sup>16</sup>

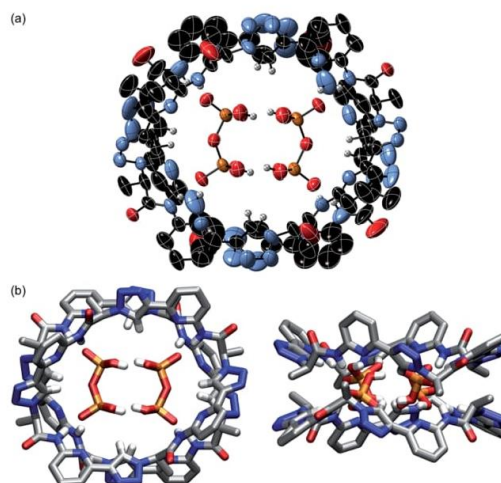


Fig. 1 Molecular structure of 2·DHPP<sub>2</sub> showing the 2 : 2 association of the pseudopeptide and two DHPP anions with the thermal ellipsoids shown at the 50% probability level (a). The TBA cations and the hydrogen atoms except those on the NH and triazole CH groups are omitted for clarity. (b) shows the same structure as a stick model from the top (left) and the side (right) to further illustrate the arrangement of the binding partners.

The pseudopeptide rings in 2·DHPP<sub>2</sub> adopt a slightly distorted conformation with a lower than the ideal C<sub>4</sub> symmetry. Each vacant oxygen atom of the anion dimer is hydrogen-bonded to two NH groups of **2**, one from the upper and one from the lower ring in the sandwich. The N···O distances range between 2.76 and 2.84 Å. Four opposing triazole CH bonds face the oxygen atoms of the anion dimer that are involved in the hydrogen-bonding interactions. The C···O distances of 3.65–3.85 Å indicate that this interaction is also weakly stabilising. The other four triazole CH bonds face the bridging oxygen atom of the anions at distances of 3.65–3.80 Å. Two TBA counterions fill the bowl-shaped cavities of the pseudopeptide rings, one on each side forming the sandwiched 2 × 2 × 2 complex (see ESI<sup>†</sup>). The remaining two TBA cations could not be located due to the severe disorder in the crystal.

The space filling model shown in Fig. S1a<sup>†</sup> illustrates that the overall structure of the complex is very compact and that the DHPP dimer perfectly fills the space between the two pseudopeptide rings. Both rings are structurally nicely complementary, allowing them to closely approach each other in the sandwich as visible in the respective side view in Fig. S1b.<sup>†</sup> The arrangement of NH and CH hydrogen bond donors from both rings above one another causes the methyl groups in the side chains of one ring to be arranged above the aromatic rings of the other pseudopeptide (Fig. 1b), indicating that dispersive interactions between the rings could contribute to stabilise the whole aggregate.

NMR spectroscopy demonstrates that the binding mode seen in the crystal structure of the DHPP complex of **2** persists in solution. The effects of TBA DHPP on the <sup>1</sup>H NMR spectrum of **2** in 2.5 vol% D<sub>2</sub>O/DMSO-*d*<sub>6</sub> are shown in Fig. 2.

**Anion binding studies**

Binding studies were restricted to 2.5 vol% water/DMSO as solvent and to the oxoanions sulfate, dihydrogenphosphate (DHP), and (di)hydrogenpyrophosphate [(D)HPP] as guests to allow comparison with the previous work on receptor **1**, whose interactions with the same anions was studied under analogous conditions.<sup>14</sup> Anions such as halides and nitrate were excluded because they did not exhibit detectable affinity to **1** in DMSO.

**Sulfate binding.** Addition of 2 equiv. of TBA sulfate to a solution of **2** in 2.5 vol% D<sub>2</sub>O/DMSO-*d*<sub>6</sub> produced downfield shifts of the triazole CH signal by 0.35 ppm and of the C\*H signal by 0.30 ppm. The extent of the shift of the triazole CH signal is significantly smaller than the one observed for the smaller pseudopeptide **1** under the same conditions (see ESI<sup>†</sup>), while that of the C\*H signal is larger.<sup>14</sup> The binding mode of the two receptors therefore seems to differ with the relatively moderate shift of the triazole CH signal indicating that interactions of **2** with the sulfate anion might be weaker than those of **1**.

The ESI mass spectrum of a solution of **2** in dichloromethane containing 1 equiv. of TBA sulfate, recorded in the negative mode, exhibits two major signals (see ESI<sup>†</sup>). Besides the signal of the deprotonated receptor also a strong signal is visible whose *m/z* ratio can be assigned to the 1 : 1 complex 2·SO<sub>4</sub><sup>2-</sup> with one TBA cation partially balancing the two negative charges. No evidence for the presence of higher complexes could be detected. The preferential formation of a 1 : 1 complex is also consistent with the shape of the ITC isotherm obtained by titrating **2** with TBA sulfate in 2.5 vol% H<sub>2</sub>O/DMSO. The resulting stability constant log *K*<sub>a</sub> amounts to 3.1 ( $\Delta H = +6.1$  kJ mol<sup>-1</sup>,  $T\Delta S = +23.6$  kJ mol<sup>-1</sup>), rendering the sulfate complex of **2** more than one order of magnitude less stable than the corresponding 1 : 1 complex of **1**.<sup>14</sup> Moreover, ring enlargement causes sulfate binding to go from exothermic for **1** to endothermic for **2** in 2.5 vol% water/DMSO.

The stoichiometry of the sulfate complex suggests that **2** can indeed fold around an anion as predicted, but binding seems to be not very efficient. While the exact mode of complex formation unfortunately could not be elucidated, it is very likely that it differs profoundly from the one observed for protonated phosphate-derived anions (*vide infra*).

**Dihydrogenpyrophosphate binding.** Crystals of the complex between **2** and DHPP with modest quality for X-ray crystallography were obtained from a solution of **2** in DMSO containing 1 equiv. of TBA DHPP. Fig. 1 shows that anion binding in the solid-state involves sandwiching of a hydrogen-bonded DHPP dimer between two pseudopeptide rings resulting in an overall C<sub>2</sub> symmetric complex. The hydrogen bonding pattern of the DHPP dimer commences through pairs of oxygen atoms on each phosphorus atom with O···O distances between 2.53 Å and 2.55 Å. The four remaining oxygen atoms point into the corners of the rectangular complex, interacting with the pseudopeptide rings. It should be noted that a similar hydrogen-bonded DHPP dimer has recently been found in the complexes of non-cyclic pyrrole-derived receptors developed in the Sessler group.<sup>16</sup>

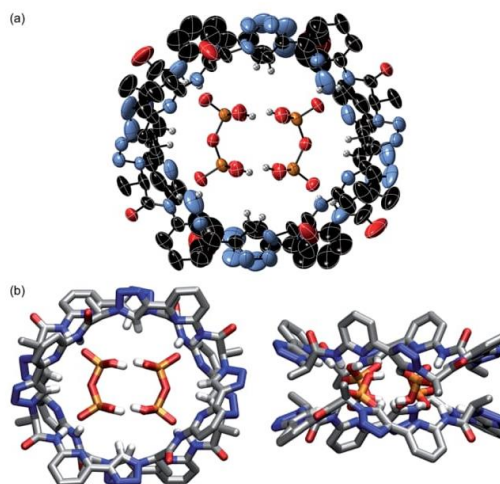


Fig. 1 Molecular structure of 2<sub>2</sub>·DHPP<sub>2</sub> showing the 2 : 2 association of the pseudopeptide and two DHPP anions with the thermal ellipsoids shown at the 50% probability level (a). The TBA cations and the hydrogen atoms except those on the NH and triazole CH groups are omitted for clarity. (b) shows the same structure as a stick model from the top (left) and the side (right) to further illustrate the arrangement of the binding partners.

The pseudopeptide rings in 2<sub>2</sub>·DHPP<sub>2</sub> adopt a slightly distorted conformation with a lower than the ideal C<sub>4</sub> symmetry. Each vacant oxygen atom of the anion dimer is hydrogen-bonded to two NH groups of **2**, one from the upper and one from the lower ring in the sandwich. The N···O distances range between 2.76 and 2.84 Å. Four opposing triazole CH bonds face the oxygen atoms of the anion dimer that are involved in the hydrogen-bonding interactions. The C···O distances of 3.65–3.85 Å indicate that this interaction is also weakly stabilising. The other four triazole CH bonds face the bridging oxygen atom of the anions at distances of 3.65–3.80 Å. Two TBA counterions fill the bowl-shaped cavities of the pseudopeptide rings, one on each side forming the sandwiched 2 × 2 × 2 complex (see ESI<sup>†</sup>). The remaining two TBA cations could not be located due to the severe disorder in the crystal.

The space filling model shown in Fig. S1a<sup>†</sup> illustrates that the overall structure of the complex is very compact and that the DHPP dimer perfectly fills the space between the two pseudopeptide rings. Both rings are structurally nicely complementary, allowing them to closely approach each other in the sandwich as visible in the respective side view in Fig. S1b.<sup>†</sup> The arrangement of NH and CH hydrogen bond donors from both rings above one another causes the methyl groups in the side chains of one ring to be arranged above the aromatic rings of the other pseudopeptide (Fig. 1b), indicating that dispersive interactions between the rings could contribute to stabilise the whole aggregate.

NMR spectroscopy demonstrates that the binding mode seen in the crystal structure of the DHPP complex of **2** persists in solution. The effects of TBA DHPP on the <sup>1</sup>H NMR spectrum of **2** in 2.5 vol% D<sub>2</sub>O/DMSO-*d*<sub>6</sub> are shown in Fig. 2.

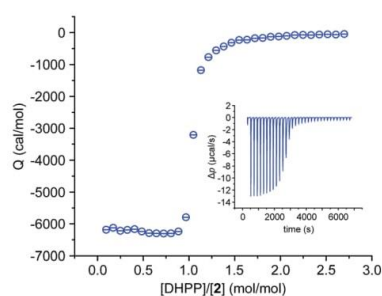


Fig. 4 ITC binding isotherm obtained by titrating a solution of TBA DHPP (6.1 mM) into a solution of **2** (0.4 mM) in 2.5 vol% H<sub>2</sub>O/DMSO. The inset shows the heat pulses of the measurement that were used to obtain the isotherm.

second one the subsequent formation of the final complex (for details, see ESI<sup>†</sup>). With a  $\log K_{11}$  of 6.3 and a  $\log K_{21}$  of 6.4 both binding constants are practically equal in size, leading to a  $\log \beta$  of 12.7 for the overall stability of the complex. This  $\log \beta$ , although not representing the actual stability constant as the dimerisation equilibrium of the anion is missing, clearly shows that DHPP binding proceeds very efficiently. The fact that the second stability constant is larger than  $\log(K_{11}/4)$  is consistent with cooperative binding,<sup>17</sup> and the thermodynamic parameters associated with the individual stability constants indicate that DHPP binding is not only enthalpically (negative  $\Delta H$ ) but also entropically favourable (positive  $\Delta S$ ).

ITC did not allow us, unfortunately, to estimate the dimerisation constant of the DHPP dimer directly because titrating a solution of TBA DHPP into 2.5 vol% H<sub>2</sub>O/DMSO produced only small exothermic heat effects. As the association constant of the DHP dimer was previously determined to amount to a  $\log K_a$  of 1.71 in DMSO,<sup>11g</sup> it is likely that also the DHPP dimer (or even the cyclic DHP tetramer, *vide infra*) is not present in 2.5 vol% H<sub>2</sub>O/DMSO to a significant extent at the concentrations used for the binding studies. Its stabilisation by **2** can therefore be attributed to the presence of the pseudopeptide rings that hold the anions together.

**Hydrogenpyrophosphate binding.** To investigate the effect of the protonation state of the anion on complex formation, also hydrogenpyrophosphate (HPP) anions were considered in the binding studies. Interestingly, no major differences are visible in the <sup>1</sup>H NMR spectra of solutions of **2** in 2.5 vol% D<sub>2</sub>O/DMSO-*d*<sub>6</sub> containing either TBA HPP or TBA DHPP (see ESI<sup>†</sup>). Also, the ESI mass spectrum of a mixture of **2** and TBA HPP exhibits the same peaks as the spectrum in Fig. 3, showing that the DHPP dimer is bound by the receptor and not HPP anions. High affinity of **2** for the DHPP dimer thus seems to cause the protonation state of the pyrophosphate anion to shift in solution to the diprotonated form, which is then bound in the form of the corresponding dimer. The protons required for this process likely derive from the water present in the mixture. Indirect evidence for the protonation equilibrium came from the following results.

X-ray crystallography showed that crystals of **2** grown from acetone in the presence of TBA HPP contain analogous  $2 \times 2 \times$

2 sandwich-type arrangements of two pseudopeptide rings and DHPP dimers as in the structure  $2_2 \cdot \text{DHPP}_2$  shown in Fig. 1. The crystals obtained were, however, centrosymmetric (space group  $P\bar{1}$ ) and thus contain both enantiomers of **2** (see Fig. S2<sup>†</sup>). The pseudopeptide rings in  $2(\text{rac})_2 \cdot \text{DHPP}_2$  adopt similar conformations, again with a lower than the ideal  $C_4$  symmetry, independent of whether the DHPP dimer is complexed by the all-*R* or the all-*S*-enantiomer of **2**. The binding modes detected in the structure in Fig. 1 are retained in  $2(\text{rac})_2 \cdot \text{DHPP}_2$ . Specifically, the vacant oxygen atoms of the DHPP dimer hydrogen-bond to NH groups of **2** with N $\cdots$ O distances ranging between 2.74 and 2.84 Å for all-*R*-**2** and 2.71 and 2.86 Å for all-*S*-**2**. Moreover, pairs of opposing triazole CH bonds in the pseudopeptide sandwiches are oriented towards the oxygen atoms of the anion dimer that are involved in the hydrogen-bonding interactions (C $\cdots$ O distances for all-*R*-**2**: 3.62–4.09 Å and all-*S*-**2**: 3.61–4.36 Å), while the other four triazole CH bonds face the bridging oxygen atom of the anions (C $\cdots$ O distances for all-*R*-**2**: 3.65–3.72 Å and all-*S*-**2**: 3.71–3.80 Å). The O $\cdots$ O distances in the DHPP dimers amount to 2.51–2.53 Å for the complex with all-*R*-**2** and 2.49–2.54 Å for the one with all-*S*-**2**. Overall,  $2(\text{rac})_2 \cdot \text{DHPP}_2$  is thus structurally closely related to the complex shown in Fig. 1 with only small differences in the distances, conformations of the pseudopeptide rings, and arrangement of the binding partners.

We attribute the presence of both enantiomers of **2** in  $2(\text{rac})_2 \cdot \text{DHPP}_2$  to the basic conditions arising upon protonation of the HPP anion. The fact that the crystals contain only the two homochiral forms of **2** can either be explained by assuming a dynamic shift of the racemisation equilibrium to the stereoisomers interacting best with the anion and/or by crystal packing effects. An additional low resolution racemic crystal structure ( $2(\text{rac})_2 \cdot \text{DHPP}_2$ -2) was obtained from crystals grown in DMSO/DCM and using HPP TBA as guest (see ESI and Fig. S3<sup>†</sup>).

Further evidence for the basic conditions of the crystallisation conditions came from the presence of several 4-hydroxy-4-methylpentan-2-one molecules, the aldol adduct of acetone, in the crystals grown from this solvent. NMR spectroscopy showed that formation of this aldol adduct is induced by TBA HPP alone and does not require the presence of **2** (see ESI<sup>†</sup>). HPP thus seems to be sufficiently basic in acetone to mediate the aldol reaction and potentially also the racemisation of **2**. In water at pH 7, HPP dominates in the HPP/DHPP protonation equilibrium by a factor of *ca.* 2,<sup>18</sup> but this situation may differ in organic solvents and the extent of HPP protonation can be further shifted by **2**. No aldol adduct forms in acetone when adding TBA DHPP (see ESI<sup>†</sup>), explaining why **2** does not racemise in the presence of this anion.

These results thus demonstrate that **2** very efficiently interacts with DHPP in 2.5 vol% water/DMSO. The cavity between two appropriately arranged pseudopeptide rings is obviously perfectly suited to host the dimer of the anion. The respective  $2_2 \cdot \text{DHPP}_2$  complex is stabilised by multiple hydrogen bonding interactions between the substrate and triazole CH and NH hydrogen bond donors of **2**, which likely cause a mutual reinforcement of the anion dimer and the pseudopeptide sandwich. Additional dispersive interactions between the closely arranged pseudopeptide rings potentially further stabilise the complex.

High overall stability is thus achieved, in spite of the entropic disadvantage associated with the 2 : 2 stoichiometry. Indications for stability are the slow complexation equilibrium on the NMR time-scale, the near complete complex formation when all components are present in the required 1 : 1 ratio, and the survival of the complex even upon transfer into the gas phase.

While pyrophosphate binding has also been observed for **1**, the information that could be derived about the complex of the smaller pseudopeptide was less clear.<sup>14</sup> ITC indicated that **1** binds one HPP anion with a stability constants  $\log K_a$  of 6.6. Higher complexes involving, for example, two pseudopeptides and one anion were also detected, however, whose composition and stabilities could not be fully characterised. In contrast, DHPP binding by **2** leads to a structurally well-defined and stable complex, demonstrating that ring enlargement significantly improves the structural complementarity between receptor and the DHPP anion in its dimeric form.

**Dihydrogenphosphate binding.** Characterisation of the interaction of DHP anions with **2** showed that the underlying binding mode is closely related to the one of DHPP anions. Structural evidence was derived from the X-ray crystallographic analysis of crystals of the complex grown from DMSO (Fig. 5). Fig. 5 shows that the complex between **2** and DHP also features two closely arranged pseudopeptide molecules that, in this case, sandwich a cyclic tetramer of DHP anions instead of a DHPP dimer. While DHP tetramers have been observed in other structures before, this cyclic arrangement is, to the best of our knowledge new. In a previously described DHP complex of

a bis(urea) type anion receptor, four DHP anions were found to be arranged in a tetrahedral fashion.<sup>10b</sup>

The four phosphorus atoms are arranged in the DHP tetramer of  $2_2 \cdot \text{DHP}_4$  at practically equal distances with two opposing phosphorus atoms located above and two below the plane of a square, rendering the whole arrangement overall  $C_{2v}$  symmetric (see Fig. S4†). Each DHP anion interacts with two neighbouring ones *via* hydrogen-bonding interactions between three of the four oxygen atoms. One of these oxygen atoms bind to oxygen atoms of both neighbours while each of the other two oxygen atoms binds to only one of the two neighbouring DHP anions. The corresponding O...O distances range between 2.57 and 2.61 Å. As a result of the arrangement of the four anions, the oxygen atoms not involved in the stabilisation of the aggregate diverge and are available for the interactions with the pseudopeptide.

Because of the square-like structure of the DHP tetramer, the conformations of the two pseudopeptide rings in  $2_2 \cdot \text{DHP}_4$  are less distorted than in  $2_2 \cdot \text{DHPP}_2$  albeit not fully  $C_4$  symmetric. As in  $2_2 \cdot \text{DHPP}_2$ , each of the four diverging hydrogen bond acceptors of the DHP tetramer binds to two NH groups of **2**, one from each ring of the sandwich ( $\text{N} \cdots \text{O}$  distances: 2.70–2.92 Å). Each of the triazole CH protons further engages in hydrogen-bonding interactions with an oxygen atom of the DHP tetramer that is involved in stabilisation of the anion aggregate ( $\text{C} \cdots \text{O}$  distances: 3.18–3.38 Å). These attractive interactions presumably contribute to the stability of the overall complex. The arrangement of the two pseudopeptide rings resembles that in  $2_2 \cdot \text{DHPP}_2$  in that the side chain methyl groups of one ring are arranged close to the aromatic planes of the other one (see Fig. S5†). The TBA cations that could be located in the structure occupy space between the  $2_2 \cdot \text{DHP}_4$  complexes rather than the bowl-shaped cavities of the pseudopeptides as in  $2_2 \cdot \text{DHPP}_2$ . Overall, the crystal structure solution contains 4  $2_2 \cdot \text{DHP}_4$  complexes, 11 TBA cations and one DMSO molecule. Due to high disorder the locations of the 5 remaining TBA cations remain unknown.

<sup>1</sup>H NMR spectroscopy and mass spectrometry demonstrated that the 2 : 4 stoichiometry found in the solid-state structure of  $2_2 \cdot \text{DHP}_4$  is also present in solution and can furthermore be transferred to the gas phase. In Fig. 6, <sup>1</sup>H NMR spectra of **2** in the presence of various amounts of TBA DHP in 2.5 vol%  $\text{D}_2\text{O}/\text{DMSO}-d_6$  are shown.

These spectra illustrate that formation of the DHP complex of **2** is again slow on the NMR time-scale and associated with a symmetry reduction, consistent with the  $C_{2v}$  symmetry of the bound DHP tetramer seen in the crystal structure of  $2_2 \cdot \text{DHP}_4$ . In contrast to DHPP binding, where one triazole CH signal moves upfield, all four triazole CH and C\*H signals are shifted downfield upon DHP binding. Moreover, the splitting of the C\*H signals is smaller than in the case of the DHPP complex and one signal in the pairs of triazole CH and C\*H signals is consistently broader than the corresponding other one. While all of these features account for slight structural differences between the DHPP and the DHP complexes of **2**, <sup>1</sup>H NMR spectroscopy supports the assumption that the binding modes found in the crystal structures of the respective complexes are preserved in solution. DHP binding to **2** seems to be somewhat

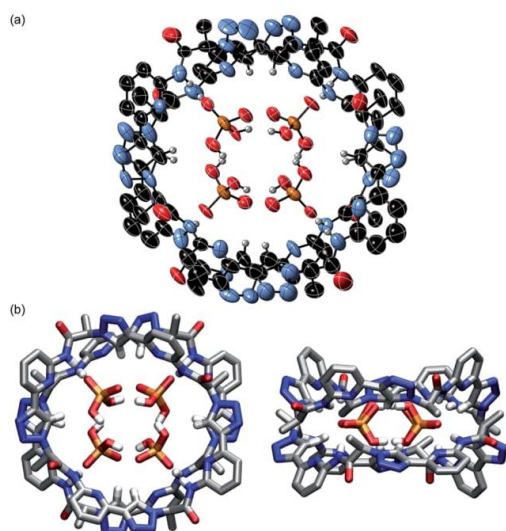


Fig. 5 Molecular structure of  $2_2 \cdot \text{DHP}_4$  showing the 2 : 4 association of the pseudopeptide and four cyclically arranged DHP anions with the thermal ellipsoids shown at the 50% probability level (a). The TBA cations and the hydrogen atoms except those on the NH and triazole CH groups are omitted for clarity. (b) Shows the same structure as a stick model from the top (left) and the side (right) to further illustrate the arrangement of the binding partners.

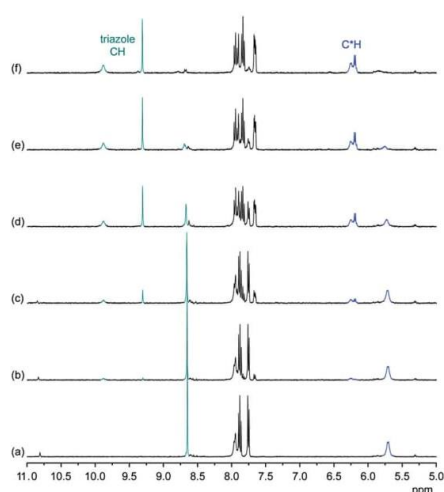


Fig. 6  $^1\text{H}$  NMR spectrum of **2** (0.5 mM) in 2.5 vol%  $\text{D}_2\text{O}/\text{DMSO}-d_6$  in the absence (a) and the presence of 0.5 equiv. (b), 1.0 equiv. (c), 2.0 equiv. (d), 3.0 equiv. (e), and 5.0 equiv. (f) of TBA DHP. The signals of the triazole and  $\text{C}^*\text{H}$  protons are marked in green and blue, respectively.

less efficient because 5 equiv. of TBA DHP are required for the almost complete disappearance of the signals of the free receptor in the  $^1\text{H}$  NMR spectrum.

The signals observed in the ESI mass spectrum of a solution of **2** (0.5 mM) containing 2 equiv. of TBA DHP confirm the 2 : 4 composition of the complex and thus support the complex stoichiometry assigned crystallographically. The major signals in this spectrum at 783.89 and at 1297.00 can be assigned to a triply negatively charged ion  $[(2 \cdot \text{DHP})_2 \cdot \text{TBA}]^{3-}$  and to a doubly negatively charged anion  $[(2 \cdot \text{DHP})_2 \cdot \text{TBA}_2]^{2-}$ , respectively (see ESI $^\ddagger$ ). A minor third signal is visible that corresponds to the 1 : 1 complex between **2** and a DHP anion. Mass spectrometry thus again provides evidence that the complex, which in this case comprises an aggregate of four negatively charged ions hold together by hydrogen-bonding and further stabilised by two pseudopeptide rings, is rather stable.

Complex formation is exothermic according to ITC and the observed binding isotherm supports formation of a complex with a higher stoichiometry (see ESI $^\ddagger$ ). Part of this isotherm could be fitted by using the model also employed for the DHPP complex and the results suggested that the DHP complex is indeed less stable than the DHPP complex. Unfortunately, the complexity of the equilibria underlying formation of the 2 : 4 DHP complex of **2** did not allow deriving more detailed quantitative information from this titration.

The binding studies with DHP thus show that efficient anion recognition by **2** is not restricted to DHPP but extends to DHP. Both anions are able to form aggregates with the DHPP dimer and the cyclic tetramer of DHP being structurally closely related in terms of size and arrangement of hydrogen bond acceptors. Both anion aggregates therefore perfectly fit into the space between two suitably arranged

pseudopeptide rings. Individual anions are connected by hydrogen bonds, while the whole aggregates are further stabilised by interactions with hydrogen bond donors of the two pseudopeptide rings that protrude into the cavity between them. The DHP complex of **2** comprises six individual components, which should render its formation entropically unfavourable. The binding studies nevertheless indicate that thermodynamic stability is substantial. The comparison of DHP binding of **2** with that of **1**, which binds two DHP anions in solution while a linear DHP trimer is bound to two pseudopeptide rings in the solid state,<sup>14</sup> again shows that the larger pseudopeptide forms the structurally better defined complex.

## Conclusions

Ring enlargement of the cyclic pseudopeptide **1**, affording the corresponding cyclic pseudooctapeptide **2**, turned out to have profound consequences on oxoanion binding in 2.5 vol% water/DMSO. In spite of the higher number of hydrogen bond donors along the ring, the larger receptor **2** binds fully deprotonated sulfate anions with a lower affinity than **1**. Protonated anions, on the other hand, which have the intrinsic ability to overcome charge repulsion by inter-anion hydrogen bond formation, can form aggregates that are strongly bound to **2**. The preferred substrates are the structurally closely related DHPP dimer and the cyclic DHP tetramer. Their incorporation into the space between two pseudopeptide rings causes the mutual reinforcement of the interactions between the individual complex components. As a consequence, the complexes persist in solution and can be transferred into the gas phase without decomposition in spite of the fact that are made up of up to six components.

Interestingly, the sandwich-type binding mode observed for the DHPP and DHP complexes of **2** is somewhat reminiscent of the binding mode we previously observed for an anion-binding cyclopeptide.<sup>19</sup> In this case, shielding of the bound anion from the surrounding solvent combined with hydrophobic interactions between the cyclopeptide rings in the sandwich complex cause anion binding to even occur in competitive aqueous media. Should similar principles govern stability of the phosphate complexes of **2**, water-soluble analogues of the pseudopeptide might be able to form such complexes even under aqueous conditions. Another attractive feature of **2** is the possibility to target large anionic aggregates that can only be formed by certain anions. Anion recognition is thus associated with characteristic properties of the anions, which could render the selectivity potentially larger than if the typically relatively small differences in shape and coordination strength of individual anions are targeted. Both aspects render **2** a highly interesting lead structure for the development of phosphate selective receptors acting in water. Work in this context is currently underway.

## Conflict of interest

There are no conflicts of interest to declare.

## Acknowledgements

We thank Johannes Lang and Sebastian Kruppa, Physical Chemistry at the Department of Chemistry in Kaiserslautern, for help with the ESI MS measurements, the Academy of Finland (KR grants no. 263256, 265328 and 292746), and the Universities of Kaiserslautern and Jyväskylä for financial support.

## Notes and references

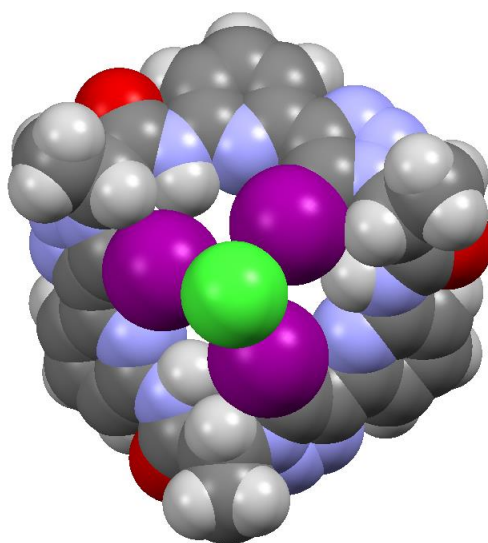
- C. A. Coulomb, *Mémoires de l'Académie Royale des Sciences*, 1788, pp. 569–577.
- (a) M. Mercer and M. R. Truter, *J. Chem. Soc., Dalton Trans.*, 1973, 2469–2473; (b) J. D. Owen and M. R. Truter, *J. Chem. Soc., Dalton Trans.*, 1979, 1831–1835; (c) J. W. Steed, *Coord. Chem. Rev.*, 2001, 215, 171–221.
- (a) A. P. Bisson, V. M. Lynch, M.-K. C. Monahan and E. V. Anslyn, *Angew. Chem., Int. Ed. Engl.*, 1997, 36, 2340–2342; (b) K. Chellappan, J. Singh, I.-C. Hwang, J. W. Lee and K. S. Kim, *Angew. Chem., Int. Ed.*, 2005, 44, 2899–2903; (c) D. Meshcheryakov, V. Böhmer, M. Bolte, V. Hubscher-Bruder, F. Arnaud-Neu, H. Herschbach, A. Van Dorselaer, I. Thondorf and W. Mögelin, *Angew. Chem., Int. Ed.*, 2006, 45, 1648–1652; (d) O. B. Berryman, C. A. Johnson II, L. N. Zakharov, M. M. Haley and D. W. Johnson, *Angew. Chem., Int. Ed.*, 2008, 47, 117–120; (e) C. A. Johnson II, O. B. Berryman, A. C. Sather, L. N. Zakharov, M. M. Haley and D. W. Johnson, *Cryst. Growth Des.*, 2009, 9, 4247–4249.
- (a) J. L. Sessler, P. A. Gale and W.-S. Cho, *Anion Receptor Chemistry*, RSC, Cambridge, 2006; (b) K. Bowman-James, A. Bianchi and E. Garcia-España, *Anion Coordination Chemistry*, Wiley-VCH, Weinheim, 2011; (c) P. A. Gale, E. N. W. Howe and X. Wu, *Chem*, 2016, 1, 351–422; (d) for an excellent review about receptors for phosphate-derived anions, see: A. E. Hargrove, S. Nieto, T. Zhang, J. L. Sessler and E. V. Anslyn, *Chem. Rev.*, 2011, 111, 6603–6782.
- (a) F. Weinhold and R. A. Klein, *Angew. Chem., Int. Ed.*, 2014, 53, 11214–11217; (b) G. Frenking and G. F. Caramori, *Angew. Chem., Int. Ed.*, 2015, 54, 2596–2599; (c) F. Weinhold and R. A. Klein, *Angew. Chem., Int. Ed.*, 2015, 54, 2600–2602.
- (a) I. Mata, I. Alkorta, E. Molins and E. Espinosa, *ChemPhysChem*, 2012, 13, 1421–1424; (b) I. Mata, I. Alkorta, E. Molins and E. Espinosa, *Chem. Phys. Lett.*, 2013, 555, 106–109; (c) I. Mata, E. Molins, I. Alkorta and E. Espinosa, *J. Phys. Chem. A*, 2015, 119, 183–194.
- (a) P. Colomban, M. Pham-Thi and A. Novak, *Solid State Ionics*, 1987, 24, 193–203; (b) M. Malchus and M. Jansen, *Acta Crystallogr., Sect. B: Struct. Sci.*, 1988, 54, 494–502; (c) P. H. Toma, M. P. Kelley, T. B. Borchardt, S. R. Byrn and B. Kahr, *Chem. Mater.*, 1994, 6, 1317–1324; (d) M. E. Light, P. A. Gale and M. B. Hursthouse, *Acta Crystallogr., Sect. E: Struct. Rep. Online*, 2001, 57, o705–o706; (e) R. Custelcean, N. J. Williams and C. A. Seipp, *Angew. Chem., Int. Ed.*, 2015, 54, 10525–10529; (f) M. N. Hoque, U. Manna and G. Das, *Supramol. Chem.*, 2016, 28, 284–292; (g) K. Pandurangan, J. A. Kitchen, S. Blasco, E. M. Boyle, B. Fitzpatrick, M. Feeney, P. E. Kruger and T. Gunnlaugsson, *Angew. Chem., Int. Ed.*, 2015, 54, 4566–4570; (h) D. A. Jose, K. Kumar, B. Ganguly and A. Das, *Inorg. Chem.*, 2007, 46, 5817–5819.
- (a) D. M. Rudkevich, W. Verboom, Z. Brzozka, M. J. Palys, W. P. R. V. Stauthamer, G. J. van Hummel, S. M. Franken, S. Harkema, J. F. J. Engbersen and D. N. Reinhoudt, *J. Am. Chem. Soc.*, 1994, 116, 4341–4351; (b) P. S. Lakshminarayanan, I. Ravikumar, E. Suresh and P. Ghosh, *Chem. Commun.*, 2007, 5214–5216; (c) J. Ju, M. Park, J. m. Suk, M. S. Lah and K.-S. Jeong, *Chem. Commun.*, 2008, 3546–3548; (d) P. Dydio, T. Zieliński and J. Jurczak, *Org. Lett.*, 2010, 12, 1076–1078.
- (a) F. A. Cotton, B. A. Frenz and D. L. Hunter, *Acta Crystallogr., Sect. B: Struct. Crystallogr. Cryst. Chem.*, 1975, 31, 302–304; (b) N. Ohama, M. Machida, T. Nakamura and Y. Kunifuji, *Acta Crystallogr., Sect. C: Cryst. Struct. Commun.*, 1987, 43, 962–964; (c) J. M. Karle and I. L. Karle, *Acta Crystallogr., Sect. C: Cryst. Struct. Commun.*, 1988, 44, 1605–1608; (d) M. E. Light, S. Camiolo, P. A. Gale and M. B. Hursthouse, *Acta Crystallogr., Sect. E: Struct. Rep. Online*, 2001, 57, o727–o729; (e) V. Amendola, M. Boiocchi, D. Esteban-Gómez, L. Fabbrizzi and E. Monzani, *Org. Biomol. Chem.*, 2005, 3, 2632–2639; (f) B. Lou, X. Guo and Q. Lin, *J. Chem. Crystallogr.*, 2009, 39, 469–473; (g) A. Rajbanshi, S. Wan and R. Custelcean, *Cryst. Growth Des.*, 2013, 13, 2233–2237; (h) B. Wu, C. Huo, S. Li, Y. Zhao and X.-J. Yang, *Z. Anorg. Allg. Chem.*, 2015, 641, 1786–1791.
- (a) M. A. Hossain, M. Işıklan, A. Pramanik, M. A. Saeed and F. R. Fronczek, *Cryst. Growth Des.*, 2012, 12, 567–571; (b) V. Blažek, K. Molčanov, K. Mlinarić-Majerski, B. Kojić-Prodić and N. Basarić, *Tetrahedron*, 2013, 69, 517–526.
- (a) R. H. Wood and D. F. Platford, *J. Solution Chem.*, 1975, 4, 977–982; (b) F. Rull, A. D. Vallel, F. Sobron and S. Veintemillas, *J. Raman Spectrosc.*, 1989, 20, 625–631; (c) S. Valiyaveetil, J. F. J. Engbersen, W. Verboom and D. N. Reinhoudt, *Angew. Chem., Int. Ed. Engl.*, 1993, 32, 900–901; (d) E. A. Katayev, J. L. Sessler, V. N. Khrustalev and Y. A. Ustynyuk, *J. Org. Chem.*, 2007, 72, 7244–7252; (e) V. Blažek, N. Bregović, K. Mlinarić-Majerski and N. Basarić, *Tetrahedron*, 2011, 67, 3846–3857; (f) G. Baggi, M. Boiocchi, L. Fabbrizzi and L. Mosca, *Chem.–Eur. J.*, 2011, 17, 9423–9439; (g) N. Bregović, N. Cindro, L. Frkanec, K. Užarević and V. Tomišić, *Chem.–Eur. J.*, 2014, 20, 15863–15871.
- E. M. Fatila, E. B. Twum, A. Sengupta, M. Pink, J. A. Karty, K. Raghavachari and A. H. Flood, *Angew. Chem., Int. Ed.*, 2016, 55, 14057–14062.
- Q. He, M. Kelliher, S. Bähring, V. M. Lynch and J. L. Sessler, *J. Am. Chem. Soc.*, 2017, 139, 7140–7143.
- D. Mungalpara, H. Kelm, A. Valkonen, K. Rissanen, S. Keller and S. Kubik, *Org. Biomol. Chem.*, 2017, 15, 102–113.
- (a) E. A. Katayev, G. D. Pantos, M. D. Reshetova, V. N. Khrustalev, V. M. Lynch, Y. A. Ustynyuk and J. L. Sessler, *Angew. Chem., Int. Ed.*, 2005, 44, 7386–7390; (b) J. L. Sessler, E. Katayev, G. D. Pantos, P. Scherbakov, M. D. Reshetova, V. N. Khrustalev, V. M. Lynch and Y. A. Ustynyuk, *J. Am. Chem. Soc.*, 2005, 127, 11442–11446;

- (c) E. A. Katayev, N. V. Boev, V. N. Khrustalev, Y. A. Ustynyuk, I. G. Tananaev and J. L. Sessler, *J. Org. Chem.*, 2007, **72**, 2886–2896; (d) J. Cai, B. P. Bay, N. J. Young, X. Yang and J. L. Sessler, *Chem. Sci.*, 2013, **4**, 1560–1567.
- 16 M. K. Deliomeroğlu, V. M. Lynch and J. L. Sessler, *Chem. Sci.*, 2016, **7**, 3843–3850.
- 17 D. D. Perrin, *Pure Appl. Chem.*, 1969, **20**, 133–236.
- 18 G. Ercolani, *J. Am. Chem. Soc.*, 2003, **125**, 16097–16103.
- 19 S. Kubik, R. Goddard, R. Kirchner, D. Nolting and J. Seidel, *Angew. Chem., Int. Ed.*, 2001, **40**, 2648–2651.

# Chapter 4

---

## **A neutral halogen bonding macrocyclic anion receptor based on a pseudocyclopeptide with three 5-iodo-1,2,3-triazole subunits**



[D. Mungalpara, S. Stegmüller, S. Kubik "A neutral halogen bonding macrocyclic anion receptor based on a pseudocyclopeptide with three 5-iodo-1,2,3-triazole subunits" *Chem. Comm.* 2017, **53**, 5095-5098]. Copyright by the Royal Society of Chemistry (RSC). Reproduced with permission.

My contributions to this publication were the development of the synthesis of the described pseudopeptide, its purification, and characterization, and I also performed all the binding investigations. Ms. Simone Stegmüller helped with some of the LC-MS experiments. Prof. Dr. Stefan Kubik acted as scientific supervisor.

- 4 Chapter 4 - A neutral halogen bonding macrocyclic anion receptor based on a pseudocyclopeptide with three 5-iodo-1,2,3-triazole subunits**

## 4.1 Scope of the Work

As described in Chapter 2, pseudopeptide **16** strongly binds to oxoanions such as sulfate, DHP or HPP, but the complexation equilibria are often complex, involving the binding of more than one anion to the pseudopeptide ring or more than one pseudopeptide to an anion. The second strategy pursued in this work to simplify anion binding involved the replacement of the protons in the 5-position of the triazole moieties of **16** with iodine atoms to afford **18** (Chart 15).

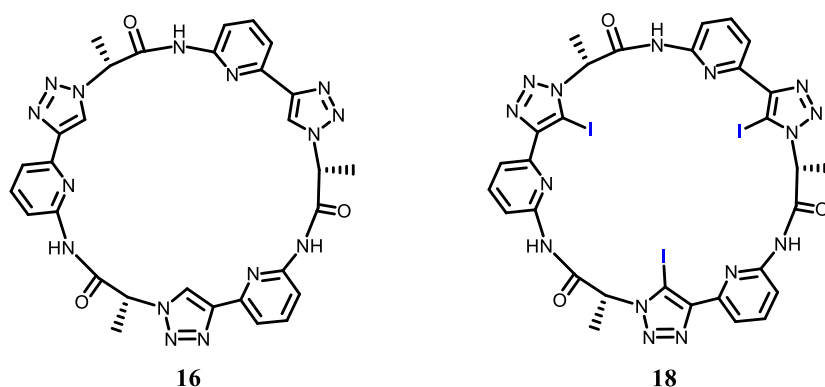
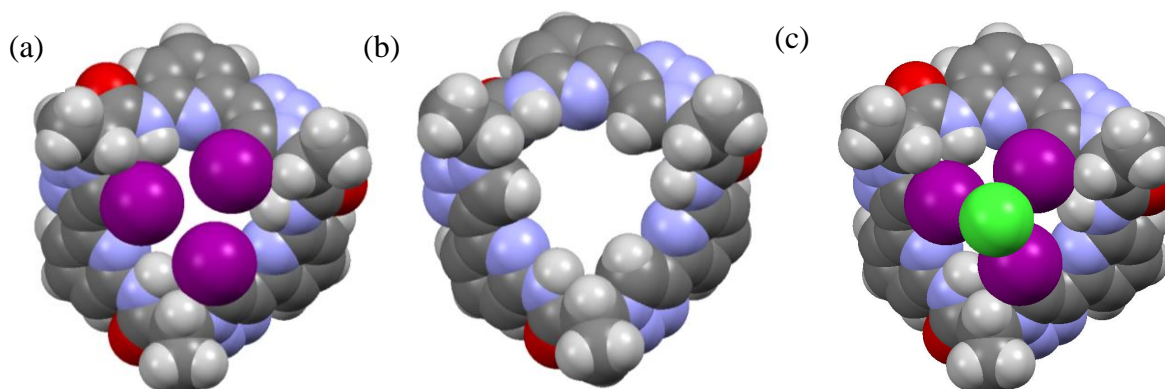


Chart 15

These iodine atoms should allow **18** to engage in anion binding by XB interactions.<sup>61</sup> They should also decrease the cavity size and therefore alter anion selectivity of **18** in comparison to that of **16** in favor of smaller anions.

DFT calculations were performed based on the crystal structure of **16** to gain insight into the influence of the iodide atoms in **18** on cavity size and anion binding. The results of these calculations are compared with the solid-state structure of **16** in Figure 28.



**Figure 28** Calculated structures of pseudopeptide **18** (a), crystal structure of **16** (b) and calculated structure of the chloride complex of **18** (c). DFT calculations were performed by using the B3LYP functional implemented in Spartan 10 (Wavefunction, Inc.) with the 6-311G\* basis set.

Figure 28 shows that the iodine atoms in **18** significantly reduce the diameter of the binding site of the pseudopeptide. Moreover, the calculated structure of the chloride

complex suggests that the distance and orientation of the iodine atoms should be well suited for binding of this small halide, which can make contact to the  $\sigma$ -holes of all three iodine atoms in the complex with no need for a major conformational reorganization of the receptor. Pseudopeptide **18** should therefore be synthesized and its anion binding properties evaluated.

## 4.2 Results

### 4.2.1 Synthesis

Synthesis of cyclic pseudoheptapeptide **18** started from the central building block **21**, which was also used for the preparation of **16**. Chain elongations and cyclization were achieved by repeated copper-catalyzed iodoalkyne-azide cycloaddition reactions (CuIAAC), yielding the desired 1,4-disubstituted 5-iodo-1,2,3-triazole subunits (Figure 29 and Figure 30).

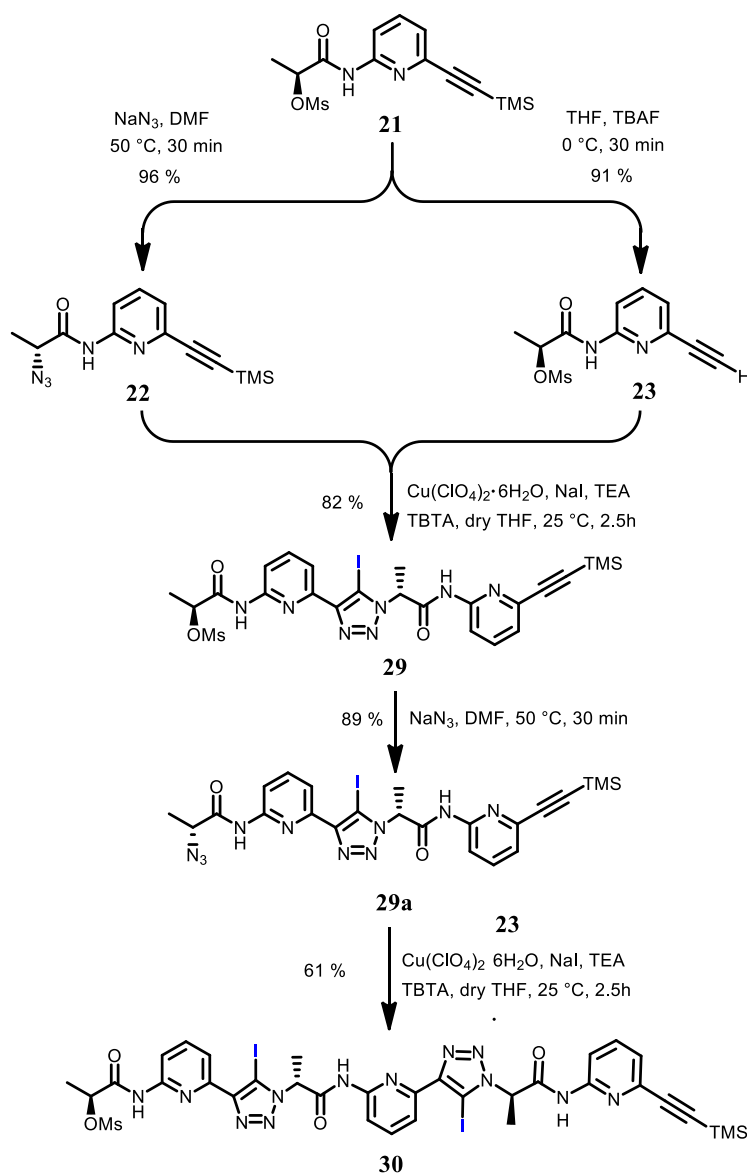


Figure 29 Synthesis of linear pseudoheptapeptide **30**.

In the first step, equal amounts of **21** were converted into the azide **22** and the alkyne **23**. Compounds **22** and **23** were coupled under appropriate conditions to yield the linear dimer **29**. This dimer was converted into the azide **29a** and coupled to **23**, again using CuIAAC, to afford the linear trimer **30** (Figure 29). Treatment of **30** with tetrabutylammonium fluoride followed by iodination afforded the iodoalkyne-containing linear trimer **30b** (Figure 30).

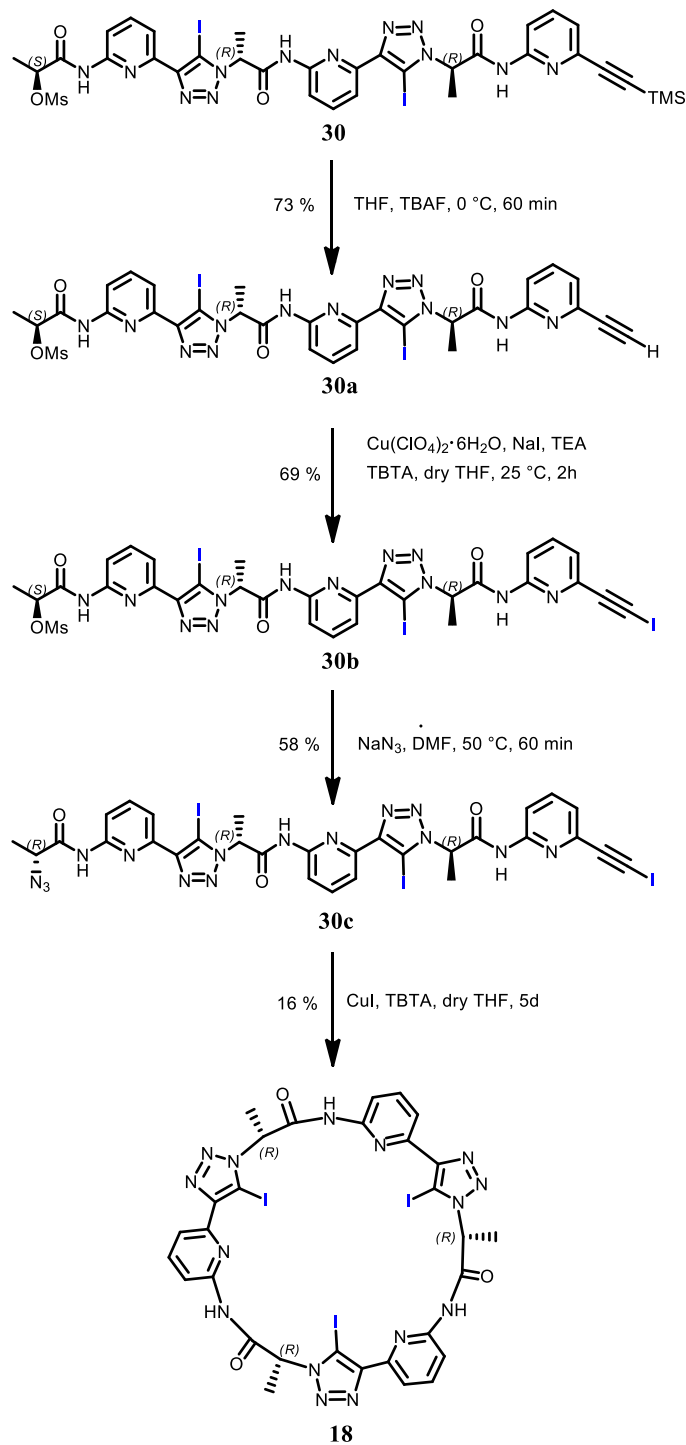
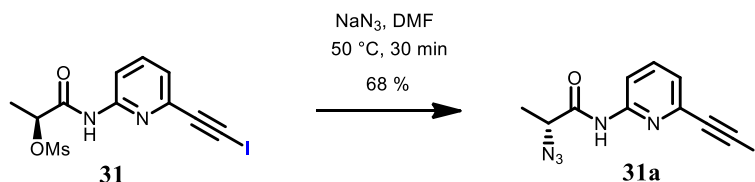


Figure 30 Synthesis of the pseudocyclohexapeptide **18**.

To test whether the iodoalkyne group is stable during the subsequent substitution reaction, the independently prepared model compound **31** was initially treated with  $\text{NaN}_3$  in DMF at  $50\text{ }^\circ\text{C}$ . Under these conditions, the corresponding azide **31a** was cleanly obtained without affecting the iodoalkyne moiety (Figure 31). The same reaction conditions were therefore used to convert **30b** into the corresponding azide **30c** (Figure 30).



**Figure 31** Conversion of the model monomer **31** into the azide **31a**.

The cyclization of the linear trimer **30c** to obtain **18** was the most challenging step of this synthesis. Initially, small scale cyclizations were performed using the conditions collected in Table 6. These conditions were chosen because examples of macrocyclization reactions using these methods are reported in the literature.<sup>84, 64, 85</sup> All small-scale cyclization reactions were performed under dilute condition using  $617\text{ }\mu\text{M}$  solutions of **30c** in various dry solvents. In the reactions **CR1** and **CR2**, 20 mol% of CuI and of TBTA were added initially to the reaction mixture and 10 mol% of both reagents were added every 24 h till the complete disappearance of the peak associated with the starting material in the HPLC chromatogram. In reaction **CR3**, a solution of **30c** in acetonitrile was passed through a coil of copper tube using a syringe pump at elevated temperature ( $70\text{ }^\circ\text{C}$ ). In this case, the copper tube should serve as a Cu(I) source.

**Table 6** Attempted cyclization reactions involving **30c** by using different copper sources and solvents. All reactions were performed at  $25\text{ }^\circ\text{C}$ .

Entry	<b>30c</b> ( $\mu\text{mol}$ )	Copper source	Cu-catalyst (mol%)	TBTA (mol%)	Solvent
<b>CR1</b>	37	CuI	20+(4x10) <sup>a</sup>	20+(4x10) <sup>a</sup>	THF
<b>CR2</b>	37	CuI	20+(4x10) <sup>a</sup>	20+(4x10) <sup>a</sup>	methanol
<b>CR3</b>	37	copper tube coil	-	-	acetonitrile <sup>b</sup>

<sup>a</sup>10 mol% of CuI and TBTA were added to the reaction mixture **CR1** and **CR2** after every 24 h, <sup>b</sup>The reaction was stirred at  $70\text{ }^\circ\text{C}$ .

Conversion in all reactions was followed by HPLC-MS. Examples of chromatograms are shown in Figure 32. According to the mass spectroscopic analysis, the peaks at 17 min and 22 min in the chromatograms correspond to the cyclic product **18** and the linear precursor **30c**, respectively. In this reaction mixture, a small amount of **30c** was degraded into its deiodinated derivative (Figure 32a). Later, the deiodinated **30c** disappeared in the HPLC chromatogram with the course of cyclization (Figure 32c). It is therefore assumed that the deiodinated side product could have either undergo oligomerization or did not elute because of poor solubility in the used eluents. Among these tested methods, only **CR1** proved to afford the desired product. Consequently, these conditions were used for the synthesis of **18** on a larger scale. Purification of **18** involves several washing and extraction steps after which the cyclic pseudopeptide is obtained in analytically pure form. More details about the synthesis are available in the publication (Chapter 4.5).

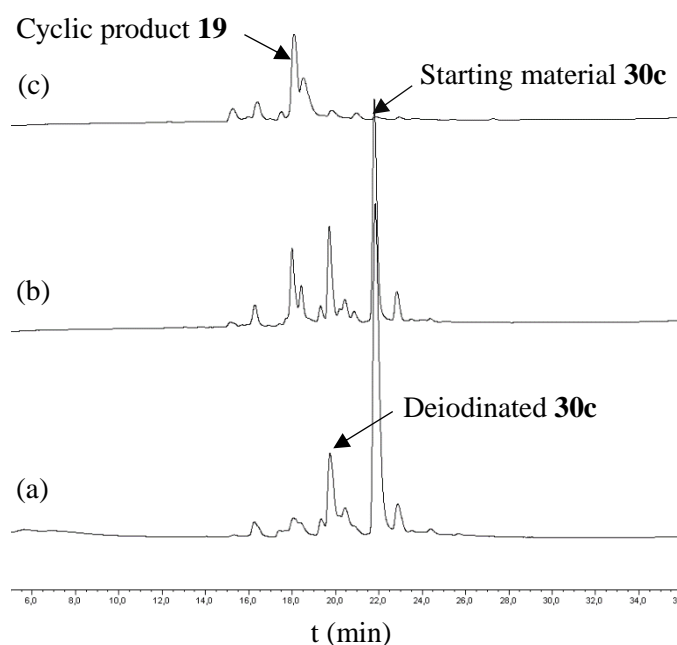


**Figure 32** HPLC chromatograms of the cyclization reaction under condition **CR1** obtained after 24 h (a) 72 h (b), and 120 h (c).

#### 4.2.2 Structural Assignment and Anion Binding Properties

The results of the structural assignment of pseudopeptide **18** and of the anion binding studies are described in the publication (Chapter 4.5). Only the most important results will therefore be summarized here.

$^1\text{H-NMR}$  spectroscopy indicates that **18** adopts an averaged  $C_3$  symmetrical conformation in  $\text{DMSO-}d_6$ . The ROESY NMR spectrum in the same solvent indicated that the N-H and the C\*-H are oriented into the same direction. Thus, the arrangement of the N-H and

C\*-H groups of **18** in solution is same as in the parent macrocycle **16**. No experimental information is available about the orientation of the C-I bonds, but the DFT calculations strongly indicate that the most stable conformation of **18** is one with C-I bonds arranged in a similar converging arrangement as the triazole C-H bonds in **16**.

Binding studies were performed in 2.5 vol% water/DMSO to allow comparison with the anion binding properties of **16**. The complexation of anions with **18** was studied by ESI mass spectrometry, <sup>1</sup>H-NMR spectroscopy, and microcalorimetry.

In the ESI mass spectra of solutions of **18** (1 mM) in 50 vol% DMSO/ACN containing 1 equiv of the TBA salts of DHP, chloride, bromide, and iodide, peaks were observed whose *m/z* ratios could be correlated with the 1:1 complexes between **18** and these anions. No such peak was observed in the presence of TBA sulfate (Table 7).

**Table 7** Main signals (*m/z*) present in the ESI mass spectra of solution of **18** (1 mM) in 50 vol% DMSO/ACN containing 1 equiv of different anions as their TBA salts.

Anion	<i>m/z</i>	Complex
chloride	1058.00	[ <b>18</b> ·Cl] <sup>-</sup>
bromide	1101.88	[ <b>18</b> ·Br] <sup>-</sup>
iodide	1149.88	[ <b>18</b> ·I] <sup>-</sup>
DHP	1119.99	[ <b>18</b> ·DHP] <sup>-</sup>

Mass spectra under analogous conditions were also recorded of solutions containing **18** together with either 1 equiv of each of the three TBA halides or 1 equiv of each TBA chloride, TBA DHP, and TBA sulfate. In the mass spectrum of the first solution, the most intense signal corresponds to the chloride complex, while smaller signals of the bromide and iodide complexes were also observed with the one of the iodide complex being the least intensive one. The other solution only gave rise to one signal in the mass spectrum corresponding to the 1:1 chloride complex of **18**.

Qualitative NMR spectroscopic binding studies were performed by adding 5 equiv of the tetrabutylammonium (TBA) salts of different anions to solutions of **18** in 2.5 vol% H<sub>2</sub>O/DMSO-*d*<sub>6</sub> and comparing the resulting NMR spectra with the one of the free pseudopeptide. H<sub>2</sub>O was used instead of D<sub>2</sub>O in the solvent mixture to prevent H/D exchange. The obtained spectra are depicted in Figure 34.

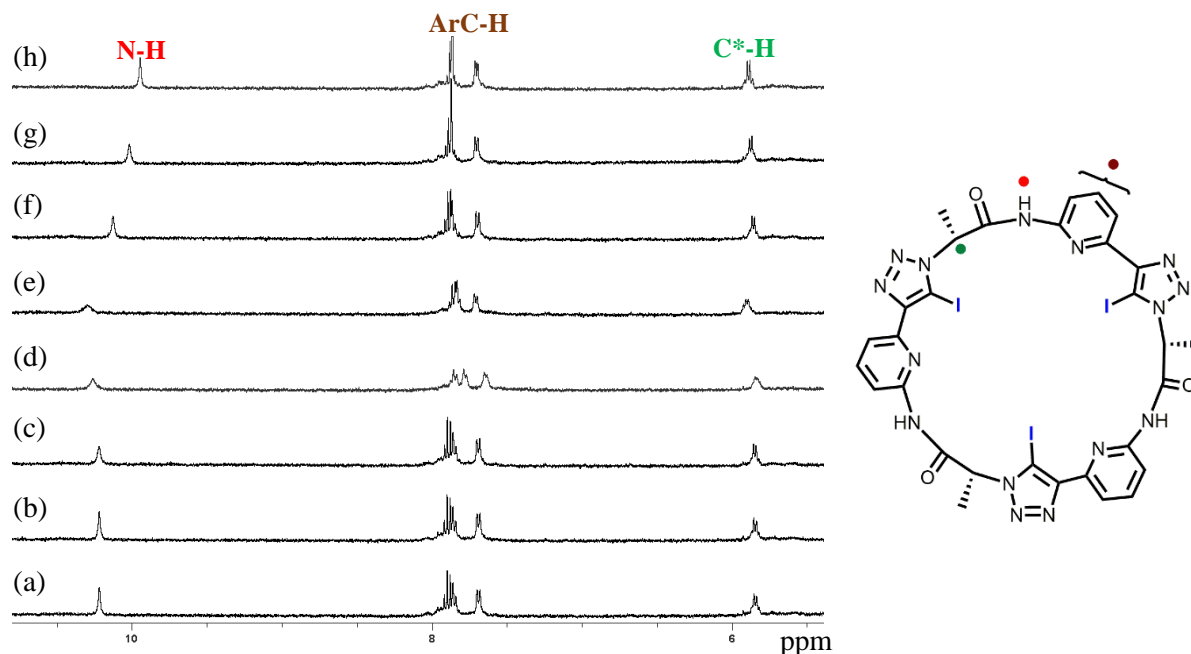


**Figure 33** <sup>1</sup>H-NMR spectrum of **18** (1 mM) in 2.5 vol% H<sub>2</sub>O/DMSO-*d*<sub>6</sub> in the absence (a) and the presence of 5 equiv. of TBA nitrate (b), DHP (c), fluoride (d), sulfate (e), iodide (f), bromide (g) chloride (h). The signals assigned are indicated in the structure on the right hand side by using the same color code.

These spectra show that only sulfate and the halides produce noticeable changes on the resonances of **18**. All of these anions cause a slight deshielding of the C\*-H protons. The N-H signal moves slightly downfield in the presence of sulfate, but upfield when a halide is present.

NMR titrations were performed by following the effects of the gradual addition of the TBA salts of chloride, bromide, iodide, sulfate, and DHP to a solution of **18** in 2.5 vol% H<sub>2</sub>O/DMSO-*d*<sub>6</sub>. Only in the cases of chloride, bromide, iodide, and sulfate could changes in the signals shifts of **18** upon addition of the anions be observed. Binding of these anions is fast on the NMR time-scale, allowing binding isotherms to be constructed from the gradual shifts of the receptor signals observed with increasing amount of the salt. The isotherms obtained from the titrations with chloride, bromide, and iodide were globally fitted to 1:1 binding model by using HypNMR2008. Binding constants obtained from this method are summarized in Table 8. The stability of the chloride complex of **18** was also determined by using tetramethylammonium (TMA) chloride instead of TBA chloride. The resulting binding constant shows that the

counterion has a negligible effect on chloride affinity. The sigmoidal binding isotherms obtained from the titration with TBA sulfate could not be fitted reliably to a reasonable binding model.

**Table 8** Stability constants and thermodynamic parameters of the TBA halide complexes of **18** in 2.5 vol% H<sub>2</sub>O/DMSO-*d*<sub>6</sub> or 2.5 vol% H<sub>2</sub>O/DMSO.

anion	log $K_a^a$	log $K_a^b$	$\Delta H^{oc}$ kJ/mol	$TAS^{oc}$ kJ/mol
chloride	3.3	3.4	-1.4	18.2
chloride <sup>d</sup>	3.6	n.d. <sup>e</sup>	n.d. <sup>e</sup>	n.d. <sup>e</sup>
bromide	2.9	n.d. <sup>e</sup>	n.d. <sup>e</sup>	n.d. <sup>e</sup>
iodide	2.2	n.d.	n.d. <sup>e</sup>	n.d. <sup>e</sup>
sulfate	- <sup>f</sup>			

<sup>a</sup>Determined by NMR titration in 2.5 vol% H<sub>2</sub>O/DMSO-*d*<sub>6</sub>; <sup>b</sup>determined by ITC in 2.5 vol% H<sub>2</sub>O/DMSO; <sup>c</sup>enthalpies and entropies; errors are estimated to amount to ca.  $\pm 10\%$ ; <sup>d</sup>TMA chloride; <sup>e</sup>not determined; <sup>f</sup>the binding isotherm could not fit to a reasonable binding model.

Among all the tested anions, chloride is most strongly bound in 2.5 vol% H<sub>2</sub>O/DMSO-*d*<sub>6</sub> followed by bromide and iodide. This stability trend therefore mirrors the signal intensities observed in the mass spectrum of **18** measured in the presence of the three halides. Anion affinity of **18** was also evaluated using isothermal titration calorimetry (ITC). The results of this investigation are also summarized in Table 8. The binding constant obtained for the chloride complex of **18** is in good agreement with the one of the NMR titration. Chloride binding in 2.5 vol% H<sub>2</sub>O/DMSO is mainly due to entropy with a small favourable enthalpic contribution. The enthalpic contribution to bromide and iodide binding proved to be too small under these conditions to allow quantification of binding strength.

### 4.3 Discussion

The results of  $^1\text{H}$ -,  $^{13}\text{C}$ -, and ROESY NMR spectra are consistent with the averaged  $C_3$  symmetrical structure of **18** in solution. Unfortunately, the spectra do not allow assignment of the orientation of the triazole rings. Because of the structural relationship between **16** and **18**, combined with the information obtained by ROESY NMR spectroscopy and the results of the DFT calculations, it is assumed that the calculated structure shown in Figure 28 reflects the averaged conformation of **18** in solution. Binding studies in 2.5 vol%  $\text{H}_2\text{O}/\text{DMSO-}d_6$  indicated that among the studied anions only sulfate and halides interact with **18**. No interaction was observed with DHP in solution although this anion is strongly bound by **16**. ESI MS suggests that DHP weakly binds to **18**. Sulfate affinity of **18** could not be quantified by NMR titration. This titration indicates that the binding mode between **18** and sulfate is complex. It also suggests that sulfate is presumably bound weaker by **18** than by **16**.

On the other hand, halides are bound by **18** in the form of 1:1 complexes, while **16** does not bind to these anions under the same conditions. The presence of the halides causes a slight deshielding of the  $\text{C}^*\text{-H}$  protons and a shielding of the  $\text{N-H}$  protons. It should be pointed out that deshielding of the  $\text{C}^*\text{-H}$  protons in the presence of anions is generally attributed to through-space effects of the bound anions arranged close to the respective protons in the complex. The upfield shift of the  $\text{N-H}$  signal in the presence of halides is, however, atypical for anion binding. Since the calculations indicate that the  $\text{N-H}$  protons and iodine atoms in **18** are likely too far apart to contribute to anion binding to the same extent, the shielding of the  $\text{N-H}$  protons upon halide binding can be attributed to receptor reorganization and/or the complexation induced release of solvent (DMSO or water) molecules solvating the  $\text{N-H}$  groups in the absence of anions. That the  $\text{N-H}$  signal moves downfield in the presence of sulfate anions could indicate that the binding modes of the halide and the sulfate complexes are different.

According to microcalorimetry, the halide binding is only slightly exothermic, supporting the assumption that the receptor has to be desolvated prior to anion binding, which is enthalpically costly. Complex stability therefore becomes mainly due to entropy.

The  $\log K_a$  of 3.3 observed for the chloride complex of **18** is sizeable, also considering that binding does not involve substantial contributions beyond XB and that it proceeds in a relatively competitive medium. Affinities of this order of magnitude have mostly been observed under similar conditions for positively charged XB receptors containing, for example, triazolium subunits, while neutral receptors typically exhibit lower affinity.<sup>61</sup>

The high chloride affinity of **18** could be attributed the rigid well preorganized macrocyclic structure of the pseudopeptide that also restricts anion binding to a relatively narrow range of anions. Thus, the iodine atoms in **18** lead to major changes in the anion binding properties with respect to **16** as they cause the cavity to become smaller and they mediate XB interactions. As a consequence, **18** exhibits affinity for halide and no or only a very weak affinity for oxoanions.

#### **4.4 Summary**

The cyclic pseudoheptapeptide **18** containing 1,4-disubstituted 5-iodo 1,2,3-triazole moieties was synthesized. ROESY NMR spectroscopy indicates that **18** adopts a conformation in DMSO-*d*<sub>6</sub> that is related to the one of the parent macrocycle **16**.

<sup>1</sup>H-NMR spectroscopy, mass spectrometry, and isothermal titration calorimetry demonstrate that **18** binds to chloride, bromide, and iodide in 2.5 vol% water/DMSO, leading to the formation of 1:1 complexes. With a log *K*<sub>a</sub> of 3.3 the chloride complex is the most stable one and complex stability decreases by one order of magnitude when going to the larger halide. Oxoanions are significantly less strongly bound by **18** than by the parent pseudopeptide **16**. No complexation of DHP could be detected while interactions of **18** with sulfate cannot be excluded. A defined stoichiometry or stability of the sulfate complex could, however, not be determined.

## 4.5 Publication



ChemComm

COMMUNICATION

View Article Online  
View Journal | View Issue



Cite this: *Chem. Commun.*, 2017, 53, 5095

Received 29th March 2017,  
Accepted 19th April 2017

DOI: 10.1039/c7cc02424j

rsc.li/chemcomm

### A neutral halogen bonding macrocyclic anion receptor based on a pseudocyclopeptide with three 5-iodo-1,2,3-triazole subunits†

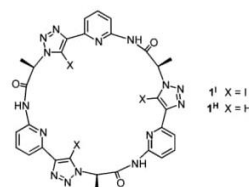
Disha Mungalpara,<sup>a</sup> Simone Stegmüller<sup>b</sup> and Stefan Kubik<sup>id</sup> \*<sup>a</sup>

**The converging arrangement of iodine atoms along its confined cavity causes a cyclic pseudopeptide with three 5-iodo-1,2,3-triazole subunits to interact with halides, in particular with chloride, in 2.5 vol% water/DMSO.**

Anion recognition relies on interactions between the electron rich substrate and electron deficient parts of a structurally complementary receptor.<sup>1</sup> Examples of structural elements in a receptor that induce anion affinity are Lewis acidic centres,<sup>2a-d</sup> hydrogen bond donors,<sup>2e-h</sup> electron deficient  $\pi$ -systems<sup>2i,j</sup> and the so-called  $\sigma$ -holes of halogen atoms residing at the terminus of the carbon-halogen bond.<sup>2k-q</sup> The latter type of interactions, termed halogen-bonding (XB),<sup>3</sup> has found widespread application in material science<sup>2k-m</sup> and has also been shown more recently to afford anion receptors,<sup>2n</sup> sensors<sup>2m</sup> and organocatalysts.<sup>2q</sup> Advantages of halogen-bonding are the high directionality and strength of the halogen bond, which often cause a halogen-containing receptor to bind anions more efficiently than the corresponding hydrogen-bonding (HB) analogue.<sup>4</sup>

The introduction of halogen-bond donors into an anion receptor is typically achieved by attaching halogenated (often iodinated and electron poor) aromatic residues to an appropriate core structure. In this context, 5-iodo-1,2,3-triazoles or respective triazolium ions are particularly attractive structural motifs<sup>5</sup> because they can easily be prepared from iodoalkynes and azides under copper(i) catalysis or from terminal alkynes and azides in the presence of an iodine source, potentially followed by alkylation.<sup>6</sup> Molecular architectures that have thus been accessed are mostly non-cyclic, containing typically between one and four halogen

atoms as binding sites.<sup>2o</sup> In addition, a variety of interlocked receptors with converging halogen-bond donors have been developed in the Beer group,<sup>2o,p,7</sup> some of which exhibit outstanding binding properties, including anion affinity in water.<sup>8</sup> Macrocyclic receptors with a converging arrangement of several halogen-bond donors are, however, rare. To the best of our knowledge, the only example is a family of cyclophanes developed by Beer *et al.* featuring two bromoimidazolium units in the ring that bind halides in 9 : 1 CH<sub>3</sub>OH/H<sub>2</sub>O by combining electrostatic interactions with XB.<sup>9a</sup> A macrocyclic crown ether-derived receptor has recently been described by the Schubert group that, however, comprises only one 5-iodo-1,2,3-triazole moiety.<sup>9b</sup>



Here, we introduce the cyclic pseudopeptide **1<sup>I</sup>** containing three 5-iodo-1,2,3-triazole subunits as a novel macrocyclic XB receptor. This pseudopeptide is based on the non-halogenated analogue **1<sup>H</sup>**, which has been shown to bind oxoanions in 2.5 vol% water/DMSO.<sup>10</sup> Anions are bound to **1<sup>H</sup>** by HB interactions to the NH and triazole CH groups that are arranged in a convergent well preorganised fashion even in the absence of guests. While oxoanions such as dihydrogenphosphate (DHP) and sulfate anions are strongly bound in 2.5 vol% water/DMSO, no complexation of halides could be observed under the same conditions.

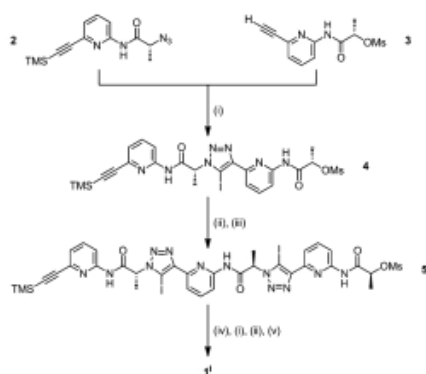
We reasoned that the iodinated receptor **1<sup>I</sup>** should possess a more confined cavity than **1<sup>H</sup>**, which is furthermore surrounded by XB donors, rendering the binding properties potentially distinctly different from those of the non-halogenated analogue. Binding studies indeed demonstrated that the iodine atoms in **1<sup>I</sup>** prevent this receptor from strongly interacting with oxoanions while they induce affinity for halides, especially for chloride. Incorporation of the iodine atoms into the rigid scaffold of the

<sup>a</sup> Technische Universität Kaiserslautern, Fachbereich Chemie – Organische Chemie, Erwin-Schrödinger-Straße, 67663, Kaiserslautern, Germany.  
E-mail: kubik@chemie.uni-kl.de

<sup>b</sup> Technische Universität Kaiserslautern, Fachbereich Chemie – Lebensmittelchemie & Toxikologie, Erwin-Schrödinger-Straße, 67663, Kaiserslautern, Germany

† Electronic supplementary information (ESI) available: Synthetic details, NMR and mass spectra of the product and the intermediates, ROESY NMR spectrum of **1<sup>I</sup>**, and details about the NMR spectroscopic and calorimetric binding studies. See DOI: 10.1039/c7cc02424j

Communication



**Scheme 1** Synthesis of **1<sup>I</sup>**. Reaction conditions: (i)  $\text{Cu}(\text{ClO}_4)_2$  (2 equiv.), TBTA (10 mol%), NaI (4 equiv.), triethylamine (1 equiv.), THF, 25 °C, 2.5 h; (ii)  $\text{NaN}_3$  (2 equiv.), DMF, 50 °C, 30 min; (iii) **3** (1.4 equiv.),  $\text{Cu}(\text{ClO}_4)_2$  (2.8 equiv.), TBTA (14 mol%), NaI (5.9 equiv.), triethylamine (1.4 equiv.), THF, 25 °C, 2.5 h; (iv) TBAF (2 equiv.), THF, 0 °C, 60 min; (v)  $\text{CuI}$  (0.60 equiv.), TBTA (0.6 equiv.), THF, 25 °C, 5 d.

cyclic pseudopeptide therefore has more pronounced effects on anion binding than typically observed for XB anion receptors.

Pseudopeptide **1<sup>I</sup>** was prepared along a similar route as the analogue **1<sup>H</sup>** (Scheme 1). In the first step, the building blocks **2** and **3**, which were also used for the synthesis of **1<sup>H</sup>**,<sup>10</sup> were coupled in the presence of  $\text{Cu}(\text{ClO}_4)_2$ , NaI, triethylamine, and tris(benzyltriazolylmethyl)amine (TBTA) to afford the 5-iodo-1,2,3-triazole derivative **4**. Coupling involves initial iodination of the terminal alkyne with the concomitant reduction of the copper(II) salt. Triazole formation is then believed to be mediated by  $\text{CuI}$ .<sup>6</sup> Chain elongation was achieved by converting **4** into the corresponding azide, which was then coupled with another equivalent of **3** to afford trimer **5**. This trimer was cyclised by using the sequence TMS deprotection, iodination of the terminal alkyne, introduction of the azide group, and triazole formation (for details, see ESI<sup>†</sup>). Cyclisation was followed by HPLC-MS, showing that it required 5 d at 25 °C for completion. The product was purified by repeated washing and extraction steps to afford analytically pure material.

Pseudopeptide **1<sup>I</sup>** has a simple <sup>1</sup>H and <sup>13</sup>C NMR spectrum, consistent with its  $C_3$  symmetric structure. To obtain information about the preferred conformation of **1<sup>I</sup>** in solution, a ROESY NMR spectrum was recorded in  $\text{DMSO-}d_6$ . This spectrum contains a crosspeak between the NH signal and the one of the C\*H protons at the stereogenic centres (see ESI<sup>†</sup>). No crosspeak is visible between the NH signal and the signal of the aromatic protons in 3 position of the pyridine units. The NH protons in **1<sup>I</sup>** are therefore preferentially oriented in the same direction as the pyridine nitrogen atoms and also the C\*H protons point into this way. A similar arrangement has been observed for **1<sup>H</sup>**. In the case of this pseudopeptide, additional crosspeaks from the NH and C\*H signals to the triazole CH signal are visible in the spectrum showing that the triazole protons also converge to the cavity centre. While the absence of protons on the triazole rings of **1<sup>I</sup>** did not allow the same assignment it is reasonable to assume that the preferred arrangement of the triazole rings is

View Article Online

ChemComm

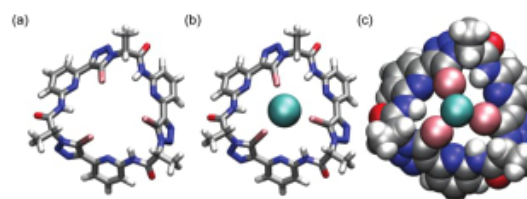


**Fig. 1** Calculated structures of pseudopeptide **1<sup>I</sup>** (a) and of its chloride complex as line (b) and space-filling model (c). DFT calculations were performed by using the B3LYP functional implemented in Spartan 10 (Wavefunction, Inc.) with the 6-311G\* basis set.

not significantly affected by the presence of the additional iodide atoms.

Unfortunately, we could not obtain crystals of sufficient quality to structurally characterise **1<sup>I</sup>** by X-ray crystallography. We therefore performed DFT calculations based on the crystal structure of **1<sup>H</sup>** to gain insight into the influence of the iodide atoms in **1<sup>I</sup>** on cavity size and anion binding. The results of these calculations are depicted in Fig. 1.

The structure of the free pseudopeptide in Fig. 1 illustrates that the three iodine atoms surround a relatively confined cavity, smaller than the one of **1<sup>H</sup>**.<sup>10</sup> The amide NH groups are located at a distance to the iodine atoms, rendering simultaneous HB and XB interactions with an anion unlikely. The calculated structure of the chloride complex suggests that the distance and orientation of the iodine atoms should be well suited for binding of this small halide. The chloride ion is located in the complex at the extension of the C-I bonds, allowing contacts with the  $\sigma$ -holes of the three iodine atoms. No major reorganisation of the pseudopeptide is necessary for binding to occur.

To test anion affinity, qualitative <sup>1</sup>H NMR spectroscopic binding studies were performed by adding 5 equiv. of the tetrabutylammonium (TBA) salts of six different anions to a solution of **1<sup>I</sup>** in 2.5 vol%  $\text{H}_2\text{O}/\text{DMSO-}d_6$  and comparing the resulting NMR spectra with the one of the free pseudopeptide.†  $\text{H}_2\text{O}$  was used instead of  $\text{D}_2\text{O}$  in the solvent mixture to prevent H/D exchange, thus allowing the effects of the anions on the shift of the NH signal to be followed. The obtained spectra are depicted in Fig. 2.

These spectra show that only sulfate and the halides produce noticeable changes on the resonances of **1<sup>I</sup>**. All of these anions cause a slight deshielding of the C\*H protons. The NH signal moves downfield in the presence of sulfate but upfield when a halide is present. The effects of anions on the NMR spectrum of **1<sup>I</sup>** thus differ from the ones observed for **1<sup>H</sup>**. In this case, pronounced signal shifts, consistent with HB interactions between the anions and the receptor, are produced by sulfate and DHP in 2.5 vol%  $\text{D}_2\text{O}/\text{DMSO-}d_6$ , while none of the halides affect the NMR spectrum of **1<sup>H</sup>** under the same conditions.<sup>10</sup>

These qualitative binding studies thus indicate that the three iodine atoms characteristically mediate anion binding of **1<sup>I</sup>**. They seem to prevent this pseudopeptide from interacting with DHP anions but induce affinity for halides. Assuming that the extents of the shifts observed in the NMR spectra correlate with binding strength, chloride seems to be the best substrate.

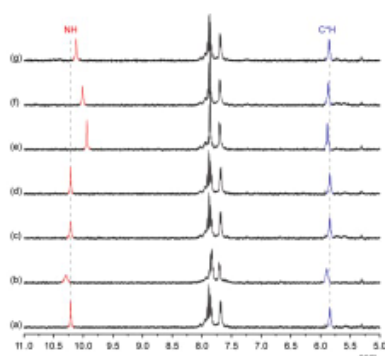


Fig. 2  $^1\text{H}$  NMR spectra of **1** (0.25 mM) in 2.5 vol%  $\text{H}_2\text{O}/\text{DMSO}-d_6$  in the absence (a) and the presence of 5 equiv. of sulfate (b), DHP (c), nitrate (d), chloride (e), bromide (f), and iodide (g). All anions were used as their respective TBA salts.

It should be pointed out that deshielding of the  $\text{C}^*\text{H}$  protons in the presence of anions has also been observed for **1**<sup>H</sup>. This effect is generally attributed to through-space effects of the bound anions arranged close to the respective protons in the complex. The upfield shift of the NH signal in the presence of halides is, however, atypical for anion binding. Since the calculations indicate that the NH protons in **1** are likely too far away from the iodine atoms to contribute to anion binding to a significant extent, we attribute the shielding of the NH protons upon halide binding to receptor reorganisation during complex formation and/or the complexation induced release of DMSO molecules that solvate the NH groups of **1** in the absence of anions. That the NH signal moves downfield in the presence of sulfate anions could account for a binding mode of the respective complex differing from the one of the halide complexes.

Further information about anion binding of **1** was obtained by ESI mass spectrometry. Fig. 3 shows the mass spectrum of a solution of **1** in DMSO/acetonitrile, 1:1 (v/v) containing 1 equiv. of each TBA chloride, bromide, and iodide. Three major signals are visible in this spectrum whose  $m/z$  ratios can be assigned to the respective 1:1 complexes between **1** and the three halides (calcd.:  $[\text{M}\cdot\text{Cl}]^-$ : 1057.90;  $[\text{M}\cdot\text{Br}]^-$ : 1101.85;  $[\text{M}\cdot\text{I}]^-$ : 1149.84). The mass spectrum thus confirms the ability of **1** to interact with halides and suggests that 1:1 complexes are preferentially formed. The decreasing intensities of the peaks assigned to the chloride, bromide, and iodide complexes mirror the trend observed by NMR spectroscopy and therefore indicate that chloride is likely most strongly bound. In the ESI mass spectrum of a solution of **1** containing 1 equiv. of TBA DHP, a signal is present at the  $m/z$  ratio of the 1:1 complex between the pseudopeptide and the DHP anion (see ESI<sup>†</sup>). Once the solution contains an additional equivalent of TBA chloride this signal completely disappears in favour of the one representing the chloride complex of **1**, which shows that this complex is more stable than the one with DHP. Signals attributable to the sulfate complex of **1** are practically absent in the ESI mass spectrum of an equimolar mixture of **1** and TBA sulfate, likely because the pseudopeptide is unable to stabilize sulfate anions in the gas phase.

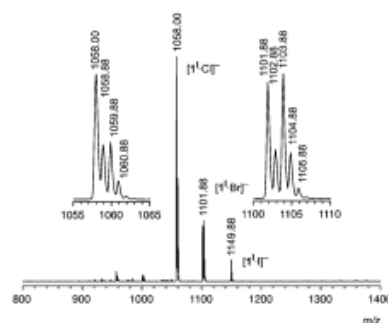


Fig. 3 ESI MS of **1** (1 mM) in DMSO/acetonitrile, 1:1 (v/v) in the presence of 1 equiv. of each TBA chloride, bromide, and iodide.

On the basis of this information, quantitative binding studies were performed by using NMR titrations and isothermal titration calorimetry (ITC). Table 1 summarises the results.

The shape of the isotherms obtained in the NMR titrations with the three halides are consistent with a simple 1:1 binding equilibrium. The resulting stability constants moreover confirm that chloride is most strongly bound. Affinity decreases with increasing size of the halides, rendering the iodide complex to be *ca.* one order of magnitude less stable than the chloride complex. This size selectivity can be attributed to the better fit of the chloride anion into the cavity of **1** with respect to the larger halides. We also determined the stability of the chloride complex of **1** by using tetramethylammonium (TMA) chloride instead of TBA chloride. The resulting binding constant  $\log K_a$  of 3.60 shows that the counterion has no major effect on chloride affinity, indicating that the interactions responsible for chloride binding are anion specific.

The binding constant resulting from the calorimetric titration is in good agreement with the one of the NMR titration. The ITC results additionally show that chloride binding is mainly controlled by entropy with a small favourable enthalpic contribution. The enthalpic contributions to bromide and iodide binding under the chosen conditions turned out to be too small to reliably determine a stability constant.

We also attempted to quantify sulfate and DHP affinity of **1** by NMR titrations. In the case of sulfate, the obtained sigmoidal binding isotherms could not be reliably fitted to a reasonable binding model. Although NMR spectroscopy thus indicates that interactions between **1** and sulfate anions take place, binding does not follow the simple 1:1 equilibria observed for the halides.

Table 1 Stability constants  $\log K_a$  and thermodynamic parameters of the halide complexes of **1** in 2.5 vol%  $\text{H}_2\text{O}/\text{DMSO}-d_6$  or 2.5 vol%  $\text{H}_2\text{O}/\text{DMSO}$

Anion	$\log K_a^a$	$\log K_a^b$	$\Delta H^\circ$ <sup>c</sup>	$T\Delta S^\circ$ <sup>c</sup>
Chloride	3.28	3.43	-1.4	18.2
Bromide	2.85	n.d. <sup>d</sup>	n.d.	n.d.
Iodide	2.15	n.d.	n.d.	n.d.

<sup>a</sup> Determined by NMR titration in 2.5 vol%  $\text{H}_2\text{O}/\text{DMSO}-d_6$ . <sup>b</sup> Determined by ITC in 2.5 vol%  $\text{H}_2\text{O}/\text{DMSO}$ . <sup>c</sup> Enthalpies and entropies in  $\text{kJ mol}^{-1}$ ; errors are estimated to amount to *ca.*  $\pm 10\%$ . <sup>d</sup> Not determined.

Moreover, a significantly higher amount of TBA sulfate is required for the isotherms to approach saturation than in the case of **1<sup>H</sup>** (12 equiv. vs. 3 equiv.).<sup>10</sup> Based on this qualitative argument we assume that binding of sulfate is weaker to **1<sup>I</sup>** than to the analogue **1<sup>H</sup>** (see ESI† for a comparison of the anion affinities of **1<sup>I</sup>** and **1<sup>H</sup>**). No signal shifts were observed in the titration with TBA DHP.

The log  $K_a$  of ca. 3.3 observed for the chloride complex of **1<sup>I</sup>** is sizeable, also considering that **1<sup>I</sup>** is neutral, that binding does not involve substantial contributions from interactions other than XB, and that it proceeds in a competitive medium. Affinities of this order of magnitude have mostly been observed under similar conditions for positively charged XB receptors containing, for example, triazolium subunits.<sup>20,p,4b</sup> Neutral receptors typically exhibit lower affinity unless XB is reinforced by, for example, HB to urea moieties.<sup>11</sup> We attribute the high chloride affinity of **1<sup>I</sup>** to the rigid well preorganised macrocyclic structure of this receptor, whose confined cavity also restricts anion binding to a relatively narrow range of anions.

Pseudopeptide **1<sup>I</sup>** therefore represents a promising platform for the development of novel halide receptors. Advantages of **1<sup>I</sup>** are high binding affinity and selectivity, mediated by the macrocyclic structure, and the possibility for further structural modifications such as the conversion of the triazole into triazolium units, which should influence not only anion affinity but also receptor solubility. Alternative means to control binding properties and/or solubility involve replacement of the peripheral methyl groups with other substituents. Finally, chirality is also structural feature not often found in XB receptors,<sup>4c,12</sup> which should render this pseudopeptide interesting for use in asymmetric organocatalysis. All of these aspects are currently being explored.

## Notes and references

‡ We also considered fluoride as a potential guest. The results were inconclusive, however. Some line broadening was observed in the <sup>1</sup>H NMR spectrum of **1<sup>I</sup>** after addition of TBA fluoride but no significant shifts and the NMR and ITC titrations did not provide reliable data to derive a binding constant.

- (a) J. L. Sessler, P. A. Gale and W.-S. Cho, *Anion Receptor Chemistry*, RSC, Cambridge, 2006; (b) K. Bowman-James, A. Bianchi and E. Garcia-España, *Anion Coordination Chemistry*, Wiley-VCH, Weinheim, 2011; P. A. Gale, E. N. W. Howe and X. Wu, *Chem*, 2016, **1**, 351–422.

- (a) P. D. Beer and E. J. Hayes, *Coord. Chem. Rev.*, 2003, **240**, 167–189; (b) V. Amendola and L. Fabbrizzi, *Chem. Commun.*, 2009, 513–531; (c) M.-O. M. Piepenbrock, G. O. Lloyd, N. Clarke and J. W. Steed, *Chem. Rev.*, 2010, **110**, 1960–2004; (d) D. J. Mercer and S. J. Loeb, *Chem. Soc. Rev.*, 2010, **39**, 3612–3620; (e) C. R. Bondy and S. J. Loeb, *Coord. Chem. Rev.*, 2003, **240**, 77–99; (f) K. Choi and A. D. Hamilton, *Coord. Chem. Rev.*, 2003, **240**, 101–110; (g) S. O. Kang, R. A. Begum and K. Bowman-James, *Angew. Chem., Int. Ed.*, 2006, **45**, 7882–7894; (h) J. Cai and J. L. Sessler, *Chem. Soc. Rev.*, 2014, **43**, 6198–6213; (i) D. Quiñero, C. Garau, C. Rotger, A. Frontera, P. Ballester, A. Costa and P. M. Deyà, *Angew. Chem., Int. Ed.*, 2002, **41**, 3389–3392; (j) A. Frontera, P. Gamez, M. Mascal, T. J. Mooibroek and J. Reedijk, *Angew. Chem., Int. Ed.*, 2011, **50**, 9564–9583; (k) M. Giese, M. Albrecht and K. Rissanen, *Chem. Commun.*, 2016, **52**, 1778–1795; (l) P. Metrangolo, F. Meyer, T. Pilati, G. Resnati and G. Terraneo, *Angew. Chem., Int. Ed.*, 2008, **47**, 6114–6127; (m) G. Cavallo, P. Metrangolo, T. Pilati, G. Resnati, M. Sansotera and G. Terraneo, *Chem. Soc. Rev.*, 2010, **39**, 3772–3783; (n) T. M. Beale, M. G. Chudzinski, M. G. Sarwar and M. S. Taylor, *Chem. Soc. Rev.*, 2013, **42**, 1667–1680; (o) L. C. Gilday, S. W. Robinson, T. A. Barendt, M. J. Langton, B. R. Mullaney and P. D. Beer, *Chem. Rev.*, 2015, **115**, 7118–7195; (p) A. Brown and P. D. Beer, *Chem. Commun.*, 2016, **52**, 8645–8658; (q) D. Bulfield and S. M. Huber, *Chem. – Eur. J.*, 2016, **22**, 14434–14450.
- G. R. Desiraju, P. S. Ho, L. Kloo, A. C. Legon, R. Marquardt, P. Metrangolo, P. Politzer, G. Resnati and K. Rissanen, *Pure Appl. Chem.*, 2013, **85**, 1711–1713.
- (a) N. L. Kilah, M. D. Wise, C. J. Serpell, A. L. Thompson, N. G. White, K. E. Christensen and P. D. Beer, *J. Am. Chem. Soc.*, 2010, **132**, 11893–11895; (b) R. Tepper, B. Schulze, M. Jäger, C. Friebe, D. H. Scharf, H. Görls and U. S. Schubert, *J. Org. Chem.*, 2015, **80**, 3139–3150; (c) A. Borissov, J. Y. C. Lim, A. Brown, K. E. Christensen, A. L. Thompson, M. D. Smith and P. D. Beer, *Chem. Commun.*, 2017, **53**, 2483–2486.
- (a) V. Haridas, S. Sahu, P. P. P. Kumar and A. R. Sapala, *RSC Adv.*, 2012, **2**, 12594–12605; (b) B. Schulze and U. S. Schubert, *Chem. Soc. Rev.*, 2014, **43**, 2522–2571.
- (a) W. S. Brotherton, R. J. Clark and L. Zhu, *J. Org. Chem.*, 2012, **77**, 6443–6455; (b) D. N. Barsoum, N. Okashah, X. Zhang and L. Zhu, *J. Org. Chem.*, 2015, **80**, 9542–9551.
- M. D. Lankshear and P. D. Beer, *Acc. Chem. Res.*, 2007, **40**, 657–668.
- (a) M. J. Langton, S. W. Robinson, I. Marques, V. Félix and P. D. Beer, *Nat. Chem.*, 2014, **6**, 1039–1043; (b) A. Rezanka, M. J. Langton and P. D. Beer, *Chem. Commun.*, 2015, **51**, 4499–4502.
- (a) A. Caballero, N. G. White and P. D. Beer, *Angew. Chem., Int. Ed.*, 2011, **50**, 1845–1848; (b) R. Tepper, B. Schulze, P. Bellstedt, J. Heidler, H. Görls, M. Jäger and U. S. Schubert, *Chem. Commun.*, 2017, **53**, 2260–2263.
- D. Mungalpara, H. Kelm, A. Valkonen, K. Rissanen, S. Keller and S. Kubik, *Org. Biomol. Chem.*, 2017, **15**, 102–113.
- M. G. Chudzinski, C. A. McClary and M. S. Taylor, *J. Am. Chem. Soc.*, 2011, **133**, 10559–10567.
- M. Kaasik, S. Kaabel, K. Kriis, I. Järving, R. Aav, K. Rissanen and T. Kanger, *Chem. – Eur. J.*, 2017, DOI: 10.1002/chem.201700618.

## 5 Conclusion and Outlook

During the experimental work of this thesis three novel cyclic pseudopeptides **16**, **17** and **18** were successfully synthesized and their anion binding properties evaluated. These compounds complement the series of anion-binding cyclopeptide and cyclopseudopeptide derivatives developed in the Kubik group by derivatives containing 1,4-disubstituted 1,2,3-triazole units along the ring. These subunits not only act as surrogates for *trans*-amide groups, they also add converging 1,2,3-triazole C-H or 5-iodo-1,2,3-triazole C-I groups to the receptors that, together with the amide N-H groups, could participate in anion binding by HB or XB interactions, respectively.

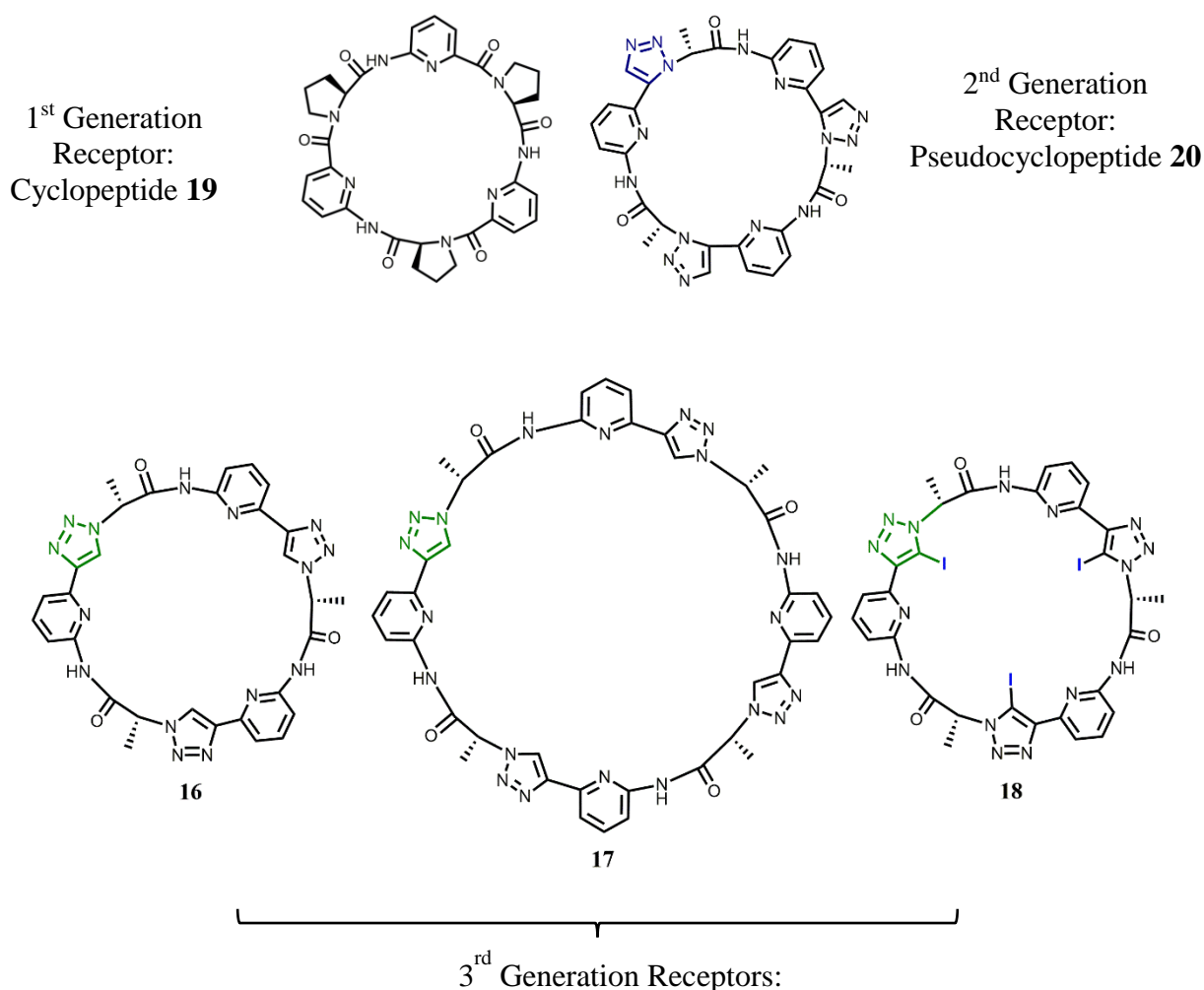


### Chart 16

Structural studies show that all three pseudopeptides can adopt conformations with the triazole C-H or C-I groups pointing into the cavity center to allow them to contribute to binding. Anion binding of **16** could only be studied in organic media because of solubility reasons. In 5 vol% DMSO-*d*<sub>6</sub>/acetone-*d*<sub>6</sub>, **16** binds to chloride, bromide, nitrate, hydrogen sulfate, sulfate, and dihydrogen phosphate anions. Quantitative binding studies demonstrated that chloride, bromide,

and hydrogen sulfate are bound in the forms of (**16**)·(anion)<sub>2</sub> complexes in this solvent mixture. The exact structure of these complexes could not be determined. The binding of sulfate and DHP in 5 vol% DMSO-*d*<sub>6</sub>/acetone-*d*<sub>6</sub> is slow on the NMR time scale. In 2.5 vol% D<sub>2</sub>O/DMSO-*d*<sub>6</sub>, **16** only binds strongly coordinating oxoanions. The respective complexes differ in their stoichiometries. In the case of DHP, two anions are bound by **16** in solution, whereas sulfate and HPP complexation involves a stepwise process comprising formation of a 1:1 complex followed by binding of second pseudopeptide ring. Receptor **16** thus has a propensity to form higher complexes with sulfate and DHP presumably because it is unable to fully saturate the acceptor sites on these anions for structural reasons.

Pseudopeptide **17** was expected to form 1:1 complexes. This complex stoichiometry was indeed observed for sulfate binding. However, the respective complex is not very stable maybe because the arrangement of hydrogen bond donors of **17** along the ring is not optimal for sulfate complexation. Phosphate-derived anions are bound in the form of sandwich-type complexes in which a dimer of DHPP or a tetramer of DHP is arranged between two pseudopeptide rings. These higher complexes are stabilized by multiple HB interactions, potentially combined with dispersive interaction between the pseudopeptides. As a consequence, the complexes persist in solution and can even be transferred without decomposition into the gas phase although they are made up of up to six components. Fitting of the binding isotherms obtained by microcalorimetric titration to a simplified model demonstrated high stability. Interestingly, the sandwich-type binding mode observed for the DHPP and DHP complexes of **17** is somewhat reminiscent of sandwich complexes of cyclopeptide **19**.

Pseudohexapeptide **18** allows anion binding by halogen bonding. In addition, introduction of iodine atoms also affects the cavity size of the pseudopeptide, thus mediating anion selectivity. Interaction of **18** with oxyanions is relatively weak but binding to halides, in particular to chloride, which were not bound in the same solvent by **16**, is strong when considering that only XB interactions are responsible.

While the unusual phosphate affinity of **17** and the halide affinity of **18** are particularly interesting, the presence of the 1,4-disubstituted 1,2,3-triazol groups in these receptors typically reduce their solubility in polar protic solvents. Therefore, future work should focus on improving water solubility without disturbing the anion binding properties to allow these pseudopeptides to be used under conditions more relevant for application. In this context, either converting the triazole subunits into triazolium subunits or replacing the methyl groups on the

stereogenic centers by the more polar side chains could be an interesting options. Examples of potential future receptors are shown in Chart 17.

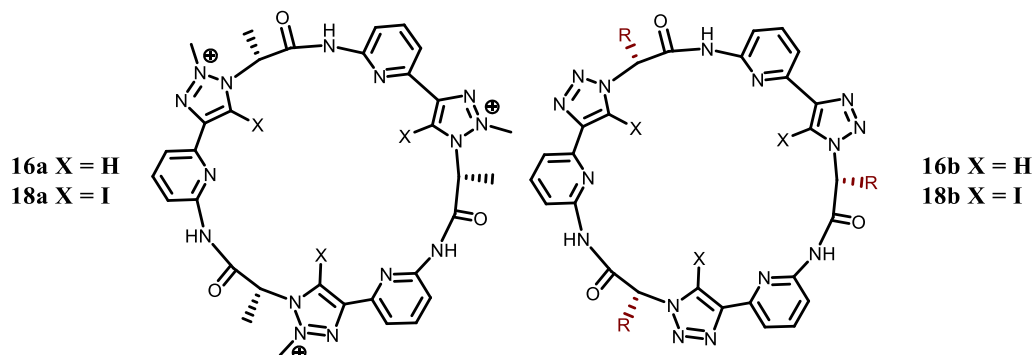


Chart 17

## 6 References

- 1 J.-M. Lehn, *Supramolecular Chemistry: Concepts and Perspectives*, Wiley-VCH, Weinheim, 1995.
- 2 D. J. Cram, *Angew. Chem., Int. Ed. Engl.*, 1986, **25**, 1039–1057.
- 3 F. P. Schmidtchen, *Chem. Soc. Rev.*, 2010, **39**, 3916–3935.
- 4 P. D. Beer and P. A. Gale, *Angew. Chem., Int. Ed.*, 2001, **40**, 486–516.
- 5 N. Busschaert, C. Caltagirone, W. Van Rossom and P. A. Gale, *Chem. Rev.*, 2015, **115**, 8038–8155.
- 6 P. A. Gale, *Acc. Chem. Res.*, 2011, **44**, 216–226.
- 7 N. H. Evans and P. D. Beer, *Angew. Chem., Int. Ed.*, 2014, **53**, 11716–11754.
- 8 M. A. Wilson, P. J. Bailey, P. A. Tasker, J. R. Turkington, R. A. Grant and J. B. Love, *Chem. Soc. Rev.*, 2014, **43**, 123–34.
- 9 M. J. Welsh and A. E. Smith, *Cell*, 1993, **73**, 1251–1254.
- 10 E. Belloni, M. Muenke, E. Roessler, G. Traverse, J. Siegel-Bartelt, A. Frumkin, H. F. Mitchell, H. Donis-Keller, C. Helms, A. V. Hing, H. H. Q. Heng, B. Koop, D. Martindale, J. M. Rommens, L.-C. Tsui and S. W. Scherer, *Nat. Genet.*, 1997, **17**, 171–178.
- 11 E. Belloni, M. Muenke, E. Roessler, G. Traverse, J. Siegel-Bartelt, A. Frumkin, H. F. Mitchell, H. Donis-Keller, C. Helms, A. V. Hing, H. H. Q. Heng, B. Koop, D. Martindale, J. M. Rommens, L.-C. Tsui and S. W. Scherer, *Nat. Genet.*, 1996, **14**, 353–6.
- 12 D. A. Scott, R. Wang, T. M. Kreman, V. C. Sheffield and L. P. Karniski, *Nat. Genet.*, 1999, **21**, 440–443.
- 13 R. H. Moseley, P. Höglund, G. D. Wu, D. G. Silberg, S. Haila, A. De La Chapelle, C. Holmberg and J. Kere, *Am. J. Physiol.*, 1999, **276**, 185–192.
- 14 S. J. Connon, *Synlett*, 2009, 354–376.
- 15 S. J. Connon, *Chem. Commun.*, 2008, 2499–2510.
- 16 S. Kubik, in *Synthetic Receptors for Biomolecules: Design Principles and Applications*, The Royal Society of Chemistry, 2015, pp. 129–176.
- 17 P. A. Gale, *Chem. Commun.*, 2011, **47**, 82–86.
- 18 P. D. Beer and E. J. Hayes, *Coord. Chem. Rev.*, 2003, **240**, 167–189.
- 19 E. J. O’Neil and B. D. Smith, *Coord. Chem. Rev.*, 2006, **250**, 3068–3080.
- 20 L. Fabbrizzi and A. Poggi, *Chem. Soc. Rev.*, 2013, **42**, 1681–1699.
- 21 C. H. Park and H. E. Simmons, *J. Am. Chem. Soc.*, 1968, **90**, 2431–2432.
- 22 F. P. Schmidtchen, *Angew. Chem., Int. Ed. Engl.*, 1977, **16**, 720–721.
- 23 J. M. L. Ernest Graf, *J. Am. Chem. Soc.*, 1976, **98**, 6403–6405.
- 24 E. Arunan, G. R. Desiraju, R. A. Klein, J. Sadlej, S. Scheiner, I. Alkorta, D. C. Clary, R. H. Crabtree, J. J. Dannenberg, P. Hobza, H. G. Kjaergaard, A. C. Legon, B. Mennucci and D. J. Nesbitt, *Pure Appl. Chem.*, 2011, **83**, 1637–1641.
- 25 T. Steiner, *Angew. Chem., Int. Ed.*, 2002, **41**, 49–76.
- 26 J. Cai and J. L. Sessler, *Chem. Soc. Rev.*, 2014, **43**, 6198–6213.
- 27 Y. Hua and A. H. Flood, *Chem. Soc. Rev.*, 2010, **39**, 1262–1271.
- 28 V. Haridas, S. Sahu, P. P. Praveen Kumar and A. R. Sapala, *RSC Adv.*, 2012, **2**, 12594–12605.
- 29 B. Schulze and U. S. Schubert, *Chem. Soc. Rev.*, 2014, **43**, 2522–2571.
- 30 H. C. Kolb, M. G. Finn and K. B. Sharpless, *Angew. Chem., Int. Ed.*, 2001, **40**, 2004–

- 2021.
- 31 A. Brown and P. D. Beer, *Chem. Commun.*, 2016, **52**, 8645–8658.
- 32 P. Metrangolo, F. Meyer, T. Pilati, G. Resnati and G. Terraneo, *Angew. Chem., Int. Ed.*, 2008, **47**, 6114–6127.
- 33 P. Politzer, P. Lane, M. C. Concha, Y. Ma and J. S. Murray, *J. Mol. Model.*, 2007, **13**, 305–311.
- 34 P. Metrangolo, H. Neukirch, T. Pilati and G. Resnati, *Acc. Chem. Res.*, 2005, **38**, 386–395.
- 35 G. R. Desiraju, P. S. Ho, L. Kloo, A. C. Legon, R. Marquardt, P. Metrangolo, P. Politzer, G. Resnati and K. Rissanen, *Pure Appl. Chem.*, 2013, **85**, 1711–1713.
- 36 P. Metrangolo and G. Resnati, *Chem. Eur. J.*, 2001, **7**, 2511–2519.
- 37 N. Ramasubbu, R. Parthasarathy and P. Murray-Rust, *J. Am. Chem. Soc.*, 1986, **108**, 4308–4314.
- 38 J. P. M. Lommerse, A. J. Stone, R. Taylor and F. H. Allen, *J. Am. Chem. Soc.*, 1996, **118**, 3108–3116.
- 39 G. A. Landrum, N. Goldberg and R. Hoffmann, *J. Chem. Soc., Dalton Trans.*, 1997, 3605–3613.
- 40 V. V. Rostovtsev, L. G. Green, V. V. Fokin and K. B. Sharpless, *Angew. Chem. Int. Ed.*, 2002, **41**, 2596–2599.
- 41 C. W. Tornøe, C. Christensen and M. Meldal, *J. Org. Chem.*, 2002, **67**, 3057–3064.
- 42 Y. Li and A. H. Flood, *Angew. Chem., Int. Ed.*, 2008, **47**, 2649–2652.
- 43 H. Juwarker, J. M. Lenhardt, D. M. Pham and S. L. Craig, *Angew. Chem., Int. Ed.*, 2008, **47**, 3740–3743.
- 44 R. M. Meudtner and S. Hecht, *Angew. Chem., Int. Ed.*, 2008, **47**, 4926–4930.
- 45 S. Kubik, in *Supramolecular Chemistry: From Molecules to Nanomaterials*, J. Wiley & Sons, Chichester, 2012, pp. 1179–1203.
- 46 S. J. Butler and K. A. Jolliffe, *Org. Biomol. Chem.*, 2011, **9**, 3471–3483.
- 47 S. Kubik, *Chem. Soc. Rev.*, 2009, **38**, 585–605.
- 48 L. Xu, Y. Li, Y. Yu, T. Liu, S. Cheng, H. Liu and Y. Li, *Org. Biomol. Chem.*, 2012, **10**, 4375–80.
- 49 L. Cao, R. Jiang, Y. Zhu, X. Wang, Y. Li and Y. Li, *Eur. J. Org. Chem.*, 2014, 2687–2693.
- 50 Y. J. Li, L. Xu-, W. L. Yang-, H. B. Liu, S. W. Lai, C. M. Che and Y. L. Li, *Chem. Eur. J.*, 2012, **18**, 4782–4790.
- 51 I. E. Valverde and T. L. Mindt, *Chimia (Aarau).*, 2013, **67**, 262–266.
- 52 D. S. Pedersen and A. Abell, *Eur. J. Org. Chem.*, 2011, 2399–2411.
- 53 Y. L. Angell and K. Burgess, *Chem. Soc. Rev.*, 2007, **36**, 1674–1689.
- 54 M. H. Palmer, R. H. Findlay and A. J. Gaskell, *J. Chem. Soc., Perkin Trans. 2*, 1974, 420–428.
- 55 W. S. Horne, M. K. Yadav, C. D. Stout and M. R. Ghadiri, *J. Am. Chem. Soc.*, 2004, **126**, 15366–15367.
- 56 I. E. Valverde, A. Bauman, C. A. Kluba, S. Vomstein, M. A. Walter and T. L. Mindt, *Angew. Chem., Int. Ed.*, 2013, **52**, 8957–8960.
- 57 Ahsanullah and J. Rademann, *Angew. Chem., Int. Ed.*, 2010, **49**, 5378–5382.
- 58 H. C. Kolb and K. B. Sharpless, *Drug Discov. Today*, 2003, **8**, 1128–1137.

- 59 M. R. Davis, E. K. Singh, H. Wahyudi, L. D. Alexander, J. B. Kunicki, L. A. Nazarova, K. A. Fairweather, A. M. Giltrap, K. A. Jolliffe and S. R. McAlpine, *Tetrahedron*, 2012, **68**, 1029–1051.
- 60 M. Tischler, D. Nasu, M. Empting, S. Schmelz, D. W. Heinz, P. Rottmann, H. Kolmar, G. Buntkowsky, D. Tietze and O. Avrutina, *Angew. Chem., Int. Ed.*, 2012, **51**, 3708–3712.
- 61 A. Brown and P. D. Beer, *Chem. Commun.*, 2016, **52**, 8645–8658.
- 62 W. S. Brotherton, R. J. Clark and L. Zhu, *J. Org. Chem.*, 2012, **77**, 6443–6455.
- 63 D. N. Barsoum, N. Okashah, X. Zhang and L. Zhu, *J. Org. Chem.*, 2015, **80**, 9542–9551.
- 64 R. Tepper, B. Schulze, P. Bellstedt, J. Heidler, H. Görls, M. Jäger and U. S. Schubert, *Chem. Commun.*, 2017, **53**, 2260–2263.
- 65 T. Clark, M. Hennemann, J. S. Murray and P. Politzer, *J. Mol. Model.*, 2007, **13**, 291–296.
- 66 R. Tepper, B. Schulze, H. Görls, P. Bellstedt, M. Jäger and U. S. Schubert, *Org. Lett.*, 2015, **17**, 5740–5743.
- 67 T. K. Mole, W. E. Arter, I. Marques, V. Félix and P. D. Beer, *J. Organomet. Chem.*, 2015, **792**, 206–210.
- 68 A. Borissov, J. Y. C. Lim, A. Brown, K. E. Christensen, A. L. Thompson, M. D. Smith and P. D. Beer, *Chem. Commun.*, 2017, **53**, 2483–2486.
- 69 M. J. Langton, Y. Xiong and P. D. Beer, *Chem. Eur. J.*, 2015, **21**, 18910–18914.
- 70 L. C. Gilday, N. G. White and P. D. Beer, *Dalton Trans.*, 2013, **42**, 15766.
- 71 S. W. Robinson, C. L. Mustoe, N. G. White, A. Brown, A. L. Thompson, P. Kennepohl and P. D. Beer, *J. Am. Chem. Soc.*, 2015, **137**, 499–507.
- 72 M. J. Langton, S. W. Robinson, I. Marques, V. Félix and P. D. Beer, *Nat. Chem.*, 2014, **6**, 1039–1043.
- 73 S. Kubik, R. Goddard, R. Kirchner, D. Nolting and J. Seidel, *Angew. Chem., Int. Ed.*, 2001, **40**, 2648–2651.
- 74 M. R. Krause, R. Goddard and S. Kubik, *J. Org. Chem.*, 2011, **76**, 7084–7095.
- 75 R. T. R. Annie Tam, Ulrich Arnold, Matthew B. Soellner, *J. Am. Chem. Soc.*, 2007, **129**, 12670–12671.
- 76 J. Zabrocki, J. J. B. Dunbar, K. W. Marshall, M. V Toth and G. R. Marshall, *J. Org. Chem.*, 1992, **57**, 202–209.
- 77 M. R. Krause, R. Goddard and S. Kubik, *Chem. Commun.*, 2010, **46**, 5307–5309.
- 78 D. Mungalpara, H. Kelm, A. Valkonen, K. Rissanen, S. Keller and S. Kubik, *Org. Biomol. Chem.*, 2017, **15**, 102–113.
- 79 A. Daryl Ariawan, J. E. A. Webb, E. N. W. Howe, P. A. Gale, P. Thordarson and L. Hunter, *Org. Biomol. Chem.*, 2017, **15**, 2962–2967.
- 80 A. Rajbanshi, S. Wan and R. Custelcean, *Cryst. Growth Des.*, 2013, **13**, 2233–2237.
- 81 J. De Cierva and E. Espinosa, *J. Phys. Chem. A*, 2015, **119**, 183–194.
- 82 M. K. Deliomeroğlu, V. M. Lynch and J. L. Sessler, *Chem. Sci.*, 2016, **7**, 3843–3850.
- 83 G. Ercolani, *J. Am. Chem. Soc.*, 2003, **125**, 16097–16103.
- 84 A. R. Bogdan and K. James, *Org. Lett.*, 2011, **13**, 4060–4063.
- 85 A. C. Bédard and S. K. Collins, *Org. Lett.*, 2014, **16**, 5286–5289.

## 7 Appendix I

Electronic Supplementary Material (ESI) for Organic & Biomolecular Chemistry.  
This journal is © The Royal Society of Chemistry 2016

*Org. Biomol. Chem.*

### **Oxoanion binding to a cyclic pseudopeptide containing 1,4-disubstituted 1,2,3-triazole moieties**

Disha Mungalpara,<sup>a</sup> Harald Kelm,<sup>b</sup> Arto Valkonen,<sup>c</sup> Kari Rissanen,<sup>c</sup>  
Sandro Keller<sup>d</sup> and Stefan Kubik<sup>\*a</sup>

<sup>a</sup> *Technische Universität Kaiserslautern, Fachbereich Chemie - Organische Chemie, Erwin-Schrödinger-Straße, 67663 Kaiserslautern, Germany. E-mail: kubik@chemie.uni-kl.de.*

<sup>b</sup> *Technische Universität Kaiserslautern, Fachbereich Chemie - Anorganische Chemie, Erwin-Schrödinger-Straße, 67663 Kaiserslautern, Germany.*

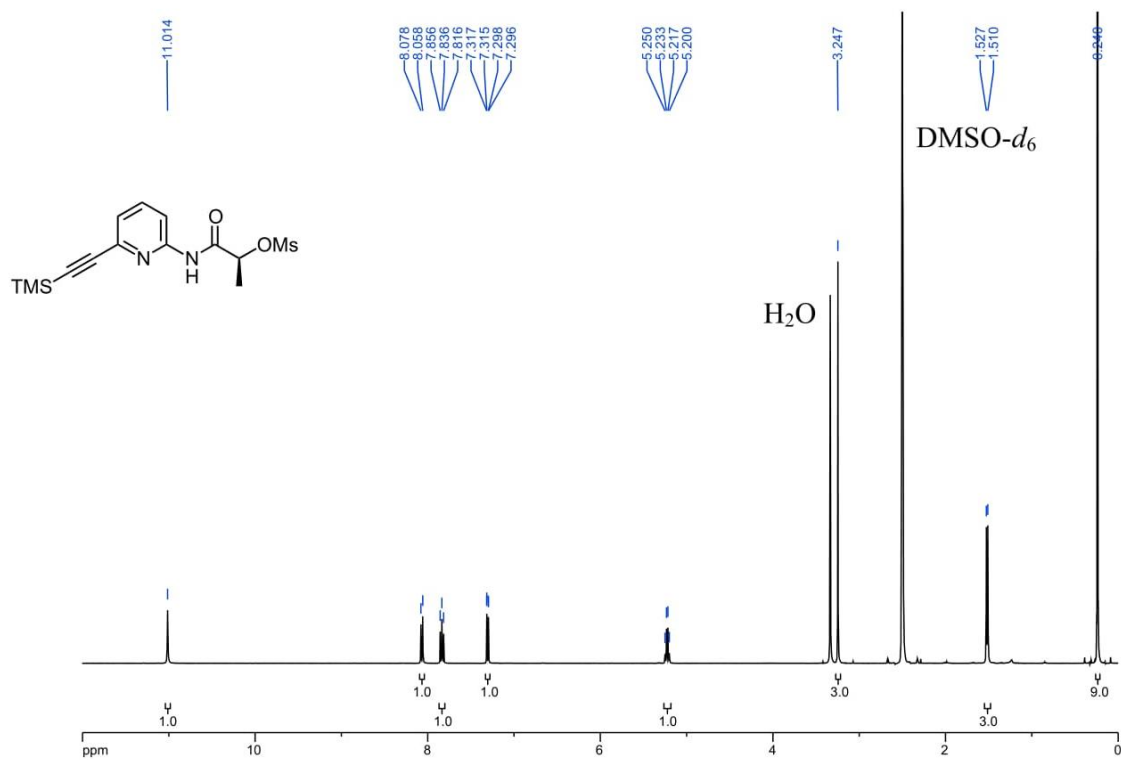
<sup>c</sup> *University of Jyväskylä, Department of Chemistry, Nanoscience Center, P.O. Box 35, Jyväskylä FI-40014, Finland.*

<sup>d</sup> *University of Kaiserslautern, Molecular Biophysics, Erwin-Schrödinger-Str. 13, 67663 Kaiserslautern, Germany.*

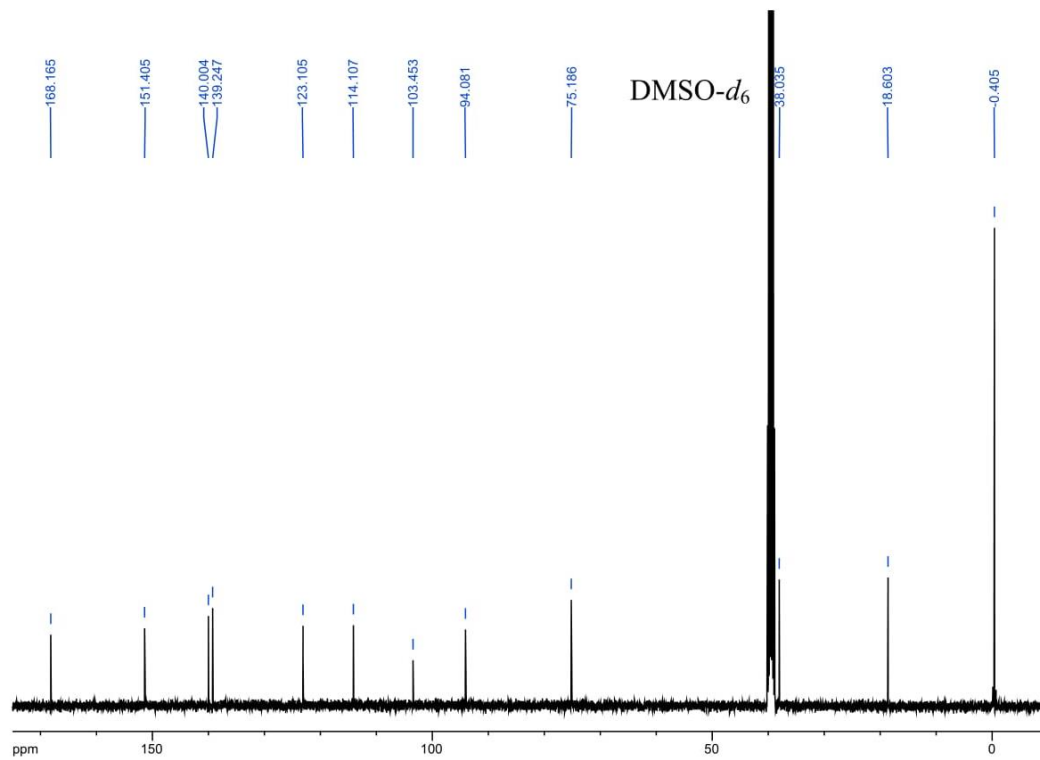
### **CONTENT**

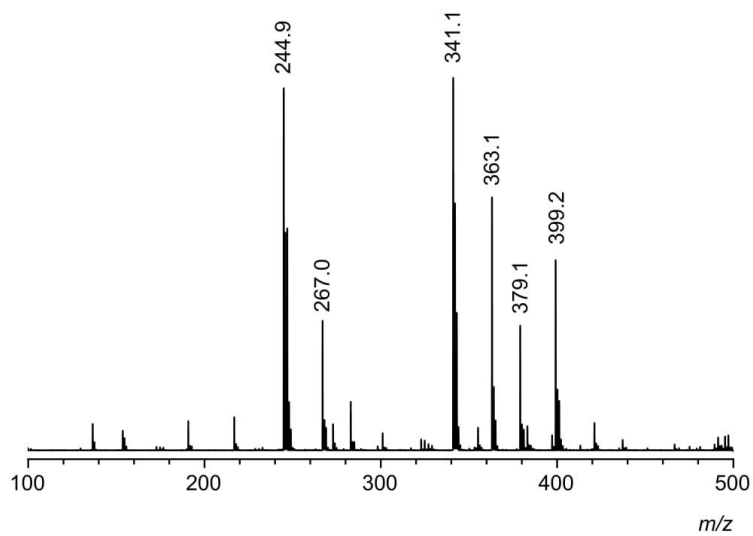
<sup>1</sup> H NMR, <sup>13</sup> C NMR, and MS Spectra of <b>5</b> , <b>7</b> , <b>8</b> , and <b>3</b> .....	S2
NOESY NMR Spectrum of <b>3</b> .....	S10
Qualitative Binding Studies in 2.5 vol% D <sub>2</sub> O/DMSO- <i>d</i> <sub>6</sub> .....	S11
Water Effect on the <sup>1</sup> H NMR Spectrum of <b>3</b> .....	S12
Water Effect on the <sup>1</sup> H NMR Spectrum of the Dihydrogenphosphate Complex of <b>3</b> .....	S13
Job Plots .....	S14
NMR Titrations .....	S16
Selected ITC Titrations .....	S21
Crystal Structures .....	S26
References .....	S29

$^1\text{H}$  NMR: TMS-Epa-(*S*)-Lac-OMs **5** (400 MHz,  $\text{DMSO-}d_6$ ).



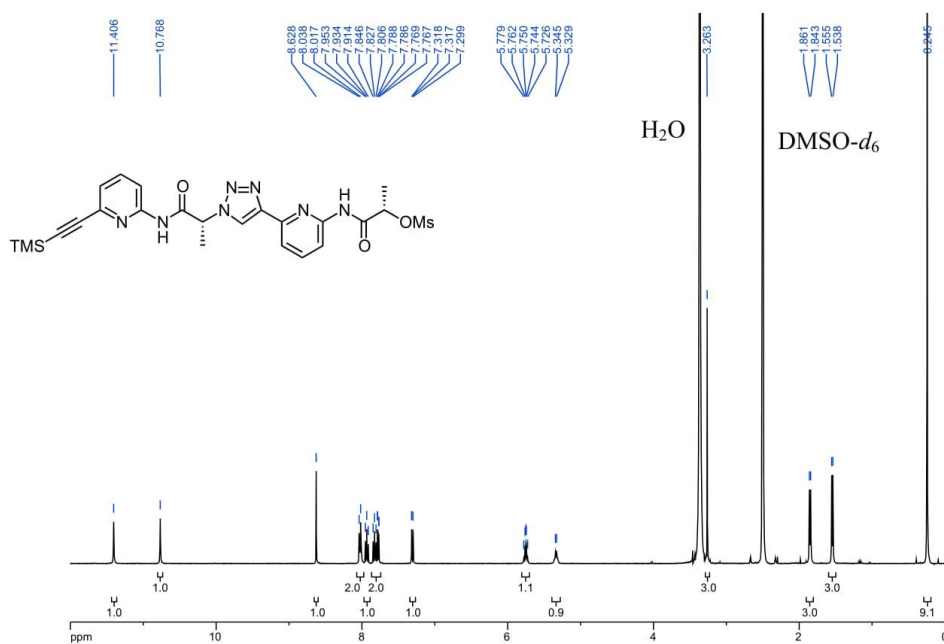
$^{13}\text{C}$  NMR: TMS-Epa-(*S*)-Lac-OMs **5** (101 MHz,  $\text{DMSO-}d_6$ ).



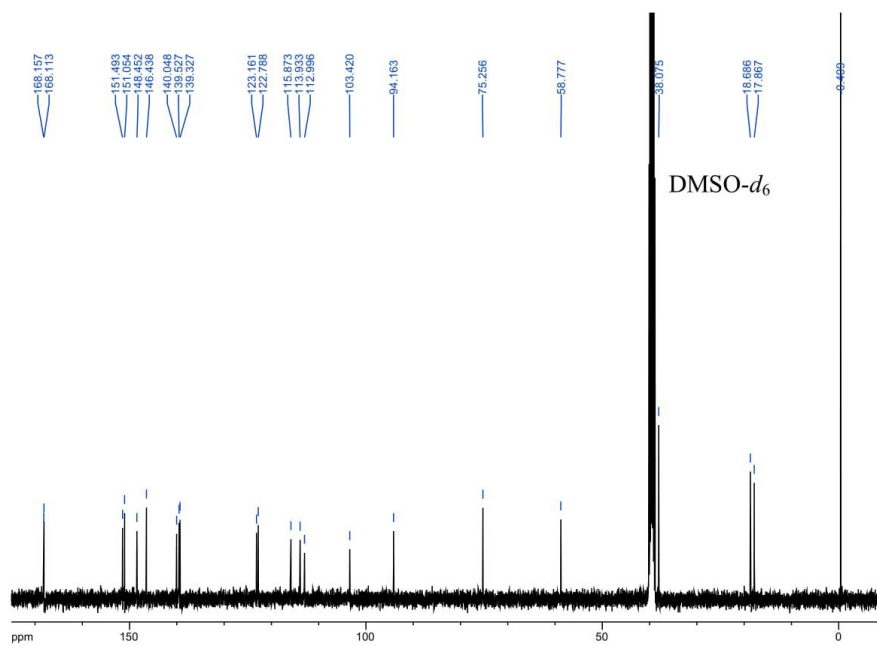
MALDI-TOF MS: TMS-Epa-(*S*)-Lac-OMs **5** (positive mode).

		<i>m/z calcd.</i>	<i>m/z exp.</i>
$[M-CH_3SO_3H+H]^+$	$C_{14}H_{20}N_2O_4SSi - CH_3SO_3H + H^+$	245.1	244.9
$[M-CH_3SO_3H+Na]^+$	$C_{14}H_{20}N_2O_4SSi - CH_3SO_3H + Na^+$	267.1	267.0
$[M+H]^+$	$C_{14}H_{20}N_2O_4SSi + H^+$	341.1	341.1
$[M+Na]^+$	$C_{14}H_{20}N_2O_4SSi + Na^+$	363.1	363.1
$[M+K]^+$	$C_{14}H_{20}N_2O_4SSi + K^+$	379.1	379.1
$[M+C_3H_6O+H]^+$	$C_{14}H_{20}N_2O_4SSi + C_3H_6O + H^+$	399.1	399.2

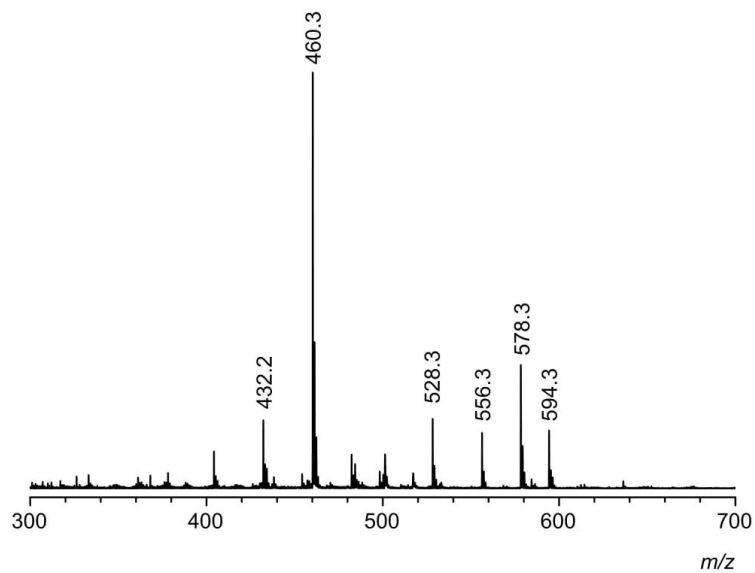
$^1\text{H}$  NMR: TMS-Epa-(*R*)-Lac-1,4-Tri-Epa-(*S*)-Lac-OMs **7** (400 MHz,  $\text{DMSO-}d_6$ ).



$^{13}\text{C}$  NMR: TMS-Epa-(*R*)-Lac-1,4-Tri-Epa-(*S*)-Lac-OMs **7** (101 MHz,  $\text{DMSO-}d_6$ ).

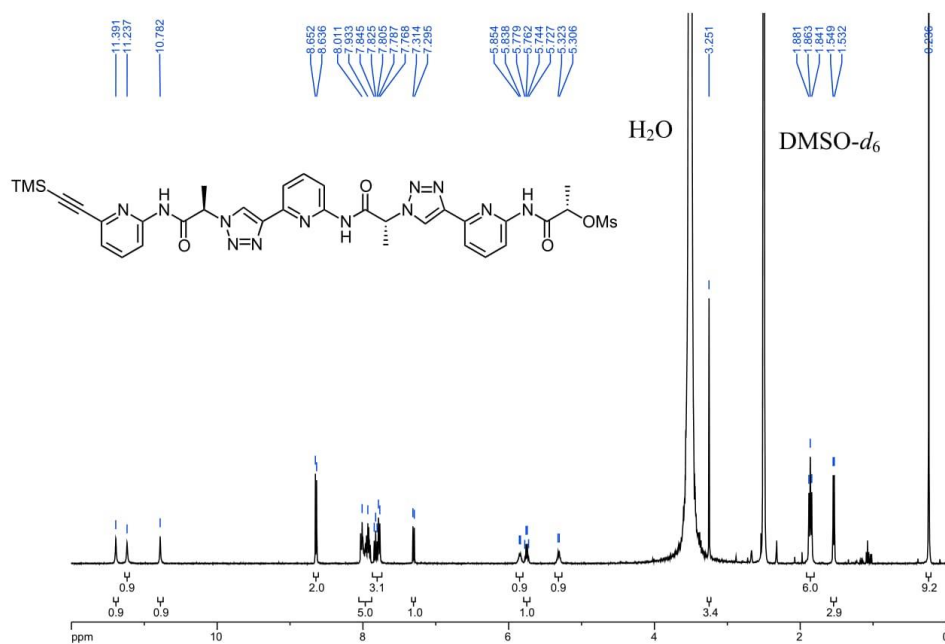


MALDI-TOF MS: TMS-Epa-(*R*)-Lac-1,4-Tri-Epa-(*S*)-Lac-OMs **7** (positive mode).

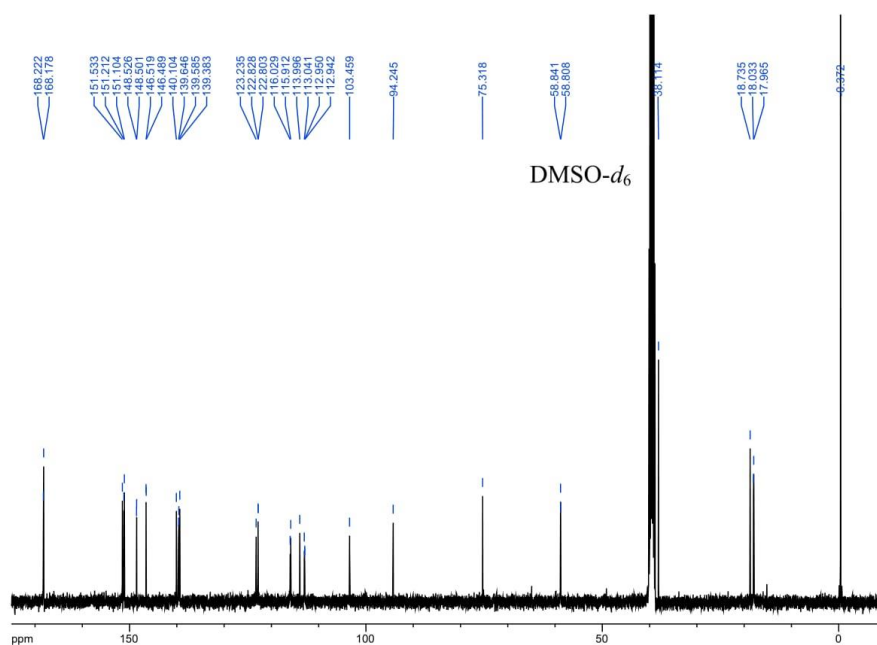


		<i>m/z</i> calcd.	<i>m/z</i> exp.
$[M-N_2-CH_3SO_3H+H]^+$	$C_{24}H_{29}N_7O_5SSi - N_2 - CH_3SO_3H + H^+$	432.6	432.2
$[M-CH_3SO_3H+H]^+$	$C_{24}H_{29}N_7O_5SSi - CH_3SO_3H + H^+$	460.6	460.3
$[M-N_2+H]^+$	$C_{24}H_{29}N_7O_5SSi - N_2 + H^+$	528.7	528.3
$[M+H]^+$	$C_{24}H_{29}N_7O_5SSi + H^+$	556.2	556.3
$[M+Na]^+$	$C_{24}H_{29}N_7O_5SSi + Na^+$	578.2	578.3
$[M+K]^+$	$C_{24}H_{29}N_7O_5SSi + K^+$	594.1	594.3

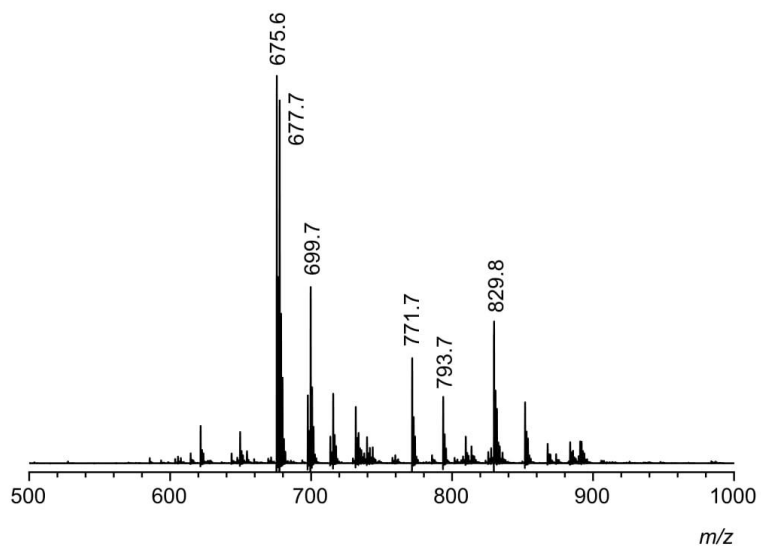
$^1\text{H NMR}$ : TMS-Epa-[(*R*)-Lac-1,4-Tri-Epa] $_2$ -(*S*)-Lac-OMs **8** (400 MHz,  $\text{DMSO-}d_6$ ).



$^{13}\text{C NMR}$ : TMS-Epa-[(*R*)-Lac-1,4-Tri-Epa] $_2$ -(*S*)-Lac-OMs **8** (101 MHz,  $\text{DMSO-}d_6$ ).

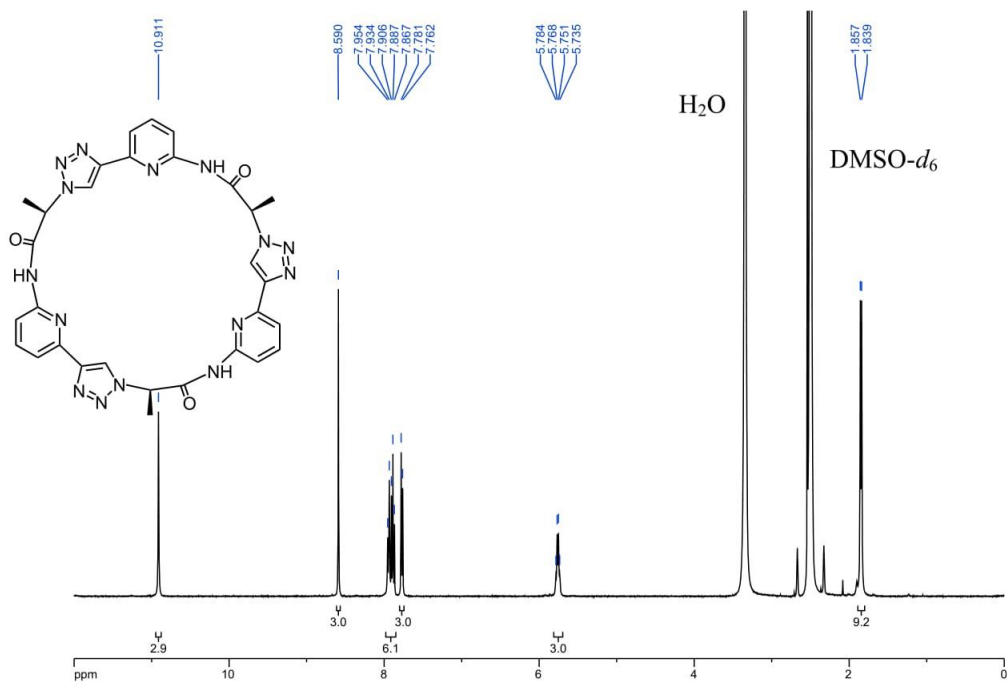


MALDI-TOF MS: TMS-Epa-[(*R*)-Lac-1,4-Tri-Epa]<sub>2</sub>-(*S*)-Lac-OMs **8** (positive mode).

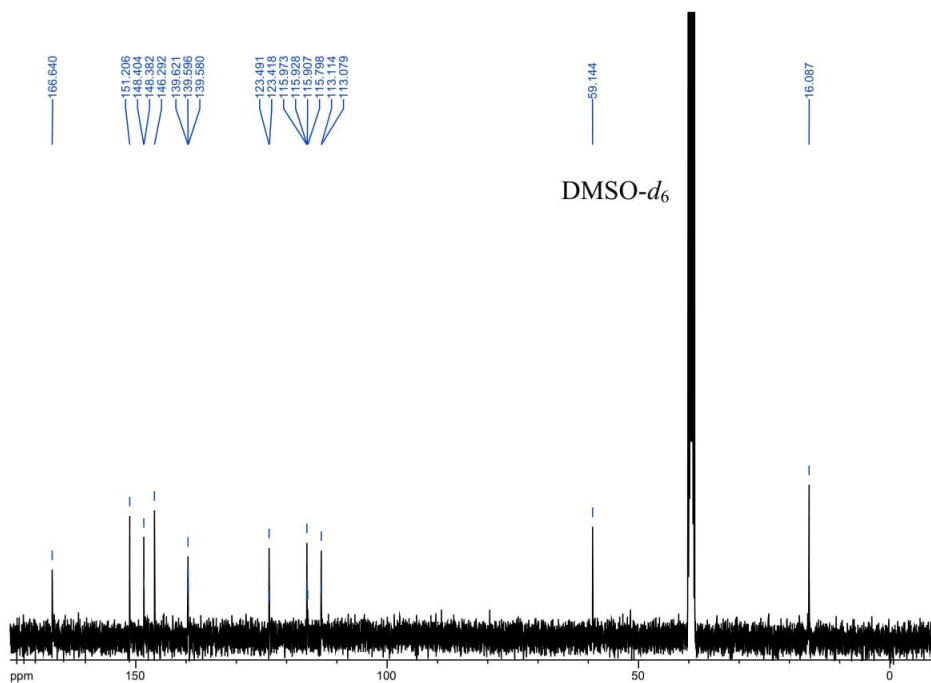


		<i>m/z calcd.</i>	<i>m/z exp.</i>
$[M-CH_3SO_3H+H]^+$	$C_{34}H_{38}N_{12}O_6SSi - CH_3SO_3H + H^+$	675.8	675.6
$[M-CH_3SO_3H+H_2+H]^+$	$C_{34}H_{38}N_{12}O_6SSi - CH_3SO_3H + H_2 + H^+$	677.8	677.7
$[M-CH_3SO_3H+H_2+Na]^+$	$C_{34}H_{38}N_{12}O_6SSi - CH_3SO_3H + H_2 + Na^+$	699.8	699.7
$[M+H]^+$	$C_{34}H_{38}N_{12}O_6SSi + H^+$	771.3	771.7
$[M+Na]^+$	$C_{34}H_{38}N_{12}O_6SSi + Na^+$	793.2	793.7
$[M+C_3H_6O+H]^+$	$C_{34}H_{38}N_{12}O_6SSi + C_3H_6O + H^+$	829.3	829.8

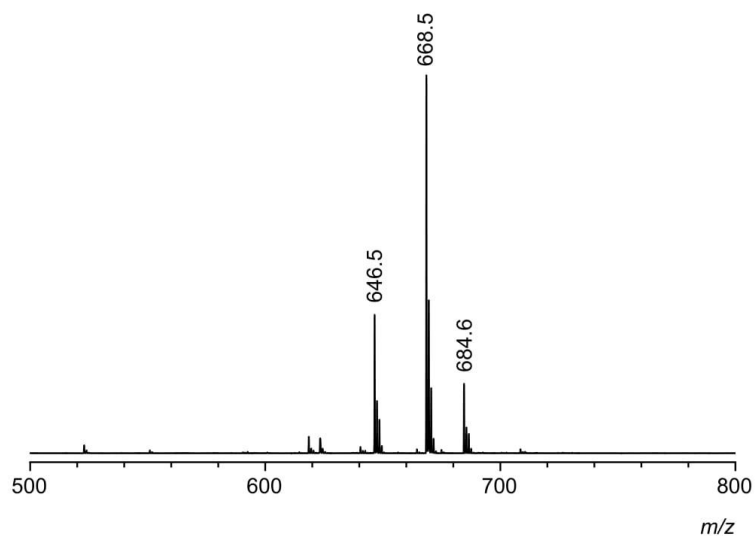
$^1\text{H}$  NMR: *cyclo*[(*R*)-Lac-1,4-Tri-Epa]<sub>3</sub> **3** (400 MHz, DMSO-*d*<sub>6</sub>).



$^{13}\text{C}$  NMR: *cyclo*[(*R*)-Lac-1,4-Tri-Epa]<sub>3</sub> **3** (101 MHz, DMSO-*d*<sub>6</sub>).

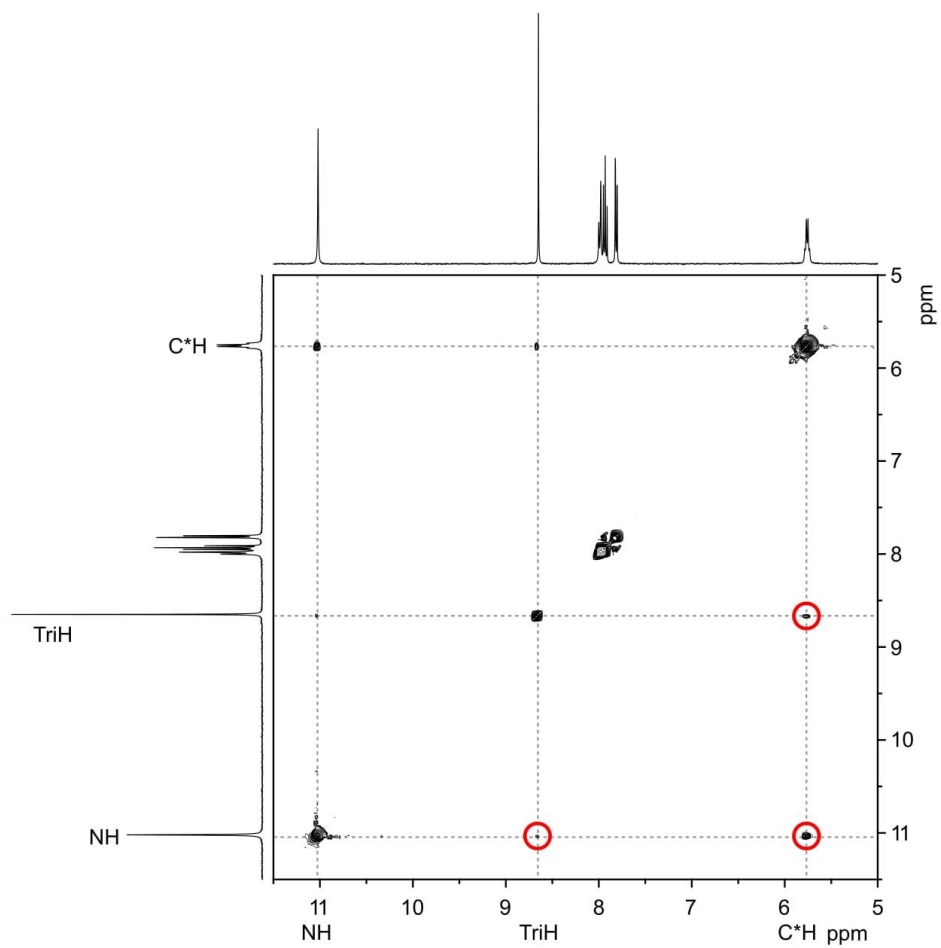


MALDI-TOF MS: *cyclo*[(*R*)-Lac-1,4-Tri-Epa]<sub>3</sub> **3** (positive mode).

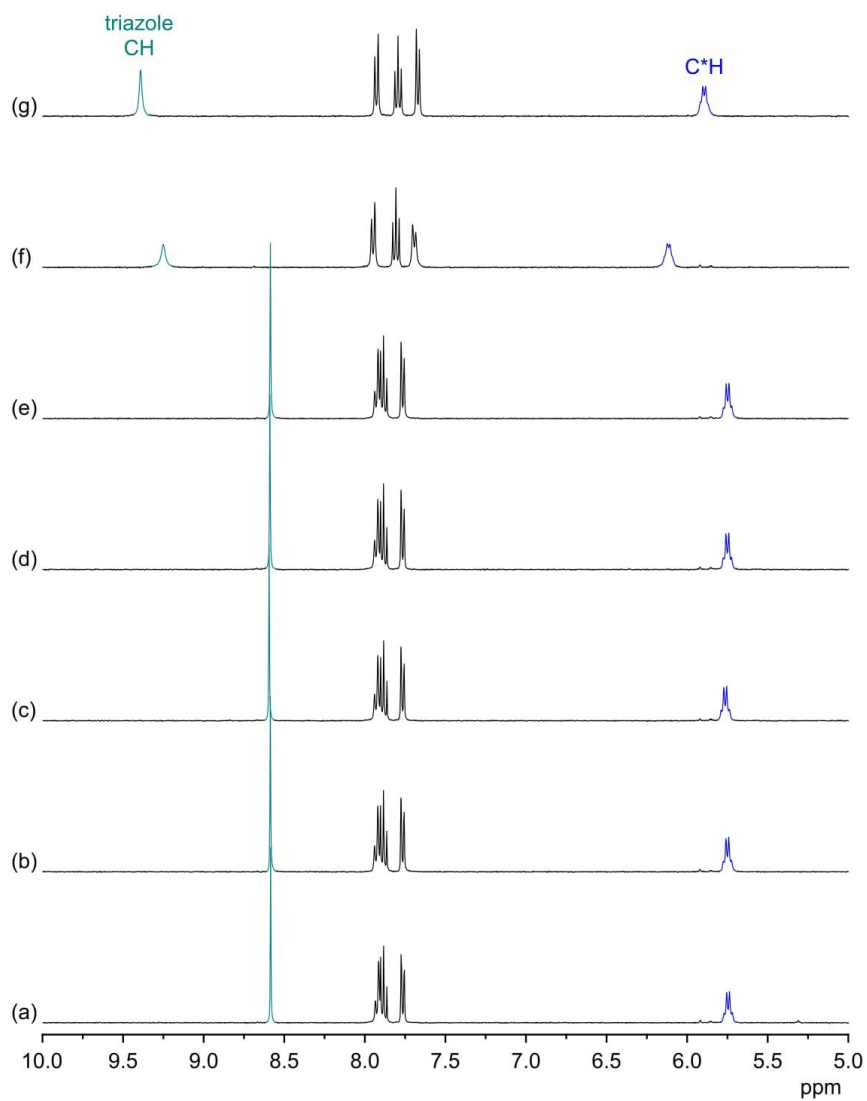


		<i>m/z</i> calcd.	<i>m/z</i> exp.
[M+H] <sup>+</sup>	C <sub>30</sub> H <sub>27</sub> N <sub>15</sub> O <sub>3</sub> + H <sup>+</sup>	646.3	646.5
[M+Na] <sup>+</sup>	C <sub>30</sub> H <sub>27</sub> N <sub>15</sub> O <sub>3</sub> + Na <sup>+</sup>	668.2	668.5
[M+K] <sup>+</sup>	C <sub>30</sub> H <sub>27</sub> N <sub>15</sub> O <sub>3</sub> + K <sup>+</sup>	684.2	684.6

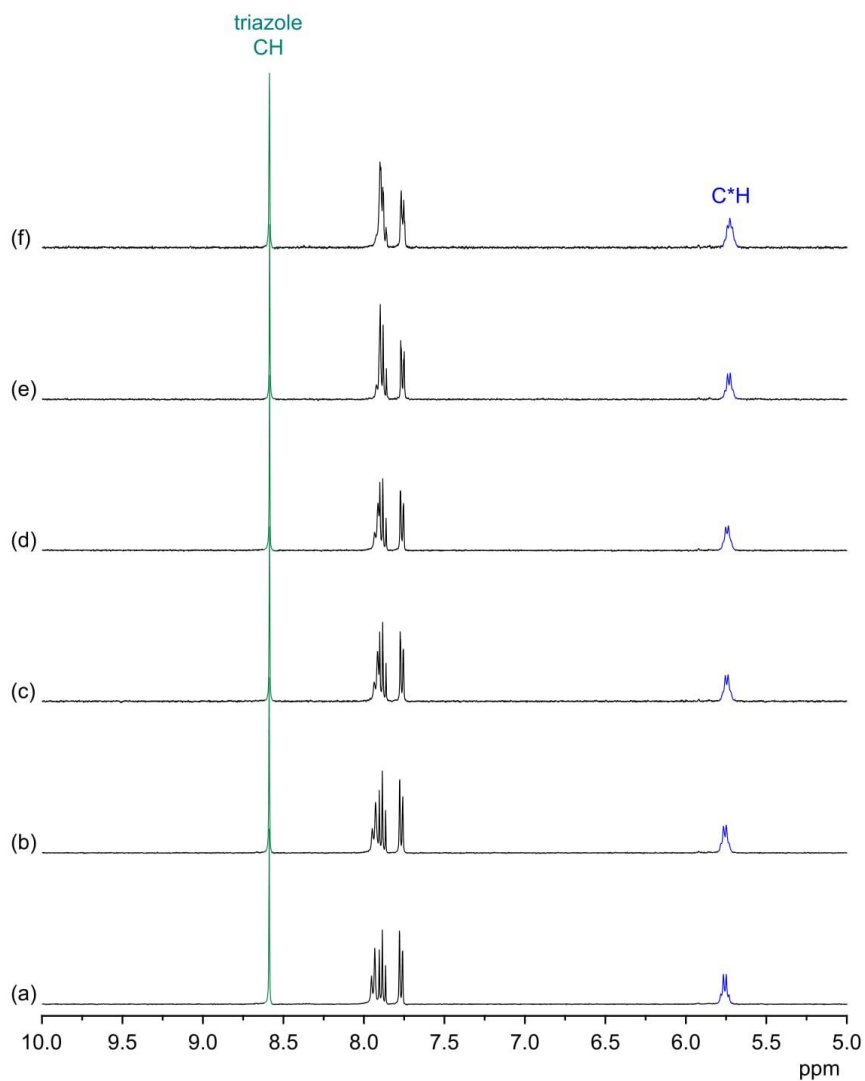
NOESY NMR Spectrum: 3 (1 mM) in DMSO- $d_6$  (mixing time 400 ms) (400 MHz).



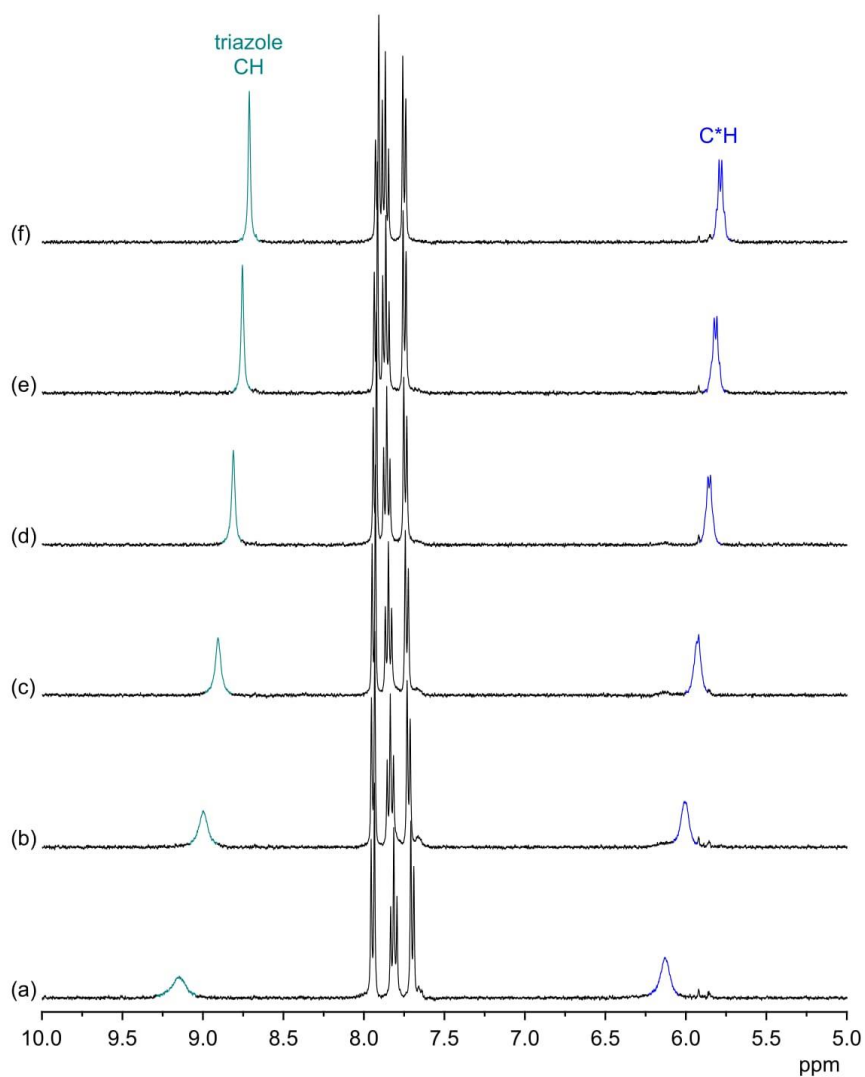
<sup>1</sup>H NMR Spectra: **3** (1 mM) in 2.5 vol% D<sub>2</sub>O/DMSO-*d*<sub>6</sub> in the absence (a) and the presence of 5 equiv of tetrabutylammonium iodide (b), bromide (c), chloride (d), nitrate (e), dihydrogenphosphate (f), and sulfate (g). The signals of the triazole CH, and C\*H protons are marked in green and blue, respectively.



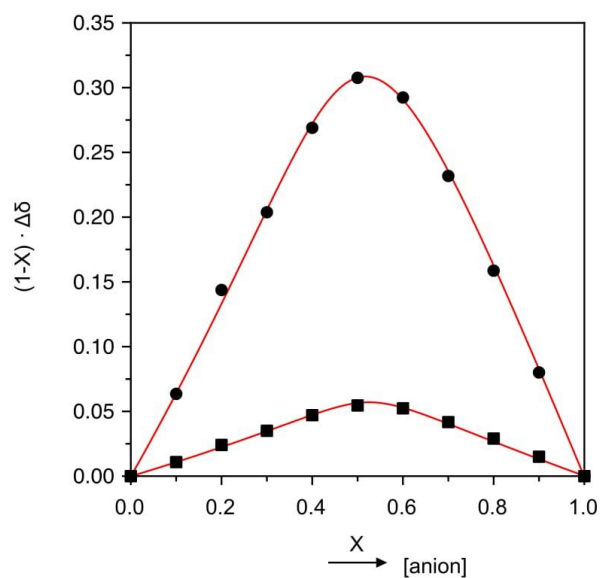
<sup>1</sup>H NMR Spectra: 3 (1 mM) in D<sub>2</sub>O/DMSO-*d*<sub>6</sub> mixtures with the D<sub>2</sub>O content amounting to 0.03 vol% (a), 1 vol% (b), 2 vol% (c), 3 vol% (d) 4 vol% (e), and 5 vol% (f). The signals of the triazole CH, and C\*H protons are marked in green and blue, respectively.



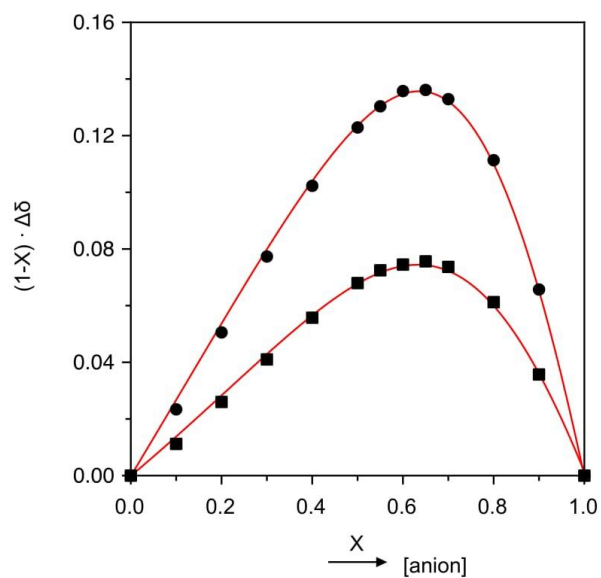
<sup>1</sup>H NMR Spectra: **3** (1 mM) in the presence of 5 equiv of tetrabutylammonium dihydrogenphosphate in D<sub>2</sub>O/DMSO-*d*<sub>6</sub> mixtures with the D<sub>2</sub>O content amounting to 0.03 vol% (a), 1 vol% (b), 2 vol% (c), 3 vol% (d) 4 vol% (e), and 5 vol% (f). The signals of the triazole CH, and C\*H protons are marked in green and blue, respectively.



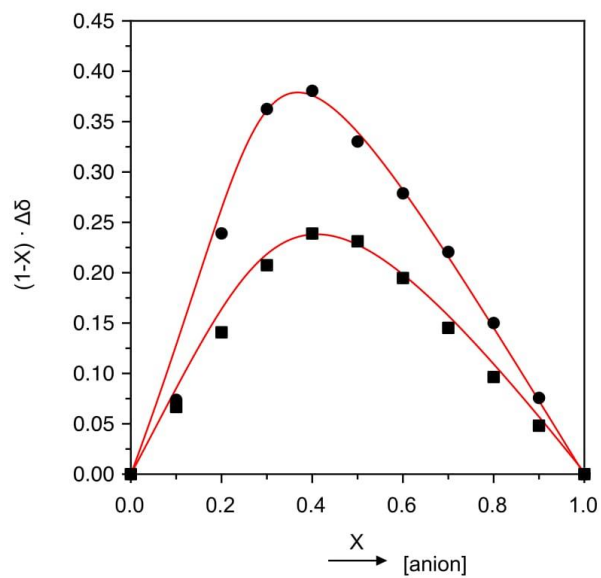
Job Plot: 3 + TBA sulfate (400 MHz, 2.5 vol% D<sub>2</sub>O/DMSO-*d*<sub>6</sub>). The circles indicate the shift of the triazole CH signal and the squares the one of the C\*H signal.



Job Plot: 3 + TBA dihydrogenphosphate (400 MHz, 2.5 vol% D<sub>2</sub>O/DMSO-*d*<sub>6</sub>). The circles indicate the shift of the triazole CH signal and the squares the one of the C\*H signal.

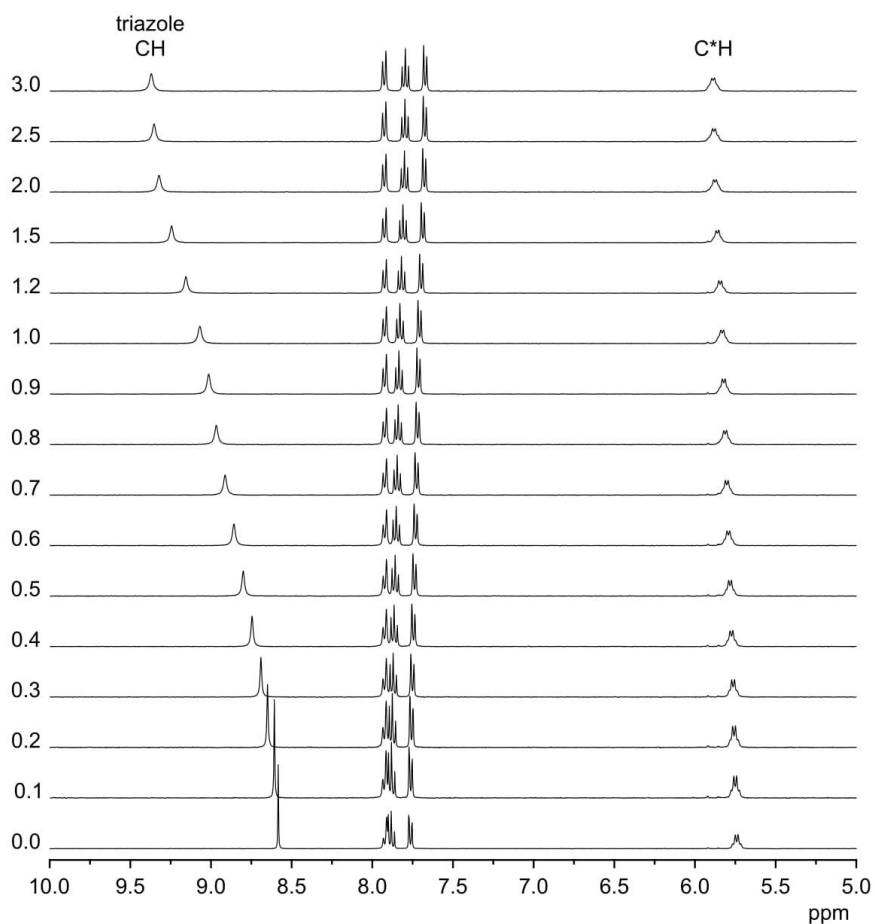


Job Plot: **3** + TBA trimetaphosphate (400 MHz, 2.5 vol% D<sub>2</sub>O/DMSO-*d*<sub>6</sub>). The circles indicate the shift of the triazole CH signal and the squares the one of the C\*H signal.



NMR Titration: 3 + TBA sulfate.

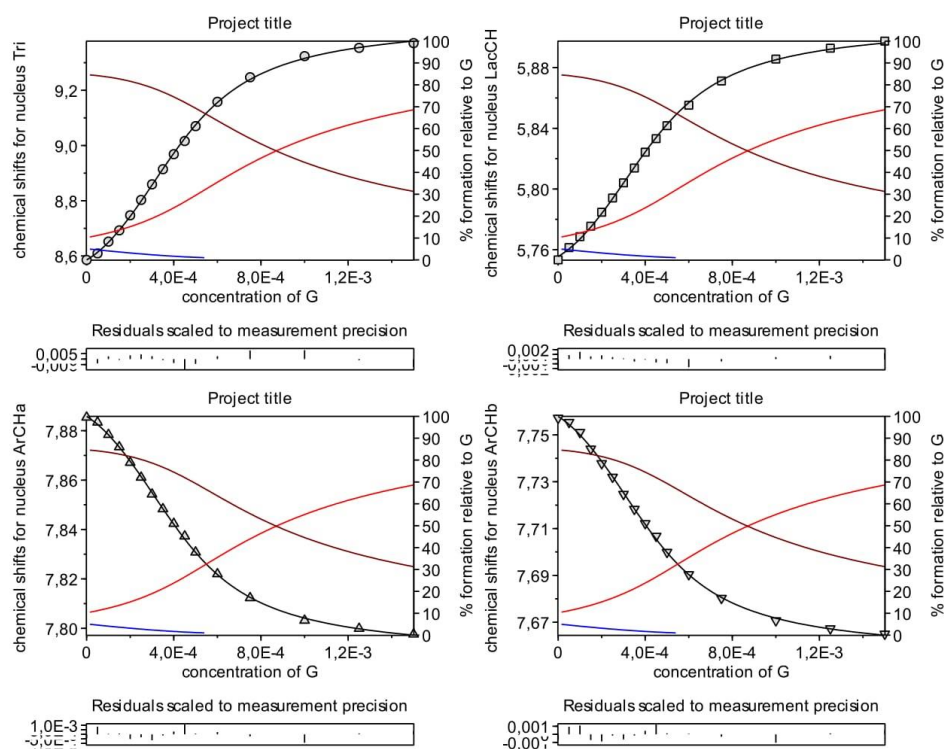
$^1\text{H}$  NMR spectra of 3 (0.5 mM) in 2.5 vol%  $\text{D}_2\text{O}/\text{DMSO-}d_6$  (400 MHz) containing the increasing equivalents of TBA sulfate specified to the left of each spectrum.



Binding isotherms and HypNMR outputs.

Converged in 1 iterations with sigma = 0.002798

	value	standard deviation	Comments
log beta (GH2)	6.3	fixed	
log beta (GH)	4.2198	0.0124	4.22 (1)



Evaluation of the stability constants of the sulfate complex with HypNMR was only possible by estimating and fixing the  $\log \beta$  value representing the overall stability of the complex. To assess the effect of varying this parameter on the outcome of the regression, fitting was performed by using different  $\log \beta$  values and the results were compared. The following table shows the dependence of  $\log K_{11}$  and of the parameter sigma, describing the goodness of the fit, on the starting value of  $\log \beta$ .

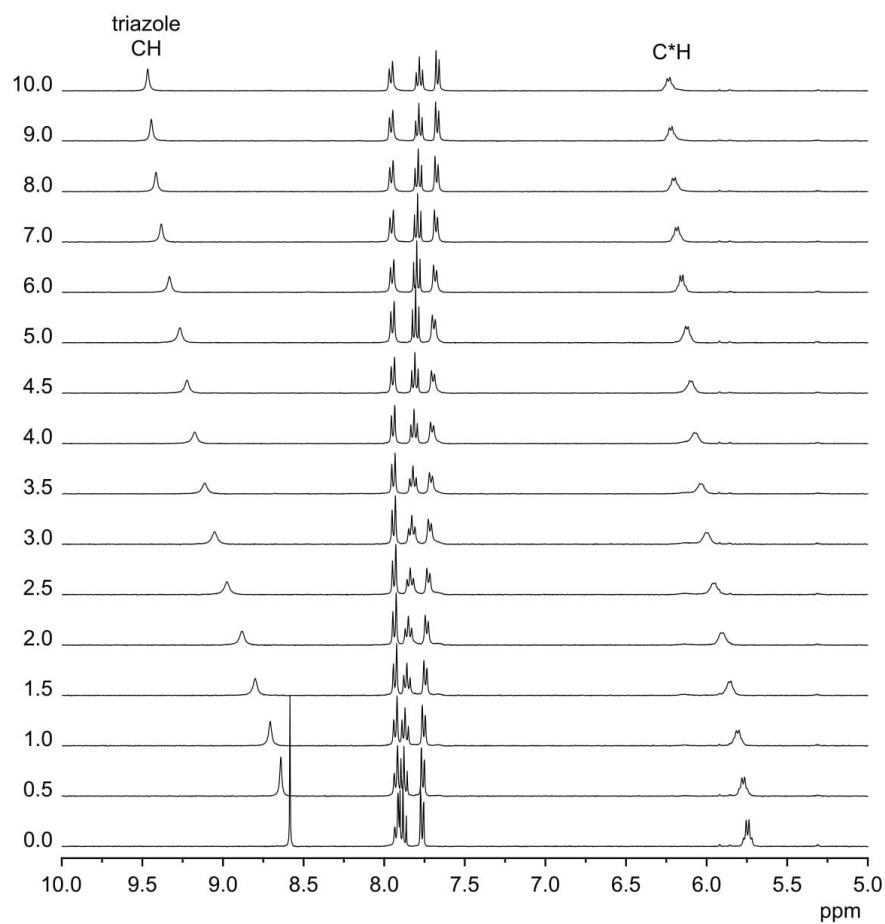
$\log \beta$	$\log K_{11}$	sigma
5.1	4.21	0.002672
5.3	4.21	0.002677
5.5	4.21	0.002685
5.7	4.21	0.002698
5.9	4.21	0.002718
6.1	4.21	0.002749
6.3	4.22	0.002798
7.0	4.26	0.003259
8.0	4.44	0.011096

No fitting was possible with  $\log \beta < 5.1$ . The goodness of the fit becomes unacceptable with  $\log \beta > 6.3$ . In the region  $5.1 < \log \beta < 6.3$  the stability constant  $\log K_{11}$  is practically unaffected by the initial choice of  $\log \beta$ , rendering the estimation of this constant reliable. In the same region the sigma value only exhibits small variations so that the exact quantification of  $\log K_{21}$  on the basis of this parameter is not possible. It is therefore safe to state that  $\log K_{21}$  ranges between 0.9 and 2.1.

Note that also the signal of the methyl groups of **3** exhibits a minor shift in the  $^1\text{H}$  NMR spectra during this titration. The resulting binding isotherm could, however, not be fitted to a reasonable binding model. As the methyl groups point away from the anion binding site, we attribute the shifts in their resonance to changes in solvation during the titration and we therefore neglected the corresponding binding isotherm in the data treatment.

NMR Titration: 3 + TBA dihydrogenphosphate.

$^1\text{H}$  NMR spectra of 3 (0.5 mM) in 2.5 vol%  $\text{D}_2\text{O}/\text{DMSO-}d_6$  (400 MHz) containing the increasing equivalents of TBA dihydrogenphosphate specified to the left of each spectrum.

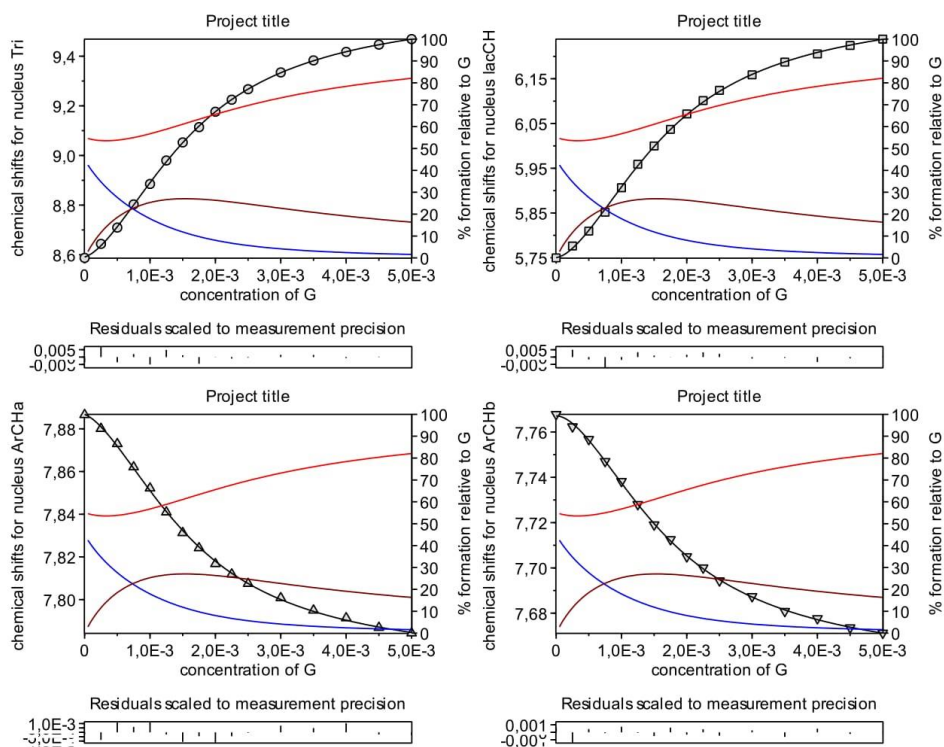


Binding isotherms and HypNMR outputs.

Converged in 1 iterations with sigma = 0.002448

	value	standard deviation	Comments
1 log beta (GH)	3.2114	0.0997	3.21 (1)
2 log beta (G2H)	6.3066	0.0634	6.31 (6)

Correlation coefficients between stability constants is 0.9858



In this case, both stability constants could be reliably fitted by using HypNMR without any initial assumptions. Only, the change of the resonance of the methyl signal of **3** was again neglected as in the sulfate titration.

## Selected ITC Titrations:

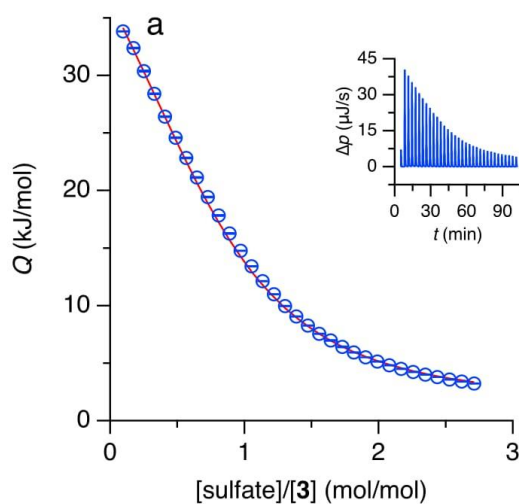
**Table S1.** Concentrations and experimental parameters of the individual titrations.

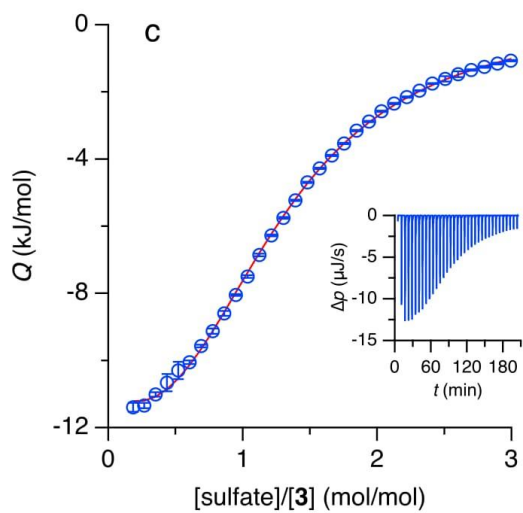
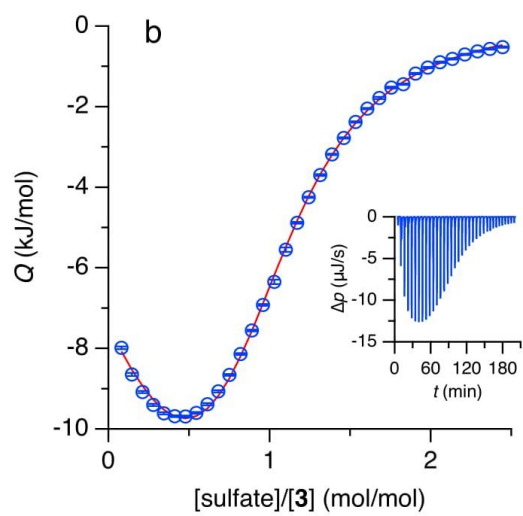
guest anion as TBA salt	vol% H <sub>2</sub> O in H <sub>2</sub> O/DMSO	<i>c</i> ( <b>3</b> ) / mM	<i>c</i> (salt) / mM	injection volume / μL	spacing time / s
sulfate	0.03	0.25	3.6	8	180
	2.5	0.37	4.4	8	360
	5	0.25	3.8	8	360
DHP	0.03	0.51	19.0	8 <sup>a</sup>	200
	2.5	0.47	33.7	8 <sup>a</sup>	180
	5	0.52	38.5	8	180
HPP	2.5	0.27	4.9	8	200
TMP	2.5	0.51	5.1	8	360

<sup>a</sup> For the first 4 injections an injection volume of 4 μL was used.

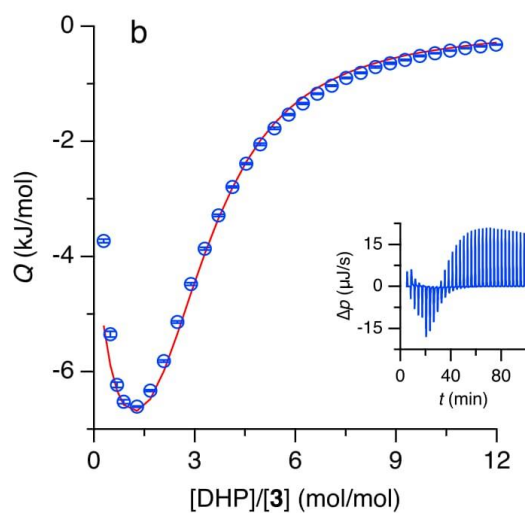
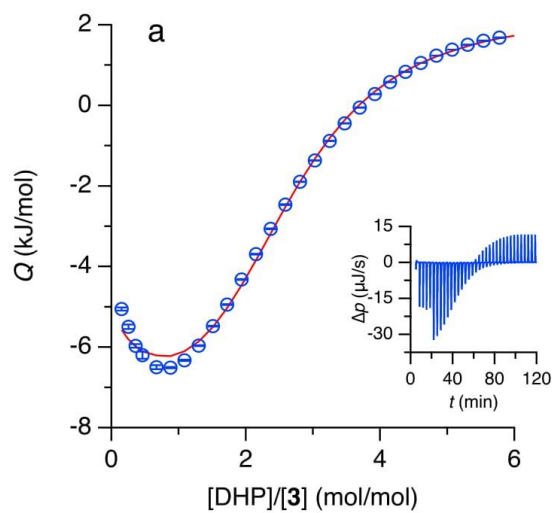
Thermograms were baseline-corrected with NITPIC,<sup>1</sup> and the resulting binding isotherms were fitted with SEDPHAT.<sup>2-4</sup> Circles in isotherms denote experimental data, and lines represent fits based on the binding models explained in the main text.

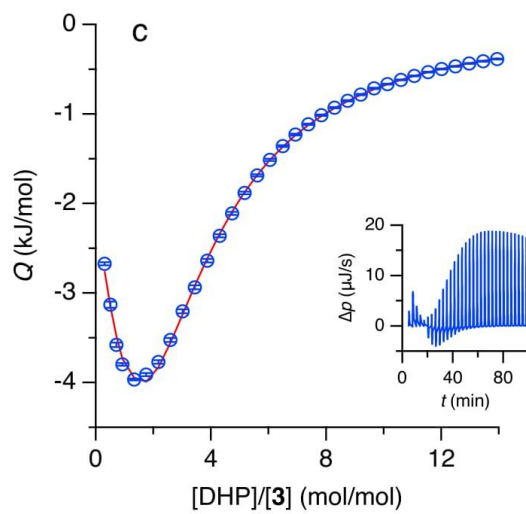
Titration of **3** with TBA sulfate (a: 0.03 vol% H<sub>2</sub>O in DMSO, b: 2.5 vol% H<sub>2</sub>O in DMSO, c: 5 vol% H<sub>2</sub>O in DMSO).



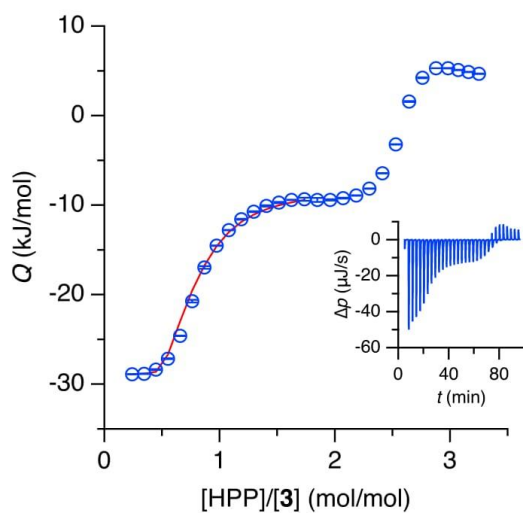


Titration of **3** with TBA dihydrogenphosphate (DHP) (a: 0.03 vol% H<sub>2</sub>O in DMSO, b: 2.5 vol% H<sub>2</sub>O in DMSO, c: 5 vol% H<sub>2</sub>O in DMSO).

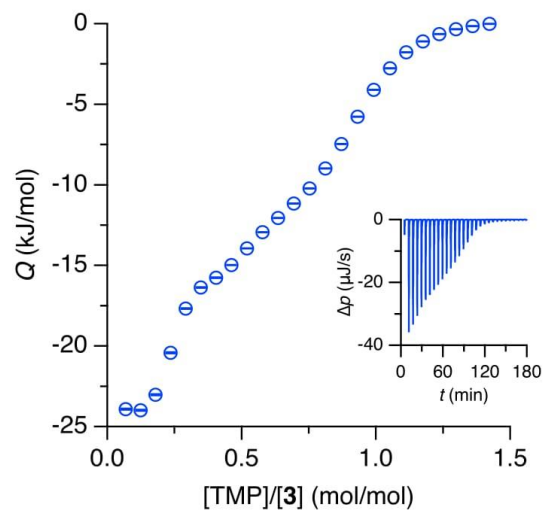




Titration of **3** with TBA hydrogenpyrophosphate (HPP) (2.5 vol% H<sub>2</sub>O in DMSO).



Titration of **3** with TBA trimetaphosphate (TMP) (2.5 vol% H<sub>2</sub>O in DMSO).



### Crystal Structures

**Structure of 3·5DMSO·0.35H<sub>2</sub>O:** 3·5DMSO·0.35H<sub>2</sub>O was crystallized as colourless plates by slow evaporation of an acetone/DMSO solution of **3**. The single crystal X-ray data was collected at 150.0(1) K on a Rigaku/Oxford diffraction Xcalibur/Gemini dual wavelength diffractometer with a Cu-K $\alpha$  ( $\lambda = 1.54184$  Å) radiation X-ray source. Program *CrysAlisPro*<sup>5</sup> was used for the data collection and reduction. The intensities were corrected for absorption using analytical face index absorption correction method<sup>6</sup> for all the data.

Both structures were solved with direct methods (*SHELXS-2014/7*<sup>8</sup>) and refined by full-matrix least squares on  $F^2$  using *SHELXL-2014/7*<sup>8</sup> program. Anisotropic displacement parameters were assigned to non-H atoms. All the hydrogen atoms were refined using riding models. The hydrogen atoms from O8 were not localized.

Crystal data: 0.58×0.35×0.03 mm, C<sub>40</sub>H<sub>57</sub>N<sub>15</sub>O<sub>8.35</sub>S<sub>5</sub>,  $M = 1041.91$ , orthorhombic, space group  $P2_12_12_1$ ,  $a = 9.3172(2)$  Å,  $b = 18.6791(4)$  Å,  $c = 29.1423(5)$  Å,  $V = 5071.84(18)$  Å<sup>3</sup>,  $Z = 4$ ,  $\mu(\text{Mo-K}\alpha) = 2.649$  mm<sup>-1</sup>,  $D_{\text{calc}} = 1.362$  g/cm<sup>3</sup>,  $F(000) = 2192$ , 15405 reflections measured ( $3.847^\circ \leq \Theta \leq 62.663^\circ$ ), 7663 unique ( $R_{\text{int}} = 0.0311$ ,  $R_{\text{sigma}} = 0.0403$ ) which were used in all calculations. Final  $R$  indices ( $I > 2\sigma(I)$ ):  $R_1 = 0.0327$ ,  $wR_2 = 0.0821$ ,  $R$  indices (all data):  $R_1 = 0.0350$ ,  $wR_2 = 0.0843$ .  $GOF = 1.033$  for 668 parameters and 18 restraints, largest diff. peak and hole 0.365/−0.293 eÅ<sup>-3</sup> with Flack parameter 0.005(8). CCDC-1505706 contains the supplementary data for this structure.

**Structure of 3·1.5TBADHP·2.5DMSO·1.7H<sub>2</sub>O:** Colourless prisms of 3·1.5TBADHP·2.5DMSO·1.7H<sub>2</sub>O were obtained by slow evaporation of acetone/DMSO solution of **3** and TBADHP. The single crystal X-ray data was collected at 120.0(1) K on a Rigaku/Agilent Super-Nova dual wavelength diffractometer with a micro-focus X-ray source and multilayer optics monochromatised Cu-K $\alpha$  ( $\lambda = 1.54184$  Å) radiation. For data collection, reduction, and absorption correction, see above.

The solution of the structure varied by using *SIR2014*<sup>7</sup> for the direct methods and the handling of one hydrogen atom. The one hydrogen (H5O) between dihydrogen phosphates was located from the difference-Fourier map and refined with  $U_{\text{eq}}(\text{H})$  of 1.5  $U_{\text{eq}}(\text{O})$  and with O-H distance restrained to value of 1.00 Å ( $s = 0.01$ ). The compound is pure enantiomer and crystallized in a chiral space group,

but due to weak disordered data the absolute structure could not be determined reliably.

Crystal data:  $0.30 \times 0.23 \times 0.15$  mm,  $C_{118}H_{198}N_{33}O_{26.40}P_3S_5$ ,  $M = 2754.69$ , orthorhombic, space group  $P2_12_12$ ,  $a = 32.0131(5)$  Å,  $b = 15.5735(2)$  Å,  $c = 14.7710(4)$  Å,  $V = 7634.2(2)$  Å<sup>3</sup>,  $Z = 2$ ,  $\mu(\text{Cu-K}\alpha) = 1.656$  mm<sup>-1</sup>,  $D_{\text{calc}} = 1.242$  g/cm<sup>3</sup>,  $F(000) = 2946$ , 27356 reflections measured ( $3.960^\circ \leq \Theta \leq 68.246^\circ$ ), 13466 unique ( $R_{\text{int}} = 0.0300$ ,  $R_{\text{sigma}} = 0.0394$ ) which were used in all calculations. Final  $R$  indices ( $I > 2\sigma(I)$ ):  $R_1 = 0.1279$ ,  $wR_2 = 0.3742$ ,  $R$  indices (all data):  $R_1 = 0.1365$ ,  $wR_2 = 0.3923$ .  $GOF = 1.760$  for 965 parameters and 511 restraints, largest diff. peak and hole  $1.15/-0.64$  eÅ<sup>-3</sup> with Flack parameter  $0.037(8)$ . CCDC-1504361 contains the supplementary data for this structure.

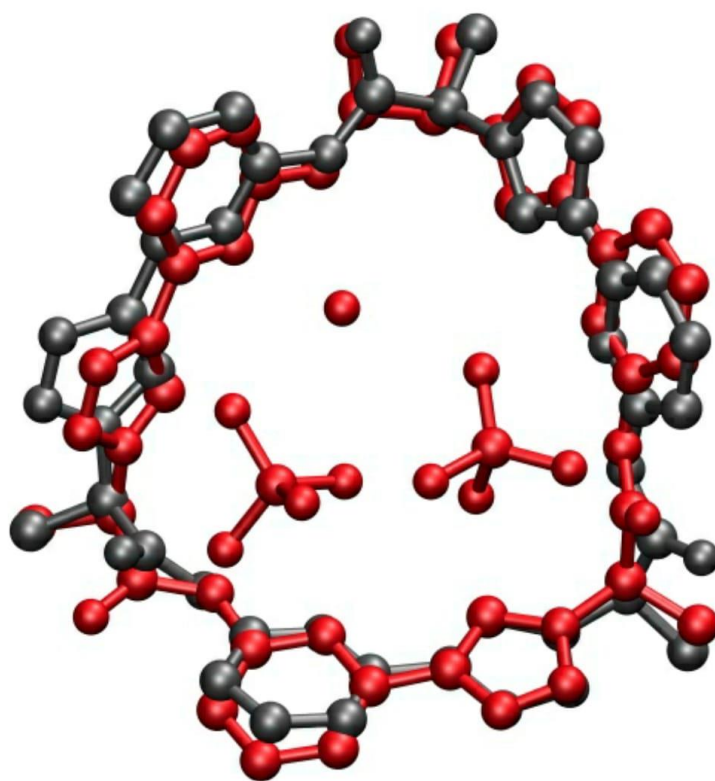


Figure S1: Overlay of the molecular structures of pseudopeptide **3** in the crystals **3**·5DMSO·0.35H<sub>2</sub>O (black) and **3**·1.5TBADHP·2.5DMSO·1.7H<sub>2</sub>O (red).

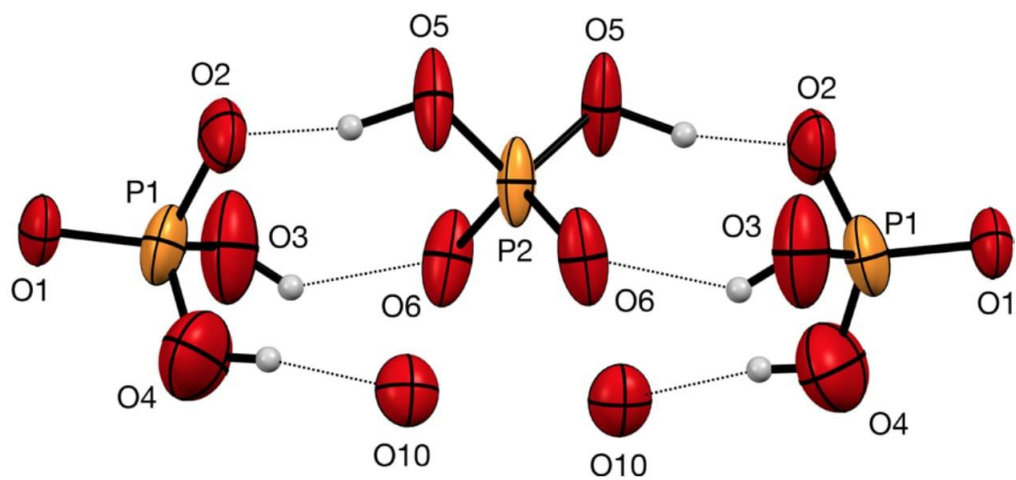


Figure S2: Detailed representation of the hydrogen bonding pattern in the DHP trimer of  $3 \cdot 1.5\text{TBADHP} \cdot 2.5\text{DMSO} \cdot 1.7\text{H}_2\text{O}$ .

References

- 1 S. Keller, C. Vargas, H. Zhao, G. Piszczek, C. A. Brautigam and P. Schuck, *Anal. Chem.*, 2012, **84**, 5066-5073.
- 2 J. C. D. Houtman, P. H. Brown, B. Bowden, H. Yamaguchi, E. Appella, L. E. Samelson and P. Schuck, *Protein Sci.*, 2007, **16**, 30-42.
- 3 G. Krainer, J. Broecker, C. Vargas, J. Fanghänel and S. Keller, *Anal. Chem.*, 2012, **84**, 10715-10722
- 4 G. Krainer, S. Keller, *Methods*, 2015, **76**, 116-123.
- 5 CrysalisPro 2015, Rigaku OD, version 1.171.38.41.
- 6 R. C. Clark, J. S. Reid, *Acta Crystallogr.*, 1995, **A51**, 887-897.
- 7 SIR2014 2014, M. C. Burla, R. Caliandro, B. Carrozzini, G. L. Cascarano, C. Giacovazzo, M. Mallamo, A. Mazzone, G. Polidori.
- 8 G. M. Sheldrick, *Acta Crystallogr.*, 2015, **A71**, 3-8.

## 8 Appendix II

*Chem. Sci.*

**Efficient stabilisation of a dihydrogenphosphate tetramer and a dihydrogenpyrophosphate dimer by a cyclic pseudopeptide containing 1,4-disubstituted 1,2,3-triazole moieties**

Disha Mungalpara,<sup>a</sup> Arto Valkonen,<sup>b</sup> Kari Rissanen,<sup>b</sup> and Stefan Kubik\*<sup>a</sup>

<sup>a</sup> *Technische Universität Kaiserslautern, Fachbereich Chemie - Organische Chemie, Erwin-Schrödinger-Straße, 67663 Kaiserslautern, Germany, Fax: +49-631-205-3921, Email:*

*kubik@chemie.uni-kl.de*

<sup>b</sup> *University of Jyväskylä, Department of Chemistry, Nanoscience Center, P.O. Box 35, Jyväskylä FI-40014, Finland.*

### CONTENT

Synthetic Procedures.....	S2
<sup>1</sup> H NMR, <sup>13</sup> C NMR, and MS Spectra of Synthetic Intermediates and Pseudopeptide <b>2</b> .....	S7
NOESY NMR Spectrum of <b>2</b> .....	S15
ROESY NMR Spectrum of the Dihydrogenpyrophosphate Complex of <b>2</b> .....	S16
Qualitative NMR Spectroscopic Binding Studies.....	S17
ESI Mass Spectrometric Binding Studies .....	S23
ITC Titrations.....	S27
Crystal Structures.....	S30
References.....	S36

### Synthetic Procedures

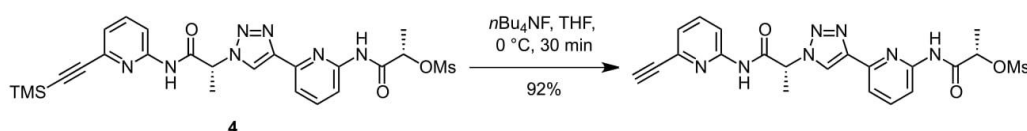
**General details.** Analyses were carried out as follows: melting points, Müller SPM-X 300; NMR, Bruker DPX 400 (peak assignments were confirmed by using H,H-COSY and HMQC spectra, spectra were referenced to the residual solvent signals (DMSO- $d_6$ :  $\delta_H = 2.50$  ppm,  $\delta_C = 39.5$  ppm);<sup>1</sup> MALDI-TOF-MS, BrukerUltraflex TOF/TOF; elemental analysis, Elementar vario Micro cube; optical rotation, Perkin Elmer 241 MC digital polarimeter ( $d = 10$  cm); ITC, Microcal VP-ITC.

The following abbreviations are used: TBA, tetrabutylammonium; Epa, 2-amino-6-ethynyl-2-pyridine; Lac, CH<sub>3</sub>CHCO; Tri, 1,2,3-triazole; PyCloP, chlorotripyrrolidinophosphonium hexafluorophosphate; TBTA, tris[(1-benzyl-1*H*-1,2,3-triazol-4-yl)methyl]amin; TBAF, tetrabutylammonium fluoride; DHP, dihydrogenphosphate; HPP, hydrogenpyrophosphate, DHPP, dihydrogenpyrophosphate.

The synthesis of the linear pseudopeptide **4** is described elsewhere.<sup>2</sup> TBA sulfate, TBA DHP, TBA HPP, and TBA DHPP are commercially available and were used after confirming purity by elemental analysis.

**ESI MS measurements.** These measurements were performed by using a Paul-type quadrupole ion trap instrument (AmaZonETD, Bruker Daltonics). The ion source was set to negative electrospray ionisation mode. Scan speed was 32500 ( $m/z$ ) s<sup>-1</sup> in standard resolution scan mode (0.3 FWHM /  $m/z$ ). Mass spectra were accumulated for at least two minutes. Sample solutions were continuously infused into the ESI chamber by a syringe pump at a flow rate of 2  $\mu\text{L min}^{-1}$ . Nitrogen was used as drying gas with a flow rate of 3.0 L min<sup>-1</sup> at 220 °C. The solutions were sprayed at a nebulizer pressure of 280 mbar (4 psi) and the electrospray needle was held at 4.5 kV.

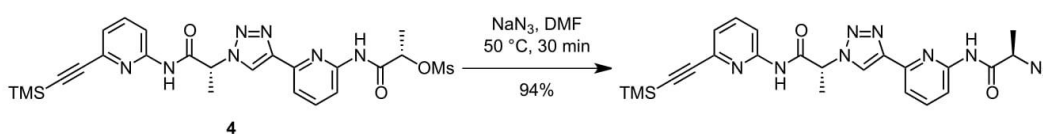
#### H-Epa-(*R*)-Lac-1,4-Tri-Epa-(*S*)-Lac-OMs.



Compound **4** (3.3 g, 5.9 mmol) was dissolved in THF (40 mL) at 0 °C. To this solution, a solution of TBAF trihydrate (3.7 g, 11.8 mmol) in THF (20 mL) was added dropwise. This mixture was stirred

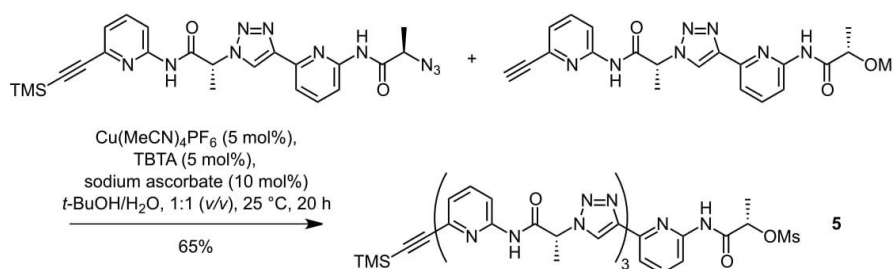
for 30 min at 0 °C. Ethyl acetate (50 mL) and water (50 mL) were added, and after separation of the organic layer the aqueous phase was extracted three times using ethyl acetate (150 mL). The combined organic layers were dried using MgSO<sub>4</sub>. The solvent was evaporated and the residue purified on silica gel column with hexane/ethyl acetate, 1:1 (v/v) as eluent. The product was obtained as a white powder. Yield: 2.6 g (5.4 mmol, 92%); MS (MALDI-TOF) *m/z* (%): [M-CH<sub>3</sub>SO<sub>3</sub>H+H]<sup>+</sup> 388.2 (100), [M+H]<sup>+</sup> 484.3 (35), [M+Na]<sup>+</sup> 506.3 (48), [M+K]<sup>+</sup> 522.3 (8).

#### TMS-Epa-(R)-Lac-1,4-Tri-Epa-(R)-Lac-N<sub>3</sub>.



Compound **4** (3.3 g, 5.9 mmol) and sodium azide (600 mg, 9.2 mmol) were dissolved in DMF (20 mL). The mixture was stirred at 50 °C for 30 min. After adding ethyl acetate (100 mL) and water (100 mL) the aqueous layer was extracted with ethyl acetate (3 × 100 mL). The combined organic layers were dried using MgSO<sub>4</sub>. Pure product was obtained by column chromatography with hexane/ethyl acetate, 1:1 (v/v) as the eluent. Yield: 2.8 g (5.6 mmol, 94%); MS (MALDI-TOF) *m/z* (%): [M-N<sub>2</sub>+H<sub>2</sub>+H]<sup>+</sup> 477.3 (14), [M+H]<sup>+</sup> 503.3 (100), [M+Na]<sup>+</sup> 525.3 (25).

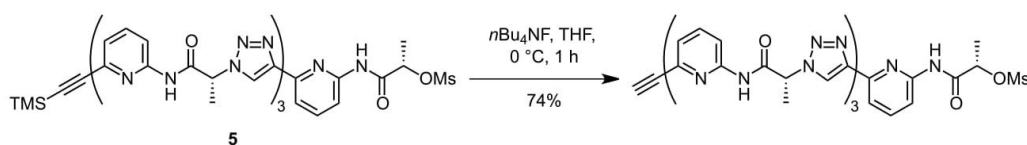
#### TMS-Epa-[(R)-Lac-1,4-Tri-Epa]<sub>3</sub>-(S)-Lac-OMs (**5**).



H-Epa-(R)-Lac-1,4-Tri-Epa-(S)-Lac-OMs (2.6 g, 5.4 mmol) and TMS-Epa-(R)-Lac-1,4-Tri-Epa-(R)-Lac-N<sub>3</sub> (2.8 g, 5.6 mmol) were dissolved in *t*-BuOH/H<sub>2</sub>O, 1:1 (v/v) (300 mL), followed by the addition of a solution of TBTA (143 mg, 270 μmol, 5 mol%), Cu(MeCN)<sub>4</sub>PF<sub>6</sub> (101 mg, 270 μmol, 5 mol%), and sodium ascorbate (107 mg, 540 μmol, 10 mol%) in *t*-BuOH/H<sub>2</sub>O, 1:1 (v/v) (20 mL). The reaction mixture was stirred at 25 °C for 20 h and extracted with ethyl acetate three times (3 × 20 mL). The

combined organic layers were washed with water twice and dried over  $\text{MgSO}_4$ . The solvent was evaporated and the residue was purified by column chromatography using ethyl acetate as the eluent. Pure product was obtained as a white solid. NMR indicated that the product thus obtained contained traces of ethyl acetate, which is why it was not characterised by elemental analysis. Purity was high enough for the next step. Yield: 3.5 g (3.5 mmol, 65%); m.p. > 200 °C (dec);  $^1\text{H}$  NMR (400 MHz, 25 °C,  $\text{DMSO-}d_6$ )  $\delta$  = 11.44 (s, 1H, NH), 11.25 (s, 2H, NH), 10.79 (s, 1H, NH), 8.66 (s, 1H, TriH), 8.65 (s, 1H, TriH), 8.64 (s, 1H, TriH), 7.91-8.05 (m, 7H, EpaH(4)+EpaH(3)), 7.84 (t, 1H,  $^3J(\text{H}, \text{H}) = 8.0$  Hz, EpaH(4)), 7.79 (d, 3H,  $^3J(\text{H}, \text{H}) = 7.6$  Hz, EpaH(5)), 7.32 (dd, 1H,  $^3J(\text{H}, \text{H}) = 7.5$  Hz,  $^4J(\text{H}, \text{H}) = 0.7$  Hz, EpaH(5)), 5.88 (m, 2H, LacCH), 5.77 (q, 1H,  $^3J(\text{H}, \text{H}) = 7.1$  Hz, LacCH), 5.34 (q, 1H,  $^3J(\text{H}, \text{H}) = 6.4$  Hz, LacCH), 3.27 (s, 3H, MsCH<sub>3</sub>), 1.85-1.89 (m, 9H, LacCH<sub>3</sub>), 1.55 (d, 3H,  $^3J(\text{H}, \text{H}) = 6.7$  Hz, LacCH<sub>3</sub>), 0.25 (s, 9H, TMSCH<sub>3</sub>) ppm;  $^{13}\text{C}$  NMR (100.6 MHz,  $\text{DMSO-}d_6$ )  $\delta$  = 168.2 (CO), 168.1 (CO), 151.5 (EpaC(2)), 151.2 (EpaC(2)), 151.1 (EpaC(2)), 148.5 (EpaC(6)), 148.6 (EpaC(6)), 146.5 (TriC(4)), 146.4 (TriC(4)), 140.1 (EpaC(6)), 139.7 (EpaC(4)), 139.6 (EpaC(4)), 139.4 (EpaC(4)), 123.2 (EpaC(5)), 122.9 (TriC(5)), 122.8 (TriC(5)), 116.0 (EpaC(5)), 115.9 (EpaC(5)), 114.0 (EpaC(3)) 113.0 (EpaC(3)), 112.9 (EpaC(3)), 103.4 (Si-C $\equiv$ C), 94.2 (Si-C $\equiv$ C), 75.3 (LacC), 58.8 (LacC), 58.7 (LacC), 38.1 (MsCH<sub>3</sub>), 18.7 (LacCH<sub>3</sub>), 18.1 (LacCH<sub>3</sub>), 18.0 (LacCH<sub>3</sub>), 17.9 (LacCH<sub>3</sub>), -0.4 (TMSCH<sub>3</sub>) ppm; MS (MALDI-TOF)  $m/z$  (%):  $[\text{M-Si}(\text{CH}_3)_3+2\text{H}]^+$  914.4 (37),  $[\text{M-CH}_3\text{SO}_3+\text{H}+\text{K}]^+$  930.4 (13),  $[\text{M}+\text{Na}]^+$  1008.4 (100),  $[\text{M}+\text{K}]^+$  1024.4 (19).

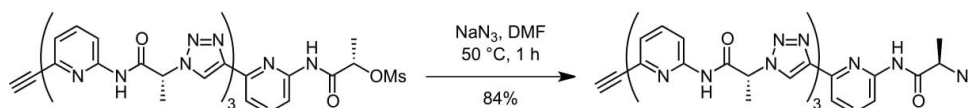
#### H-Epa-[(R)-Lac-1,4-Tri-Epa]<sub>3</sub>-(S)-Lac-OMs.



Compound **5** (3.4 g, 3.5 mmol) was dissolved in THF (40 mL) at 0 °C. To this solution, a solution of TBAF trihydrate (2.2 g, 7.0 mmol) in THF (20 mL) was added dropwise. The reaction mixture was stirred for 1 h at 0 °C. Ethyl acetate (150 mL) and water (150 mL) were added, and the organic layer was separated. The aqueous layer was extracted four times with ethyl acetate (4 × 50 mL), and the combined organic layers were dried using  $\text{MgSO}_4$ . The solvent was evaporated, and the residue purified on a silica gel column with ethyl acetate as eluent. The product was obtained as a white

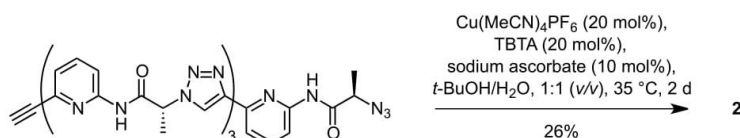
powder. Yield: 2.4 g (2.6 mmol, 74%); MS (MALDI-TOF)  $m/z$  (%):  $[M-CH_3SO_3H+H]^+$  818.4 (93),  $[M+H]^+$  914.4 (100),  $[M+Na]^+$  936.4 (15).

#### H-Epa-[(*R*)-Lac-1,4-Tri-Epa]<sub>3</sub>-(*R*)-Lac-N<sub>3</sub>.



This reaction was performed with 0.19 mmol of starting material to avoid having to store larger amounts of the product, which is potentially prone to oligomerisation via thermal 1,3-dipolar cycloaddition, and because the subsequent cyclisation step turned out to be more efficient when performed on a smaller scale. H-Epa-[(*R*)-Lac-1,4-Tri-Epa]<sub>3</sub>-(*S*)-Lac-OMs (170 mg, 0.19 mmol) and sodium azide (250 mg, 0.36 mmol) were dissolved in DMF (10 mL), and the reaction mixture was heated at 50 °C for 1 h. Ethyl acetate (30 mL) and water (30 mL) were added, and the organic layer was separated. The aqueous layer was extracted three times with ethyl acetate (3 × 50 mL), and the combined organic layers were dried over MgSO<sub>4</sub>. The solvent was evaporated and the residue purified on a silica gel column with ethyl acetate as the eluent to afford pure product as a white powder. Yield: 135 mg (0.16 mmol, 84%); MS (MALDI-TOF)  $m/z$  (%):  $[M-N_2+H_2+H]^+$  835.6 (14),  $[M+H]^+$  861.6 (100),  $[M+Na]^+$  883.6 (86).

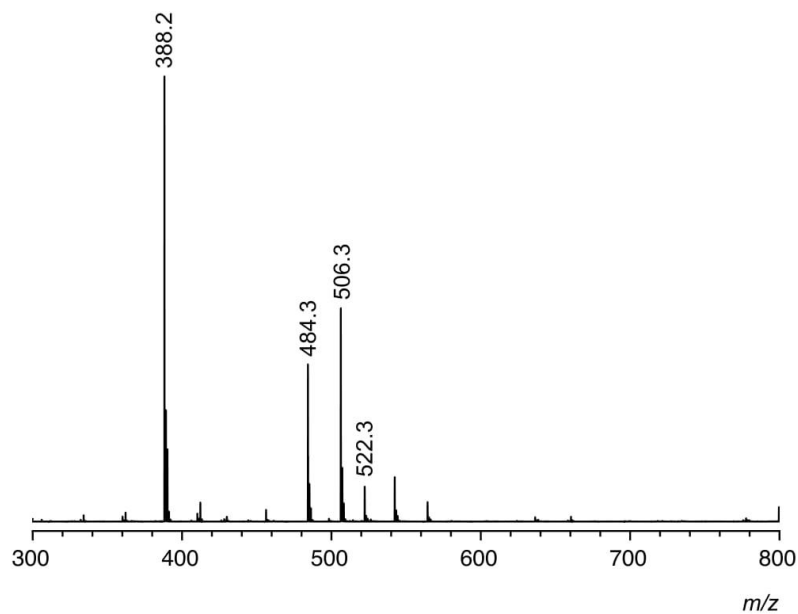
#### cyclo[(*R*)-Lac-1,4-Tri-Epa]<sub>4</sub> (2).



H-Epa-[(*R*)-Lac-1,4-Tri-Epa]<sub>3</sub>-(*R*)-Lac-N<sub>3</sub> (130 mg, 151 μmol) was dissolved in a mixture of DMF (20 mL) and *t*-BuOH/H<sub>2</sub>O, 1:1 (*v/v*) (50 mL). The resulting solution was added to a suspension of TBTA (8 mg, 15 μmol, 10 mol%), sodium ascorbate (3.0 mg, 15 μmol, 10 mol%), and Cu(MeCN)<sub>4</sub>PF<sub>6</sub> (6 mg, 16 μmol, 10 mol%) in *t*-BuOH/H<sub>2</sub>O, 1:1 (*v/v*) (250 mL). The reaction mixture was stirred at 35 °C and progress was followed by HPLC. Additional solid TBTA (9 mg, 18 μmol, 10 mol %) and Cu(MeCN)<sub>4</sub>PF<sub>6</sub> (7 mg, 18 μmol, 10 mol%) were added every 24 h until HPLC

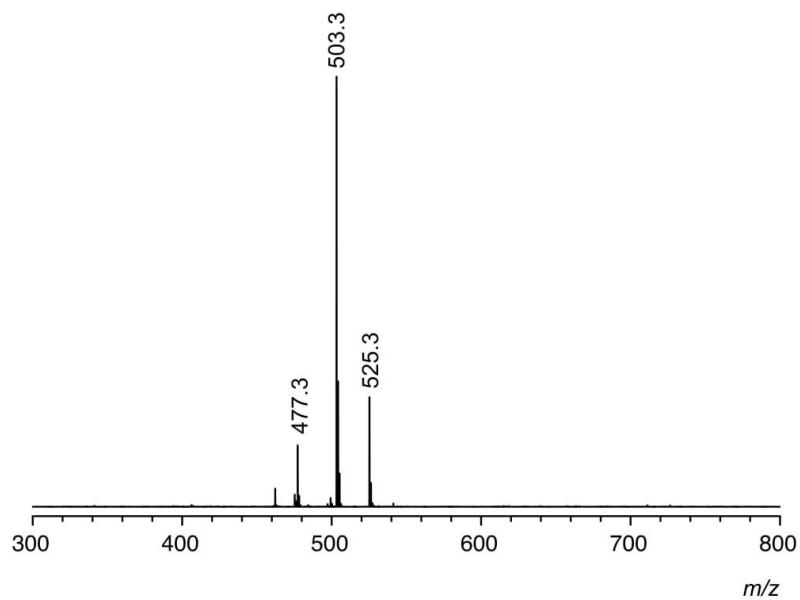
indicated full conversion, typically after 2 d. Ethyl acetate was added to the reaction mixture and the aqueous layer was removed. The organic solvent was evaporated, and the residue was purified on flash silica gel column using a gradient of dichloromethane/acetone (5:1, 3:2, 1:1, 1:2, pure acetone) to afford ca. 95 % pure product. Pure product was obtained after another chromatographic step using the same solvent mixtures as eluents. Yield: 34 mg (40  $\mu$ mol, 26%); m.p. > 200 °C (dec);  $[\alpha]_{\text{D}}^{25} = -31.0$  ( $c = 0.1$ , DMSO);  $^1\text{H}$  NMR (400 MHz, 25 °C, DMSO- $d_6$ )  $\delta = 10.80$  (s, 4H, NH), 8.67 (s, 4H, TriH), 7.96 (d, 4H,  $^3J(\text{H}, \text{H}) = 7.3$  Hz, EpaH(4)), 7.89 (t, 4H,  $^3J(\text{H}, \text{H}) = 7.8$  Hz, EpaH(5)), 7.76 (d, 4H,  $^3J(\text{H}, \text{H}) = 8.0$  Hz, EpaH(3)), 5.66-5.78 (m, 4H, LacCH), 1.85 (d, 9H,  $^3J(\text{H}, \text{H}) = 7.1$  Hz, LacCH<sub>3</sub>);  $^{13}\text{C}$  NMR (100.6 MHz, 25 °C, DMSO- $d_6$ )  $\delta = 167.4$  (CO), 151.2 (EpaC(2)), 148.4 (EpaC(6)), 146.1 (TriC(4)), 139.5 (EpaC(4)), 123.9 (TriC(5)), 115.8 (EpaC(5)), 112.9 (EpaC(3)), 59.0 (LacC), 17.2 (LacCH<sub>3</sub>); MS (MALDI-TOF)  $m/z$  (%):  $[\text{M}+\text{Na}]^+$  883.3 (100),  $[\text{M}+\text{K}]^+$  899.4 (29); elemental analysis calcd (%) for C<sub>40</sub>H<sub>36</sub>N<sub>20</sub>O<sub>4</sub>·6.5H<sub>2</sub>O: C 49.13, N 28.65, H 5.05 found C 49.20, N 28.58, H 5.48.

MALDI-TOF MS: H-Epa-(*R*)-Lac-1,4-Tri-Epa-(*S*)-Lac-OMs (positive mode).



		<i>m/z</i> calcd.	<i>m/z</i> exp.
$[M-CH_3SO_3H+H]^+$	$C_{21}H_{21}N_7O_5S - CH_3SO_3H + H^+$	388.2	388.2
$[M+H]^+$	$C_{21}H_{21}N_7O_5S + H^+$	484.1	484.3
$[M+Na]^+$	$C_{21}H_{21}N_7O_5S + Na^+$	506.1	506.3
$[M+K]^+$	$C_{14}H_{20}N_2O_4SSi + Na^+$	522.1	522.3

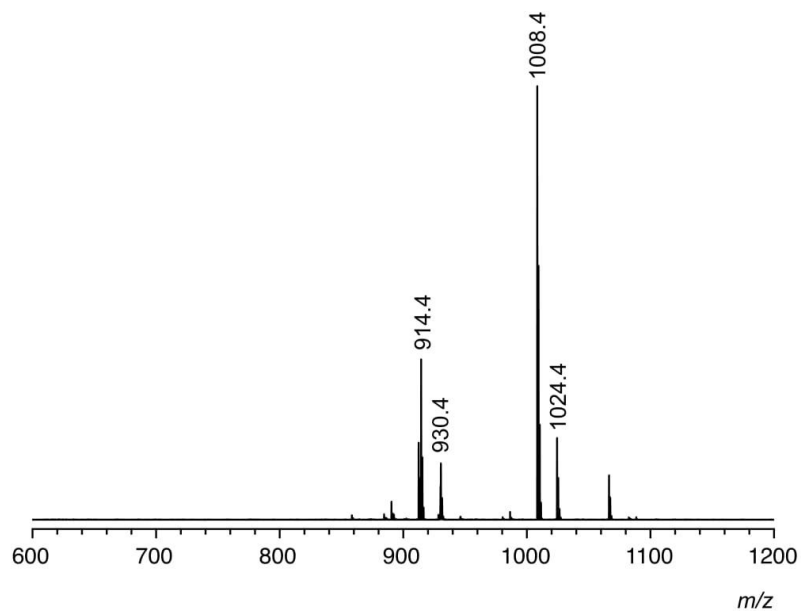
MALDI-TOF MS: TMS-Epa-(R)-Lac-1,4-Tri-Epa-(R)-Lac-N<sub>3</sub> (positive mode).



		<i>m/z calcd.</i>	<i>m/z exp.</i>
$[M-N_2+H_2+H]^+$	$C_{23}H_{28}N_8O_2Si + H^+$	477.2	477.3
$[M+H]^+$	$C_{23}H_{26}N_{10}O_2Si + H^+$	503.2	503.3
$[M+Na]^+$	$C_{23}H_{26}N_{10}O_2Si + Na^+$	525.2	525.3

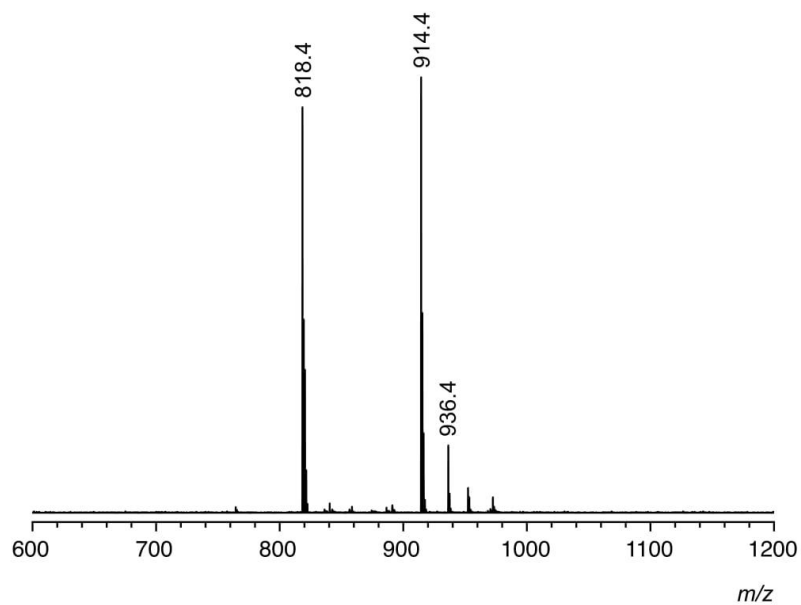


MALDI-TOF MS: TMS-Epa-[(*R*)-Lac-1,4-Tri-Epa]<sub>3</sub>-(*S*)-Lac-OMs **5** (positive mode).



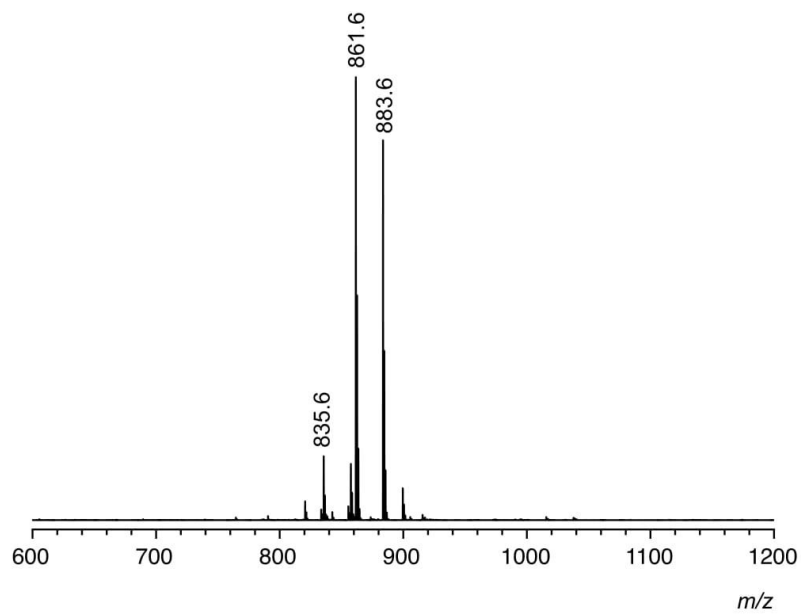
		<i>m/z calcd.</i>	<i>m/z exp.</i>
[M-Si(CH <sub>3</sub> ) <sub>3</sub> +2H] <sup>+</sup>	C <sub>41</sub> H <sub>39</sub> N <sub>17</sub> O <sub>7</sub> S + H <sup>+</sup>	914.3	914.4
[M-CH <sub>3</sub> SO <sub>3</sub> +H+K] <sup>+</sup>	C <sub>43</sub> H <sub>45</sub> N <sub>17</sub> O <sub>4</sub> Si + Na <sup>+</sup>	930.3	930.4
[M+Na] <sup>+</sup>	C <sub>44</sub> H <sub>47</sub> N <sub>17</sub> O <sub>7</sub> SSi + Na <sup>+</sup>	1008.3	1008.4
[M+K] <sup>+</sup>	C <sub>44</sub> H <sub>47</sub> N <sub>17</sub> O <sub>7</sub> SSi + K <sup>+</sup>	1024.3	1024.4

MALDI-TOF MS: H-Epa-[(*R*)-Lac-1,4-Tri-Epa]<sub>3</sub>-(*S*)-Lac-OMs (positive mode).



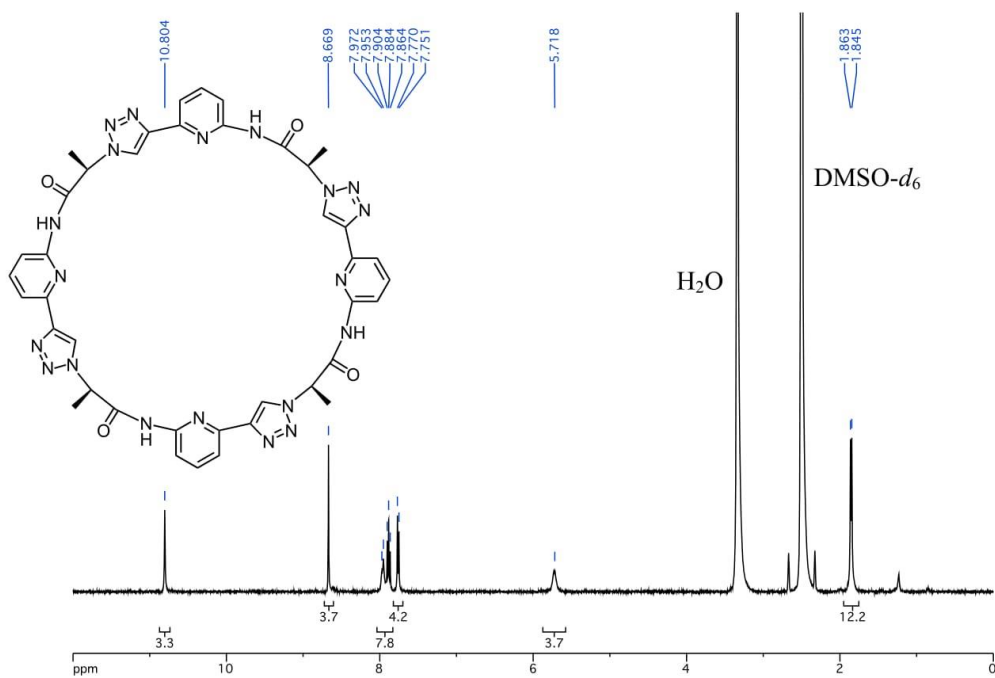
		<i>m/z calcd.</i>	<i>m/z exp.</i>
$[M-CH_3SO_3H+H]^+$	$C_{40}H_{35}N_{17}O_4 + H^+$	818.3	818.4
$[M+H]^+$	$C_{41}H_{39}N_{17}O_7S + H^+$	914.3	914.4
$[M+Na]^+$	$C_{41}H_{39}N_{17}O_7S + Na^+$	936.3	936.4

MALDI-TOF MS: H-Epa-[(R)-Lac-1,4-Tri-Epa]<sub>3</sub>-(R)-Lac-N<sub>3</sub> (positive mode).

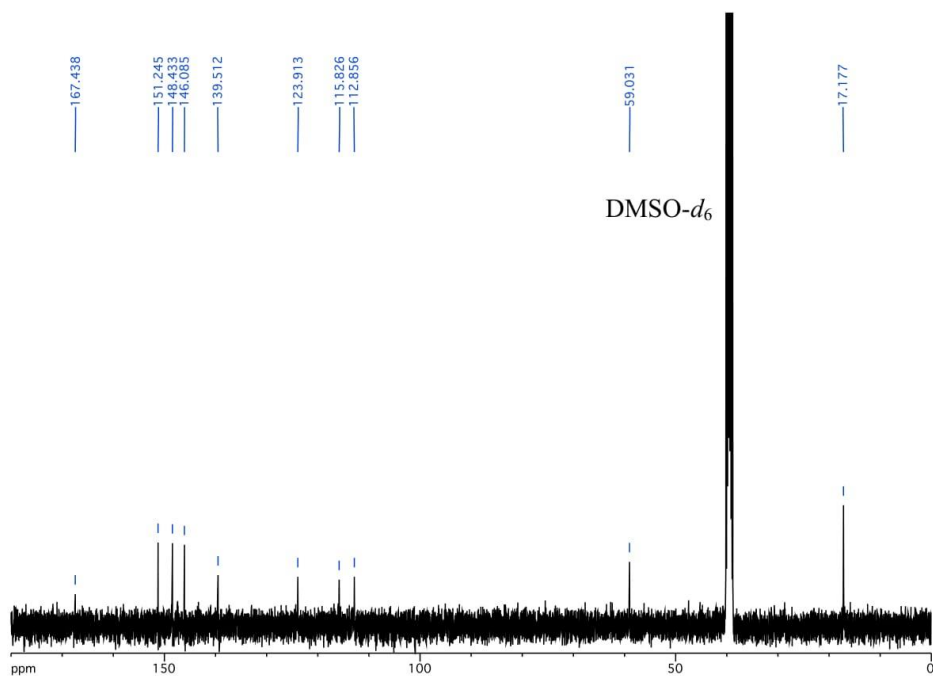


		<i>m/z calcd.</i>	<i>m/z exp.</i>
$[M-N_2+H_2+H]^+$	$C_{40}H_{38}N_{18}O_4 + H^+$	835.3	835.6
$[M+H]^+$	$C_{40}H_{36}N_{20}O_4 + H^+$	861.3	861.6
$[M+Na]^+$	$C_{40}H_{36}N_{20}O_4 + Na^+$	883.3	883.6

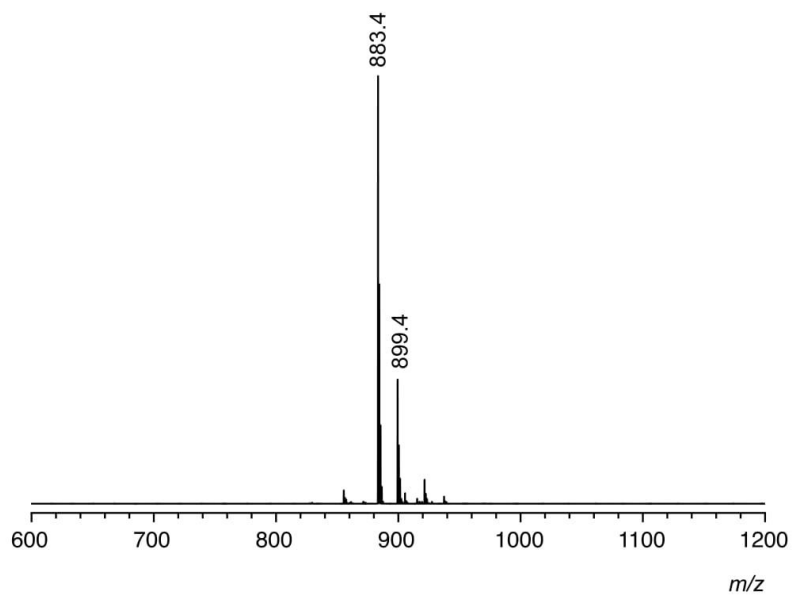
$^1\text{H}$  NMR: **2** (400 MHz,  $\text{DMSO-}d_6$ , 25 °C).



$^{13}\text{C}$  NMR: **2** (100.6 MHz,  $\text{DMSO-}d_6$ , 25 °C).

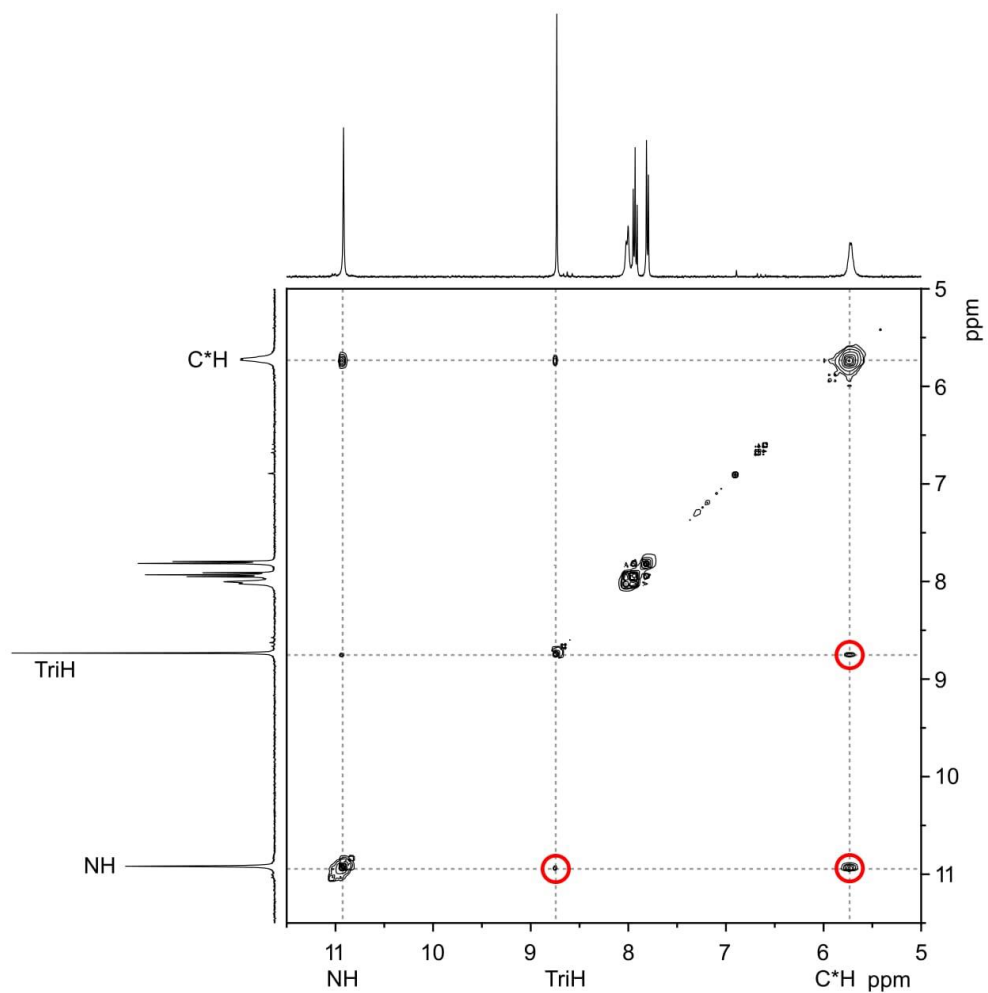


MALDI-TOF MS: **2** (positive mode).

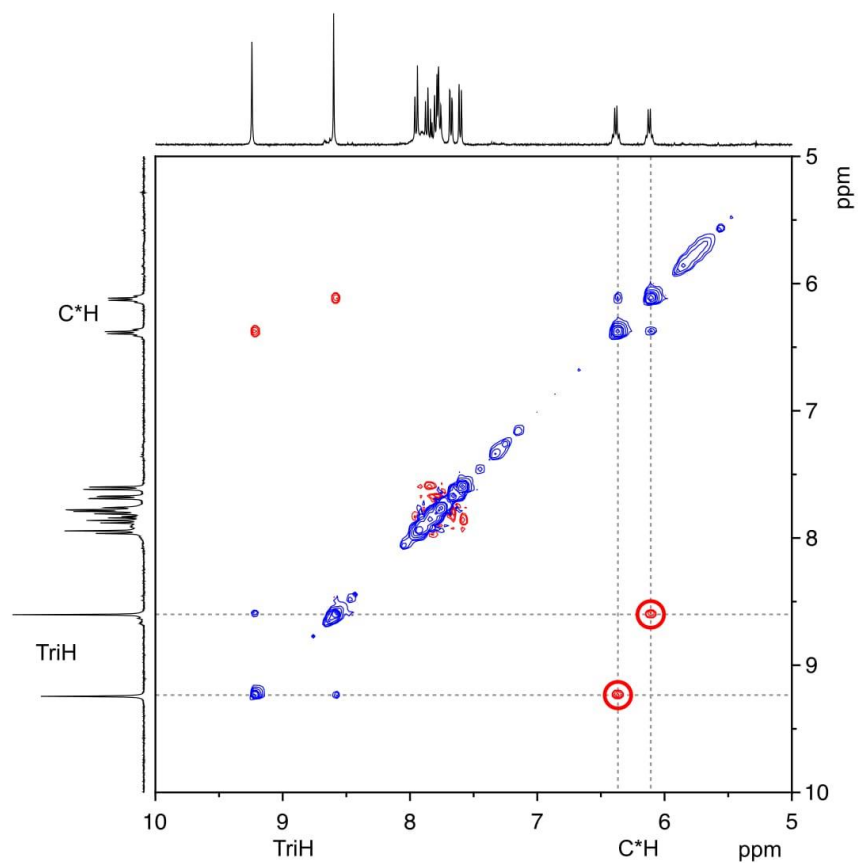


		<i>m/z calcd.</i>	<i>m/z exp.</i>
$[M+Na]^+$	$C_{40}H_{36}N_{20}O_4 + Na^+$	883.3	883.4
$[M+K]^+$	$C_{40}H_{36}N_{20}O_4 + K^+$	899.3	899.4

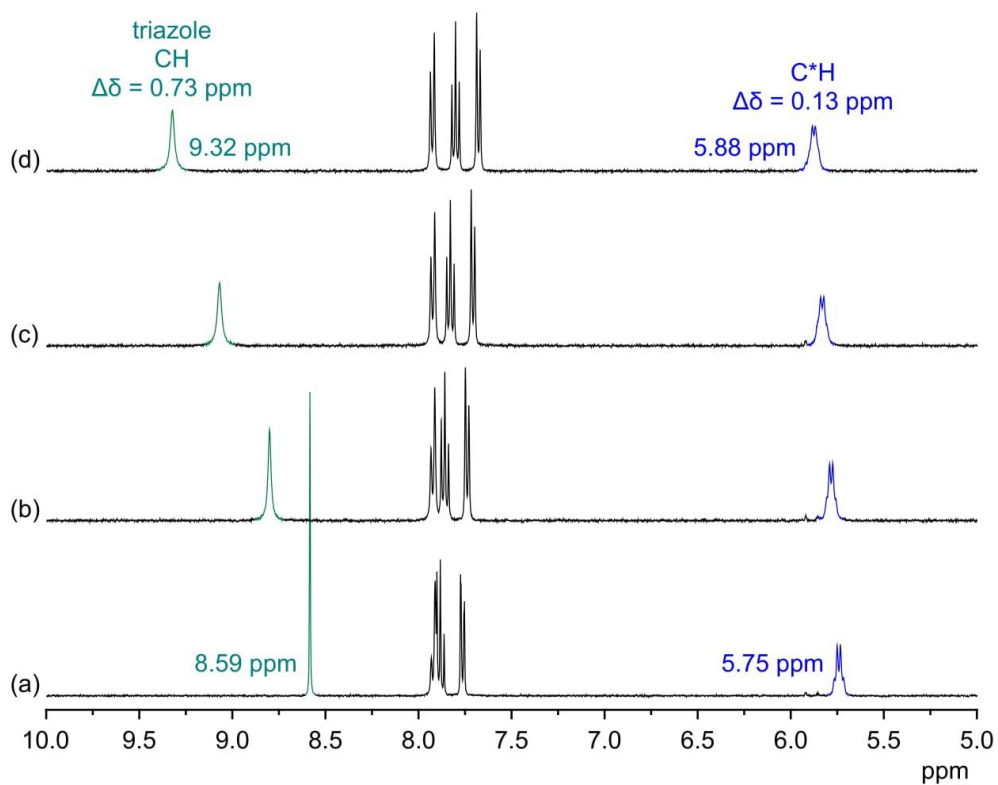
NOESY NMR Spectrum: **2** (1 mM) in DMSO- $d_6$  (mixing time 300 ms) (400 MHz, 25 °C).



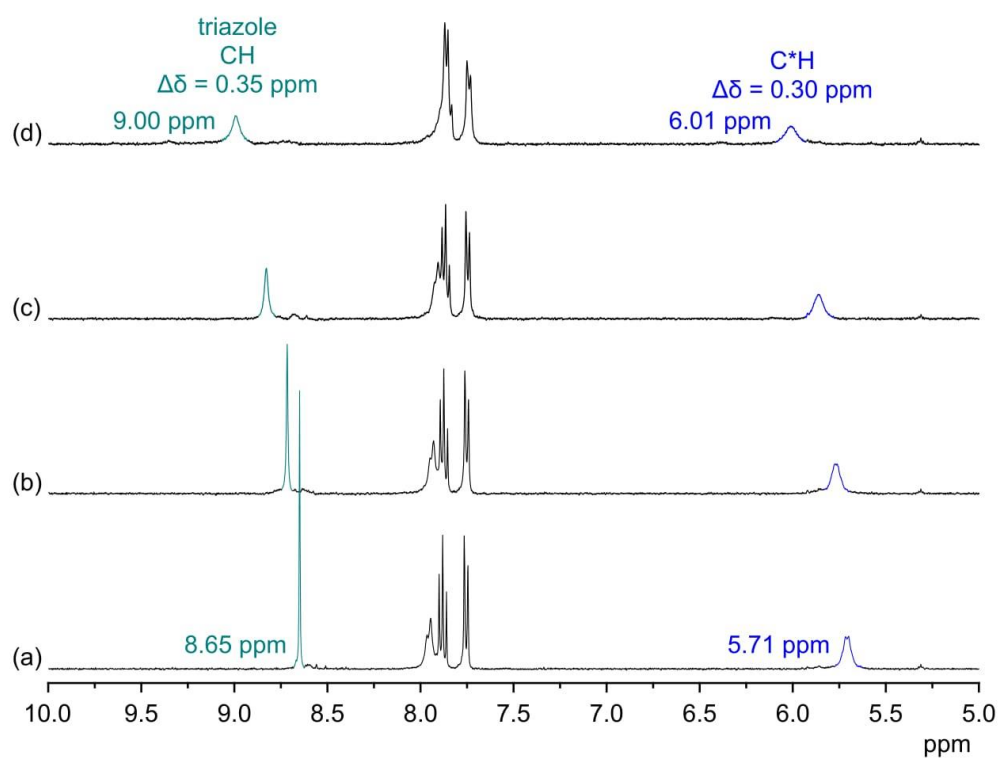
ROESY NMR Spectrum: **2** (0.5 mM) in DMSO- $d_6$  (mixing time 300 ms) in the presence of 1 equiv of tetrabutylammonium dihydrogenpyrophosphate (400 MHz, 25 °C, red - positive, blue - negative).



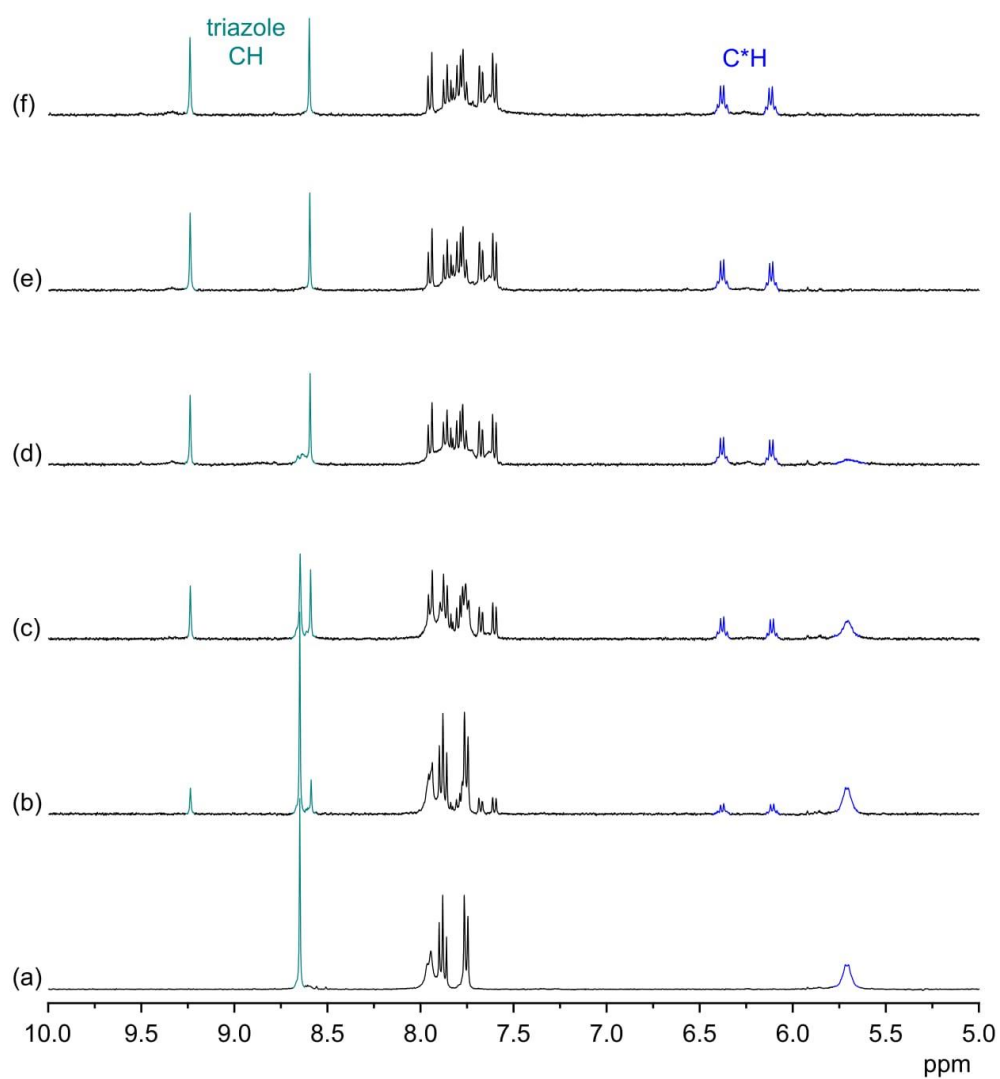
$^1\text{H}$  NMR Spectra: **1** (0.5 mM) in 2.5 vol%  $\text{D}_2\text{O}/\text{DMSO-}d_6$  in the absence (a) and the presence of 0.50 equiv (b), 1.00 equiv (c), and 2.00 equiv (d) of TBA sulfate. The signals of the triazole and C\*H protons are marked in green and blue, respectively.



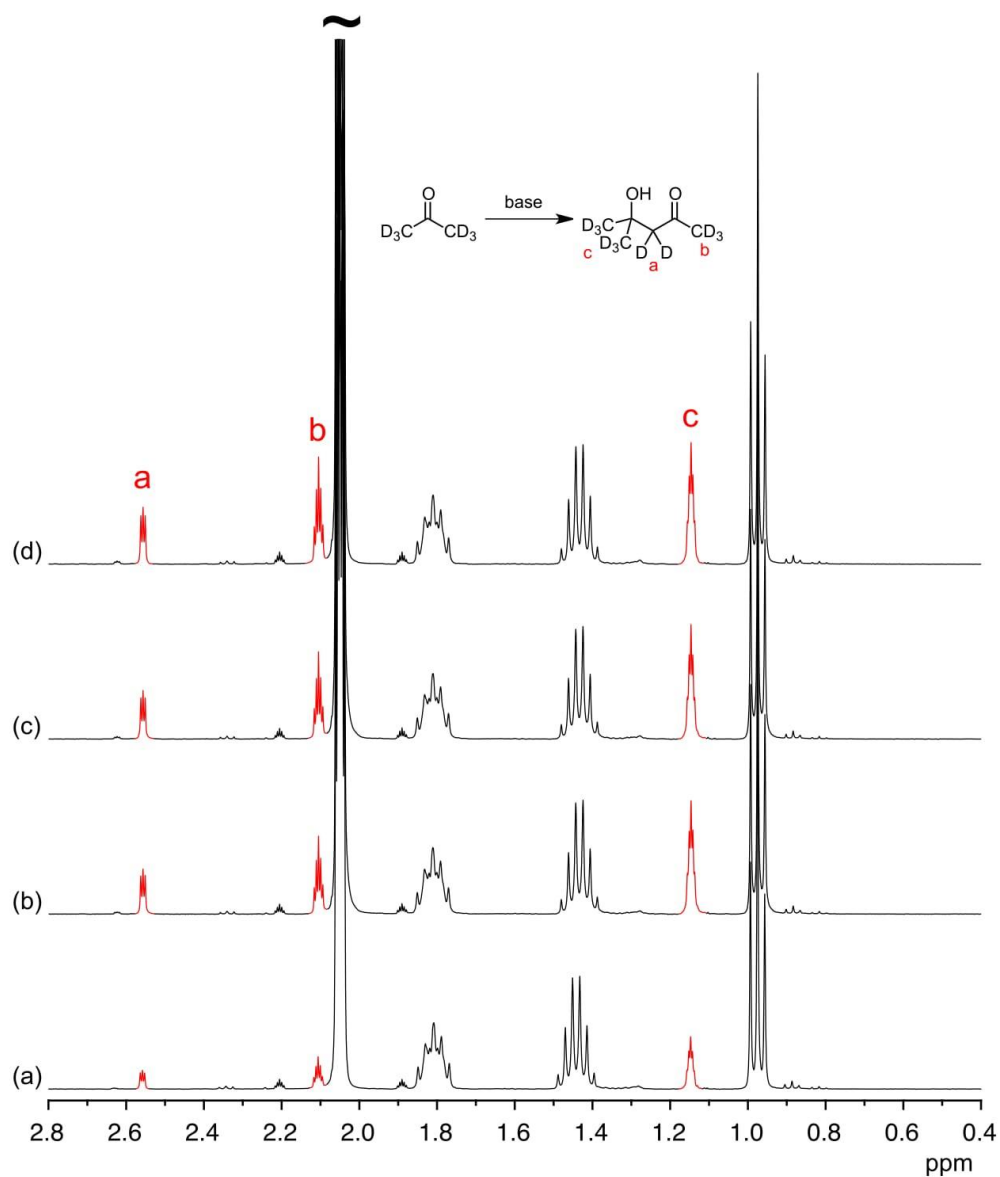
$^1\text{H}$  NMR Spectra: **2** (0.5 mM) in 2.5 vol%  $\text{D}_2\text{O}/\text{DMSO-}d_6$  in the absence (a) and the presence of 0.50 equiv (b), 1.00 equiv (c), and 2.00 equiv (d) of TBA sulfate. The signals of the triazole and C\*H protons are marked in green and blue, respectively.



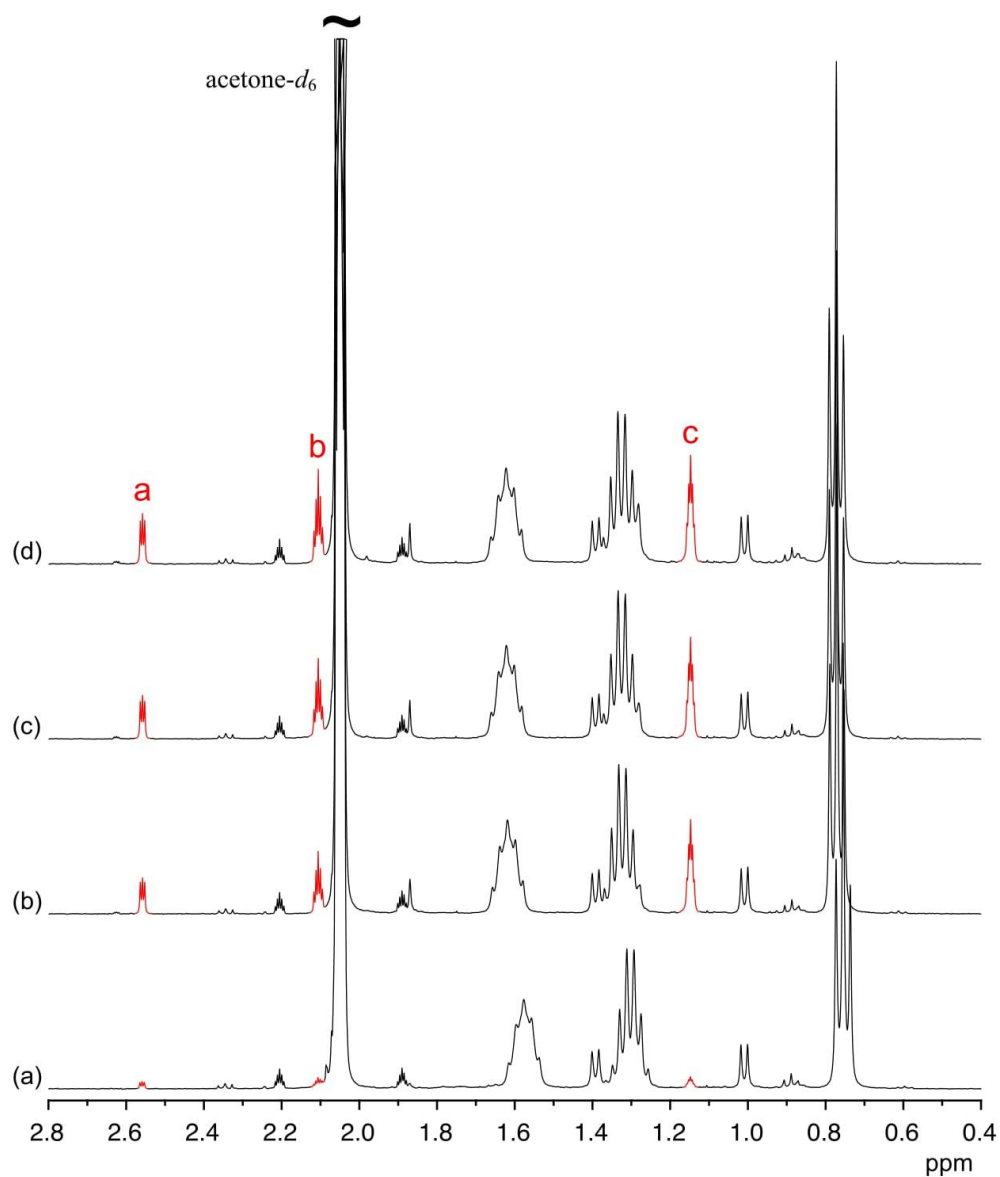
$^1\text{H}$  NMR Spectra: **2** (0.5 mM) in 2.5 vol%  $\text{D}_2\text{O}/\text{DMSO-}d_6$  in the absence (a) and the presence of 0.25 equiv (b), 0.5 equiv (c), 0.75 equiv (d), 1.0 equiv (e), and 2.0 equiv (f) of TBA HPP. The signals of the triazole and C\*H protons are marked in green and blue, respectively.



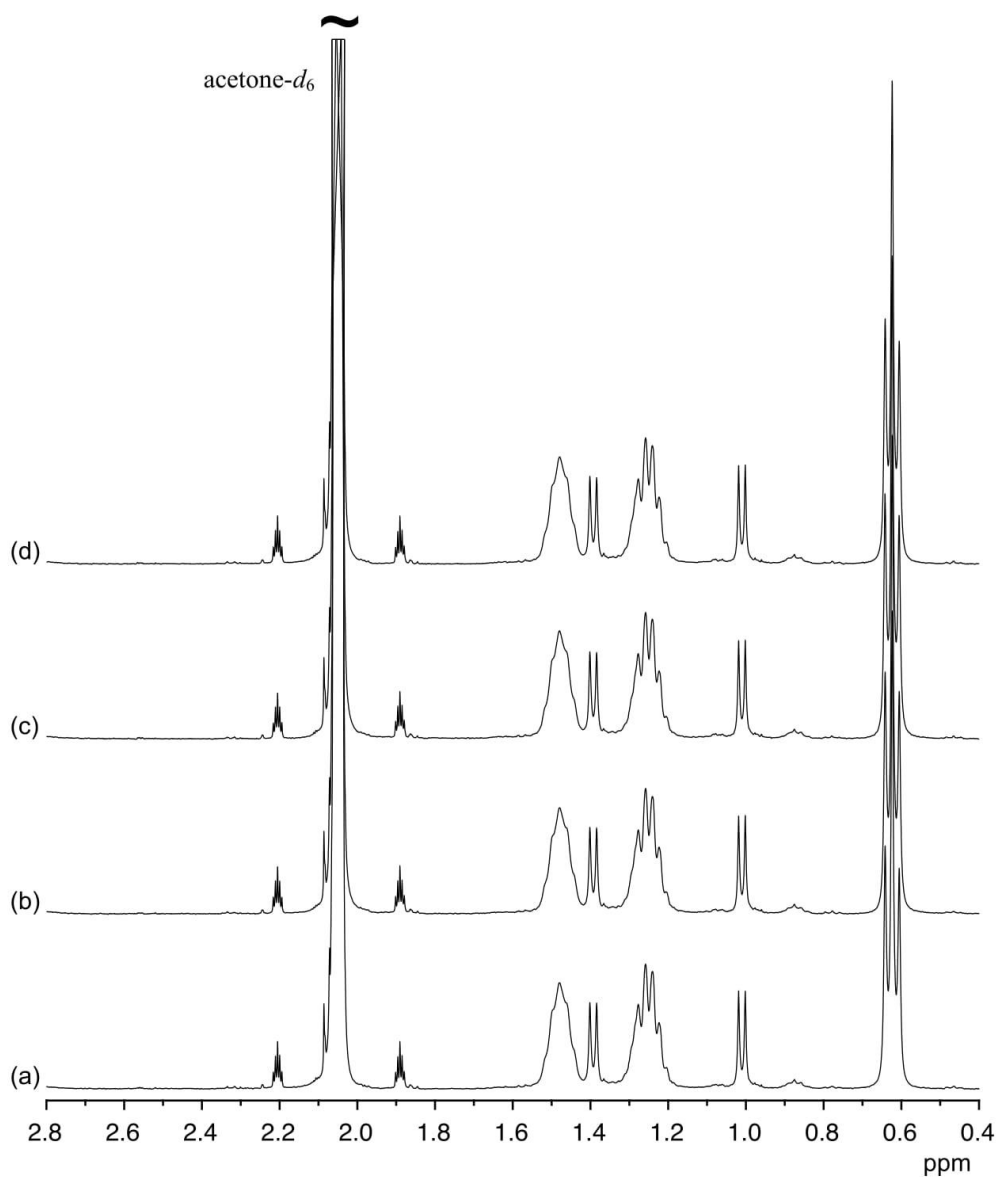
$^1\text{H}$  NMR Spectra: TBA HPP (0.75 mM) in acetone- $d_6$  after 0 d (a), 3 d (b), 5 d (c), 7 d (d), showing the formation of the aldol adduct of the solvent, deuterated 4-hydroxy-4-methylpentan-2-one. The signals assigned in red represent the residual protons of the mostly deuterated product.



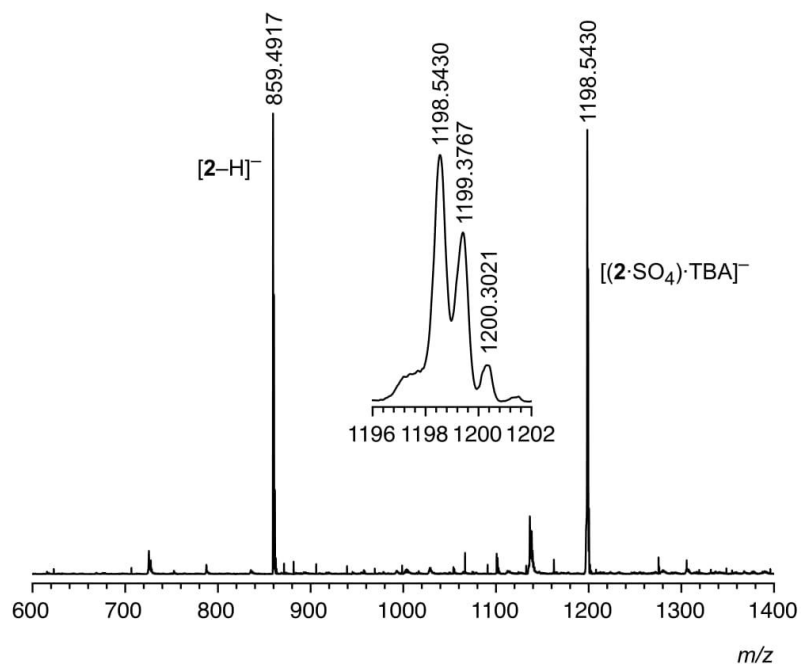
$^1\text{H}$  NMR Spectra: **2** (0.5 mM) in acetone- $d_6$  in the presence of 1.5 equiv of TBA HPP after 0 d (a), 3 d, (b), 5 d (c), 7 d (d). The signals marked red again indicate the presence of the aldol adduct of the solvent, deuterated 4-hydroxy-4-methylpentan-2-one.



$^1\text{H}$  NMR Spectra: **2** (0.5 mM) in acetone- $d_6$  in the presence of 1.5 equiv of TBA DHPP after 0 d (a), 3 d (b), 5 d (c), 7 d (d). No signals of the aldol adduct are visible, indicating that the aldol adduct of acetone does not form in the presence of TBA DHPP.

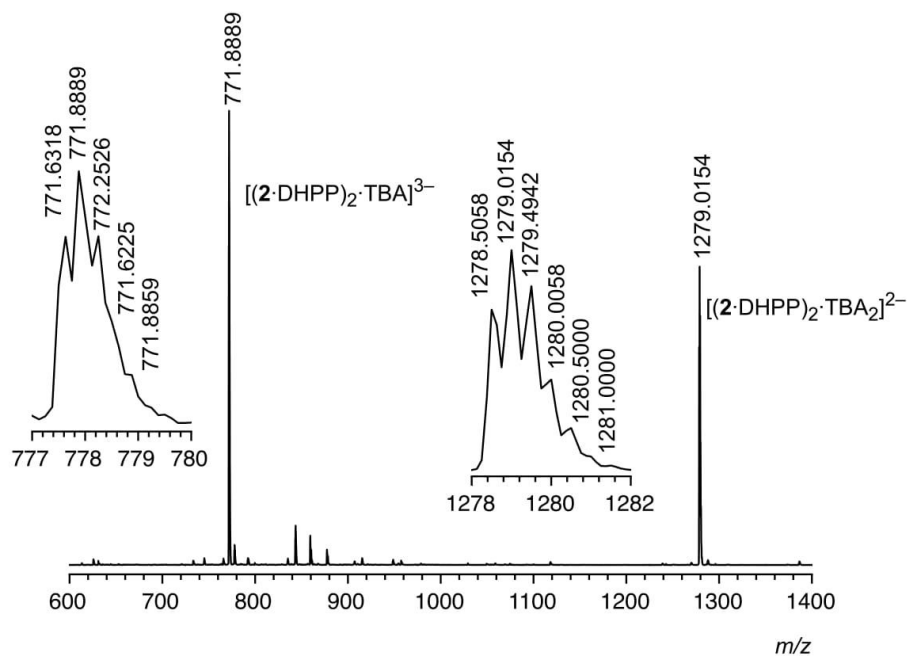


ESI MS: **2** (0.5 mM) in dichloromethane after the addition of TBA sulfate (1 equiv).



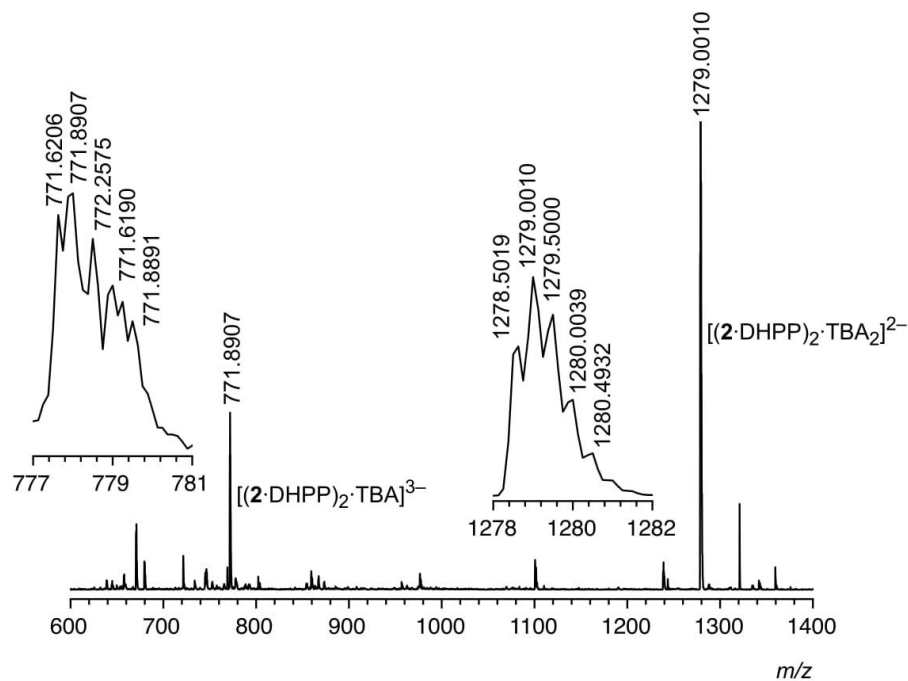
		$m/z$ calcd.	$m/z$ exp.
$[2-H]^-$	$C_{40}H_{36}N_{20}O_4 - H^+$	859.3558	859.4917
$[(2 \cdot SO_4) \cdot TBA]^-$	$C_{40}H_{36}N_{20}O_4 + SO_4^{2-} + C_{16}H_{36}N^+$	1198.5598	1198.5430

ESI MS: **2** (0.5 mM) in dichloromethane after the addition of TBA DHPP (1 equiv).



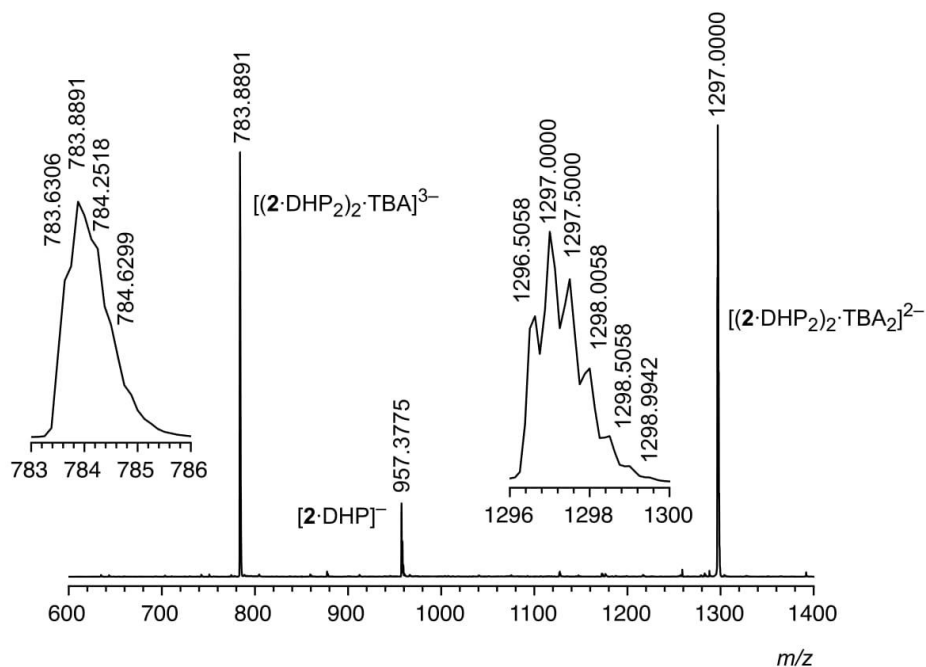
		<i>m/z calcd.</i>	<i>m/z exp.</i>
$[(2\cdot\text{DHPP})_2\cdot\text{TBA}]^{3-}$	$(\text{C}_{40}\text{H}_{36}\text{N}_{20}\text{O}_4 + \text{H}_2\text{O}_7\text{P}_2)_2^{4-} + \text{C}_{16}\text{H}_{36}\text{N}^+$	771.9302	771.8889
$[(2\cdot\text{DHPP})_2\cdot\text{TBA}_2]^{2-}$	$(\text{C}_{40}\text{H}_{36}\text{N}_{20}\text{O}_4 + \text{H}_2\text{O}_7\text{P}_2)_2^{4-} + 2 \text{C}_{16}\text{H}_{36}\text{N}^+$	1279.0374	1279.0154

ESI MS: **2** (0.5 mM) in dichloromethane after the addition of TBA HPP (1 equiv).



		<i>m/z</i> calcd.	<i>m/z</i> exp.
$[(2\cdot\text{DHPP})_2\cdot\text{TBA}]^{3-}$	$(\text{C}_{40}\text{H}_{36}\text{N}_{20}\text{O}_4 + \text{H}_2\text{O}_7\text{P}_2)_2^{4+} + \text{C}_{16}\text{H}_{36}\text{N}^+$	771.9302	771.8907
$[(2\cdot\text{DHPP})_2\cdot\text{TBA}_2]^{2-}$	$(\text{C}_{40}\text{H}_{36}\text{N}_{20}\text{O}_4 + \text{H}_2\text{O}_7\text{P}_2)_2^{4+} + 2 \text{C}_{16}\text{H}_{36}\text{N}^+$	1279.0374	1279.0010

ESI MS: **2** (0.5 mM) in dichloromethane after the addition of TBA DHP (2 equiv).



		<i>m/z calcd.</i>	<i>m/z exp.</i>
$[(2\cdot\text{DHP})_2\cdot\text{TBA}]^{3-}$	$(\text{C}_{40}\text{H}_{36}\text{N}_{20}\text{O}_4 + (\text{H}_2\text{O}_4\text{P})_2)^{4-} + \text{C}_{16}\text{H}_{36}\text{N}^+$	783.9372	783.8891
$[2\cdot\text{DHP}]^-$	$\text{C}_{40}\text{H}_{36}\text{N}_{20}\text{O}_4 + \text{H}_2\text{O}_4\text{P}^-$	957.2924	957.3775
$[(2\cdot\text{DHP})_2\cdot\text{TBA}_2]^{2-}$	$(\text{C}_{40}\text{H}_{36}\text{N}_{20}\text{O}_4 + (\text{H}_2\text{O}_4\text{P})_2)^{4-} + 2 \text{C}_{16}\text{H}_{36}\text{N}^+$	1297.0480	1297.0000

ITC Titrations:

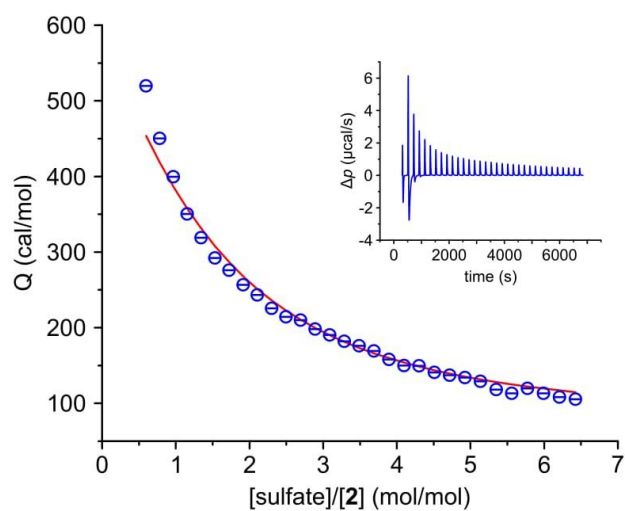
The ITC experiments were carried out in 2.5 vol% water/DMSO. The anionic substrates were used as their TBA salts. The salts and receptor **2** were weighed using an analytical precision balance, dissolved in known volumes of the respective solvent mixture, and loaded into the system for immediate analysis.

The measurements were carried out at 25 °C using a reference power of 25  $\mu$ J/s, a filter period of 2 s, a stirrer speed of 307 rpm. Other experimental parameters of the individual titrations are specified in the Table S1. Automated baseline assignment and peak integration of raw thermograms were accomplished by singular value decomposition and peak-shape analysis using NITPIC.<sup>3a</sup> Estimation of best-fit parameter values by weighted nonlinear least-squares fitting and calculation of 68.3% confidence intervals were performed with the public-domain software SEDPHAT,<sup>3b</sup> as explained in detail elsewhere.<sup>3c,d</sup>

**Table S1.** Concentrations and experimental parameters of the individual titrations.

guest anion as TBA salt	$c(\mathbf{2})$ / mM	$c(\text{salt})$ / mM	injection volume / $\mu$ L	no. of injections	spacing time / s
sulfate	0.4	13.6	8	32	200
DHPP	0.4	6.1	8	32	200
DHP	0.4	12.9	8	34	200

Titration of **2** with TBA sulfate: The blue spheres show the experimental results and the red line the fitted curve calculated by using the one site binding model. The inset shows the heat pulses of the measurement from which the isotherm was generated.



Titration of **2** with TBA DHPP: The blue spheres show the experimental results and the red line the fitted curve calculated by assuming that the dimer of the anion binds to two molecules of **2** in a stepwise fashion. The inset shows the heat pulses of the measurement from which the isotherm was generated.

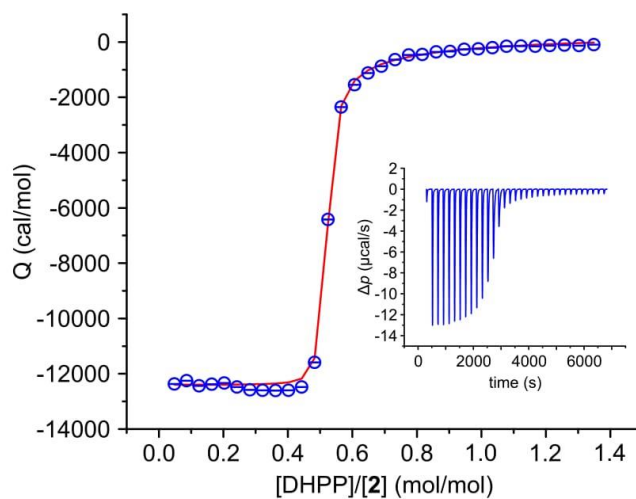
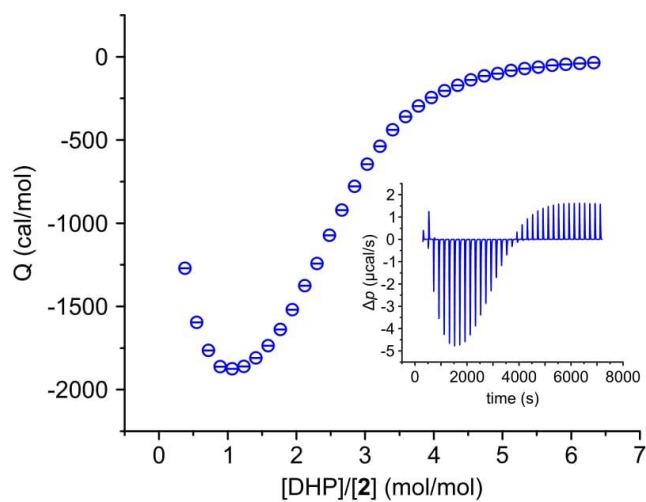


**Table S2.** Thermodynamic parameters for the binding of TBA DHPP to **2** under the assumption that the dimer of the anion (DHPP)<sub>2</sub> binds as a single entity to two molecules of **2** in a stepwise fashion.<sup>a</sup>

reaction	log $K_a$	$\Delta G$	$\Delta H$	$T\Delta S$
<b>2</b> + (DHPP) <sub>2</sub> $\rightleftharpoons$ [ <b>2</b> ·(DHPP) <sub>2</sub> ]	6.3	-36.2	-33.2	3.0
<b>2</b> + [ <b>2</b> ·(DHPP) <sub>2</sub> ] $\rightleftharpoons$ [ <b>2</b> ·(DHPP) <sub>2</sub> ] <sub>2</sub>	6.4	-36.2	-20.1	16.1
2 <b>2</b> + (DHPP) <sub>2</sub> $\rightleftharpoons$ [ <b>2</b> ·(DHPP) <sub>2</sub> ] <sub>2</sub>	12.7	-72.2	-53.3	19.1

<sup>a</sup>  $\Delta G$ ,  $\Delta H$ , and  $T\Delta S$  in kJ mol<sup>-1</sup>.

Titration of **2** with TBA DHP: The blue spheres show the experimental results and the inset shows the heat pulses of the measurement from which the isotherm was generated.



Crystal Structures:

**General details.** Single crystal X-ray data were collected at 120 K on an Agilent Super-Nova dual wavelength diffractometer with a micro-focus X-ray source and multilayer optics monochromatised CuK $\alpha$  ( $\lambda = 1.54184 \text{ \AA}$ ) radiation. Program *CrysAlisPro*<sup>4</sup> was used for the data collection and reduction. The diffraction intensities were corrected for absorption using analytical face index absorption correction method<sup>5</sup> for all the data. The structures were solved with direct methods (*SHELXT*<sup>6</sup>) and refined by full-matrix least squares on  $F^2$  using *SHELXL-2016/6*.<sup>7</sup> SQUEEZE module of PLATON<sup>8</sup> was utilised in the structure refinement to remove the residual electron densities, which were not possible to be reliably assigned and refined. Anisotropic displacement parameters were assigned to non-H atoms. Positional disorder in the structures was treated by restraining or constraining the geometric and anisotropic displacement parameters as gently as possible. All hydrogen atoms (except O-H in **2**<sub>2</sub>·DHPP<sub>2</sub> as well as O-H and N-H in **2**(rac)<sub>2</sub>·DHPP<sub>2</sub>) were refined using riding models with  $U_{eq}(\text{H})$  of  $1.5U_{eq}(\text{C},\text{O})$  for terminal methyl and hydroxyl groups, and 1.2 of  $U_{eq}(\text{C},\text{N})$  for other groups. The hydrogens found from the difference Fourier maps and bonded to O or N were refined with restrained ideal O-H (0.84  $\text{\AA}$ ) or N-H (0.91  $\text{\AA}$ ) distances and with  $U_{eq}(\text{H})$  of  $1.5 U_{eq}(\text{O})$  or  $1.2 U_{eq}(\text{N})$ . The additional details of each novel crystal data, data collection, and the refinement results are documented below (see also Table S3).

**Structure of **2**<sub>2</sub>·DHPP<sub>2</sub>:** **2**<sub>2</sub>·DHPP<sub>2</sub> was crystallised as colourless prisms from a solution of **2** in DMSO containing 1 equiv of TBA DHPP. The structure found from the solution contains one (**2**<sub>2</sub>·DHPP<sub>2</sub>)<sup>4+</sup> and only two TBA<sup>+</sup> cations, while other molecular entities could not be located. The data is so badly disordered that according to analysis by PLATON/SQUEEZE<sup>8</sup> approximately 4500 electrons were removed in the procedure, which includes the ones of missing cations (and other unknown entities) and exceeds the  $F(000)$  value.

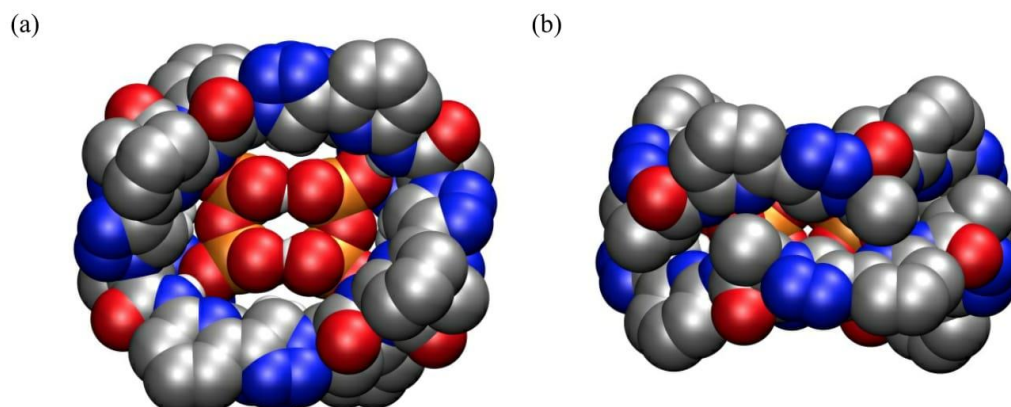


Figure S1: Molecular structure of  $2_2\cdot\text{DHPP}_2$  as space-filling models showing the sandwich-type arrangement of the two pseudopeptide rings and the DHPP anion from the top (a) and the side (b). The TBA cations and the hydrogen atoms except those on the anion, NH and triazole CH groups are omitted for clarity.

**Structure of  $2(\text{rac})_2\cdot\text{DHPP}_2$ :**  $2(\text{rac})_2\cdot\text{DHPP}_2$  with the exact composition  $4(2(\text{rac})_2\cdot\text{DHPP}_2)^{4-}\cdot 13(\text{C}_{16}\text{H}_{36}\text{N}^+)\cdot 9(\text{C}_6\text{H}_{12}\text{O}_2)\cdot (\text{C}_3\text{H}_6\text{O})\cdot (\text{H}_2\text{O})$  was crystallised as colourless plates from a solution of **2** in acetone containing 1 equiv of TBA HPP.

All the cations for the charge balance could not be located from the data. Almost 2000 electrons were removed in PLATON/SQUEEZE<sup>8</sup> procedure. The DHPP anions, as in  $2_2\cdot\text{DHPP}_2$ , form pairs by hydrogen bonds with  $\text{O}\cdots\text{O}$  distances between 2.49 and 2.55 Å. Similarly, the two pseudopeptides are holding the anion pair in the cavity between the rings with hydrogen bonds, which show  $\text{N}\cdots\text{O}$  distances between 2.71 and 2.86 Å, as well as,  $\text{C}\cdots\text{O}$  between 3.60 and 4.00 Å. The TBA cations outside the bowl-shaped cavity are filling the spaces between the complexes, which applies also for 4-hydroxy-4-methylpentan-2-one, acetone and water molecules. The nitrogen atoms in triazole molecules are accepting hydrogen bonds donated by 4-hydroxy-4-methylpentan-2-one and water molecules ( $\text{O}\cdots\text{N}$  between 2.87 and 3.00 Å).

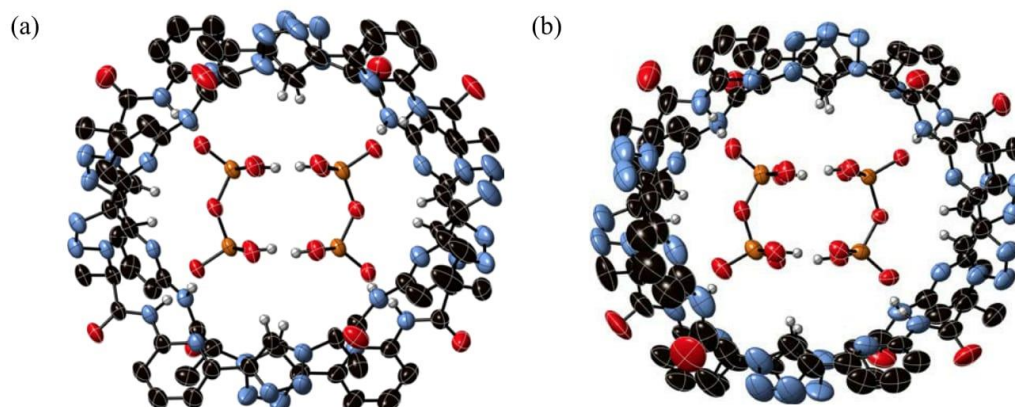


Figure S2: Molecular structure of  $2(\text{rac})_2 \cdot \text{DHPP}_2$  showing the 2:2 association of the pseudopeptide and two DHPP anions with the thermal ellipsoids shown at the 50% probability level. Figure S2a shows the complex of the all-*R* enantiomer of **2** and Figure S2b the one with the all-*S* enantiomer. TBA cations and the hydrogen atoms except those on the anion, NH and triazole CH groups are omitted for clarity.

Another batch of  $2(\text{rac})_2 \cdot \text{DHPP}_2$  crystals was obtained from DMSO/DCM, 1:1 ( $v/v$ ). The structure solution of these crystals has the composition  $3(2(\text{rac})_2 \cdot \text{DHPP}_2)^4 \cdot 12(\text{C}_{16}\text{H}_{36}\text{N})^+ \cdot 8(\text{C}_2\text{H}_6\text{OS}) \cdot 3.2\text{H}_2\text{O}$  (H atoms for water molecules were not found). In this  $2(\text{rac})_2 \cdot \text{DHPP}_2$  structure only 200 electrons were removed by PLATON/SQUEEZE.<sup>8</sup> Hydrogen bonding  $\text{O} \cdots \text{O}$  distances in DHPP dimer shows values between 2.51 and 2.67 Å. Hydrogen bonds between pseudopeptides and anions show  $\text{N} \cdots \text{O}$  distances between 2.67 and 2.98 Å, and  $\text{C} \cdots \text{O}$  distances between 2.98 and 3.80 Å. Five of the six bowl-shaped cavities of pseudopeptide rings are filled by TBA cations, while one cavity is occupied by DMSO molecules. The remaining TBA cations are located between the complexes.

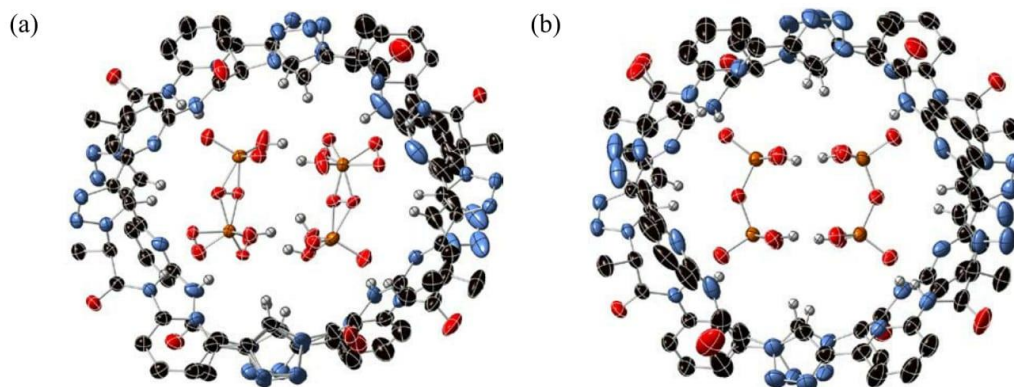


Figure S3: Molecular structure of **2(rac)<sub>2</sub>·DHPP<sub>2</sub>-2** showing the 2:2 association of the pseudopeptide and two DHPP anions with the thermal ellipsoids shown at the 50% probability level. Figure. S3a shows the complex of the all-*R* enantiomer of **2** and Figure S3b the one with the all-*S* enantiomer. TBA cations and the hydrogen atoms except those on the anion, NH and triazole CH groups are omitted for clarity.

**Structure of 2<sub>2</sub>·DHP<sub>4</sub>:** **2<sub>2</sub>·DHP<sub>4</sub>** with the exact composition  $4(2_2 \cdot \text{DHP}_4)^{4+} \cdot 11(\text{C}_{16}\text{H}_{36}\text{N})^+ \cdot (\text{C}_2\text{H}_6\text{OS})$  was crystallised as colourless plates from a solution of **2** in DMSO, containing 2 equiv of TBA DHP. Note that also in this structure not all of the TBA cations could be located because of substantial disorder. In addition, part of the structure containing almost 3500 electrons was removed by PLATON/SQUEEZE.<sup>8</sup>

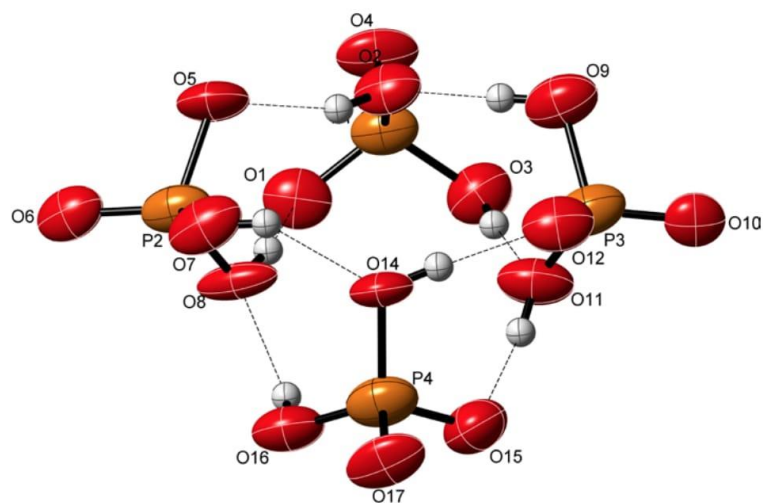


Figure S4: Detailed representation of the hydrogen bonding pattern in the DHP tetramer of  $2_2\cdot\text{DHP}_4$ .

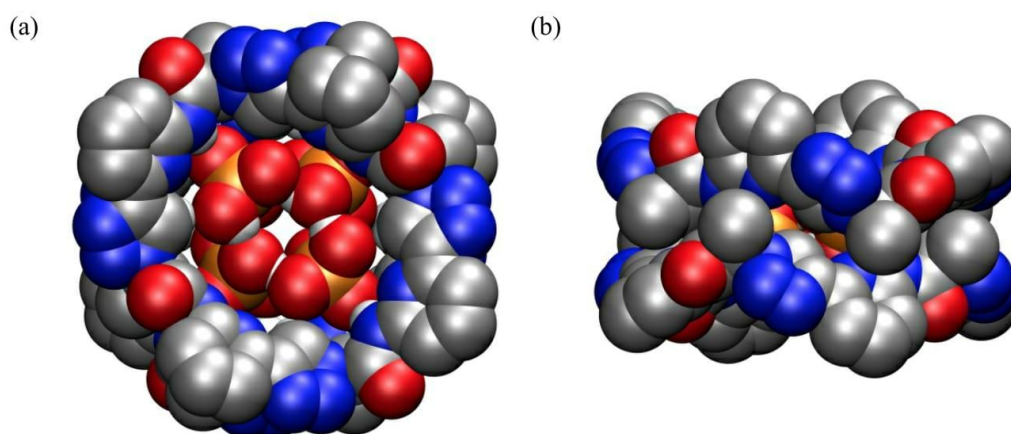


Figure S5: Molecular structure of  $2_2\cdot\text{DHP}_4$  as space-filling models showing the sandwich-type arrangement of the two pseudopeptide rings and the DHPP anion from the top (a) and the side (b). The TBA cations and the hydrogen atoms except those on the anion, NH and triazole CH groups are omitted for clarity.

**Table S3.** Crystal data and parameters for **2<sub>2</sub>·DHPP<sub>2</sub>**, **2(rac)<sub>2</sub>·DHPP<sub>2</sub>**, **2(rac)<sub>2</sub>·DHPP<sub>2</sub>-2**, and **2<sub>2</sub>·DHP<sub>4</sub>**.

	<b>2<sub>2</sub>·DHPP<sub>2</sub></b>	<b>2(rac)<sub>2</sub>·DHPP<sub>2</sub></b>	<b>2(rac)<sub>2</sub>·DHPP<sub>2</sub>-2</b>	<b>2<sub>2</sub>·DHP<sub>4</sub></b>
CCDC number	1555955	1555956	1555957	1555958
Empirical formula	C <sub>56</sub> H <sub>74</sub> N <sub>21</sub> O <sub>11</sub> P <sub>2</sub>	C <sub>585</sub> H <sub>888</sub> N <sub>173</sub> O <sub>108</sub> P <sub>16</sub>	C <sub>224</sub> H <sub>354</sub> N <sub>66</sub> O <sub>38.61</sub> P <sub>6</sub> S <sub>4</sub>	C <sub>498</sub> H <sub>722</sub> N <sub>171</sub> O <sub>97</sub> P <sub>16</sub> S
<i>F</i> <sub>w</sub> [g/mol]	1279.30	12568.15	4903.61	11184.00
Crystal system	Trigonal	Triclinic	Triclinic	Monoclinic
Space group	<i>P</i> 321 <sup>a</sup>	<i>P</i> -1	<i>P</i> -1	<i>P</i> 2 <sub>1</sub> <sup>b</sup>
Unit cell dimensions				
<i>a</i> [Å]	28.3369(4)	22.1903(3)	28.2322(3)	26.9085(8)
<i>b</i> [Å]	28.3369(4)	31.9713(4)	28.4659(3)	36.1230(11)
<i>c</i> [Å]	58.9056(13)	61.8821(4)	39.1611(5)	41.160(3)
$\alpha$ [°]	90	76.0283(8)	72.4310(10)	90
$\beta$ [°]	90	79.8139(8)	82.4440(10)	92.306(4)
$\gamma$ [°]	120	73.4101(11)	60.3890(10)	90
<i>V</i> [Å <sup>3</sup> ]	40963.0(15)	40554.3(8)	26079.5(6)	39975(3)
<i>Z</i>	6	2	4	2
$\rho$ [Mg/m <sup>3</sup> ]	0.311	1.029	1.249	0.929
$\mu$ [mm <sup>-1</sup> ]	0.290	0.878	1.330	0.857
<i>F</i> (000)	4050	13426	10492	11878
Crystal size [mm]	0.25×0.25×0.07	0.30×0.21×0.08	0.40×0.27×0.09	0.18×0.15×0.04
$\theta$ range [°]	3.462 – 67.994	3.511 – 69.999	3.365 – 67.999	3.448 – 67.700
Reflections collected	121482	238782	453951	237482
Independent reflections	49626	147346	94326	141768
<i>R</i> <sub>int</sub>	0.0697	0.0446	0.0656	0.2577
Reflections [ <i>I</i> >2 $\sigma$ ( <i>I</i> )]	35387	91821	72636	
Restraints / parameters	561 / 789	1968 / 8199	2100 / 6486	3051 / 6845
Completeness to $\theta$ [%]	99.9	97.5	99.4	99.8
Max.&min transmission	0.951 & 0.879	0.925 & 0.806	0.921 & 0.762	0.949 & 0.844
Goodness-of-fit on <i>F</i> <sup>2</sup>	1.355	1.025	1.671	0.941
Final <i>R</i> [ <i>I</i> >2 $\sigma$ ( <i>I</i> )]	<i>R</i> 1 = 0.1378 w <i>R</i> 2 = 0.3698	<i>R</i> 1 = 0.0800 w <i>R</i> 2 = 0.2302	<i>R</i> 1 = 0.1161 w <i>R</i> 2 = 0.3604	<i>R</i> 1 = 0.1303 w <i>R</i> 2 = 0.3123
<i>R</i> (all data)	<i>R</i> 1 = 0.1571 w <i>R</i> 2 = 0.3929	<i>R</i> 1 = 0.1171 w <i>R</i> 2 = 0.2710	<i>R</i> 1 = 0.1375 w <i>R</i> 2 = 0.3926	<i>R</i> 1 = 0.2948 w <i>R</i> 2 = 0.4534
Largest peak&hole [e./Å <sup>3</sup> ]	0.563 & -0.544	0.873 & -0.678	1.967 & -2.065	0.578 & -0.591

Absolute structure parameter: <sup>a</sup> meaningless and removed; <sup>b</sup> 0.11(4)

## 9 Appendix III

Electronic Supplementary Material (ESI) for ChemComm.  
This journal is © The Royal Society of Chemistry 2017

*Chem. Commun.*

### **A neutral halogen bonding macrocyclic anion receptor based on a pseudocyclopeptide with three 5-iodo-1,2,3-triazole subunits**

Disha Mungalpara,<sup>a</sup> Simone Stegmüller<sup>b</sup> and Stefan Kubik\*<sup>a</sup>

<sup>a</sup> *Technische Universität Kaiserslautern, Fachbereich Chemie - Organische Chemie, Erwin-Schrödinger-Straße, 67663 Kaiserslautern, Germany, Fax: +49-631-205-3921, Email: kubik@chemie.uni-kl.de*

<sup>b</sup> *Technische Universität Kaiserslautern, Fachbereich Chemie - Lebensmittelchemie & Toxikologie, Erwin-Schrödinger-Straße, 67663 Kaiserslautern, Germany.*

#### CONTENT

Synthetic Procedures.....	S2
<sup>1</sup> H NMR, <sup>13</sup> C NMR, and MS Spectra of Synthetic Intermediates and Pseudopeptide <b>1<sup>I</sup></b> .....	S8
ROESY NMR Spectrum of <b>1<sup>I</sup></b> .....	S18
ESI-MS Measurements .....	S19
NMR Titrations .....	S22
ITC Titrations.....	S34
Comparison of the Anion Affinities of <b>1<sup>I</sup></b> and <b>1<sup>H</sup></b> .....	S35
References.....	S36

### Synthetic Procedures

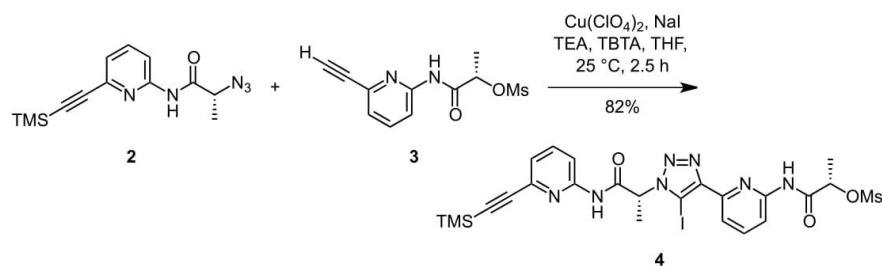
**General details.** Analyses were carried out as follows: melting points, Müller SPM-X 300; NMR, Bruker DPX 400 (peak assignments were confirmed by using H,H-COSY and HMQC spectra, spectra were referenced to the residual solvent signals (DMSO-*d*<sub>6</sub>:  $\delta_{\text{H}} = 2.50$  ppm,  $\delta_{\text{C}} = 39.5$  ppm);<sup>1</sup> elemental analysis, Elementar vario Micro cube; optical rotation, Perkin Elmer 241 MC digital polarimeter (*d* = 10 cm); ITC, Microcal VP-ITC.

The following abbreviations are used: TBA, tetrabutylammonium; TMA, tetramethylammonium Epa, 2-amino-6-ethynyl-2-pyridine; Lac, CH<sub>3</sub>CHCO; ITri, 5-iodo-1,2,3-triazole; TBTA, tris[(1-benzyl-1*H*-1,2,3-triazol-4-yl)methyl]amin; TBAF, TBA fluoride; TEA, triethylamine.

The syntheses of building blocks **2** and **3** are described elsewhere.<sup>2</sup> TBA sulfate, TBA dihydrogenphosphate, TBA nitrate, TBA chloride, TBA bromide, TBA iodide, and TMA chloride are commercially available and were used after confirming purity by elemental analysis.

**LC-ESI-MS measurements.** These measurements were performed by using an Agilent 1100 HPLC coupled with an API 2000 MS. For HPLC, a gradient from 30 to 100 vol% acetonitrile in water over 30 minutes with a flow rate of 1 mL/min was used. The parameter settings for ESI were as follows: curtain gas, 35 psi; ion spray voltage, 5500 V; temperature, 450 °C; nebulizer gas, 50 psi; heater gas, 60 psi; declustering potential, 40 V; focusing potential, 200 V; entrance potential, 10 V. The measurements were performed in full scan mode with a mass range from 500 to 1300 Da.

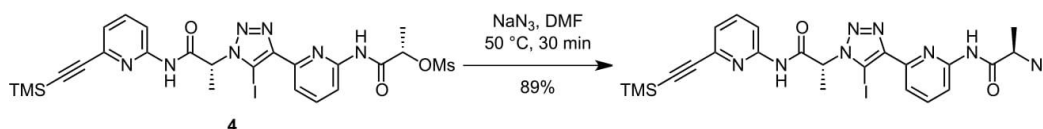
#### TMS-Epa-(*R*)-Lac-1,4-ITri-Epa-(*S*)-Lac-OMs **4**.



Thoroughly dried Cu(ClO<sub>4</sub>)<sub>2</sub>·6H<sub>2</sub>O (3.0 g, 8.2 mmol), TBTA (220 mg, 0.41 mmol), and NaI (2.6 g, 17.2 mmol) were suspended in dry THF (30 mL), followed by the addition of TEA (0.57 mL, 4.1 mmol). To this suspension, H-Epa-(*S*)-Lac-OMs **3** (1.1 g, 4.1 mmol) was added and the reaction

mixture was stirred for 20 min at 25 °C. A solution of TMS-Epa-(*R*)-Lac-N<sub>3</sub> **2** (1.4 g, 4.9 mmol) in dry THF (5 mL) was added and the resulting reaction mixture was stirred for 2 h at 25 °C. After adding water (100 mL) and a 1:1 (*v/v*) mixture of 25% aqueous NH<sub>3</sub> and 25% aqueous NH<sub>4</sub>Cl (10 mL), the mixture was extracted twice with ethyl acetate (2×100 mL). The combined organic layers were washed with water three times (3×50 mL) and dried over MgSO<sub>4</sub>. Pure product was obtained by column chromatography with hexane/ethyl acetate, 3:2 (*v/v*) as the eluent. Yield: 2.3 g (3.4 mmol, 82%); m.p. 105-107 °C;  $[\alpha]_D^{25} = -41.94$  ( $c = 0.1$ , acetone); <sup>1</sup>H NMR (400 MHz, 25 °C, DMSO-*d*<sub>6</sub>)  $\delta = 11.51$  (s, 1H, NH), 10.64 (s, 1H, NH), 8.08 (d, 1H, <sup>3</sup>*J*(H, H) = 8.3 Hz, EpaH(3)), 8.02 (d, 1H, <sup>3</sup>*J*(H, H) = 8.4 Hz, EpaH(3)), 7.96 (t, 1H, <sup>3</sup>*J*(H, H) = 8.0 Hz, EpaH(4)), 7.83 (t, 1H, <sup>3</sup>*J*(H, H) = 8.0 Hz, EpaH(4)), 7.71 (d, 1H, <sup>3</sup>*J*(H, H) = 7.5 Hz, EpaH(5)); 7.31 (dd, 1H, <sup>3</sup>*J*(H, H) = 7.5 Hz, <sup>4</sup>*J*(H, H) = 0.9 Hz, EpaH(5)), 5.58 (q, 1H, <sup>3</sup>*J*(H, H) = 7.0 Hz, LacCH), 5.40 (q, 1H, <sup>3</sup>*J*(H, H) = 6.6 Hz, LacCH), 3.26 (s, 3H, MsCH<sub>3</sub>), 1.97 (d, 3H, <sup>3</sup>*J*(H, H) = 7.0 Hz, LacCH<sub>3</sub>), 1.55 (d, 3H, <sup>3</sup>*J*(H, H) = 6.7 Hz, LacCH<sub>3</sub>), 0.25 (s, 9H, TMSCH<sub>3</sub>) ppm; <sup>13</sup>C NMR (100.6 MHz, 25 °C, DMSO-*d*<sub>6</sub>)  $\delta = 168.2$  (CO), 168.1 (CO), 151.7 (EpaC(2)), 150.7 (EpaC(2)), 148.4 (EpaC(6)), 147.7 (ITriC(4)), 140.1 (EpaC(6)), 139.4 (EpaC(4)), 139.3 (EpaC(4)), 123.0 (EpaC(5)), 118.3 (EpaC(5)), 113.9 (EpaC(3)), 113.3 (EpaC(3)), 103.5 (Si-C≡C), 94.1 (Si-C≡C), 84.4 (ITriC(5)); 75.2 (LacC), 60.3 (LacC), 38.2 (MsCH<sub>3</sub>), 18.8 (LacCH<sub>3</sub>), 17.1 (LacCH<sub>3</sub>), -0.4 (TMSCH<sub>3</sub>) ppm; MS (ESI) *m/z* (%): 586.0 (37) [M-CH<sub>3</sub>SO<sub>3</sub>H+H]<sup>+</sup>, 682.0 (4) [M+H]<sup>+</sup>, 704.0 (100) [M+Na]<sup>+</sup>, 720.0 (8) [M+K]<sup>+</sup>; elemental analysis calcd (%) for C<sub>24</sub>H<sub>28</sub>IN<sub>7</sub>O<sub>5</sub>SSi: C 42.29, N 14.39, H 4.14, S 4.70 found C 42.73, N 14.14, H 4.52, S 4.74.

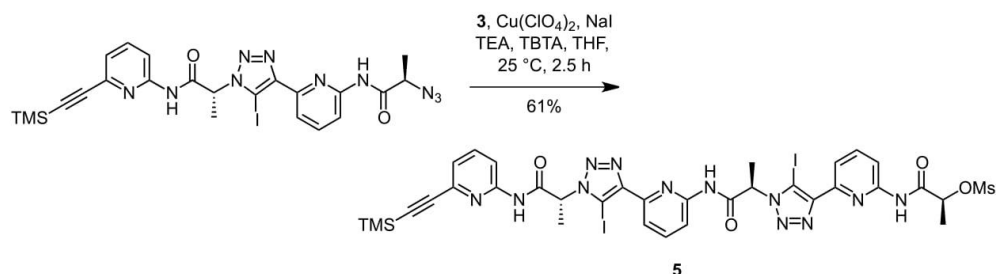
**TMS-Epa-(*R*)-Lac-1,4-ITri-Epa-(*R*)-Lac-N<sub>3</sub>.**



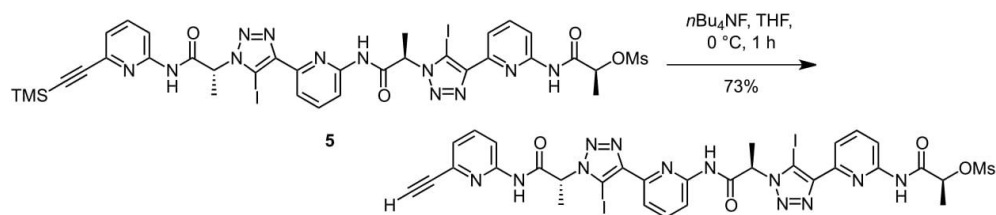
TMS-Epa-(*R*)-Lac-1,4-ITri-Epa-(*S*)-Lac-OMs **4** (2.2 g, 3.2 mmol) and sodium azide (416 mg, 6.4 mmol) were dissolved in DMF (25 mL). The mixture was stirred at 50 °C for 30 min. After adding water (100 mL), the mixture was extracted with three times with ethyl acetate (3×100 mL). The combined organic layers were dried over MgSO<sub>4</sub>. Pure product was obtained by column chromatography with hexane/ethyl acetate, 2:1 (*v/v*) as the eluent. Yield: 1.8 g (2.8 mmol, 89%); MS

(ESI)  $m/z$  (%): 525.2 (12)  $[M-I+H+Na]^+$ , 629.0 (18)  $[M+H]^+$ , 651.0 (100)  $[M+Na]^+$ .

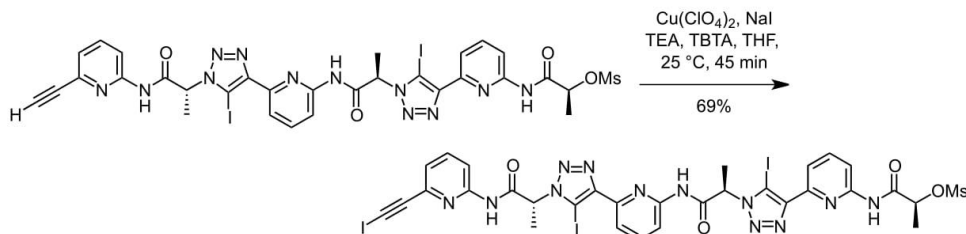
**TMS-Epa-[(*R*)-Lac-1,4-ITri-Epa]<sub>2</sub>-(*S*)-Lac-OMs 5.**



Thoroughly dried  $Cu(ClO_4)_2 \cdot 6H_2O$  (889 mg, 2.4 mmol), TBTA (64 mg, 0.12 mmol), and NaI (760 mg, 5.0 mmol) were suspended in dry THF (15 mL), followed by the addition of TEA (167  $\mu$ L, 1.20 mmol). To this suspension, H-Epa-(*S*)-Lac-OMs **3** (322 mg, 1.20 mmol) was added and the reaction mixture was stirred for 20 min at 25 °C. A solution of H-Epa-(*R*)-Lac-1,4-ITri-Epa-(*S*)-Lac-OMs **4** (534 mg, 0.85 mmol) in dry THF (10 mL) was added and the resulting reaction mixture was stirred for 2 h at 25 °C. After adding water (100 mL) and a 1:1 (*v/v*) mixture of 25% aqueous  $NH_3$  and 25% aqueous  $NH_4Cl$  (10 mL), the mixture was extracted twice with ethyl acetate ( $2 \times 100$  mL). The combined organic layers were washed with water three times ( $3 \times 50$  mL) and dried over  $MgSO_4$ . Pure product was precipitated from hexane/ethyl acetate, 1:1 (*v/v*) as a white powder. Yield: 530 mg (0.52 mmol, 61%);  $^1H$  NMR (400 MHz,  $DMSO-d_6$ )  $\delta$  = 11.51 (s, 1H, NH), 11.19 (s, 1H, NH), 10.63 (s, 1H, NH), 7.93-8.09 (m, 5H, EpaH(5) + EpaH(3)), 7.83 (t, 1H,  $^3J(H, H) = 8.0$  Hz, EpaH(4)), 7.70 (t, 2H,  $^3J(H, H) = 7.9$  Hz, EpaH(4)), 7.31 (dd, 1H,  $^3J(H, H) = 7.5$  Hz,  $^4J(H, H) = 0.7$  Hz, EpaH(5)), 5.73 (bs, 1H, LacCH), 5.59 (q, 1H,  $^3J(H, H) = 6.9$  Hz, LacCH), 5.38 (q, 1H,  $^3J(H, H) = 6.6$  Hz, LacCH), 3.25 (s, 3H, MsCH<sub>3</sub>), 2.00 (d, 3H,  $^3J(H, H) = 7.1$  Hz, LacCH<sub>3</sub>), 1.98 (d, 3H,  $^3J(H, H) = 7.0$  Hz, LacCH<sub>3</sub>), 1.54 (d, 3H,  $^3J(H, H) = 6.7$  Hz, LacCH<sub>3</sub>), 0.25 (s, 9H, TMSCH<sub>3</sub>) ppm; MS (ESI)  $m/z$  (%): 1023.0 (12)  $[M+H]^+$ , 1045.0 (100)  $[M+Na]^+$ , 1060.9 (28)  $[M+K]^+$ .

**H-Epa-[(R)-Lac-1,4-ITri-Epa]<sub>2</sub>-(S)-Lac-OMs.**

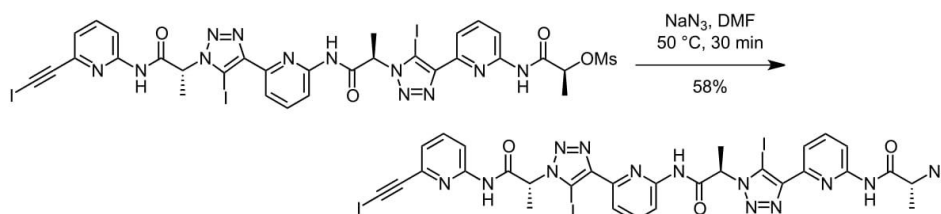
TMS-Epa-[(R)-Lac-1,4-ITri-Epa]<sub>2</sub>-(S)-Lac-OMs **5** (501 mg, 0.49 mmol) was dissolved in THF (30 mL) and the solution was cooled to 0 °C. A solution of TBAF (256 mg, 0.98 mmol) in THF (5 mL) was added dropwise. The reaction mixture was stirred for 1 h at 0 °C. Ethyl acetate (150 mL) and water (150 mL) were added, and the organic layer was separated. The aqueous layer was extracted four times with ethyl acetate (4×50 mL), and the combined organic layers were dried using MgSO<sub>4</sub>. The solvent was evaporated, and the residue precipitated from ethyl acetate. The product was obtained as a white powder. Yield: 340 mg (0.36 mmol, 73%); MS (ESI) *m/z* (%): 855.0 (9) [M-CH<sub>3</sub>SO<sub>3</sub>H+H]<sup>+</sup>, 950.9 (25) [M+H]<sup>+</sup>, 972.9 (100) [M+Na]<sup>+</sup>, 988.9 (5) [M+K]<sup>+</sup>.

**I-Epa-[(R)-Lac-1,4-ITri-Epa]<sub>2</sub>-(S)-Lac-OMs.**

Thoroughly dried Cu(ClO<sub>4</sub>)<sub>2</sub>·6H<sub>2</sub>O (252 mg, 0.68 mmol), TBTA (18 mg, 0.03 mmol), and NaI (207 mg, 1.36 mmol) were suspended in dry THF (5 mL), followed by the addition of TEA (47.0 μL, 0.34 mmol). H-Epa-[(R)-Lac-1,4-ITri-Epa]<sub>2</sub>-(S)-Lac-OMs (320 mg, 0.34 mmol) was immediately added, and the reaction mixture was stirred for 45 min under an inert atmosphere. After adding water (100 mL) and a 1:1 (v/v) mixture of 25% aqueous NH<sub>3</sub> and 25% aqueous NH<sub>4</sub>Cl (10 mL), the mixture was extracted twice with ethyl acetate (2×100 mL). The combined organic layers were washed with water three times (3×50) and dried over MgSO<sub>4</sub>. White product was precipitated from ethyl acetate. Yield: 210 mg (0.23 mmol, 69%); MS (ESI) *m/z* (%): 972.9 (17) [M-I+H+Na]<sup>+</sup>, 1076.8 (42) [M+H]<sup>+</sup>, 1098.8

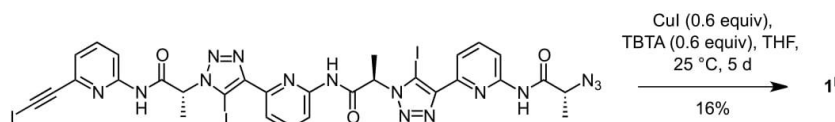
(100)  $[M+Na]^+$ , 1114.8 (15)  $[M+K]^+$ .

**I-Epa-[(R)-Lac-1,4-ITri-Epa]<sub>2</sub>-(R)-Lac-N<sub>3</sub>.**



I-Epa-[(R)-Lac-1,4-ITri-Epa]<sub>2</sub>-(S)-Lac-OMs (205 mg, 0.19 mmol) and sodium azide (25 mg, 0.38 mmol) were dissolved in DMF (10 mL). The mixture was stirred at 50 °C for 30 min. After adding water (100 mL), the mixture was extracted with three times ethyl acetate (3×100 mL). The combined organic layers were dried over MgSO<sub>4</sub>. Pure product was obtained by column chromatography with ethyl acetate as the eluent. Yield: 112 mg (0.11 mmol, 58%); MS (ESI)  $m/z$  (%): 920.0 (19)  $[M+H+Na]^+$ , 1045.9 (100)  $[M+Na]^+$ , 1061.8 (5)  $[M+K]^+$ .

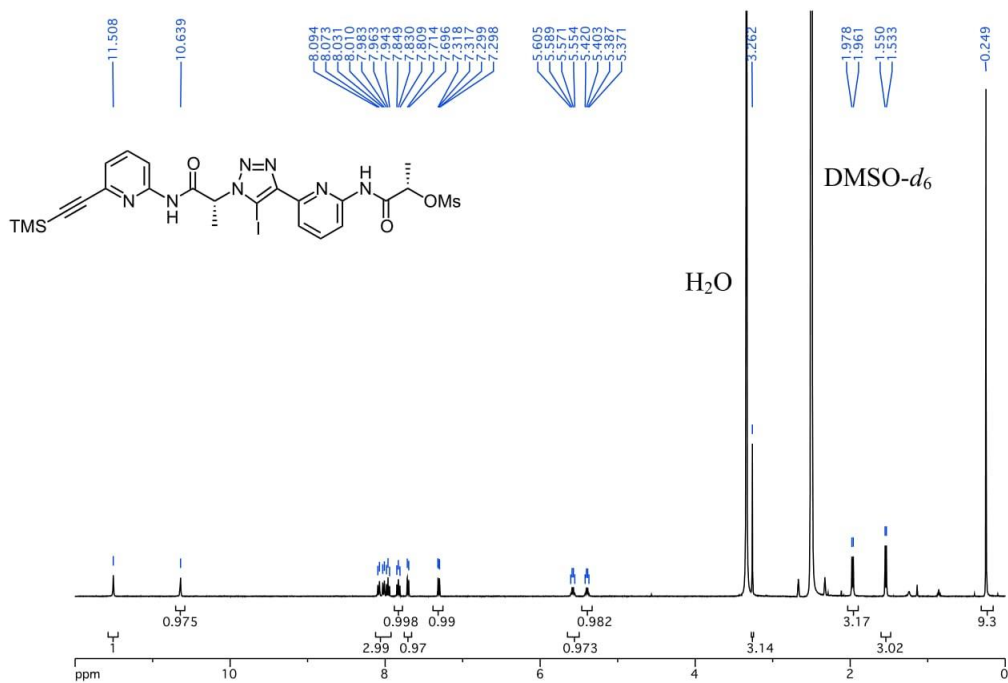
**cyclo[(R)-Lac-1,4-ITri-Epa]<sub>3</sub> 1<sup>1</sup>.**



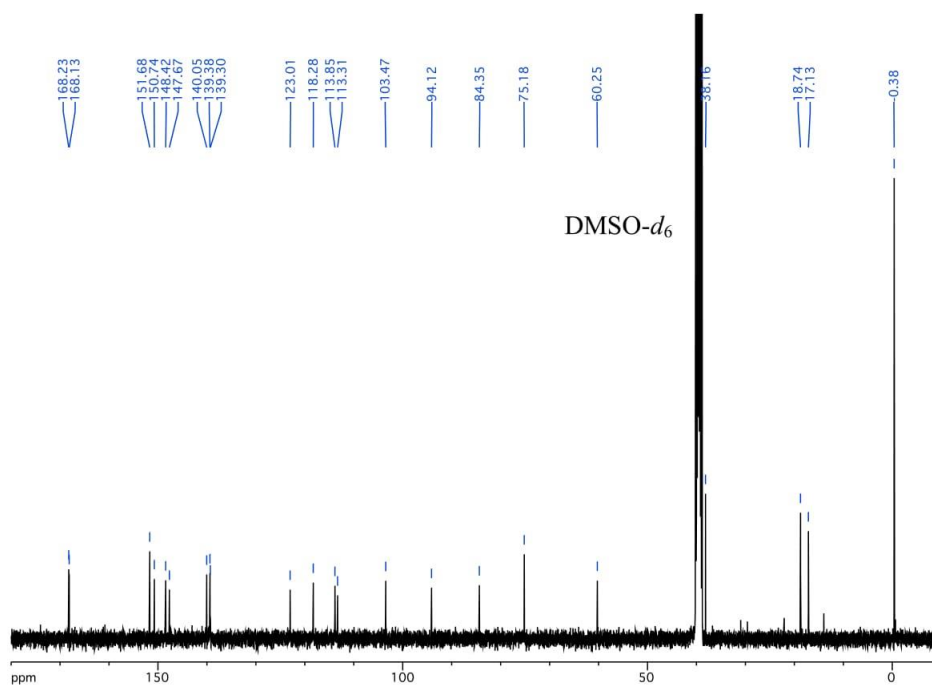
I-Epa-[(R)-Lac-1,4-ITri-Epa]<sub>2</sub>-(R)-Lac-N<sub>3</sub> (102 mg, 0.10 mmol), CuI (2 mg 10 μmol), and TBTA (5 mg, 10 μmol) were dissolved in dry THF (360 mL). The reaction mixture was stirred at 25 °C and its progress was followed by HPLC. Additional CuI (2 mg 10 μmol) and TBTA (5 mg 10 μmol) were added every 24 h until HPLC indicated full conversion, typically after 5 d. Isolation and purification of the cyclic product was achieved by, first, removing the solid materials from the reaction mixture by centrifugation. After adding water (50 mL) and a 1:1 (v/v) mixture of 25% aqueous NH<sub>3</sub> and 25% aqueous NH<sub>4</sub>Cl (10 mL), the mixture was extracted three times with ethyl acetate (1×400 mL, 2×100 mL). The combined organic layers were washed with water three times (3×25 mL). The solvent was removed to afford yellowish solid. This crude product was washed with dichloromethane (3×30 mL), followed by acetone/water, 1:1 (v/v) (3×10 mL), and finally THF (5×45 mL) to obtain the product in analytically pure form after drying. Yield: 16 mg (16 μmol, 16%); m.p. > 200 °C (dec);  $[\alpha]_D^{25} =$

-23.7 ( $c = 0.1$ , DMSO);  $^1\text{H}$  NMR (400 MHz, DMSO- $d_6$ )  $\delta = 10.21$  (s, 3H, NH), 7.90 (t, 3H,  $^3J(\text{H}, \text{H}) = 7.8$  Hz, EpaH(4)), 7.85 (d, 3H,  $^3J(\text{H}, \text{H}) = 8.1$  Hz, EpaH(5)), 7.70 (d, 3H,  $^3J(\text{H}, \text{H}) = 7.9$  Hz, EpaH(3)), 5.86 (q, 3H,  $^3J(\text{H}, \text{H}) = 6.5$  Hz, LacCH), 1.99 (d, 9H,  $^3J(\text{H}, \text{H}) = 6.7$  Hz, LacCH<sub>3</sub>) ppm;  $^{13}\text{C}$  NMR (100.6 MHz, DMSO- $d_6$ )  $\delta = 166.6$  (CO), 149.2 (EpaC(2)), 148.3 (EpaC(6)), 145.4 (ITriC(4)) 139.3 (EpaC(4)), 117.2 (EpaC(5)), 115.1 (EpaC(3)), 83.5 (ITriC(5)), 59.4 (LacC), 16.1 (LacCH<sub>3</sub>) ppm; MS (ESI)  $m/z$  (%): 1023.8 (16)  $[\text{M}+\text{H}]^+$ , 1045.8 (100)  $[\text{M}+\text{Na}]^+$ , 1061.8 (5)  $[\text{M}+\text{K}]^+$ ; elemental analysis calcd (%) for C<sub>30</sub>H<sub>24</sub>I<sub>3</sub>N<sub>15</sub>O<sub>3</sub>: C 35.21, N 20.53, H 2.36 found C 35.32, N 20.09, H 2.45.

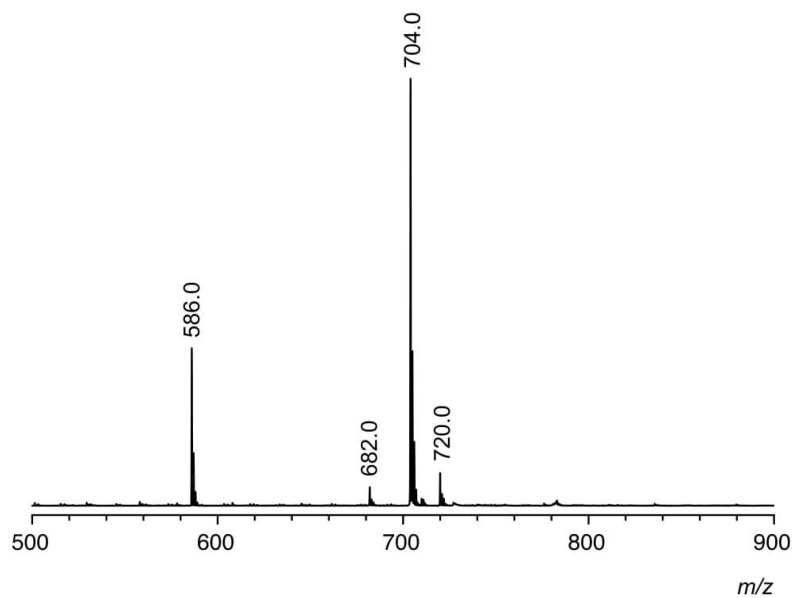
$^1\text{H}$  NMR: TMS-Epa-(*R*)-Lac-1,4-ITri-Epa-(*S*)-Lac-OMs **4** (400 MHz,  $\text{DMSO-}d_6$ , 25 °C).



$^{13}\text{C}$  NMR: TMS-Epa-(*R*)-Lac-1,4-ITri-Epa-(*S*)-Lac-OMs **4** (100.6 MHz,  $\text{DMSO-}d_6$ , 25 °C).

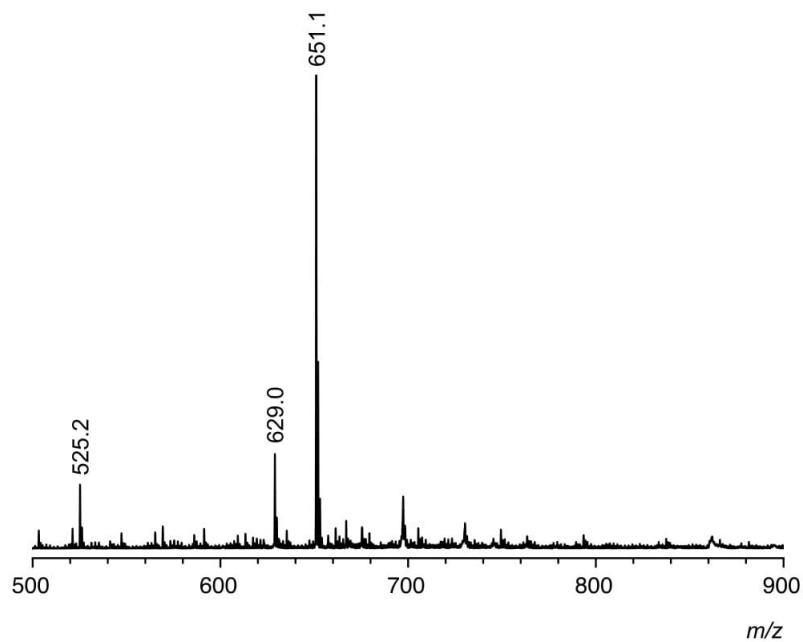


ESI-TOF MS: TMS-Epa-(*R*)-Lac-1,4-ITri-Epa-(*S*)-Lac-OMs **4** (positive mode).



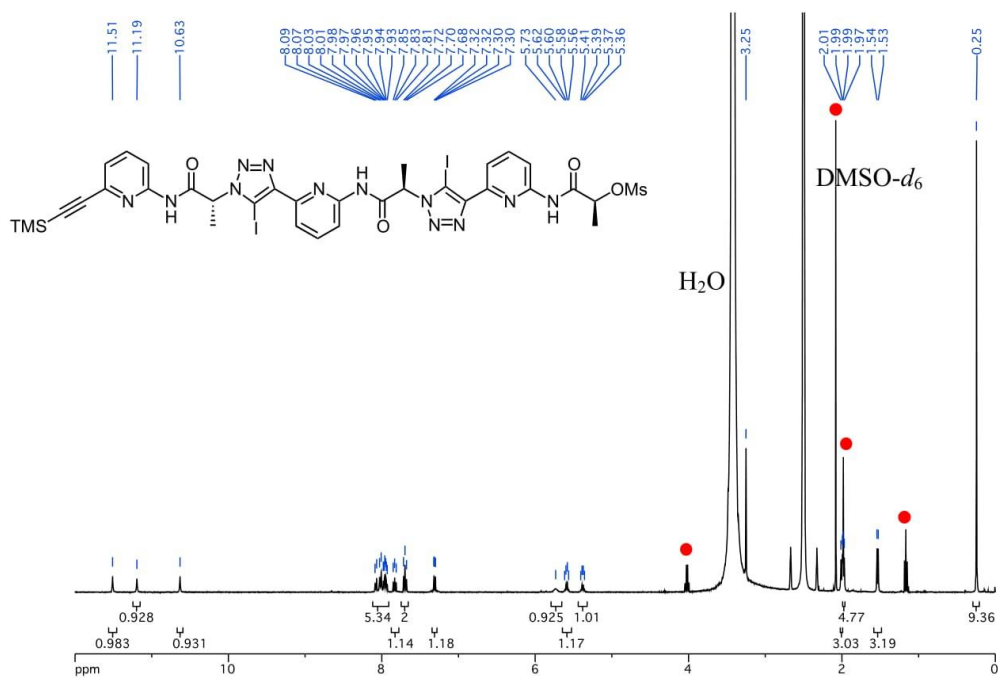
		<i>m/z</i> calcd.	<i>m/z</i> exp.
$[M-CH_3SO_3H+H]^+$	$C_{23}H_{24}IN_7O_2Si + H^+$	586.1	586.0
$[M+H]^+$	$C_{24}H_{28}IN_7O_5SSi + H^+$	682.1	682.0
$[M+Na]^+$	$C_{24}H_{28}IN_7O_5SSi + Na^+$	704.1	704.0
$[M+K]^+$	$C_{24}H_{28}IN_7O_5SSi + K^+$	720.0	720.0

ESI-TOF MS: TMS-Epa-(R)-Lac-1,4-I-Tri-Epa-(R)-Lac-N<sub>3</sub> (positive mode).



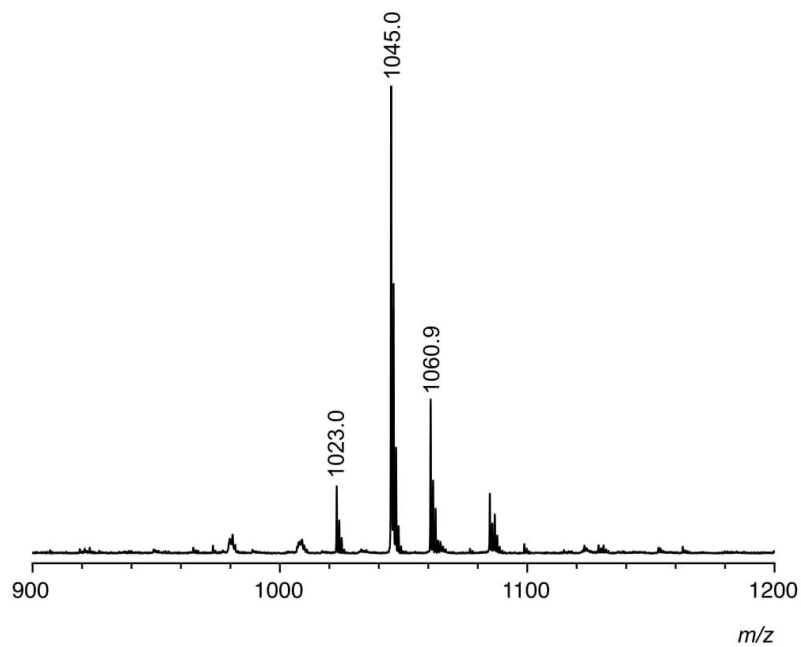
		<i>m/z calcd.</i>	<i>m/z exp.</i>
$[M-I+H+Na]^+$	$C_{23}H_{26}N_{10}O_2Si + Na^+$	525.2	525.2
$[M+H]^+$	$C_{23}H_{25}IN_{10}O_2Si + H^+$	629.1	629.0
$[M+Na]^+$	$C_{23}H_{25}IN_{10}O_2Si + Na^+$	651.1	651.0

$^1\text{H NMR}$ : TMS-Epa-[(*R*)-Lac-1,4-ITri-Epa]<sub>2</sub>-(*S*)-Lac-OMs **5** (400 MHz,  $\text{DMSO-}d_6$ , 25 °C).



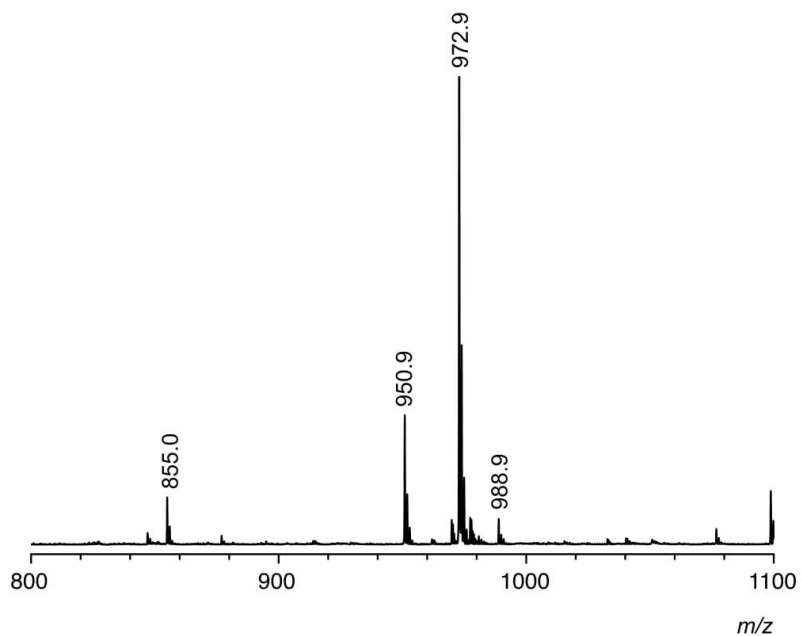
Signals of impurities (ethyl acetate, acetone) are marked with red dots.

ESI-TOF MS: TMS-Epa-[(*R*)-Lac-1,4-I<sub>2</sub>Tri-Epa]<sub>2</sub>-(*S*)-Lac-OMs **5** (positive mode).



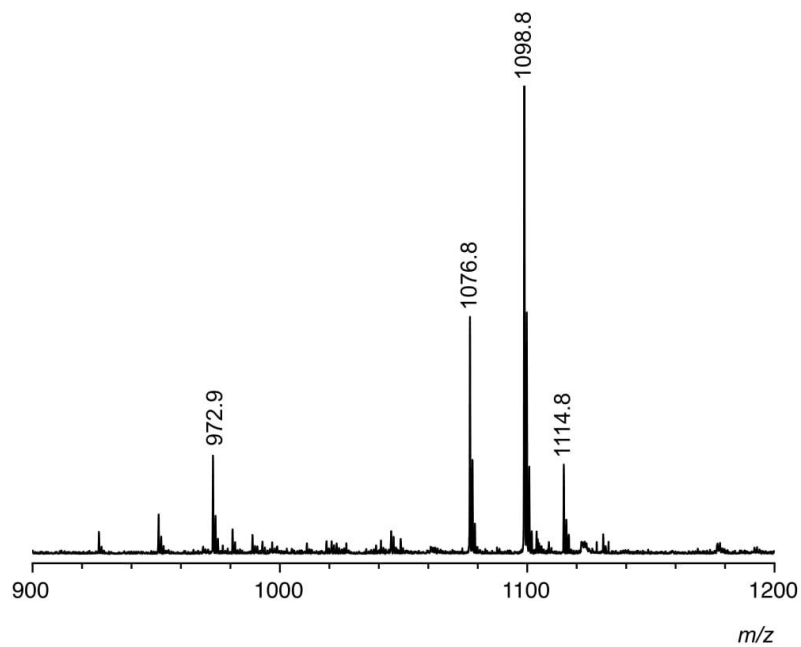
		<i>m/z</i> calcd.	<i>m/z</i> exp.
[M+H] <sup>+</sup>	C <sub>34</sub> H <sub>36</sub> I <sub>2</sub> N <sub>12</sub> O <sub>6</sub> SSi + H <sup>+</sup>	1023.1	1023.0
[M+Na] <sup>+</sup>	C <sub>34</sub> H <sub>36</sub> I <sub>2</sub> N <sub>12</sub> O <sub>6</sub> SSi + Na <sup>+</sup>	1045.0	1045.0
[M+K] <sup>+</sup>	C <sub>34</sub> H <sub>36</sub> I <sub>2</sub> N <sub>12</sub> O <sub>6</sub> SSi + K <sup>+</sup>	1061.0	1060.9

ESI-TOF MS: H-Epa-[(*R*)-Lac-1,4-I-Tri-Epa]<sub>2</sub>-(*S*)-Lac-OMs (positive mode).



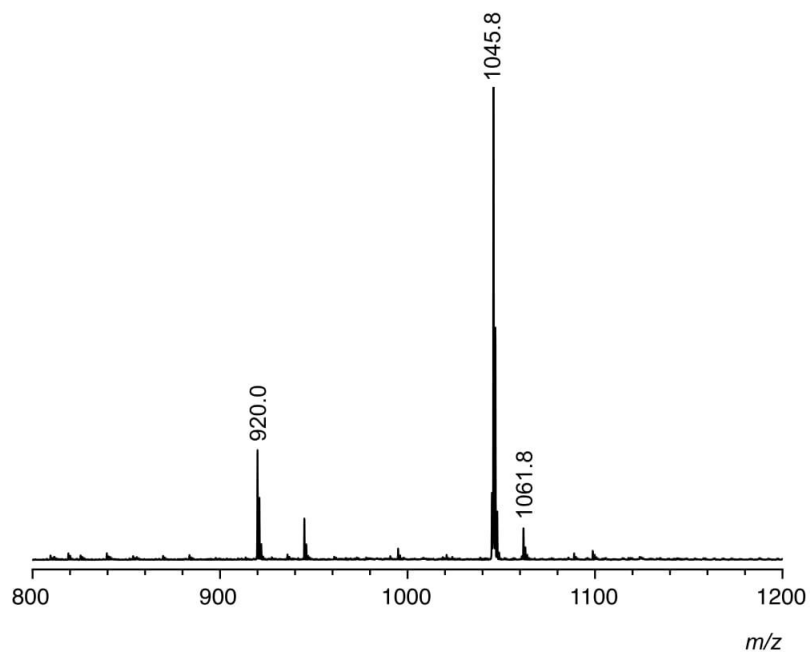
		<i>m/z calcd.</i>	<i>m/z exp.</i>
$[M-CH_3SO_3H+H]^+$	$C_{30}H_{24}I_2N_{12}O_3 + H^+$	855.0	855.0
$[M+H]^+$	$C_{31}H_{28}I_2N_{12}O_6S + H^+$	951.0	950.9
$[M+Na]^+$	$C_{31}H_{28}I_2N_{12}O_6S + Na^+$	973.0	972.9
$[M+K]^+$	$C_{31}H_{28}I_2N_{12}O_6S + K^+$	989.0	988.9

ESI-TOF MS: I-Epa-[(R)-Lac-1,4-ITri-Epa]<sub>2</sub>-(S)-Lac-OMs (positive mode).



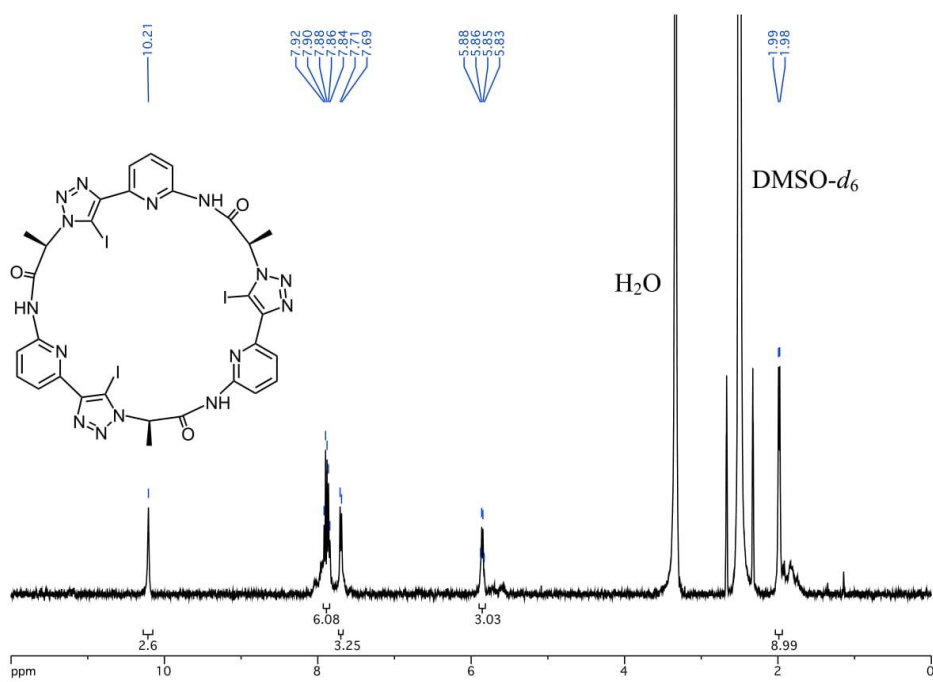
		<i>m/z calcd.</i>	<i>m/z exp.</i>
[M-I+H+Na] <sup>+</sup>	C <sub>30</sub> H <sub>24</sub> I <sub>2</sub> N <sub>12</sub> O <sub>3</sub> + Na <sup>+</sup>	973.0	972.9
[M+H] <sup>+</sup>	C <sub>31</sub> H <sub>27</sub> I <sub>3</sub> N <sub>12</sub> O <sub>6</sub> S + H <sup>+</sup>	1076.9	1076.8
[M+Na] <sup>+</sup>	C <sub>31</sub> H <sub>27</sub> I <sub>3</sub> N <sub>12</sub> O <sub>6</sub> S + Na <sup>+</sup>	1098.9	1098.8
[M+K] <sup>+</sup>	C <sub>31</sub> H <sub>27</sub> I <sub>3</sub> N <sub>12</sub> O <sub>6</sub> S + K <sup>+</sup>	1114.9	1114.8

ESI-TOF MS: I-Epa-[(R)-Lac-1,4-I-Tri-Epa]<sub>2</sub>-(R)-Lac-N<sub>3</sub> (positive mode).

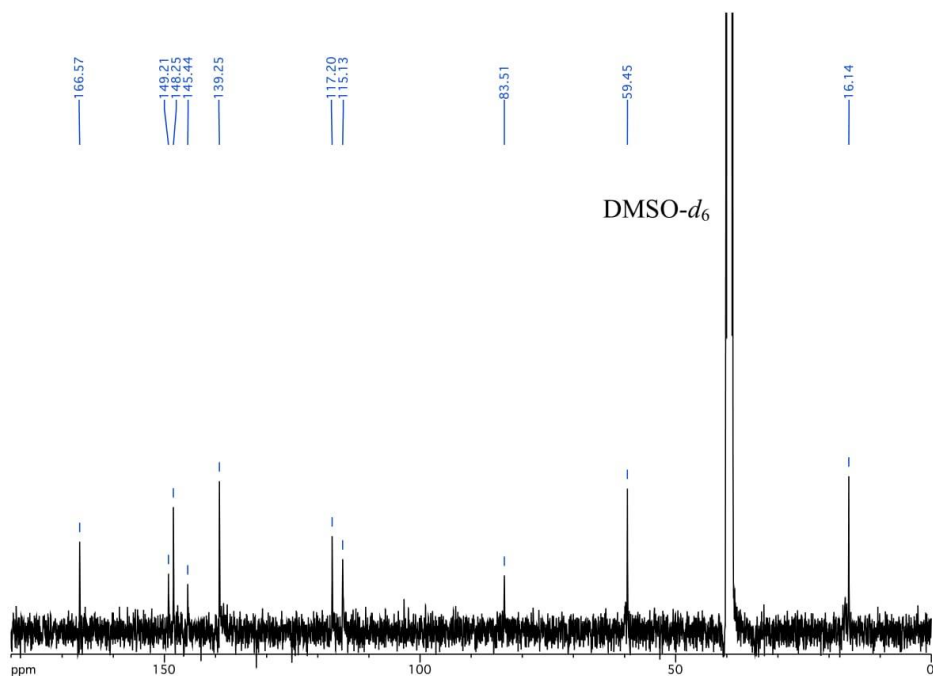


		<i>m/z calcd.</i>	<i>m/z exp.</i>
$[M-I+H+Na]^+$	$C_{30}H_{25}I_2N_{15}O_3 + Na^+$	920.0	920.0
$[M+Na]^+$	$C_{30}H_{24}I_3N_{15}O_3 + Na^+$	1045.9	1045.8
$[M+K]^+$	$C_{30}H_{24}I_3N_{15}O_3 + K^+$	1061.9	1061.8

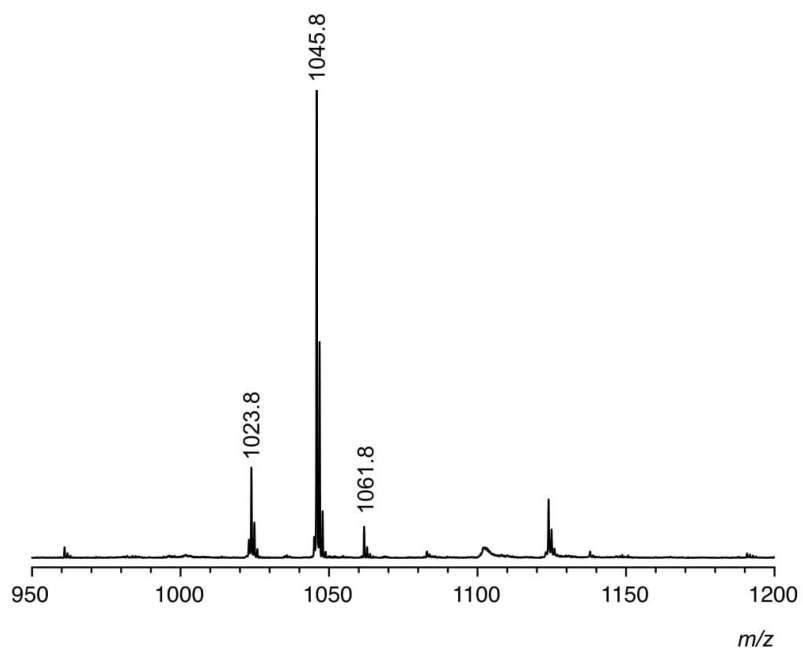
$^1\text{H}$  NMR: *cyclo*[(*R*)-Lac-1,4-ITri-Epa]<sub>3</sub> **1**<sup>I</sup> (400 MHz, DMSO-*d*<sub>6</sub>, 25 °C).



$^{13}\text{C}$  NMR: *cyclo*[(*R*)-Lac-1,4-ITri-Epa]<sub>3</sub> **1**<sup>I</sup> (100.6 MHz, DMSO-*d*<sub>6</sub>, 25 °C).

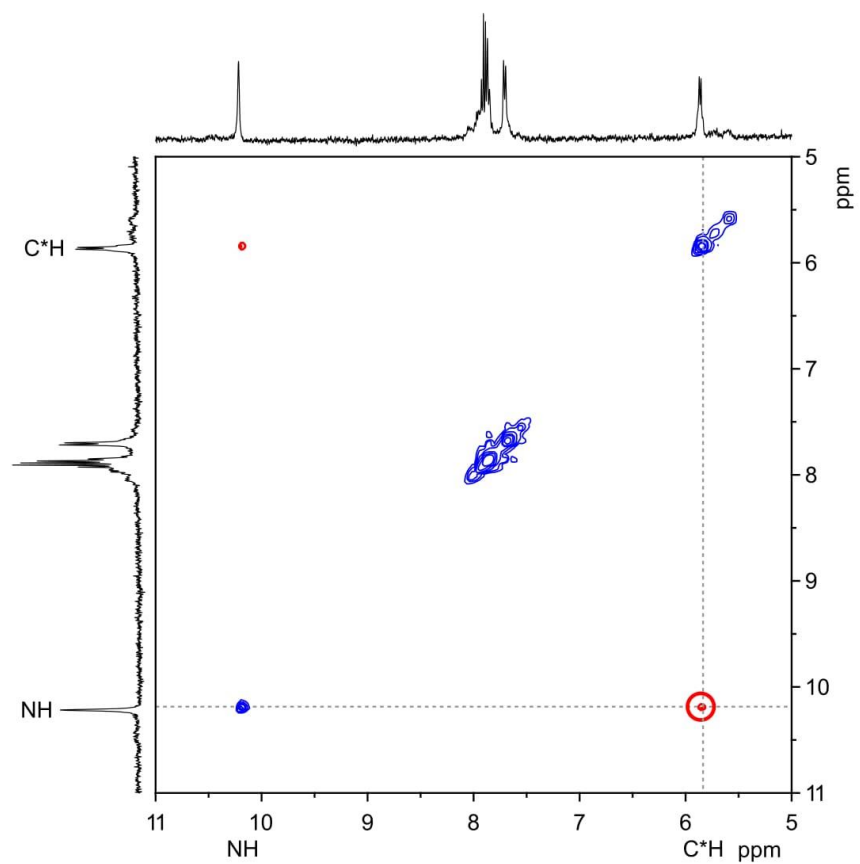


ESI-TOF MS: *cyclo*[(*R*)-Lac-1,4-ITri-Epa]<sub>3</sub> 1<sup>I</sup> (positive mode).



		<i>m/z calcd.</i>	<i>m/z exp.</i>
[M+H] <sup>+</sup>	C <sub>30</sub> H <sub>24</sub> I <sub>3</sub> N <sub>15</sub> O <sub>3</sub> + H <sup>+</sup>	1023.9	1023.8
[M+Na] <sup>+</sup>	C <sub>30</sub> H <sub>24</sub> I <sub>3</sub> N <sub>15</sub> O <sub>3</sub> + Na <sup>+</sup>	1045.9	1045.8
[M+K] <sup>+</sup>	C <sub>30</sub> H <sub>24</sub> I <sub>3</sub> N <sub>15</sub> O <sub>3</sub> + K <sup>+</sup>	1061.9	1061.8

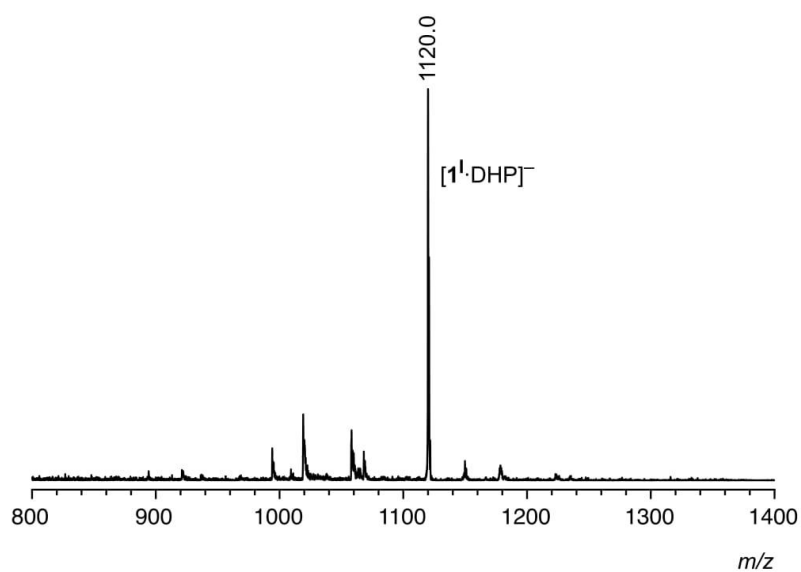
ROESY NMR Spectrum: **1**<sup>1</sup> (0.5 mM) in DMSO-*d*<sub>6</sub> (mixing time 300 ms) (400 MHz, 25 °C).



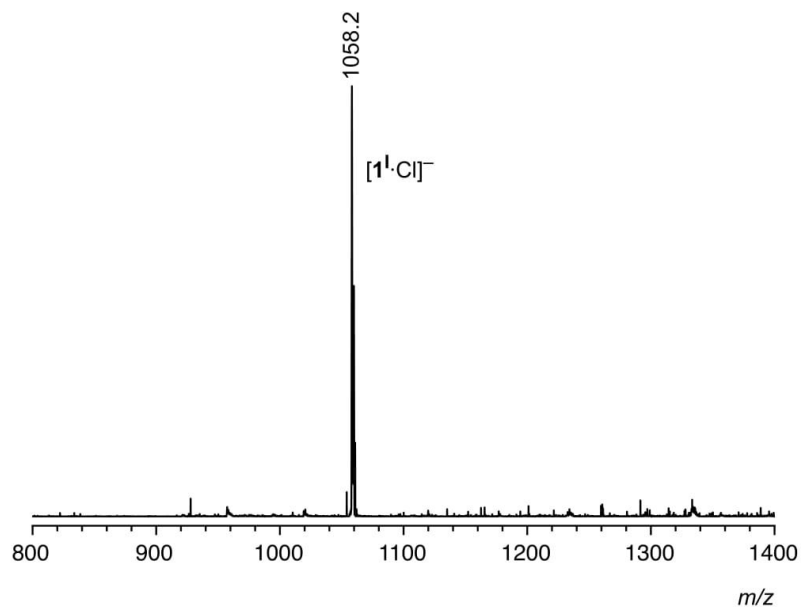
## ESI-MS Measurements:

		<i>m/z calcd.</i>
$[\mathbf{1}^{\mathbf{I}}+\text{Cl}]^{-}$	$\text{C}_{30}\text{H}_{24}\text{I}_3\text{N}_{15}\text{O}_3 + \text{Cl}^{-}$	1057.9
$[\mathbf{1}^{\mathbf{I}}+\text{DHP}]^{-}$	$\text{C}_{30}\text{H}_{24}\text{I}_3\text{N}_{15}\text{O}_3 + \text{H}_2\text{PO}_4^{-}$	1119.9
$[\mathbf{1}^{\mathbf{I}}+\text{TBA}+\text{SO}_4]^{-}$	$\text{C}_{30}\text{H}_{24}\text{I}_3\text{N}_{15}\text{O}_3 + \text{C}_{16}\text{H}_{36}\text{N}^{+} + \text{SO}_4^{2-}$	1361.2

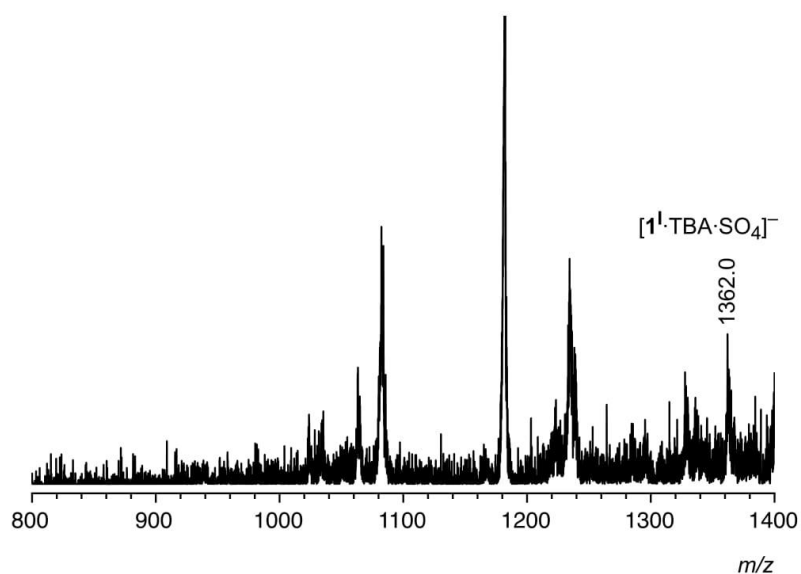
ESI MS:  $\mathbf{1}^{\mathbf{I}}$  (1 mM) in DMSO/acetonitrile, 1:1 (v/v) in the presence of 1 equiv of TBA DHP.



ESI MS: **1**<sup>1</sup> (1 mM) in DMSO/acetonitrile, 1:1 (v/v) in the presence of each 1 equiv of TBA DHP and TBA chloride.

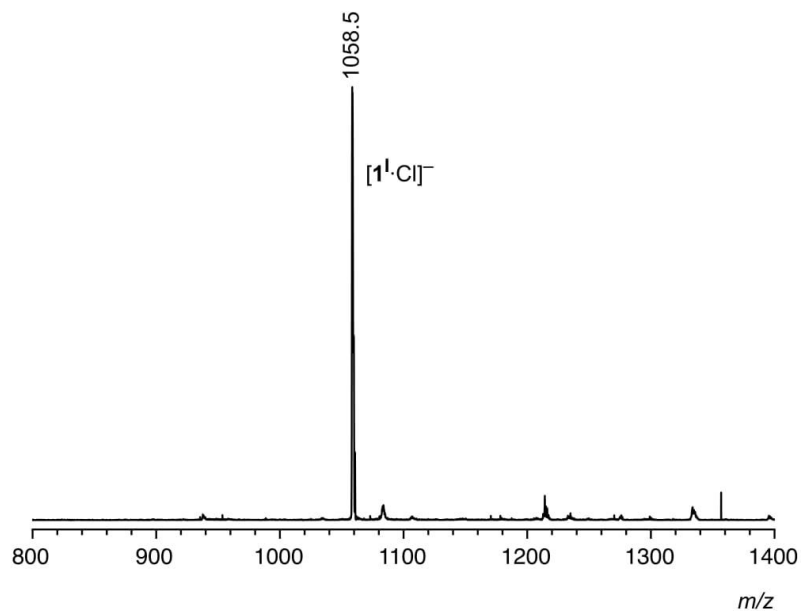


ESI MS: **1**<sup>1</sup> (1 mM) in DMSO/acetonitrile, 1:1 (v/v) in the presence of 1 equiv of TBA sulfate.

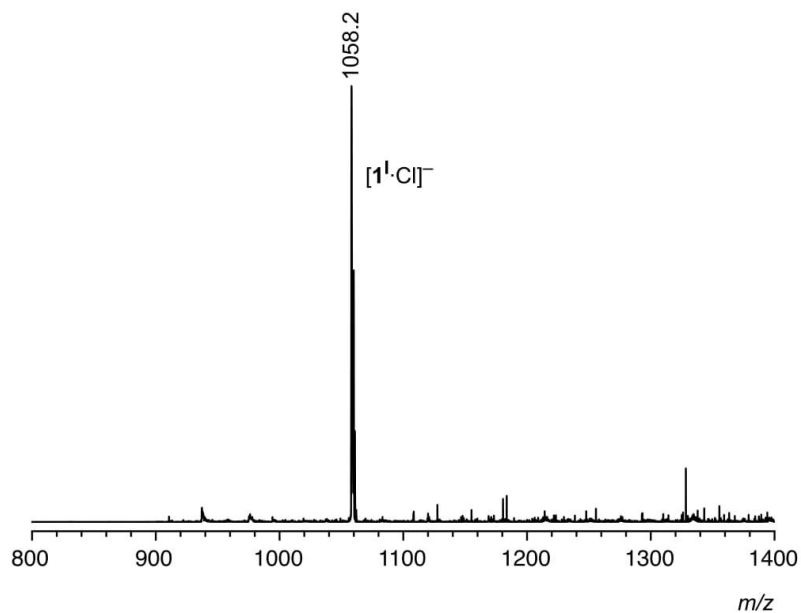


That only a very small peak is visible attributable to the sulfate complex of **1**<sup>1</sup> indicates that the pseudopeptide is not able to stabilize the sulfate anion in the gas phase.

ESI MS: **1**<sup>1</sup> (1 mM) in DMSO/acetonitrile, 1:1 (v/v) in the presence of 1 equiv of each TBA sulfate and TBA chloride.



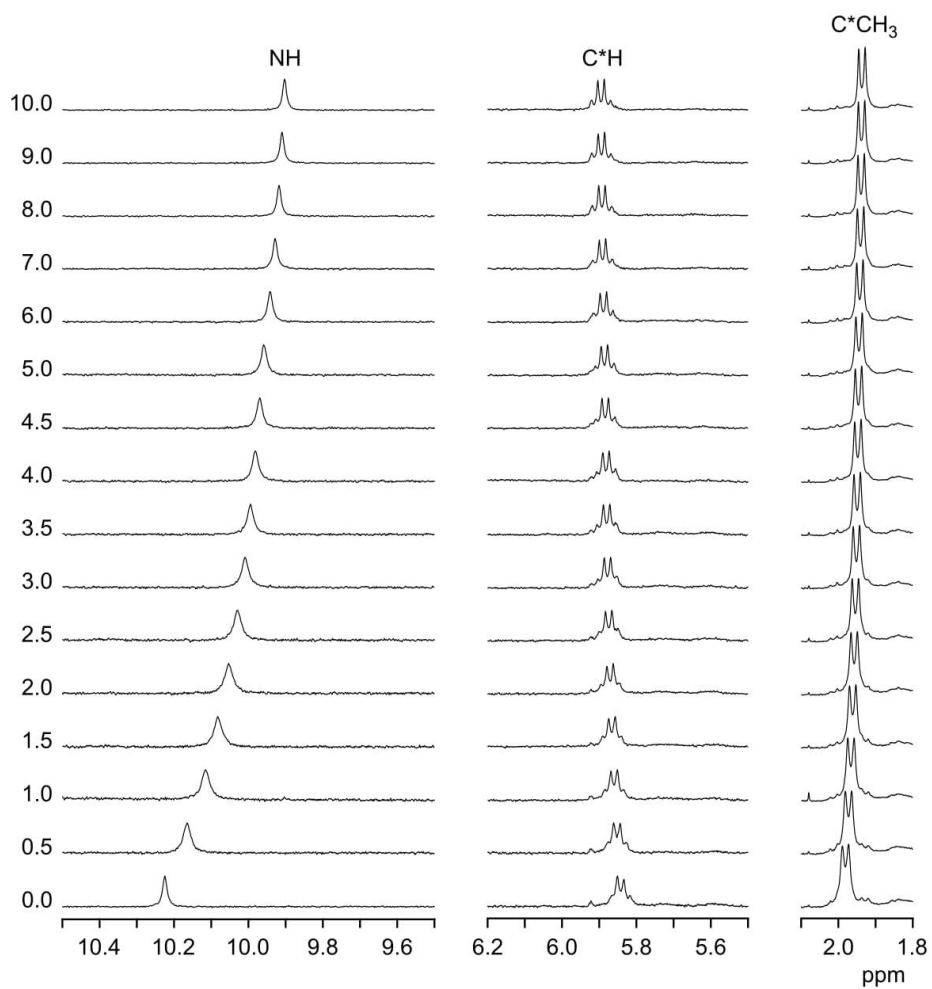
ESI MS: **1**<sup>1</sup> (1 mM) in DMSO/acetonitrile, 1:1 (v/v) in the presence of 1 equiv of each TBA DHP, TBA sulfate, and TBA chloride.



NMR Titration:

Stock solutions of **I**<sup>1</sup> (0.5 mM), TBA chloride (5 mM), TMA chloride (5 mM), TBA bromide (5 mM), TBA iodide (5 mM), TBA sulfate (5 mM), and TBA DHP (5 mM) were prepared separately in 2.5 vol% H<sub>2</sub>O/DMSO-*d*<sub>6</sub>. Increasing amounts (0 to 300 μL) of the salt stock solution were added to 16 NMR tubes (13 NMR tubes in the case of TBA sulfate, 10 NMR tubes in the case of TMA chloride, and 11 NMR tubes in the case of TBA DHP), each containing 300 μL of the receptor stock solution. The total volume in each tube was made up to 600 μL with 2.5 vol% H<sub>2</sub>O/DMSO-*d*<sub>6</sub>. All tubes were thoroughly shaken and the <sup>1</sup>H NMR spectra were recorded (256 scans, 400 MHz). Stability constants of the anion-receptor complexes were calculated by following the shifts of the NH, C\*H and C\*CH<sub>3</sub> signals and using HypNMR2008 for global fitting.<sup>3</sup>

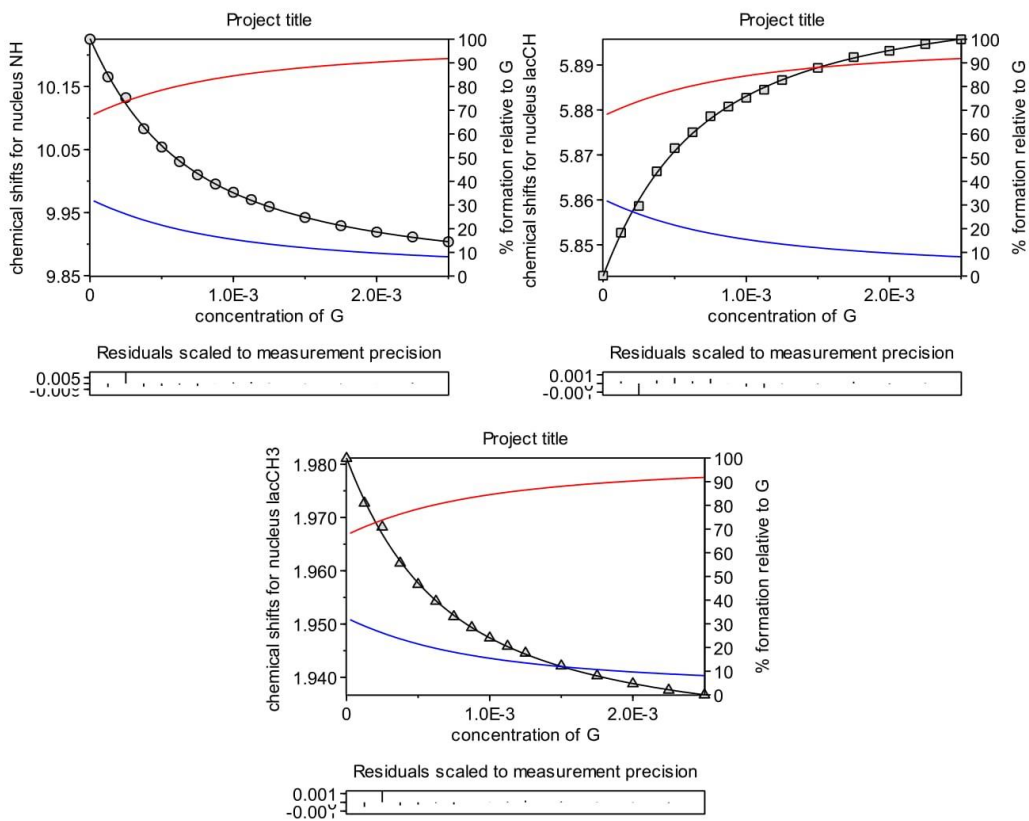
$^1\text{H}$  NMR spectra of **1**<sup>I</sup> (0.25 mM) in 2.5 vol%  $\text{H}_2\text{O}/\text{DMSO-}d_6$  (400 MHz) containing the increasing equivalents of TBA chloride specified to the left of each spectrum.



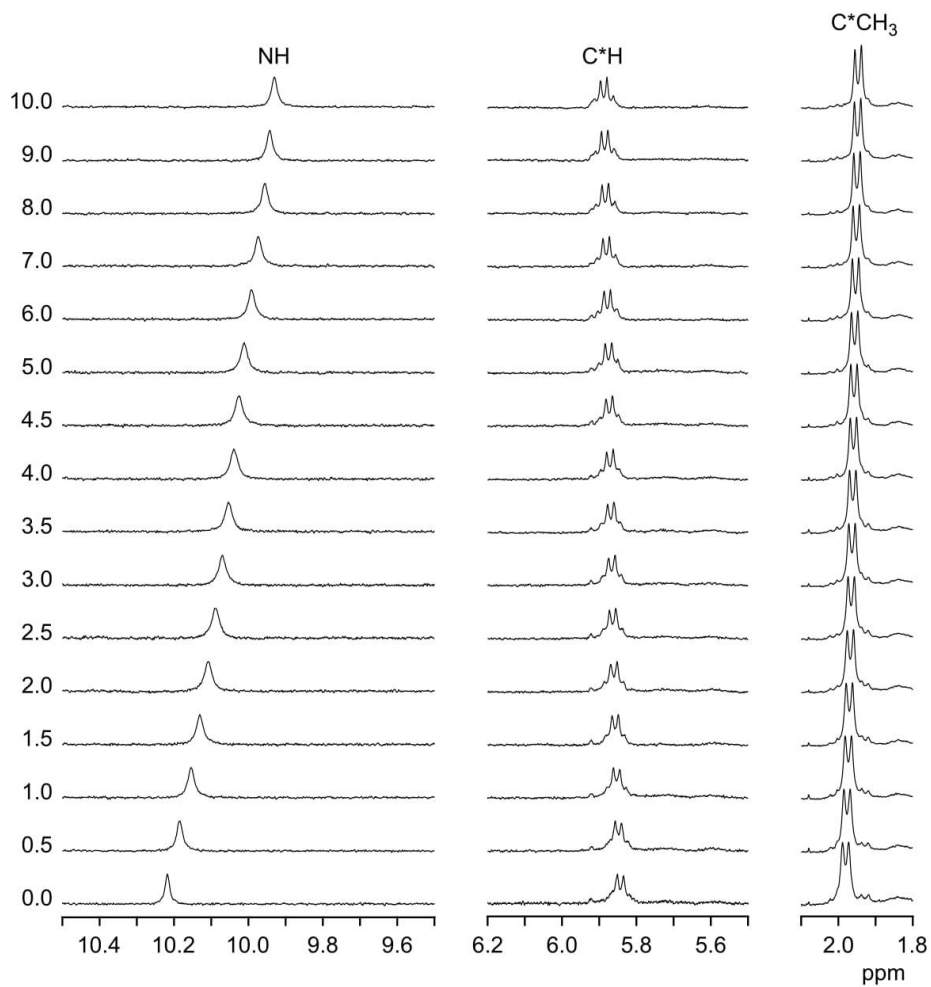
Binding isotherms and HypNMR outputs

Converged in 1 iterations with sigma = 0.001783

	value	standard deviation	Comments
1 log beta(GH)	3.2838	0.0104	3.28(1)



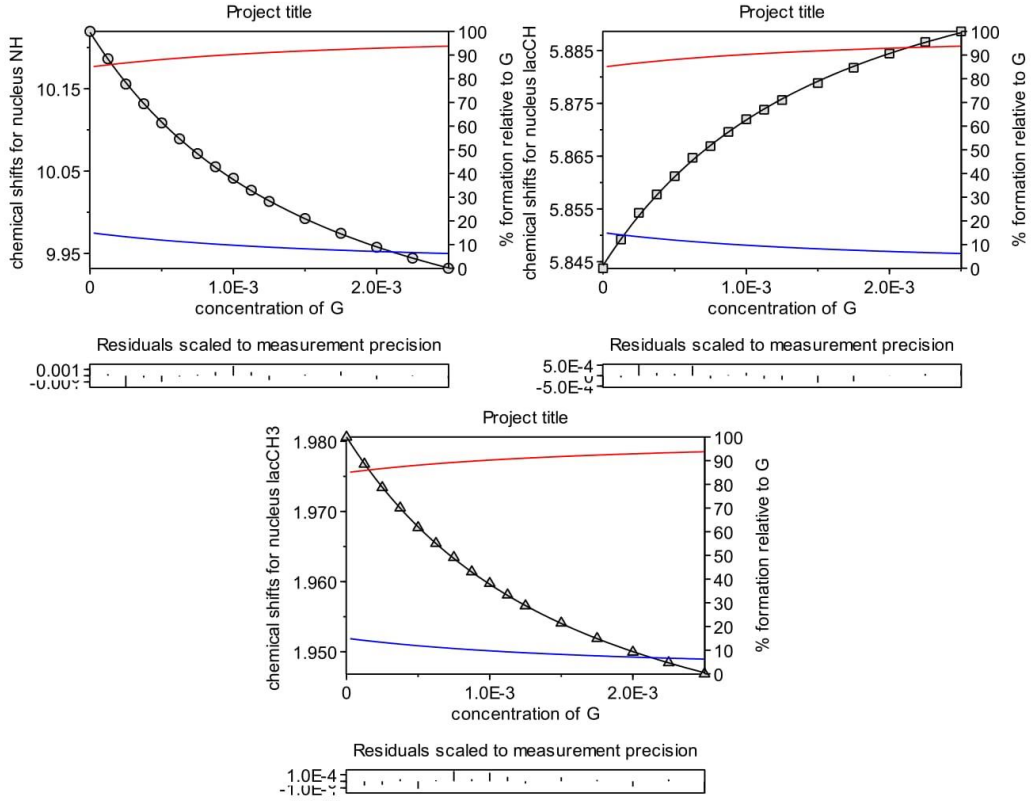
$^1\text{H}$  NMR spectra of **1**<sup>I</sup> (0.25 mM) in 2.5 vol%  $\text{H}_2\text{O}/\text{DMSO-}d_6$  (400 MHz) containing the increasing equivalents of TBA bromide specified to the left of each spectrum.



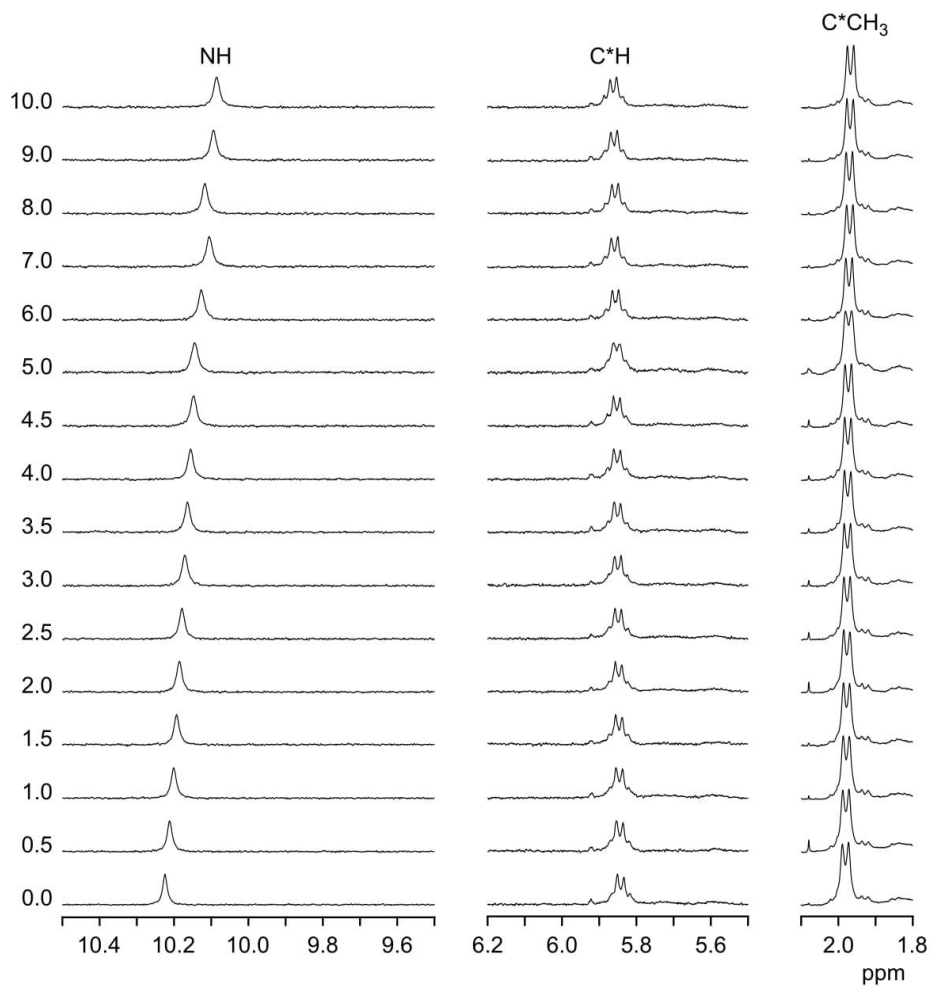
Binding isotherms and HypNMR outputs

Converged in 4 iterations with sigma = 0.000534

	value	standard deviation	Comments
1 log beta (GH)	2.8506	0.0043	2.851 (4)



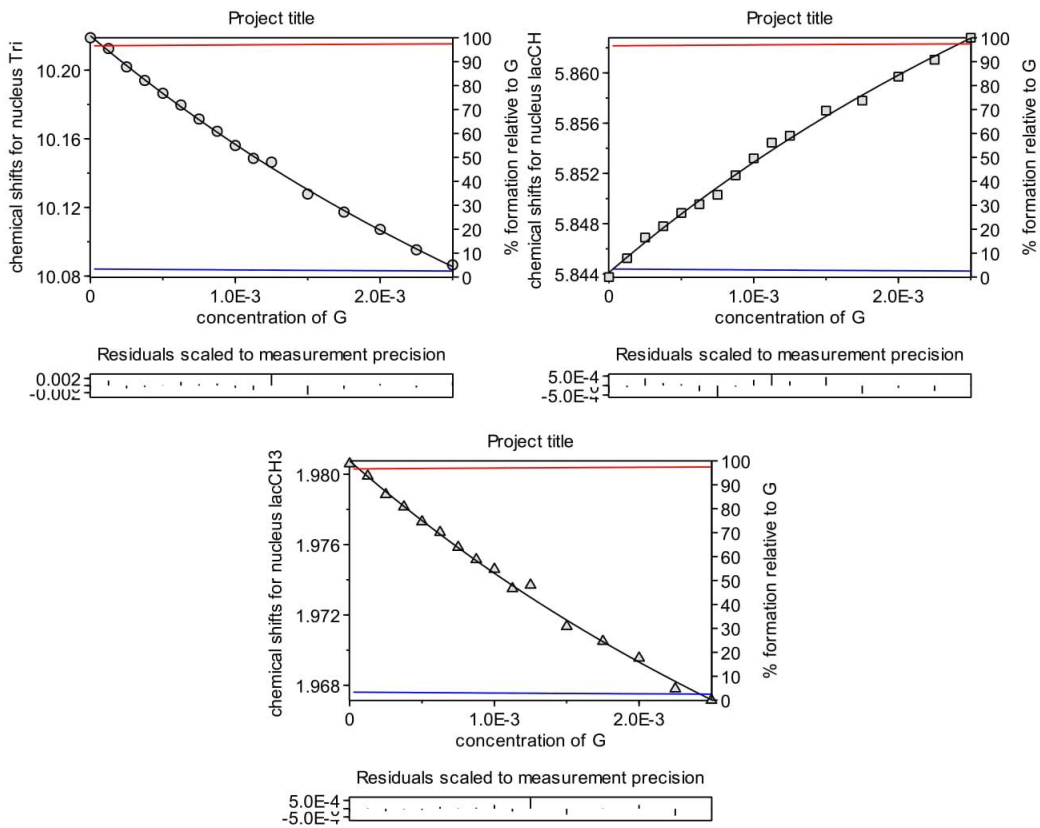
$^1\text{H}$  NMR spectra of **1**<sup>I</sup> (0.25 mM) in 2.5 vol%  $\text{H}_2\text{O}/\text{DMSO-}d_6$  (400 MHz) containing the increasing equivalents of TBA iodide specified to the left of each spectrum.



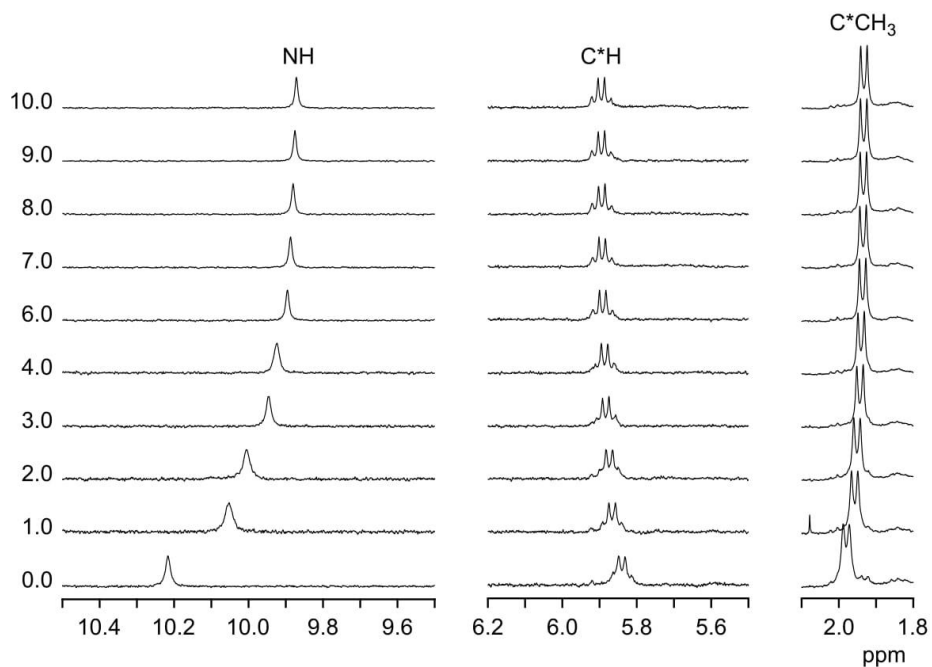
Binding isotherms and HypNMR outputs

Converged in 4 iterations with sigma = 0.000849

	value	standard deviation	Comments
1 log beta (GH)	2.1477	0.0335	2.15 (3)



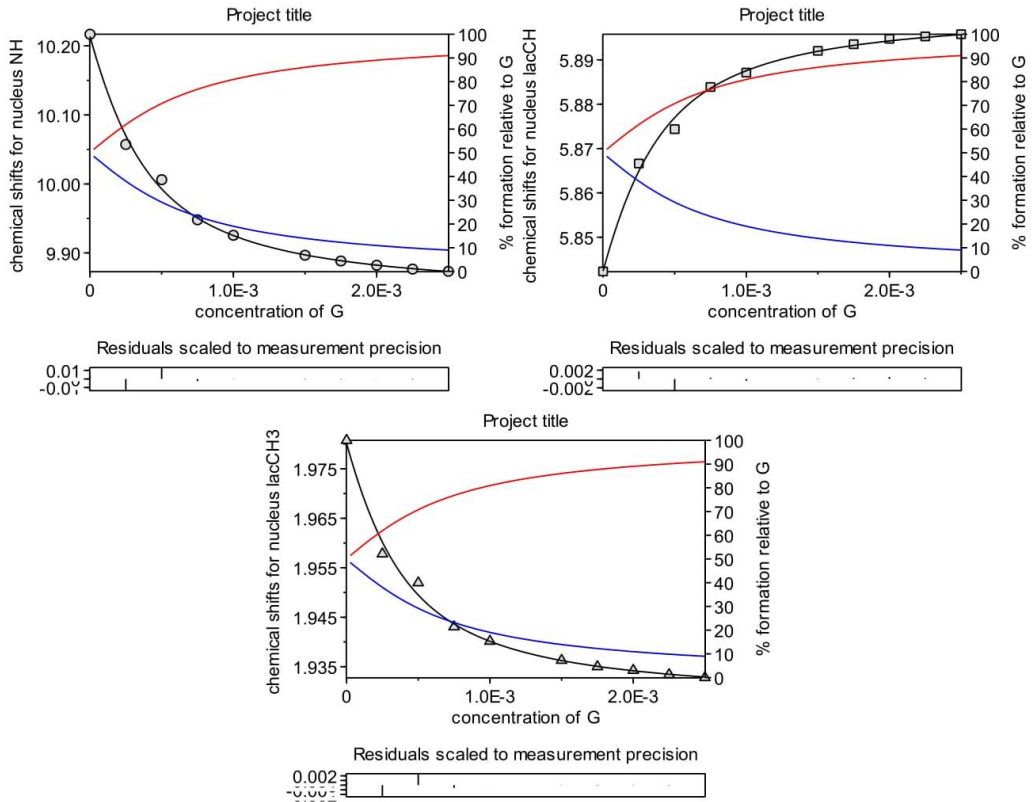
$^1\text{H}$  NMR spectra of **1**<sup>I</sup> (0.25 mM) in 2.5 vol%  $\text{H}_2\text{O}/\text{DMSO-}d_6$  (400 MHz) containing the increasing equivalents of TMA chloride specified to the left of each spectrum.



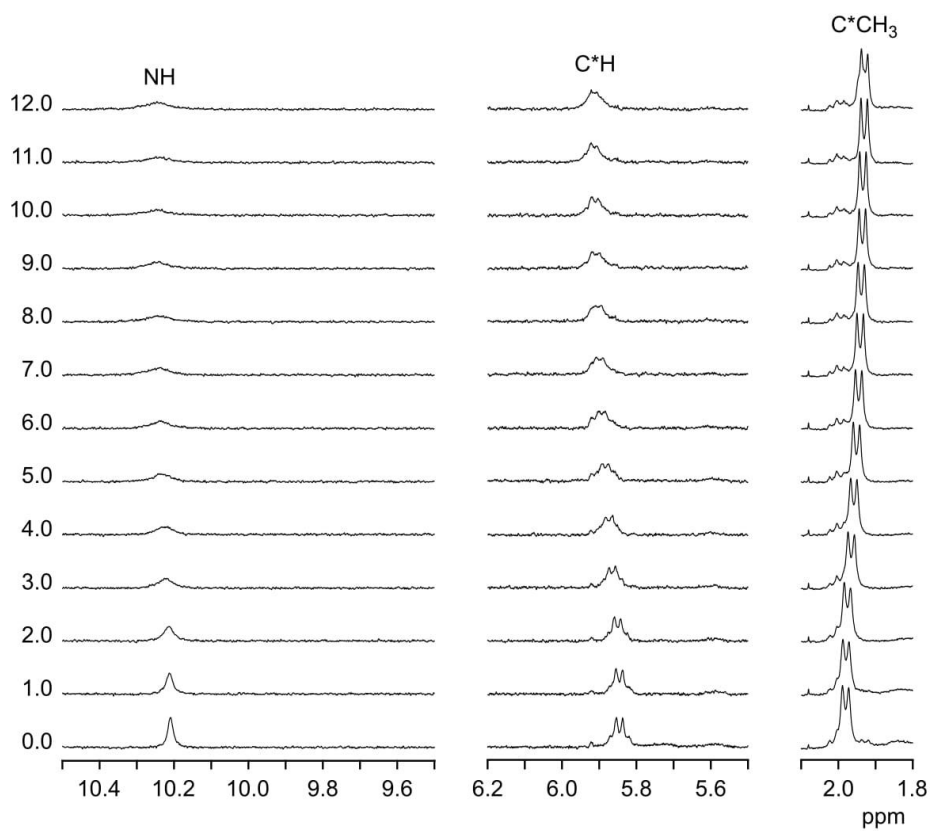
Binding isotherms and HypNMR outputs

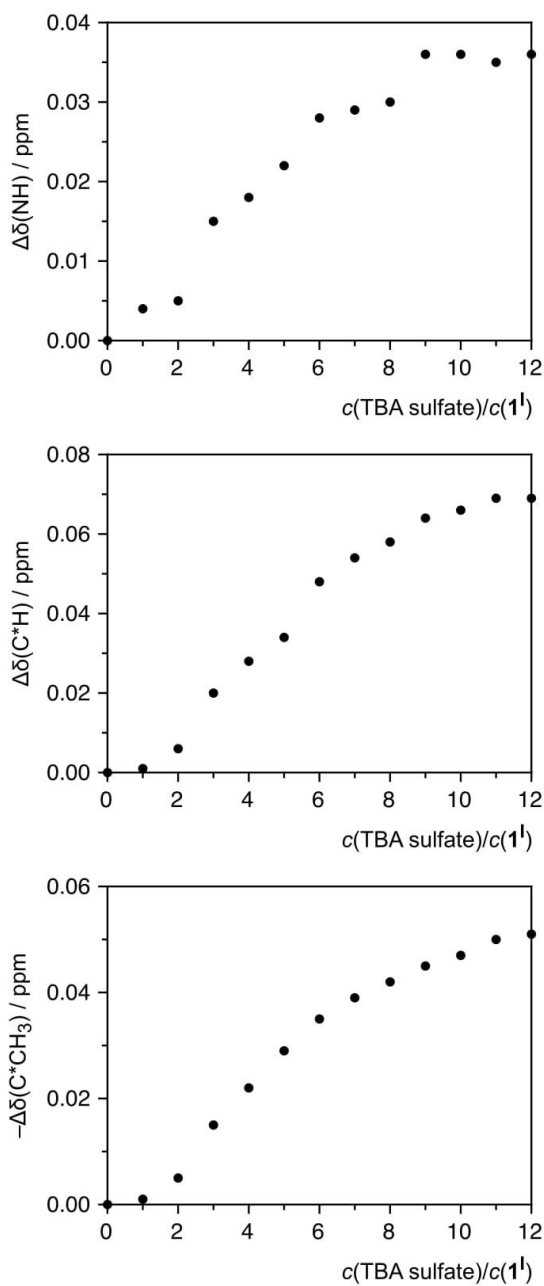
Converged in 1 iterations with sigma = 0.004043

	value	standard deviation	Comments
1 log beta (GH)	3.5987	0.0261	3.6(3)



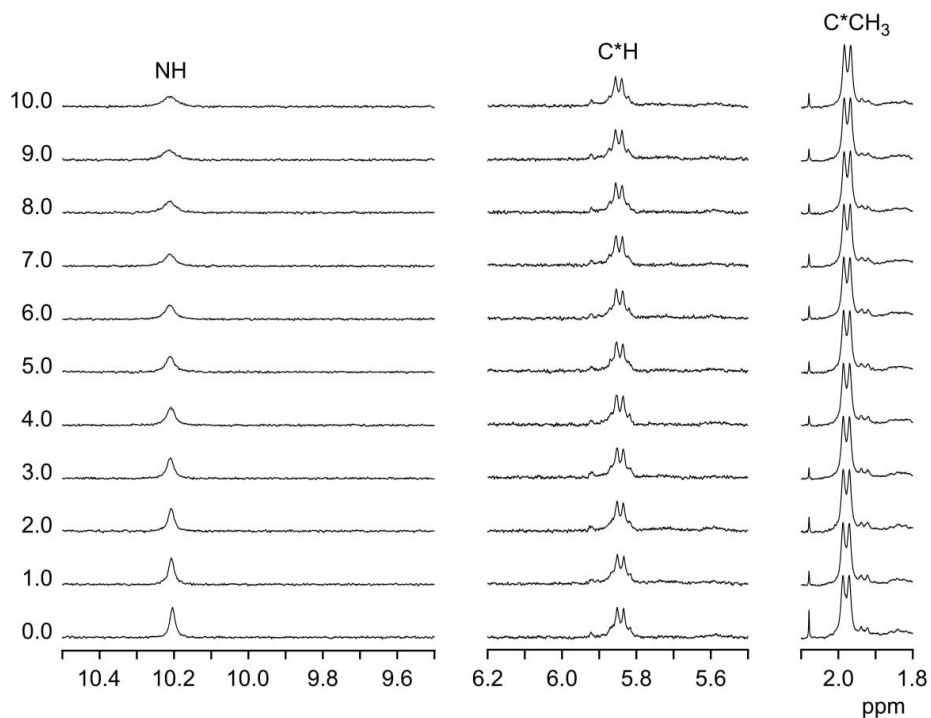
$^1\text{H}$  NMR spectra of **1**<sup>I</sup> (0.25 mM) in 2.5 vol%  $\text{H}_2\text{O}/\text{DMSO-}d_6$  (400 MHz) containing the increasing equivalents of TBA sulfate specified to the left of each spectrum.



Binding isotherms

The binding isotherms observed in the titration with TBA sulfate exhibited a sigmoidal shape, indicating that complex formation is not consistent with a simple 1:1 equilibrium. We did not succeed, however, to fit these isotherms to a reasonable other binding model.

$^1\text{H}$  NMR spectra of  $\mathbf{1}^{\text{I}}$  (0.25 mM) in 2.5 vol%  $\text{H}_2\text{O}/\text{DMSO-}d_6$  (400 MHz) containing the increasing equivalents of TBA DHP specified to the left of each spectrum.



No signal shifts are visible, indicating that DHP is not bound by  $\mathbf{1}^{\text{I}}$  under these conditions.

ITC Titrations:

The ITC experiments were carried out in 2.5 vol% water/DMSO. The anionic substrates were used as their TBA salts. The salts and receptor **1**<sup>1</sup> were weighed using an analytical precision balance, dissolved in known volumes of the respective solvent mixture, and loaded into the system for immediate analysis.

The measurements were carried out at 25 °C using a reference power of 25  $\mu$ J/s, a filter period of 2 s, a stirrer speed of 307 rpm. Other experimental parameters of the individual titrations are specified in the Table S1. Automated baseline assignment and peak integration of raw thermograms were accomplished by singular value decomposition and peak-shape analysis using NITPIC.<sup>4a</sup> Estimation of best-fit parameter values by weighted nonlinear least-squares fitting and calculation of 68.3% confidence intervals were performed with the public-domain software SEDPHAT,<sup>4b</sup> as explained in detail elsewhere.<sup>4c,d</sup>

**Table S1.** Concentrations and experimental parameters of the individual titrations.

guest anion as TBA salt	$c(\mathbf{1}^1)$ / mM	$c(\text{salt})$ / mM	injection volume / $\mu$ L	no. of injections	spacing time / s
chloride	0.7	26.5	8	29	180
bromide	0.9	32.5	8	29	180

The heat changes observed during the titration with TBA bromide turned out to be too small to allow reliable quantification of binding strength.

Titration of **1**<sup>I</sup> with TBA chloride: The blue spheres show the experimental results and the red line the fitted curve calculated by using the one site binding model. The inset shows the heat pulses of the measurement from which the isotherm was generated.

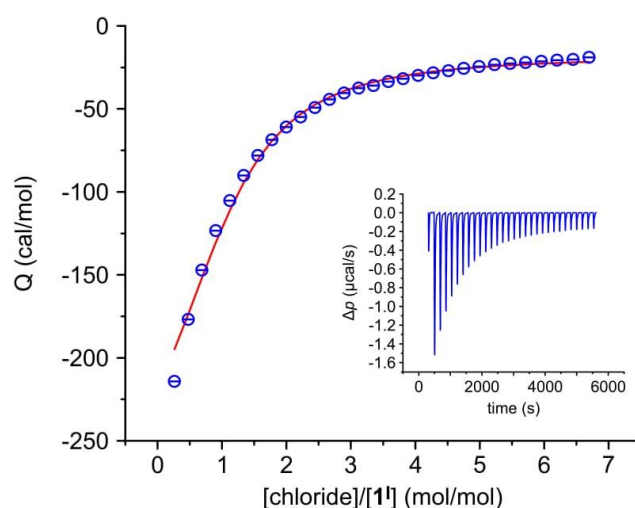


**Table S2.** Comparison of the anion affinity of **1**<sup>I</sup> in 2.5 vol% H<sub>2</sub>O/DMSO-*d*<sub>6</sub> with that of the corresponding prototriazole derivative **1**<sup>H</sup> in 2.5 vol% D<sub>2</sub>O/DMSO-*d*<sub>6</sub>.<sup>2</sup>

anion	<b>1</b> <sup>I</sup>	<b>1</b> <sup>H</sup>
chloride	$\log K_{1:1} = 3.28$	no binding detectable in solution
bromide	$\log K_{1:1} = 2.85$	no binding detectable in solution
iodide	$\log K_{1:1} = 2.15$	no binding detectable in solution
DHP	no binding detectable in solution complex binding equilibrium	$\log K_{1:1} = 3.21$ ; $\log K_{1:2} = 3.10^a$
sulfate	saturation is reached only in the presence of 12 equiv of TBA sulfate	$\log K_{1:1} = 4.22$ ; $\log K_{2:1} < 2.1^b$

<sup>a</sup> binding constant referring to the formation of a 1:2 complex with two DHP anions binding to one pseudopeptide; <sup>b</sup> binding constant referring to the formation of a 2:1 complex with two pseudopeptides binding to one sulfate anion.

References

- 1 H. E. Gottlieb, V. Kotlyar and A. Nudelman, *J. Org. Chem.*, 1997, **62**, 7512-7515.
- 2 D. Mungalpara, H. Kelm, A. Valkonen, K. Rissanen, S. Keller and S. Kubik, *Org. Biomol. Chem.*, 2017, **15**, 102-113.
- 3 C. Frassinetti, S. Ghelli, P. Gans, A. Sabatini, M. S. Moruzzi and A. Vacca, *Anal. Biochem.*, 1995, **231**, 374-382.
- 4 (a) S. Keller, C. Vargas, H. Zhao, G. Piszczek, C. A. Brautigam and P. Schuck, *Anal. Chem.*, 2012, **84**, 5066-5073; (b) J. C. D. Houtman, P. H. Brown, B. Bowden, H. Yamaguchi, E. Appella, L. E. Samelson and P. Schuck, *Protein Sci.*, 2007, **16**, 30-42; (c) G. Krainer, J. Broecker, C. Vargas, J. Fanghänel and S. Keller, *Anal. Chem.*, 2012, **84**, 10715-10722; (d) G. Krainer, S. Keller, *Methods*, 2015, **76**, 116-123.

## CURRICULUM VITAE

**Disha Mungalpara**

### **EDUCATION**

---

06/2013-06/2017	Doktor der Naturwissenschaften (Very Good) Technical University Kaiserslautern, Germany
06/2012-05/2013	Zulassungsarbeit zur Promotion (Good) Technical University Kaiserslautern, Germany
2009-2011	Master of Pharmacy (Excellent) Indian Institute of Technology (BHU), Varanasi, India
2005-2009	Bachelor of Pharmacy (First Class) Gujarat University, India

### **PUBLICATIONS**

---

**D. Mungalpara**, H. Kelm, A. Valkonen, K. Rissanen, S. Keller, S. Kubik "Oxoanion binding to a cyclic pseudopeptide containing 1,4-disubstituted 1,2,3-triazole moieties" *Org. Biomol. Chem.* 2017, **15**, 102-113.

**D. Mungalpara**, S. Stegmüller, S. Kubik "A neutral halogen bonding macrocyclic anion receptor based on a pseudocyclopeptide with three 5-iodo-1,2,3-triazole subunits" *Chem. Commun.* **2017**, **53**, 5095-5098.

**D. Mungalpara**, A. Valkonen, K. Rissanen, S. Kubik "Efficient stabilisation of a dihydrogenphosphate tetramer and a dihydrogenpyrophosphate dimer by a cyclic pseudopeptide containing 1,4-disubstituted 1,2,3-triazole moieties" *Chem. Sci.* 2017, **8**, 6005-6013.

**D. Mungalpara**, S. Kubik "Amino acid-based receptors" in: *Comprehensive Supramolecular Chemistry II*, Vol. 3, J. L. Atwood, (ed.), Elsevier: Oxford, p. 293-310.